

PASSIVE LOAD FOLLOW ANALYSIS
OF THE STAR-LM AND STAR-H2 SYSTEMS

A Dissertation

by

ANTON MOISSEYTSEV

Submitted to the Office of Graduate Studies of
Texas A&M University
in partial fulfillment of the requirements for the degree of

DOCTOR OF PHILOSOPHY

December 2003

Major Subject: Nuclear Engineering

PASSIVE LOAD FOLLOW ANALYSIS
OF THE STAR-LM AND STAR-H2 SYSTEMS

A Dissertation

by

ANTON MOISSEYTSEV

Submitted to Texas A&M University
in partial fulfillment of the requirements
for the degree of

DOCTOR OF PHILOSOPHY

Approved as to style and content by:

Kenneth L. Peddicord
(Chair of Committee)

Yassin A. Hassan
(Member)

Paul Nelson, Jr.
(Member)

Robert A. Gustafson
(Member)

William E. Burchill
(Head of Department)

December 2003

Major Subject: Nuclear Engineering

ABSTRACT

Passive Load Follow Analysis of the STAR-LM and STAR-H2 Systems.

(December 2003)

Anton Moisseytsev, B.S., Moscow State Engineering and Physics Institute;

M.S., Moscow State Engineering and Physics Institute

Chair of Advisory Committee: Dr. Kenneth L. Peddicord

A steady-state model for the calculation of temperature and pressure distributions, and heat and work balance for the STAR-LM and the STAR-H2 systems was developed. The STAR-LM system is designed for electricity production and consists of the lead cooled reactor on natural circulation and the supercritical carbon dioxide Brayton cycle. The STAR-H2 system uses the same reactor which is coupled to the hydrogen production plant, the Brayton cycle, and the water desalination plant. The Brayton cycle produces electricity for the on-site needs. Realistic models for each system component were developed. The model also performs design calculations for the turbine and compressors for the CO₂ Brayton cycle. The model was used to optimize the performance of the entire system as well as every system component. The size of each component was calculated.

For the 400 MWt reactor power the STAR-LM produces 174.4 MWe (44% efficiency) and the STAR-H2 system produces 7450 kg H₂/hr.

The steady state model was used to conduct quasi-static passive load follow analysis. The control strategy was developed for each system; no control action on the reactor is required.

As a main safety criterion, the peak cladding temperature is used. It was demonstrated that this temperature remains below the safety limit during both normal operation and load follow.

ACKNOWLEDGMENTS

I would like to thank Dr. Kenneth Peddicord for his support during the work on this dissertation and for the opportunity to study at Texas A&M University.

I would like to thank Dr. David Wade, Dr. James Sienicki, and Dr. Joe Braun for making it possible to work on this dissertation in Argonne National Laboratory. I would also like to thank Dr. Richard Doctor, Dr. Diana Matonis, Dr. Ron Kulak, and Dr. Ike Therios of the Argonne National laboratory for their cooperation and help and Vaclav Dostal from MIT for his consultations during the work.

I would like to thank Sheri Anderson and Nicholas Lugansky for help during the preparation of this manuscript.

Finally, I would like to thank my wife Vera for her love and support.

TABLE OF CONTENTS

	Page
ABSTRACT	iii
ACKNOWLEDGMENTS.....	iv
TABLE OF CONTENTS	v
LIST OF FIGURES.....	vii
LIST OF TABLES	ix
INTRODUCTION.....	1
STAR Systems	1
STAR-LM System.....	1
STAR-H2 System.....	3
Goals of the Analysis	3
STEADY-STATE MODEL	5
Brayton Cycle Submodel	5
Brayton Cycle Optimization.....	35
Reactor Submodel	51
Hydrogen Production Plant and Intermediate Loop Submodel (STAR-H2)	55
Reactor Heat Exchanger Module	58
Results of the Steady-State Model	102
PASSIVE LOAD FOLLOW ANALYSIS	106
Reactor Reactivity Feedbacks and Passive Load Follow	106
Load Follow for the STAR-LM System	109
Load Follow for the STAR-H2 System.....	121
CONCLUSION	130
REFERENCES.....	131
APPENDIX A	135
APPENDIX B	145
APPENDIX C	153

	Page
APPENDIX D	164
APPENDIX E.....	169
APPENDIX F	174
APPENDIX G	181
APPENDIX H	188
VITA	193

LIST OF FIGURES

	Page
Figure 1. STAR-LM system.....	2
Figure 2. STAR-H2 system.....	4
Figure 3. Carbon dioxide properties near critical point.....	7
Figure 4. Inlet and outlet temperatures in recuperator.	8
Figure 5. Effectiveness of ideal recuperator.....	10
Figure 6. Multi region approach for recuperators.	17
Figure 7. Optimization of the number of regions for recuperators.	21
Figure 8. Compression process.	22
Figure 9. Turbine stage dimensions.	25
Figure 10. Gas velocities in a turbine stage.	26
Figure 11. Turbine design results.....	31
Figure 12. Results of the cooler module calculations.	36
Figure 13. Simple Brayton cycle.....	37
Figure 14. Effect of intercooling and interheating.	38
Figure 15. Maximum pressure and flow split optimization.	40
Figure 16. Minimum temperature optimization.	41
Figure 17. Fins and their efficiency.	43
Figure 18. Recuperator length optimization.....	45
Figure 19. HEATRIC heat exchanger.....	46
Figure 20. HEATRIC heat exchanger parameters optimization.	47
Figure 21. Coolant, cladding, and fuel temperatures.	54
Figure 22. Reactor heat exchanger.....	59
Figure 23. U-tube.	61
Figure 24. RHX tube with two lead flows.	63
Figure 25. Comparison of two approaches.....	68
Figure 26. Flow areas in concentric tubes.....	74
Figure 27. Straight tubes HX flow areas.	77

	Page
Figure 28. Number of the helical coil HXs.	82
Figure 29. Dimensions of helical coil HX.....	84
Figure 30. Plate type RHX	87
Figure 31. HEATRIC HX channel.....	90
Figure 32. Tube projections.	94
Figure 33. Comparison of the tube projections correlations.	96
Figure 34. Comparison of RHX designs (STAR-LM).....	98
Figure 35. Comparison of RHX designs (STAR-H2).....	99
Figure 36. Effect of the tube projections.....	100
Figure 37. Temperature distribution inside U-tube (#1) and straight tube (#4).....	101
Figure 38. Result of the steady-state model (STAR-LM).....	103
Figure 39. Results of the steady-state model (STAR-H2).	104
Figure 40. STAR-LM at 50 % load (mass flow rate controlled).....	112
Figure 41. STAR-LM at 60 % load (flow split controlled).....	115
Figure 42. CO ₂ inventory change.....	118
Figure 43. Inventory control system.	119
Figure 44. STAR-H2 at 50% load (reagent steam flow rate).....	124
Figure 45. STAR-H2 at 50% load (bromine flow rate).....	126
Figure 46. STAR-H2 under compressor over speed accident.....	129

LIST OF TABLES

	Page
Table 1. Results of turbine and compressors design	32
Table 2. Estimation of benefit from increase in cycle efficiency by 1%	37
Table 3. Effect of tube fins on recuperators' effectiveness and cycle efficiency	44
Table 4. Minimum temperature in cycle and cooler length	49
Table 5. Number of tubes for the stacked U-tube HX	60
Table 6. Results for outlet temperatures.....	69
Table 7. RHX cross section area occupied by a tube	70
Table 8. Fraction of RHX cross section area occupied by secondary fluid	77
Table 9. Results of RHX optimization (STAR-LM).....	98
Table 10. Results of RHX optimization (STAR-H2).....	99
Table 11. CO ₂ inventory at nominal power.....	117
Table 12. Accident scenarios for STAR-H2	127

INTRODUCTION

STAR Systems

The Secure Transportable Autonomous Reactor (STAR) was designed by Argonne National Laboratory (Sienicki et al., 1999; Sienicki and Spencer, 2002; Spencer et al., 2000; Spencer, 2000; Spencer et al., 2000) as a Generation IV reactor. It is a fast reactor utilizing liquid lead or lead-bismuth eutectic as a coolant allowing for natural circulation. The reactor was designed to meet the goals of economics, proliferation resistance, and sustainability and for the possibility of long term operation (15-20 years) without refueling.

The other design feature is the possibility to use the STAR reactor in various systems, including electrical and non-electrical applications. Several systems were designed based on the STAR reactor. For the purpose of this work two systems were selected: STAR-LM System which uses the STAR reactor with supercritical carbon dioxide Brayton cycle for electricity production and STAR-H2 System which uses the STAR reactor for hydrogen production. Both these systems utilize lead as a coolant and are described below in more details.

STAR-LM System

The STAR-LM System is designed for electricity production and consists of the STAR reactor, reactor heat exchanger (RHX) and supercritical carbon dioxide (S-CO₂) Brayton cycle (Figure 1). The S-CO₂ Brayton cycle was selected for the power conversion system because of its high thermal efficiency and small component size (Dostal et al., 2001; Dostal et al., 2002) and it suits the STAR reactor for temperature regimes, chemical compatibility between CO₂ and lead, and power level. The reactor power level is set to be 400 MWt, and the goal of the design analysis was to produce as much electricity as possible.

This dissertation follows the style and format of Nuclear Engineering and Design.

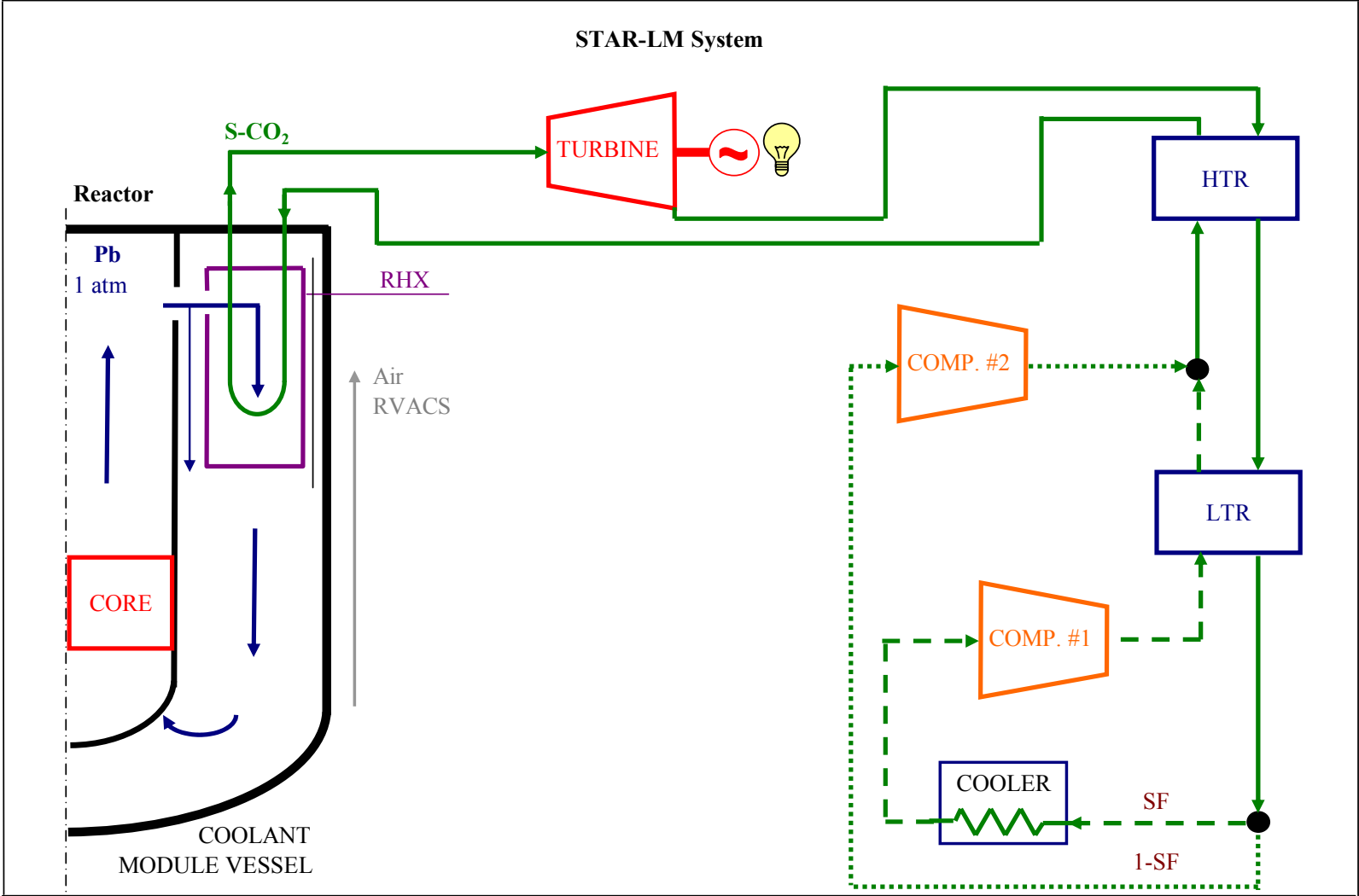


Figure 1. STAR-LM system.

STAR-H2 System

The STAR-H2 system is designed to produce hydrogen from seawater using heat from the STAR nuclear reactor. The system is designed in such a way that it requires no off-site electricity and produces the maximum amount of hydrogen possible.

The system consists of a reactor, reactor vessel air cooling system (RVACS), intermediate loop, hydrogen production plant, Brayton cycle, and desalination plant (Figure 2). The reactor produces heat. The reactor vessel air cooling system cools the reactor vessel under normal operation and in the event of an accident. The intermediate loop serves to deliver the heat from the reactor to the hydrogen production plant, where the heat is used for thermo-chemical cracking of steam. The Brayton cycle provides electricity for the whole plant. The desalination plant produces fresh water from the seawater, and steam for the hydrogen production plant.

Goals of the Analysis

The goals of this work are:

1. Develop a steady-state thermo hydraulic computer model of the STAR-LM and STAR-H2 systems to calculate pressure and temperature distribution of all working fluids, their mass flow rates, and the whole-system heat balance
2. Use the steady-state model to optimize the systems' design and calculate the optimal sizes of the components
3. Modify steady-state model for quasi-static passive load follow analysis
4. Modify steady-state model for final-state accident analysis

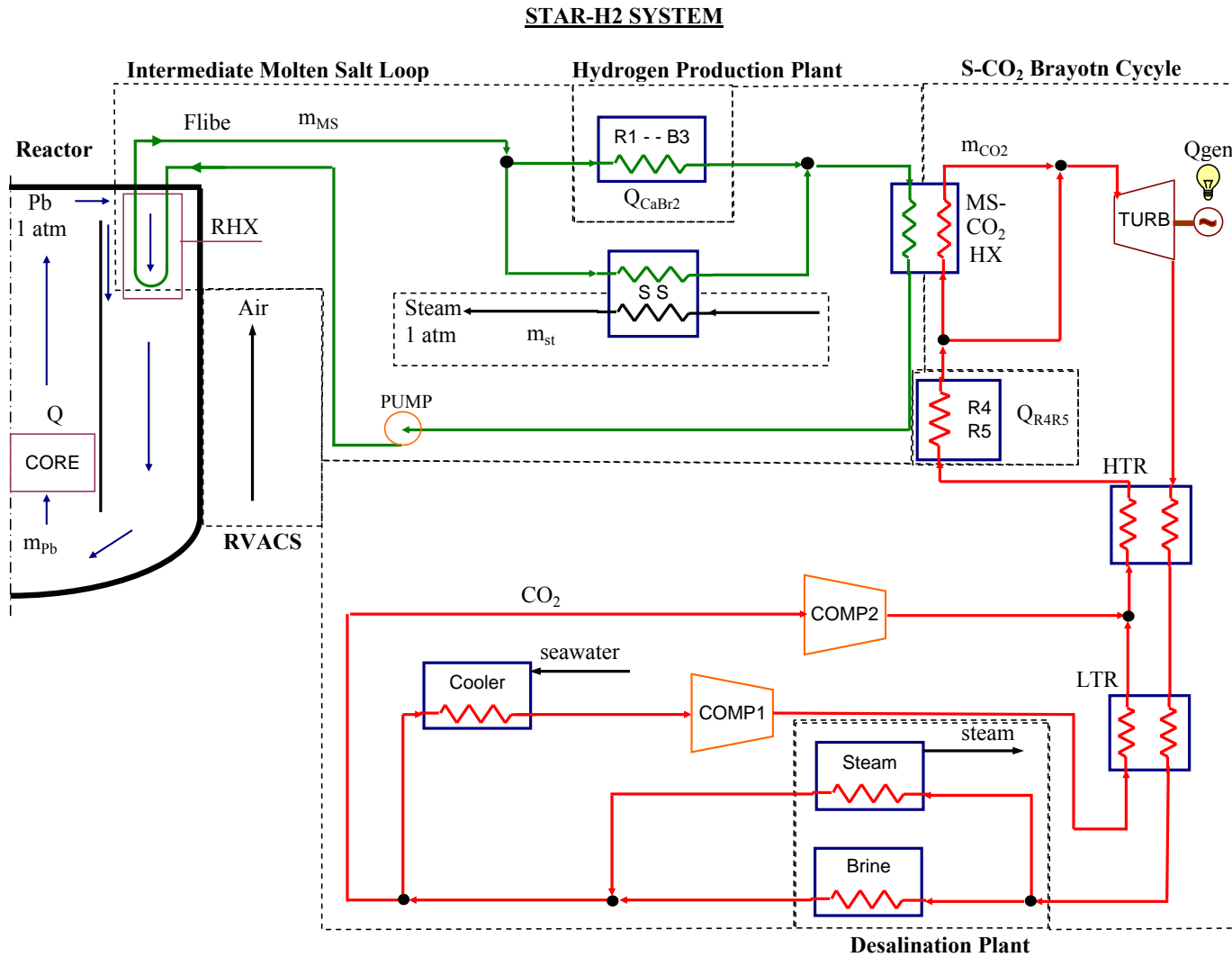


Figure 2. STAR-H2 system.

STEADY-STATE MODEL

The goals of the steady-state model are to calculate temperature and pressure distribution of the working fluids, their mass flow rates, amount of heat transferred in each heat exchanger, electricity produced by the generator, electricity required to run pumps and compressors, and amount of hydrogen and fresh water produced (STAR-H2 system). The temperatures should be compared to the limiting temperatures to ensure safe operation of the systems.

The steady-state model was developed using FORTRAN programming language. It consists of several submodels for each subsystem, such as reactor, reactor heat exchanger, Brayton cycle, and intermediate loop (STAR-H2). There is also a main program which serves to connect these submodels. Big submodels, like Brayton cycle, use a module for each component, i.e. turbine, compressors, heat exchangers etc.

The steady-state model is used to optimize the systems for maximum performance. To do this, the optimization should be done on two levels: component level and system level. On the component level, the optimal design (dimensions, configuration) is found for every component (heat exchangers, turbine etc.) to give the maximum performance. On the system level the parameters of working fluids (pressure and temperature region) are selected to maximize the systems' performance.

Brayton Cycle Submodel

For the STAR system, the Brayton cycle with supercritical carbon dioxide as a working fluid was selected for electricity production because it is shown to have a high thermodynamic efficiency. The cycle has common components for all gas cycles: reactor heat exchanger (RHX), turbine, compressors, cooler and recuperators (Figure 1). After the CO₂ is heated in the RHX, it then expands in the turbine, producing expansion work which is converted into electricity in the generator. Next the CO₂ is cooled in the recuperators, and further cooled in the cooler, then the CO₂ is compressed by the compressors, heated up in the recuperators and returned to the RHX.

It was shown that working in the supercritical regime (CO₂ pressure and temperature above critical point value¹) gives the best performance of the cycle. This is due to the fact that the CO₂ properties change rapidly near critical point, allowing for significant reduction in the compression work, compared to similar cycles with ideal gases, like helium. This unique feature of carbon dioxide on one hand makes it possible to design a high-efficient cycle and, on the other hand, requires very accurate calculations of the CO₂ properties near critical point. Therefore, the ideal gas approach, which is usually used for gas cycle analysis, cannot be implemented for the CO₂ Brayton cycle, and realistic models for each component that use accurate CO₂ properties should be developed.

CO₂ Properties

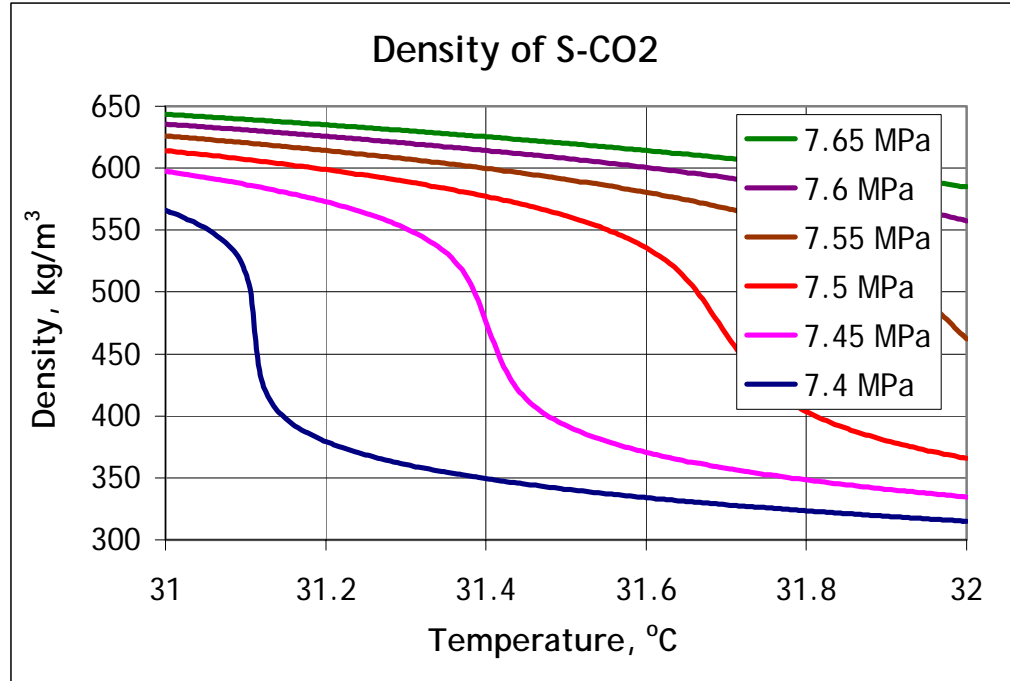
CO₂ properties above critical point have two special features which influence Brayton cycle calculations.

First, the CO₂ properties change rapidly near the critical point. A sharp increase in the density (Figure 3a) leads to reduction in compression work and, therefore, higher cycle efficiency. Due to this feature, the carbon dioxide Brayton cycle was selected for energy production. The change in specific heat (Figure 3b) means that cooling down the CO₂ to near critical point is difficult, thus a large heat exchanger is required.

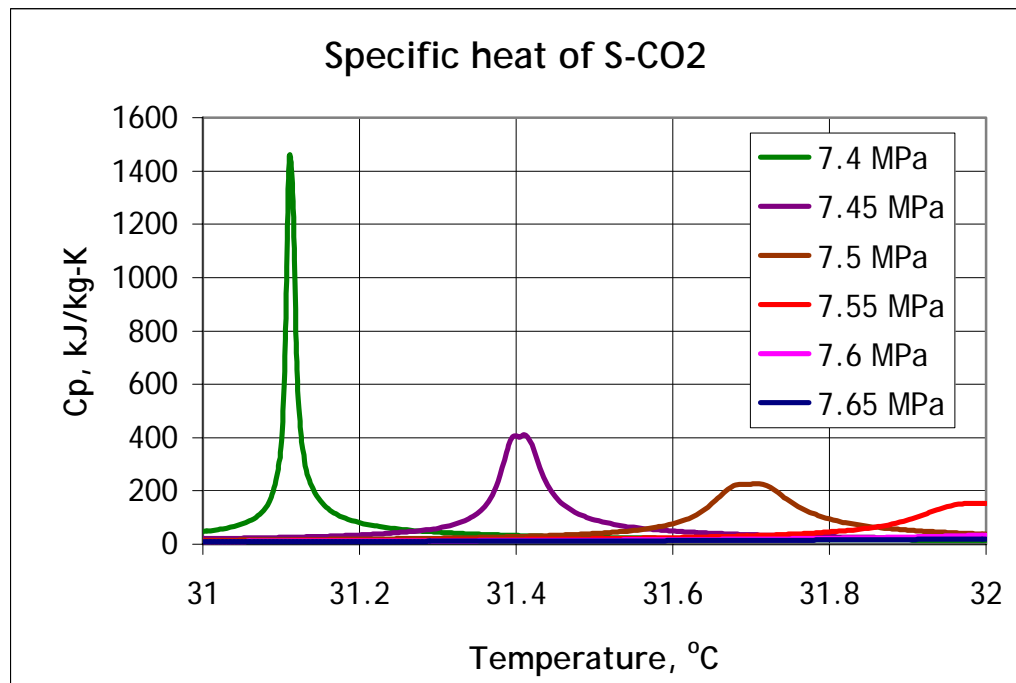
Second, the properties of CO₂ depend on pressure, unlike an ideal gas. This means that heat transfer from one CO₂ flow with one pressure to the other CO₂ flow with different pressure is not very efficient, causing problems for the recuperators design.

Because of the CO₂ behavior, accurate calculation of the CO₂ properties is important for the cycle analysis. In this work, the properties were calculated using equations recommended by (Vesovic et al., 1990; Span and Wagner, 1996), which are accurate to within 0.03% of the density near critical point with maximum error of 0.2% for the working region of the cycle.

¹ Critical point of the CO₂ is $p_{crit}=7.3773 \text{ MPa}$, $T_{crit}=30.98 \text{ }^\circ\text{C}$.



a) Density



b) Specific heat

Figure 3. Carbon dioxide properties near critical point.

Recuperator Module

The recuperative heat exchangers (or recuperators) are used in Brayton cycle to transfer heat between two CO₂ flows. This heat transfer decreases the CO₂ temperature for compression (for the given turbine inlet temperature) resulting in lower compression work and, therefore, higher cycle efficiency. There are two recuperators used in the cycle (Figure 1) – high temperature recuperator (HTR) and low temperature recuperator (LTR)¹.

The goal of the recuperator module is to calculate CO₂ temperatures at the recuperator outlets the given temperatures at the inlets (Figure 4).

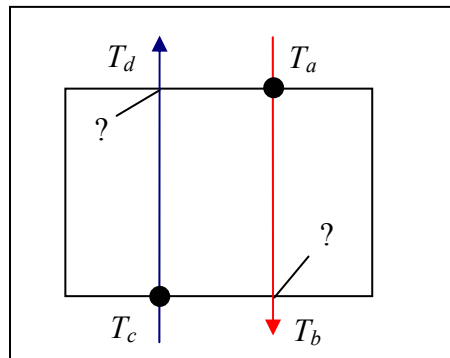


Figure 4. Inlet and outlet temperatures in recuperator.

Ideal Recuperator

Before performing the calculations for any real design of the recuperator, it is useful to know what are the theoretical limits for the heat exchanger performance. These limits are defined by the differences in the thermal properties of the two CO₂ flows in the recuperator, particularly, specific heats. In an ideal case, the outlet temperatures will be equal to the corresponding inlet temperatures ($T_d=T_a$, $T_b=T_c$, Figure 4). However, if the specific heats of these two flows are different, the change in temperature for one flow will be less than that of the other flow, since the amount of heat (which is equal to

¹ See section on cycle analysis for the reasons why two recuperators are needed.

the change in temperature times the specific heat) is the same for both flows. Also since the CO₂ properties, including specific heat, depend on pressure, and the pressures of the flows inside the recuperator are different, the outlet temperatures will not match the inlet temperatures.

In order to find out how close the outlet temperature can possibly be to the inlet temperature, the ideal recuperator model was developed. This model calculates the CO₂ temperature change in the infinite recuperator with no pressure loss, thus providing the theoretical limit for the CO₂-to-CO₂ heat exchanger performance.

The ideal recuperator model uses the energy conservation equation which states that the amount of energy transferred from the cold flow is equal to the amount of energy accepted by the cold flow:

$$\dot{m}_{hot} \cdot \Delta h_{hot} = \dot{m}_{cold} \cdot \Delta h_{cold}, \quad (1)$$

where $\dot{m}_{hot}, \dot{m}_{cold}$ - mass flow rates of hot and cold flows,

$\Delta h_{hot} = h_a - h_b$ - enthalpy change for the hot flow,

$\Delta h_{cold} = h_d - h_c$ - enthalpy change for the cold flow.

In the infinite heat exchanger, heat transfer occurs at some point of the heat exchanger while the temperature of the hot flow is greater than the temperature of the cold flow. This means that either the hot outlet temperature should be equal to the cold inlet temperature ($T_b=T_c$) or the cold outlet temperature should be equal to the hot inlet temperature ($T_d=T_a$). Let's assume that the $T_b=T_c$. Then, the T_b is known (T_c is given) and the enthalpy h_b is an enthalpy for T_b and the hot flow pressure. Then, the enthalpy at the cold flow outlet can be calculated using Equation (1):

$$h_d = h_c + \frac{\dot{m}_{hot}}{\dot{m}_{cold}} (h_a - h_b) \quad (2)$$

The enthalpy and pressure at point d define the cold outlet temperature T_d . If this temperature is greater than T_a , then the assumption is that $T_b=T_c$ was wrong and, therefore, $T_d=T_a$. In this case the same technique will be used to find T_b .

Figure 5 shows the dependence of the recuperator effectiveness on the hot and cold flow inlet temperatures for the equal mass flow rates. The recuperator effectiveness shows how close the cold outlet temperature is to the hot inlet and is defined as:

$$\varepsilon_{HX} = \frac{T_d - T_c}{T_a - T_c} \cdot 100\% \quad (3)$$

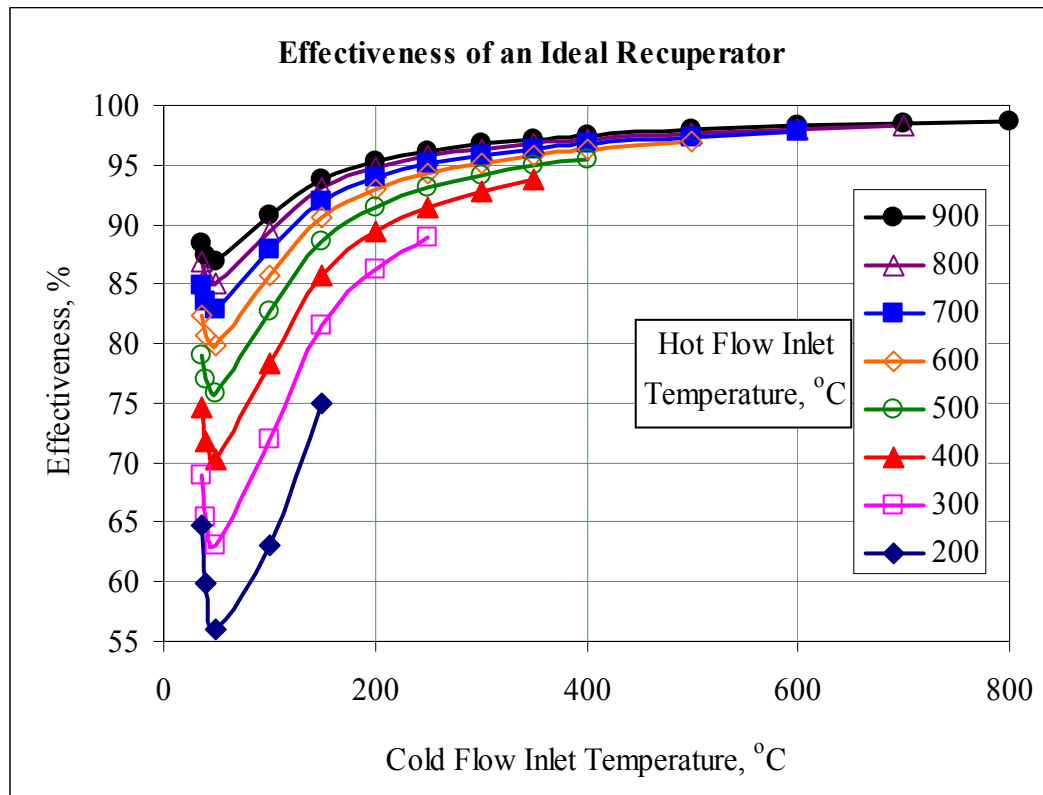


Figure 5. Effectiveness of ideal recuperator.

Realistic Recuperator Model

Unlike the ideal recuperator, the real recuperator has a finite length. Therefore, its effectiveness will be lower than that of an ideal one and will depend on the length.

Consider one element of a heat exchanger where hot fluid is flowing on one side of the tube and cold fluid on the other. The mass flow rates of both fluids are known as well as the dependence of thermodynamic properties as a function of temperature and pressure. The parameters of the hot and cold flows will be referred as those with indexes 1 and 2, respectively.

Heat transfer from the hot fluid to the cold fluid at any point in the heat exchanger along its axis is defined (Todreas and Kazimi, 1990) by Equation (4):

$$q(z) = \frac{T_1(z) - T_2(z)}{\frac{1}{h_1 WP_1 \eta_1} + \frac{\ln(r_o/r_i)}{2\pi k_w} + \frac{1}{h_2 WP_2 \eta_2}} \quad \left[\frac{kW}{m} \right] \quad (4)$$

where

T – fluid temperature (K)

h – heat transfer coefficient (kW/(m²-K))

WP – wetted perimeter (m)

η – fin efficiency (if fins are used)

r_o, r_i – tube outer and inner radii (m)

k_w – wall thermal conductivity, (kW/(m-K))

The amount of heat transferred on the infinitely small region dz is equal to $q(z)dz$. This heat transfer causes a change in the fluid temperature on both sides:

$$\dot{m}_1 c_{p1} dT_1 = -q(z)dz = \dot{m}_2 c_{p2} dT_2 \quad (5)$$

The minus sign reflects the fact that, on one hand, the heat is taken away from the hot fluid, and on the other hand, the cold flow direction is opposite to the z -axis, which is chosen here to be the direction of the hot flow.

Equations (4) and (5) can be written as a system of differential equations:

$$\begin{cases} \frac{dT_1}{dz} = -\frac{q(z)}{m_1 c_{p1}} = -\frac{1}{m_1 c_{p1}} \frac{1}{\frac{1}{h_1 W P_1 \eta_1} + \frac{\ln(r_o/r_i)}{2\pi k_w} + \frac{1}{h_2 W P_2 \eta_2}} (T_1(z) - T_2(z)) \\ \frac{dT_2}{dz} = -\frac{q(z)}{m_2 c_{p2}} = -\frac{1}{m_2 c_{p2}} \frac{1}{\frac{1}{h_1 W P_1 \eta_1} + \frac{\ln(r_o/r_i)}{2\pi k_w} + \frac{1}{h_2 W P_2 \eta_2}} (T_1(z) - T_2(z)) \end{cases} \quad (6)$$

Or,

$$\begin{cases} \frac{dT_1}{dz} = -k \cdot T_1(z) + k \cdot T_2(z) \\ \frac{dT_2}{dz} = -k \cdot n \cdot T_1(z) + k \cdot n \cdot T_2(z) \end{cases} \quad (7)$$

where

$$k = \frac{1}{m_1 c_{p1}} \frac{1}{\frac{1}{h_1 W P_1 \eta_1} + \frac{\ln(r_o/r_i)}{2\pi k_w} + \frac{1}{h_2 W P_2 \eta_2}}$$

$$n = \frac{m_1 c_{p1}}{m_2 c_{p2}}$$

The coefficients k and n are functions of the fluid properties and, hence, a function of the fluid temperatures. This means that System (7) cannot be solved analytically. However, if we assume that the heat exchanger is divided into several regions and the fluid properties do not change inside each region, we can solve this system for every region.

Let's assume that the fluid properties are constant inside the heat exchanger, i.e. the coefficients k and n are not functions of z . Then System (7) is a system of linear differential equations. The boundary conditions for System (7) are given inlet temperatures:

$$\begin{aligned} T_1(0) &= T_a \\ T_2(L) &= T_c \end{aligned} \quad (8)$$

To solve System (7) take Laplace transform of each equation. Denoting $t_i(s) = \mathcal{L}\{T_i(z)\}$, we get:

$$\begin{aligned} s \cdot t_1(s) - T_1(0) &= -k \cdot t_1(s) + k \cdot t_2(s) \\ s \cdot t_2(s) - T_2(0) &= -k \cdot n \cdot t_1(s) + k \cdot n \cdot t_2(s) \end{aligned} \quad (9)$$

Solving the second equation for $t_2(s)$:

$$t_2(s) = \frac{T_2(0) - k \cdot n \cdot t_1(s)}{s - k \cdot n} \quad (10)$$

Substituting (10) into first equation of (9) and solving for $t_1(s)$:

$$(s + k) \cdot t_1(s) = T_1(0) + k \cdot \frac{T_2(0) - k \cdot n \cdot t_1(s)}{s - k \cdot n}$$

$$\left[(s + k)(s - k \cdot n) + k^2 \cdot n \right] \cdot t_1(s) = (s - k \cdot n) \cdot T_1(0) + k \cdot T_2(0)$$

$$\left[s^2 + k \cdot s - k \cdot n \cdot s \right] \cdot t_1(s) = (s - k \cdot n) \cdot T_1(0) + k \cdot T_2(0)$$

$$t_1(s) = \frac{(s - k \cdot n) \cdot T_1(0) + k \cdot T_2(0)}{s(s - k(n - 1))} \quad (11)$$

To find $T_1(z)$ use the method of residues (Mertyurek, 2002) at poles $s=0$ and $s=k(n-1)$:

$$T_1(z) = R_{s=0} + R_{s=k(n-1)}$$

$$R_{s=0} \equiv \left[s \cdot t_1(s) \cdot e^{s \cdot z} \right]_{s=0} = \frac{T_1(0) \cdot (-k \cdot n) + k \cdot T_2(0)}{-k \cdot (n-1)} = \frac{n \cdot T_1(0) + T_2(0)}{n-1}$$

$$\begin{aligned} R_{s=k(n-1)} &\equiv \left[(s - k \cdot (n-1)) \cdot t_1(s) \cdot e^{s \cdot z} \right]_{s=k(n-1)} = \frac{T_1(0) \cdot (k \cdot (n-1) - k \cdot n) + k \cdot T_2(0)}{k \cdot (n-1)} e^{k(n-1) \cdot z} \\ &= \frac{-T_1(0) + T_2(0)}{n-1} e^{k(n-1) \cdot z} \end{aligned}$$

$$T_1(z) = \frac{n - e^{k(n-1)z}}{n-1} T_1(0) + \frac{-1 + e^{k(n-1)z}}{n-1} T_2(0) \quad (12)$$

Temperature $T_2(z)$ can be found from the first equation of System (7):

$$T_2(z) = \frac{1}{k} \frac{dT_1}{dz} + T_2(z)$$

$$\frac{dT_1}{dz} = \frac{1}{k} \left[\frac{-k \cdot (n-1)}{n-1} \cdot e^{k(n-1)z} \cdot T_1(0) + \frac{k \cdot (n-1)}{n-1} \cdot e^{k(n-1)z} \cdot T_2(0) \right] = [-T_1(0) + T_2(0)] \cdot e^{k(n-1)z}$$

$$\begin{aligned} T_2(z) &= [-T_1(0) + T_2(0)] \cdot e^{k(n-1)z} + \frac{n - e^{k(n-1)z}}{n-1} T_1(0) + \frac{-1 + e^{k(n-1)z}}{n-1} T_2(0) \\ &= \frac{-(n-1) \cdot e^{k(n-1)z} + n - e^{k(n-1)z}}{n-1} T_1(0) + \frac{(n-1) \cdot e^{k(n-1)z} - 1 + e^{k(n-1)z}}{n-1} T_2(0) \end{aligned}$$

$$T_2(z) = \frac{n}{n-1} (1 - e^{k(n-1)z}) T_1(0) + \frac{n}{n-1} \left(-\frac{1}{n} + e^{k(n-1)z} \right) T_2(0) \quad (13)$$

So, the solution of System (7) is:

$$\boxed{\begin{aligned} T_1(z) &= \frac{n - e^{k(n-1)z}}{n-1} T_1(0) + \frac{-1 + e^{k(n-1)z}}{n-1} T_2(0) \\ T_2(z) &= \frac{n}{n-1} (1 - e^{k(n-1)z}) T_1(0) + \frac{n}{n-1} \left(-\frac{1}{n} + e^{k(n-1)z} \right) T_2(0) \end{aligned}} \quad (14)$$

In this solution $T_1(0)=T_a$ is given, while $T_2(0)$ is to be found using boundary conditions (8).

$$T_c = T_2(L) = \frac{n}{n-1} (1 - e^{k(n-1)L}) T_a + \frac{n}{n-1} \left(-\frac{1}{n} + e^{k(n-1)L} \right) T_2(0)$$

$$\boxed{T_2(0) = \frac{T_c \frac{n-1}{n} - (1 - e^{k(n-1)L}) T_a}{\left(-\frac{1}{n} + e^{k(n-1)L} \right)}} \quad (15)$$

Solution (14) can be written in the form

$$\begin{aligned} T_1(z) &= A(z) \cdot T_1(0) + B(z) \cdot T_2(0) \\ T_2(z) &= C(z) \cdot T_1(0) + D(z) \cdot T_2(0) \end{aligned} \quad (16)$$

where expressions for parameters A , B , C , and D are obvious from comparison of (16) and (14).

It can be noted here that all initial equations in System (6) depend on temperature difference, not absolute temperature. This means that the temperature in System (6) can be either in °C or K. Therefore, solution (16) cannot depend on the choice between °C and K. Let's suppose that the temperature is in degrees Kelvin. Then the temperature in degree Centigrade is

$$\begin{aligned} T_1(z) - 273.15 &= A(z) \cdot (T_1(0) - 273.15) + B(z) \cdot (T_2(0) - 273.15) \\ T_2(z) - 273.15 &= C(z) \cdot (T_1(0) - 273.15) + D(z) \cdot (T_2(0) - 273.15) \end{aligned} \quad (17)$$

which holds only if

$$\begin{aligned} A(z) + B(z) &\equiv 1 \\ C(z) + D(z) &\equiv 1 \end{aligned} \quad (18)$$

Check if System (18) is satisfied:

$$\begin{aligned} A(z) + B(z) &= \frac{n - e^{k(n-1)z}}{n-1} + \frac{-1 + e^{k(n-1)z}}{n-1} = \frac{n-1 - e^{k(n-1)z} + e^{k(n-1)z}}{n-1} \equiv 1 \\ C(z) + D(z) &= \frac{n(1 - e^{k(n-1)z})}{n-1} + \frac{n\left(-\frac{1}{n} + e^{k(n-1)z}\right)}{n-1} = \frac{n-1 - n \cdot e^{k(n-1)z} + n \cdot e^{k(n-1)z}}{n-1} \equiv 1 \end{aligned} \quad (19)$$

Indeed, the solutions (16) and (14) do not depend on the choice between °C or K. Moreover, using result (18), the solution can be written in the following form:

$$\begin{aligned} T_1(z) &= A(z) \cdot T_1(0) + (1 - A(z)) \cdot T_2(0) \\ T_2(z) &= C(z) \cdot T_1(0) + (1 - C(z)) \cdot T_2(0) \end{aligned} \quad (20)$$

where

$$\begin{aligned} A(z) &= \frac{n - e^{k(n-1)z}}{n-1} \\ C(z) &= \frac{n - n \cdot e^{k(n-1)z}}{n-1} \end{aligned} \quad (21)$$

Solution (20) was derived from the assumption that the properties of the fluids do not change inside the heat exchanger, which is not necessarily true. Instead, one can divide the heat exchanger length into several regions (Figure 6). Inside each region it is assumed that the properties of the fluid are constant and solution (20) can be used.

For every region, the solution (20) gives the temperatures inside the region,
 $0 \leq z \leq \Delta z$:

$$\begin{aligned} T_1^i(z) &= A_i(z) \cdot T_1^{i-1} + (1 - A_i(z)) \cdot T_2^{i-1} \\ T_2^i(z) &= C_i(z) \cdot T_1^{i-1} + (1 - C_i(z)) \cdot T_2^{i-1} \end{aligned} \quad i=1,2,\dots,N \quad (22)$$

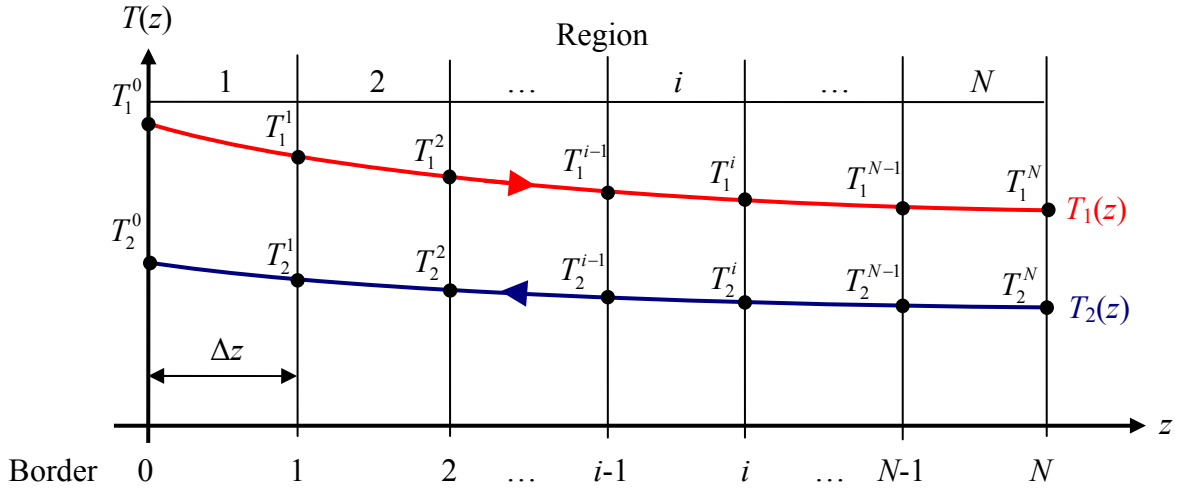


Figure 6. Multi region approach for recuperators.

And the temperatures at the right border are

$$\begin{aligned} T_1^i &= A_i \cdot T_1^{i-1} + (1 - A_i) \cdot T_2^{i-1} \\ T_2^i &= C_i \cdot T_1^{i-1} + (1 - C_i) \cdot T_2^{i-1} \end{aligned} \quad i=1,2,\dots,N \quad (23)$$

where

$$\begin{aligned} A_i &\equiv A_i(\Delta z) = \frac{n_i - e^{k_i(n_i-1)\Delta z}}{n_i - 1} \\ C_i &\equiv C_i(\Delta z) = \frac{n_i - n_i \cdot e^{k_i(n_i-1)\Delta z}}{n_i - 1} \end{aligned} \quad (24)$$

Note that the coefficients k and n are different for different regions since they are defined by the fluid properties through Equation (7).

But T_2^0 is still unknown. To find T_2^0 one needs to relate it with T_2^N which is given. To do this one can express temperatures on the right border of each region through the temperatures at zero:

$$\begin{aligned} T_1^i &= F_i \cdot T_1^0 + G_i \cdot T_2^0 \\ T_2^i &= L_i \cdot T_1^0 + M_i \cdot T_2^0 \end{aligned} \quad i=1,2,\dots,N \quad (25)$$

The goal is to find F_N , G_N , L_N , and M_N . In that case T_2^0 will be expressed through T_2^N . First, note from system (23) for $i=1$ that

$$F_1 = A_1 \quad G_1 = 1 - A_1 \quad L_1 = C_1 \quad M_1 = 1 - C_1 \quad (26)$$

Now, suppose that F_{i-1} , G_{i-1} , L_{i-1} , and M_{i-1} are known, i.e.:

$$\begin{aligned} T_1^{i-1} &= F_{i-1} \cdot T_1^0 + G_{i-1} \cdot T_2^0 \\ T_2^{i-1} &= L_{i-1} \cdot T_1^0 + M_{i-1} \cdot T_2^0 \end{aligned} \quad (27)$$

Substituting these expressions into (23):

$$\begin{aligned} T_1^i &= A_i \cdot [F_{i-1} \cdot T_1^0 + G_{i-1} \cdot T_2^0] + (1 - A_i) \cdot [L_{i-1} \cdot T_1^0 + M_{i-1} \cdot T_2^0] \\ &= [A_i \cdot F_{i-1} + (1 - A_i) \cdot L_{i-1}] \cdot T_1^0 + [A_i \cdot G_{i-1} + (1 - A_i) \cdot M_{i-1}] \cdot T_2^0 \end{aligned} \quad (28)$$

$$\begin{aligned} T_2^i &= C_i \cdot [F_{i-1} \cdot T_1^0 + G_{i-1} \cdot T_2^0] + (1 - C_i) \cdot [L_{i-1} \cdot T_1^0 + M_{i-1} \cdot T_2^0] \\ &= [C_i \cdot F_{i-1} + (1 - C_i) \cdot L_{i-1}] \cdot T_1^0 + [C_i \cdot G_{i-1} + (1 - C_i) \cdot M_{i-1}] \cdot T_2^0 \end{aligned}$$

By comparison of (28) and (25):

$$\begin{aligned}
 F_i &= A_i \cdot F_{i-1} + (1 - A_i) \cdot L_{i-1} \\
 G_i &= A_i \cdot G_{i-1} + (1 - A_i) \cdot M_{i-1} \\
 L_i &= C_i \cdot F_{i-1} + (1 - C_i) \cdot L_{i-1} \\
 M_i &= C_i \cdot G_{i-1} + (1 - C_i) \cdot M_{i-1}
 \end{aligned} \tag{29}$$

It is not hard to see that $G_i=1-F_i$ and $M_i=1-L_i$. This clearly holds for $i=1$ (Equation (26)). Suppose it is true for $i-1$. Then

$$\begin{aligned}
 F_i &= A_i \cdot F_{i-1} + (1 - A_i) \cdot L_{i-1} \\
 G_i &= A_i \cdot (1 - F_{i-1}) + (1 - A_i) \cdot (1 - L_{i-1}) = A_i - A_i \cdot F_{i-1} + 1 - A_i - L_{i-1} + A_i \cdot L_{i-1} \\
 &= 1 - A_i \cdot F_{i-1} - (1 - A_i) \cdot L_{i-1} = 1 - F_i
 \end{aligned} \tag{30}$$

$$\begin{aligned}
 L_i &= C_i \cdot F_{i-1} + (1 - C_i) \cdot L_{i-1} \\
 M_i &= C_i \cdot (1 - F_{i-1}) + (1 - C_i) \cdot (1 - L_{i-1}) = C_i - C_i \cdot F_{i-1} + 1 - C_i - L_{i-1} + C_i \cdot L_{i-1} \\
 &= 1 - C_i \cdot F_{i-1} - (1 - C_i) \cdot L_{i-1} = 1 - L_i
 \end{aligned}$$

And, by induction, this is true for every $i=1,2,\dots,N$.

Using that, Equation (25) becomes:

$$\begin{aligned}
 T_1^i &= F_i \cdot T_1^0 + (1 - F_i) \cdot T_2^0 \\
 T_2^i &= L_i \cdot T_1^0 + (1 - L_i) \cdot T_2^0
 \end{aligned} \quad i=1,2,\dots,N \tag{31}$$

where

$$\begin{aligned}
 F_1 &= A_1 & F_i &= A_i \cdot F_{i-1} + (1 - A_i) \cdot L_{i-1} & i &= 2 \dots N \\
 L_1 &= C_1 & L_i &= C_i \cdot F_{i-1} + (1 - C_i) \cdot L_{i-1} & i &= 2 \dots N
 \end{aligned} \tag{32}$$

Now F_N and L_N can be calculated using the recursive relation (32). And Equation (31) for the last region becomes:

$$\begin{aligned} T_1^N &= F_N \cdot T_1^0 + (1 - F_N) \cdot T_2^0 \\ T_2^N &= L_N \cdot T_1^0 + (1 - L_N) \cdot T_2^0 \end{aligned} \quad (33)$$

Since the given data are the inlet temperatures, $T_1^0 = T_a$ and $T_2^N = T_c$, from the second equation of system (33):

$$T_2^0 = \frac{T_c - L_N \cdot T_a}{1 - L_N} \quad (34)$$

Once the temperatures at zero are known, the temperatures at other nodes can be found using Equation (31). The problem is that the coefficients F and L are defined through the coefficients A and C (or k and n), which are a function of the region-average properties and, therefore, the region-average temperatures. Thus, iterations on the temperatures are necessary.

The iteration procedure works as follows: first, on every iteration step, the temperatures at the region borders are known from the previous iteration (for the first step, an average value between the given inlet temperatures can be taken). Then, the region-average temperature is calculated for each region, and the region-average fluid properties are calculated. Next, coefficients k_i and n_i are calculated as they are defined in (7). Coefficients A_i and C_i are calculated for all regions using Equation (24); coefficients F_i and L_i are calculated for each region using Equation (32); and Equation (34) is used to calculate T_2^0 . Finally, the new temperature distribution is calculated using Equation (31); and the outlet temperatures are $T_b = T_1^N$, $T_d = T_2^0$. The iterations are repeated while the outlet temperatures change more than the convergence criteria.

Since the CO₂ properties depend on pressure as well as on temperature, it is required to calculate the pressure drop inside the heat exchanger. The pressure drop is calculated for each region using the Colebrook and White correlation (Kestin, 1960)

every time the properties are known. Then new region-average pressure is used for the next iteration when the properties are recalculated.

The optimal number of regions for each recuperator is found for the Brayton cycle. The accuracy of the calculations increases with the number of regions. However, too many regions can slow the calculation process while not providing significant increase in the accuracy. The absolute error in the Brayton cycle efficiency was plotted as a function of the number of regions for both recuperators. Figure 7 shows an example of such a graph for the low temperature recuperator. It can be concluded from the figure that 11 points (10 regions) is sufficient, and that even 3 or 5 points produces rather accurate results. For the high temperature recuperator the graph is very similar, and again, 11 points are selected as an optimum.

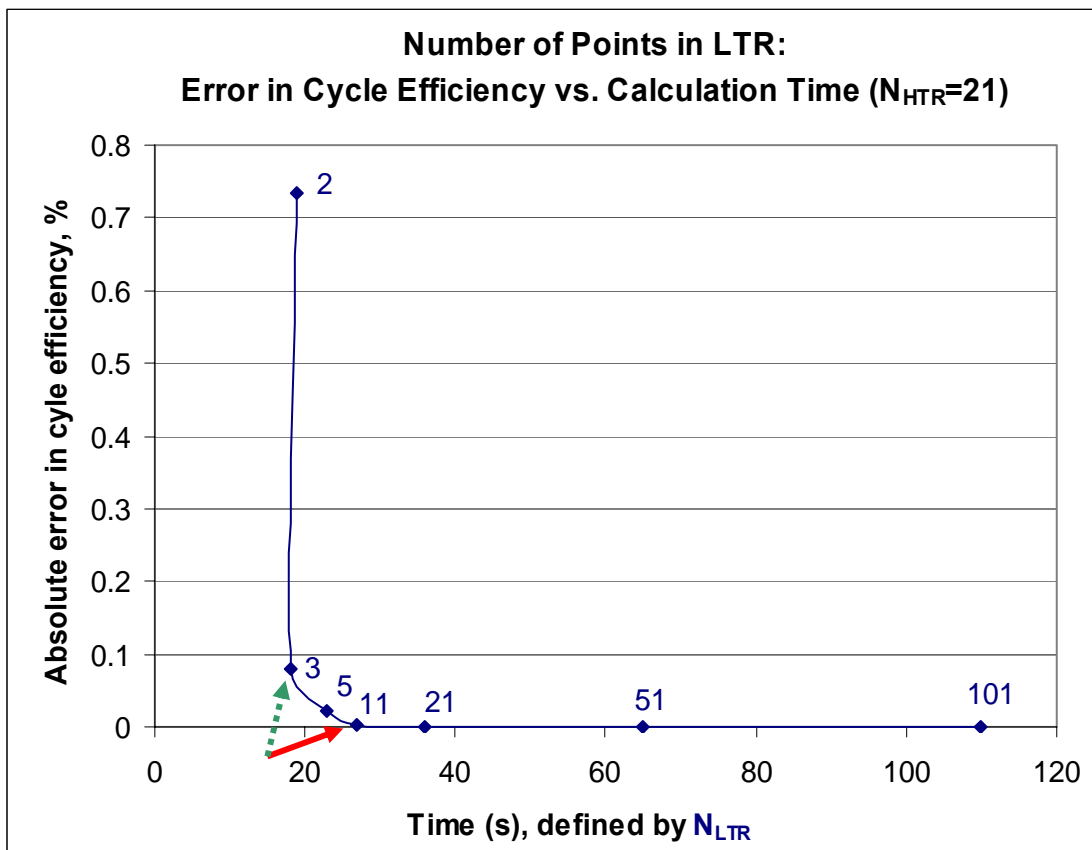


Figure 7. Optimization of the number of regions for recuperators.

Turbine and Compressor Module

The goal of this module is to calculate the change in CO₂ temperature inside the turbine or compressor given the CO₂ parameters (pressure and temperature) at inlet, CO₂ mass flow rate and outlet pressure. Once the inlet and outlet parameters are found, the amount of work done by the turbine or required for the compressor can be calculated.

Two different approaches are used in the model. First, the turbine or compressor efficiency is used as a given and the outlet temperature are calculated, while the second approach actually performs the turbine or compressor design analysis to calculate its efficiency.

Temperature after Compressor or Turbine with Given Efficiency

The goal of the first approach is to calculate temperature at compressor (or turbine) outlet. The given data are the inlet temperature (T_1) and pressure (p_1), outlet pressure (p_2) and compressor's (or turbine's) efficiency (ε). The compressor case is considered below, and the differences in the turbine case are described after.

The enthalpy-entropy diagram of a compression process (ideal 1-2s and actual 1-2) is shown in Figure 8.

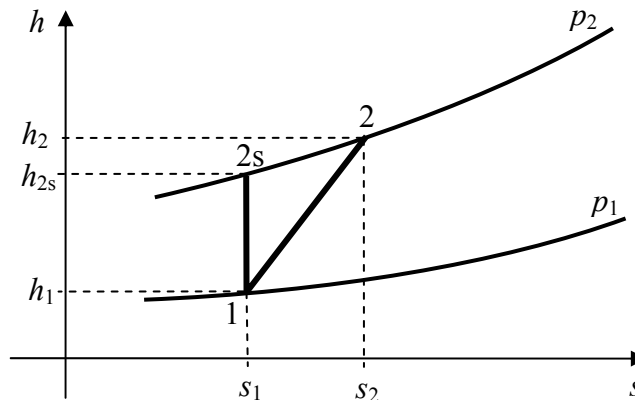


Figure 8. Compression process.

Inlet temperature and pressure define properties at point 1 – h_1 and s_1 :

$$\begin{aligned} s_1 &= s(T_1, p_1) \\ h_1 &= h(T_1, p_1) \end{aligned} \quad (35)$$

In an ideal compression the entropy does not change, i.e. $s_{2s}=s_1$, and entropy at point 2s (s_1) and outlet pressure (p_2) define temperature and enthalpy (h_{2s}) at this point:

$$h_{2s} = h(T_{2s}, p_2), \quad \text{where } T_{2s} = T(s_{2s} = s_1, p_2) \quad (36)$$

To find the enthalpy at point 2, the compressor's efficiency definition is used. By definition, the compressor's efficiency is the ratio of work done in an ideal process to that in a real process:

$$\mathcal{E}_{comp} = \frac{h_{2s} - h_1}{h_2 - h_1} \quad (37)$$

From Equation (37), the outlet enthalpy for real process is:

$$h_2 = h_1 + \frac{1}{\mathcal{E}_{comp}} (h_{2s} - h_1) \quad (38)$$

Once the outlet enthalpy (h_2) is known, it and the outlet pressure (p_2) give the outlet temperature:

$$T_2 = T(h_2, p_2) \quad (39)$$

The approach to calculate the turbine-outlet temperature is similar to that described above for compressor except for the fact that turbine's efficiency is defined as the ratio of work produced in a real process to that in an ideal process:

$$\varepsilon_{turb} = \frac{h_2 - h_1}{h_{2s} - h_1} \quad (40)$$

And the turbine-outlet enthalpy is:

$$h_2 = h_1 + \varepsilon_{turb} (h_{2s} - h_1) \quad (41)$$

The turbine-outlet temperature is again calculated by (39).

*Turbine or Compressor Design**

In this approach, the turbine or compressor efficiency is actually calculated as a result of design calculations. The goal of this approach is to design a turbine or compressor which gives the required outlet pressure for a given inlet temperature and pressure. To design a turbine or compressor means to find out what the number of stages are required, how large each stage is, what the dimensions of the blades are etc. First, the turbine design approach is described here and then the differences in the compressor design are described.

The axial flow turbine consists of several stages. Each stage consists of nozzles and a rotor. In a rotor, the expanding gas forces the blades to rotate producing a mechanical energy of rotation which is converted into electricity in the generator. In the nozzles, the gas is accelerated so it can produce more energy in the rotor. Both nozzles

* Reprinted with permission from "Turbine Design for a Supercritical Carbon Dioxide Gas Turbine Brayton Cycle", ICAPP'03-3064. Proceedings of ICAPP 03, 2003 International Congress on Advances in Nuclear Power Plants, Cordoba, Spain, May 4-7, 2003. Copyright 2003 by the American Nuclear Society, La Grange Park, Illinois.

and rotor have blades which are designed to achieve the required change in gas pressure. The blades are mounted on the hub, which is connected to the shaft (Figure 9).

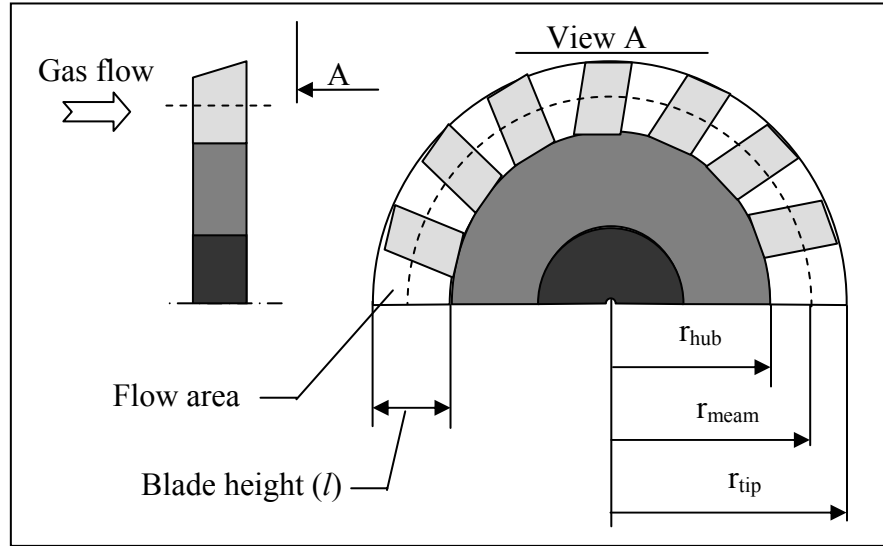


Figure 9. Turbine stage dimensions.

The gas flow is usually characterized by its velocity (C) and enthalpy (h) in turbine design analysis. There are several approaches to describe gas velocity. A two-dimensional analysis is used here because it is much simpler than the three-dimensional model, while producing results with satisfactory accuracy. Under this approach, the gas velocity is expressed in terms of axial and tangential components. The axial component (C_x) is parallel to the turbine axis, while the tangential component (C_θ) is perpendicular to the axis.

The following notation is used in the analysis. For every stage, index 1 is used for the gas flow before the nozzles, index 2 for the flow between the nozzles and the rotor, and index 3 for the flow after the rotor (Figure 10). The rotor blade speed, measured at medium blade radius, is referred as u , and it can be expressed in terms of this radius and the shaft revolution speed:

$$u = 2\pi \cdot r_m \cdot n_r, \quad (42)$$

where n_r – shaft revolution speed (rev/s).

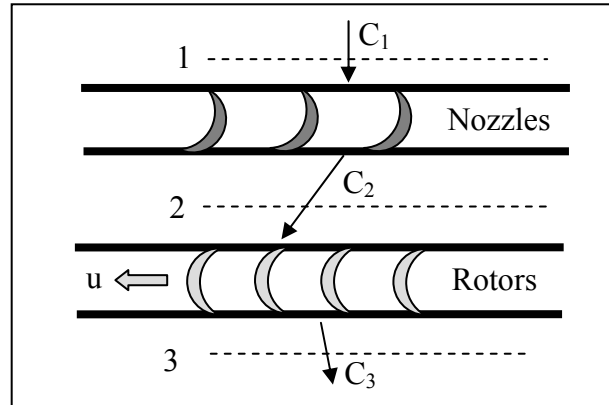


Figure 10. Gas velocities in a turbine stage.

The relationship between change in gas flow parameter and rotor blade speed is defined by the Euler's equation (Horlock, 1966):

$$\Delta h_0 = u \Delta C_\theta \quad (43)$$

where h_0 – total enthalpy $\equiv h + \frac{C^2}{2}$.

It follows from Equation (43) that the total entropy is conserved in the nozzles ($u=0$).

The change in the gas velocity is defined by the continuity equation, taking into account that the gas mass flow rate is a constant:

$$\rho \cdot C \cdot A = \dot{m} = const \quad (44)$$

where ρ – gas density,

A – flow area.

Several assumptions were made to simplify the analysis. First, it was assumed that the axial component of gas speed is constant everywhere in the turbine. This is a

common assumption for turbine design (Horlock, 1966). Second, the rotor geometry is selected in such a way that the flow at every stage inlet and outlet is pure axial, i.e. tangential component is equal to zero. This makes every stage calculation similar and independent from other stages. Also, the stage reaction, which is defined as the ratio of change in enthalpy to the change in total enthalpy (Horlock, 1966), was set to be 50%. This means that half of the pressure decrease in the stage occurs in the nozzles and half in the rotor. This is also a common choice for the turbine design.

The stage reaction (R) can be related to the blade speed and tangential component of the gas speed at rotor inlet and outlet (Horlock, 1966):

$$R = 1 - \frac{C_{2\theta} + C_{3\theta}}{2u} \quad (45)$$

Using the assumptions described above and Equations (43) and (45) the following relations between enthalpy change, flow speed and blade speed could be derived:

$$\begin{cases} C_{2\theta} = u \\ C_2^2 = C^2 + C_{2\theta}^2 \\ h_2 = h_1 + \frac{C^2}{2} - \frac{C_2^2}{2} \\ h_3 = h_2 + \frac{C_2^2}{2} - \frac{C^2}{2} - u^2 \end{cases} \quad (46)$$

where C – axial component of the flow speed = $C_1 = C_3$.

System (46) is derived for the ideal process (no losses). In actual process enthalpy at the nozzle or rotor outlet would be higher than those calculated by System (46). The approach to count for the losses described by Boyce, 2002 was used:

$$h_2 = h_{2s} + \omega \frac{C_2^2}{2} \quad (47)$$

where h_{2s} – enthalpy at nozzle outlet for ideal process (System (46)),

ω – loss coefficient, which is defined as

$$\omega = \left(\frac{10^5}{\text{Re}} \right)^{1/4} [(1 + \omega_\theta)(0.975 + 0.075/AR) - 1] \omega_i$$

Re – Reynolds number,

ω_θ, ω_i – blade geometry and incident loss factors (defined in Boyce, 2002),

AR – aspect ratio, ratio of the blade height to the blade chord.

The losses in the rotor are calculated similar to the losses in the nozzle.

It also can be seen from the last two equations of the System (46) that in an ideal process the change in enthalpy inside a stage is equal to u^2 . Therefore, the average u for an ideal turbine is equal to the square root of the ratio of the overall change in enthalpy to the number of stages. According to the System (46) this is also equal to the average $C_{2\theta}$:

$$\bar{C}_{2\theta} = \bar{u} = \sqrt{\frac{h_1 - h_{s,out}}{N}} \quad (48)$$

where $h_{s,out}$ – enthalpy at the turbine outlet in ideal (isentropic) expansion. It is define by the outlet pressure and inlet entropy.

N – number of stages.

The blade angle (α) is defined as a change in angle of flow velocity in the blade row. For the 50% reaction stages the blade angle for the rotor is equal to the blade angle for the nozzles and equal to:

$$\tan(\alpha) = \frac{C_{2\theta}}{C} \quad (49)$$

It is convenient to have blade rows inside one turbine with an approximately equal blade angle. So, if the average blade angle is given, then the axial velocity of the gas can be found using Equations (48) and (49):

$$C = \frac{\sqrt{\frac{h_1 - h_{s,out}}{N}}}{\tan(\bar{\alpha})} \quad (50)$$

To separate the stage calculations from each other, the pressure after each stage should be known. There are several schemes for pressure reduction in a turbine. They are:

1. Equal pressure ratio for every stage. In this case the ratio of the pressure before the stage to the pressure after stage is equal for all stages.
2. Equal pressure change for every stage. The difference between the stage inlet and outlet pressures is kept constant.
3. Equal energy stages. The enthalpy change in an ideal expansion from the stage inlet to the stage outlet pressures is equal for every stage. This gives the every stage outlet pressure as a pressure for the turbine inlet entropy and the stage outlet enthalpy.
4. Equal hub radii. In this case, the enthalpy changes in every stage are selected such that the stage hub radii are approximately the same throughout the turbine.

All these schemes were programmed and the results were compared. Although the difference in terms of turbine performance is small, the equal pressure change scheme gives the best results, so it is used in further discussion.

The design calculations are as follows.

1. Calculate gas properties before the stage.
2. Calculate pressure after each stage. For the equal pressure change scheme, the total pressure change in the turbine is divided by the number of stages to get the pressure

change for the stage. The stage inlet pressure is known, so the stage outlet pressure can be calculated.

3. Calculate the axial flow speed using Equation (50).
4. Using Equation (48), calculate the first guess for the blade speed.
5. Calculate mean blade radius using Equation (42).
6. Calculate the flow area using continuity Equation (44).
7. Flow area and mean radius give other radial dimensions, like blade height, hub and tip radii.
8. Calculate the enthalpy for ideal expansion in nozzles using System (46).
9. Calculate loss coefficient for nozzles and actual enthalpy after nozzles.
10. Calculate the enthalpy for ideal expansion in rotor using the last equation of System (46).
11. Based on the rotor outlet enthalpy and the nozzle outlet entropy, calculate the pressure after the stage.
12. Compare this pressure with required value. Correct the blade speed, if needed, and repeat steps 5-12.
13. Calculate the loss coefficient for the rotor and actual enthalpy after the nozzles.
14. Repeat calculations for each stage.
15. Calculate the turbine efficiency using its definition (40) (indexes 1 and 2 mean turbine inlet and outlet, respectively).

For the loss coefficient, the blade chord is calculated based on the stress criteria on the blade (Horlock, 1966; Kulak and Therios, 2003).

Figure 11 shows the results of the turbine design analysis for the Brayton cycle. Although the efficiency increases with the number of stages, adding more stages requires higher fabrication costs. Since the increase in efficiency after four stages is small, the four-stage design can be considered optimal. It follows from Figure 11 that the efficiency of the turbine is about 96 %. However, because some simplifications were made and some phenomena, like tip leakages, were not taken into account, some efficiency decrease (5 %) was assumed due to secondary effects.

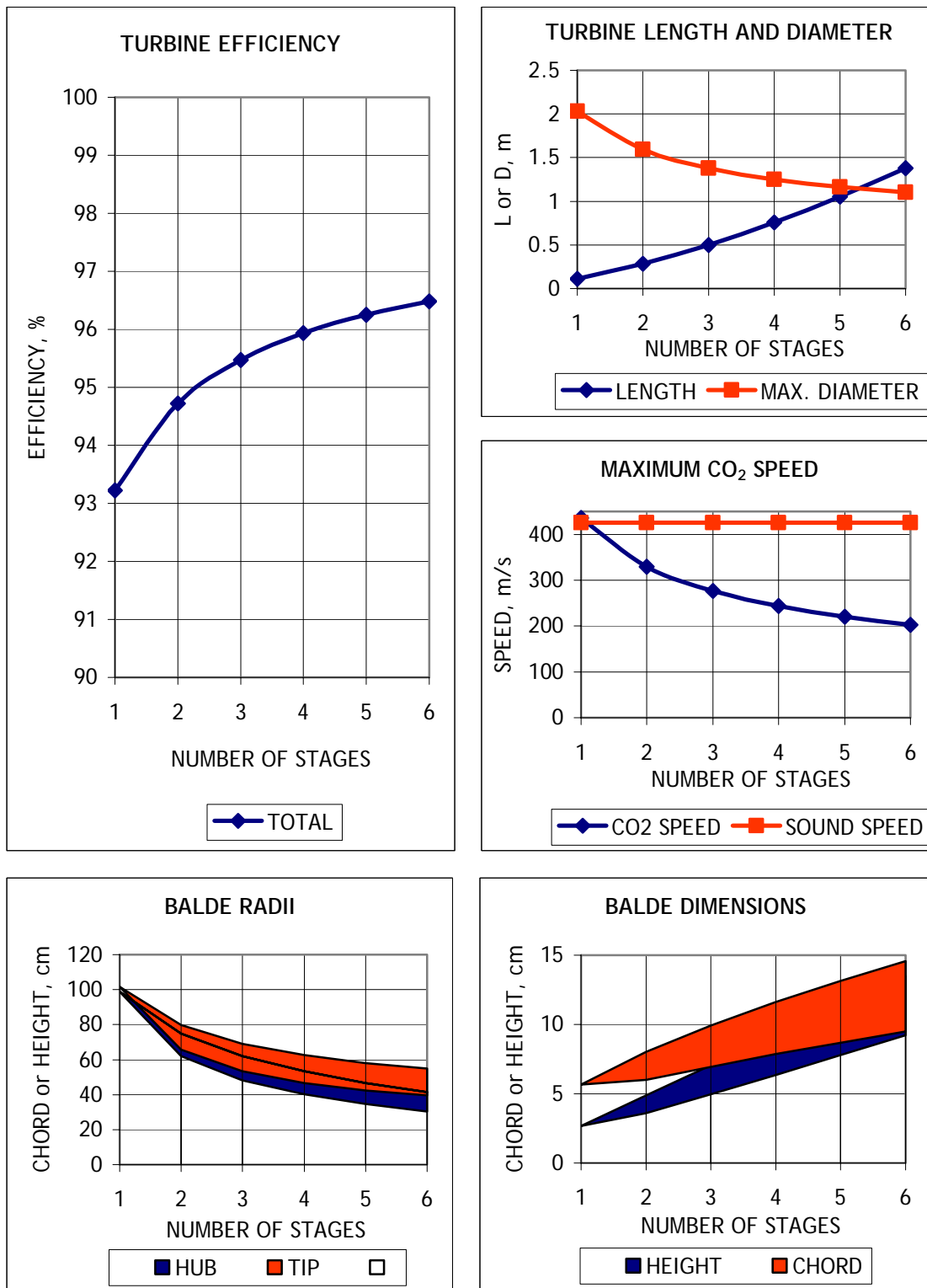


Figure 11. Turbine design results.

The design process for the compressor is very similar to that for the turbine. There are only a few differences. First, since the goal of the compressor is opposite to the turbine's goal (put energy into gas), the compressor stage is organized in the reverse order: the rotor is followed by the nozzle. Also, it is a common approach to design a compressor (Boyce, 2002) with equal-energy stages, so no comparison of the pressure increase schemes is necessary.

Table 1 shows the summary of results of turbine and compressors design calculations. There is a turbine and two compressors in the cycle.

Table 1. Results of turbine and compressors design

	Turbine	Compressors	
		1	2
Number of stages	4	4	4
Length, m	0.8	0.5	0.3
Max. Diameter, m	1.25	0.5	0.7
Efficiency, %	95.9	96.0	95.3

Cooler Module

The purpose of this module is to calculate the required length of the cooler for S-CO₂ Brayton cycle and pressure drop in the cooler. For this module the following data are given:

- CO₂ temperature and pressure at the cooler outlet (specified by user for cycle calculations)
- CO₂ temperature at the cooler inlet (result of LT recuperator calculations)
- CO₂ mass flow rate (result of cycle calculations)
- Cooler design data: number of tubes, tube inner and outer diameters, tube material, and fins parameters, if any (specified by a user)
- Cooling fluid temperature (specified by a user).

It is assumed for these calculations that cooling fluid is at constant temperature and heat transfer coefficient is large on the cooling fluid side compared to that on CO₂ side. These assumptions simulate boiling fluid on the cooling side.

Heat transfer equations are the same as those used in the recuperator model. The amount of heat transferred at any point of the cooler is defined by Equation (4), and for the cooler module subscribe “1” refers to the CO₂ flow; “2” refers to the cooling fluid.

The amount of heat transferred during infinitely small region dz is equal to $q(z)dz$. This heat transfer causes change in the CO₂ temperature:

$$\dot{m}_1 c_{p1} dT_1 = -q(z)dz \quad (51)$$

Using the assumptions described above and denoting the cooling fluid temperature by T_c and dropping index 1 for the CO₂ fluid, Equations (4) and (51) will combine into a differential equation for the CO₂ temperature:

$$\frac{dT}{dz} = -\frac{1}{\dot{m}c_p} \frac{1}{\frac{1}{h_1 WP_1 \eta_1} + \frac{\ln(r_o/r_i)}{2\pi k_w}} (T(z) - T_c) \quad (52)$$

Or, in simplified form:

$$\frac{dT}{dz} = -k(T(z) - T_c) \quad (53)$$

where $k = \frac{1}{\dot{m}c_p} \frac{1}{\frac{1}{h_1 WP_1 \eta_1} + \frac{\ln(r_o/r_i)}{2\pi k_w}}$.

Equation (53) can be easily solved in the case of constant fluid properties ($k=const$):

$$T(z) = (T(0) - T_c) \cdot e^{-k \cdot z} + T_c \quad (54)$$

If fluid properties are changing, one can divide a cooler tube into several regions and assuming that properties are constant get the solution (54) for each region.

The temperature and pressure change are calculated for every region starting from the last one (at the cooler outlet). The length of the region is specified by a user and can be very small (say 1 mm). The calculations start at cooler outlet point. The properties are calculated at that point, and the temperature change in the last region is found using Equation (54):

$$T_i^{in} = (T_i^{out} - T_c) \cdot e^{k \cdot \Delta z} + T_c \quad (55)$$

where Δz – region length.

Then, pressure drop and region-inlet pressure are calculated:

$$p_i^{in} = p_i^{out} + \Delta p_i = p_i^{out} + \left. \frac{dp}{dz} \right|_i \cdot L_i \quad (56)$$

where the derivative of pressure (pressure drop) is calculated as a function of fluid parameters at the region outlet.

If the region length is small enough, the average properties of the fluid for a region can be considered constant and equal to those at the region outlet. Although the properties near the critical point (Figure 3), where the cooler is operated, can change significantly, high specific heat means low temperature changes in the region. So, for a fixed region length, temperature change is defined by specific heat, and the peak region will be calculated with greater accuracy.

These calculations are repeated for each region until the region-inlet temperature is greater than the cooler-inlet temperature. The cooler tube length is then the sum of all the region lengths, however many regions there are.

The tube dimensions (inner and outer diameters) are assumed to be equal to those of the recuperator (1 cm and 1.4 cm, respectively). The effect of the number of tubes and the presence of fins on the inside (CO₂) surface of the tubes was investigated. Figure 12 shows the required cooler tube length, cooler pressure drop and cycle efficiency as a function of the number of tubes for bare and finned tubes.

Although the fins increase heat transfer, they partly block the flow area resulting in an increase in CO₂ speed. This effect can sometimes be more significant than the benefits from the increased heat transfer; in that case, the bare tubes perform better than the finned.

From Figure 12 one can conclude that the cooler with 50,000 bare tubes is an optimal design, since the decrease in number of tubes results in a rapid increase in the tube length, and increase in the number of tubes does not add much benefit to the cycle efficiency or the tube length.

As an alternative approach, the calculations were made on the assumption that the temperature difference between CO₂ and the cooling fluid stays constant. The results, in terms of the pressure drop inside the cooler, are very similar in both approaches. However, to get the same cooler length, the cooling fluid temperature should be decreased from 30 °C down to 25 °C. The first approach can be used if CO₂ is being cooled by a boiling fluid and it is used in the STAR-LM System where there are no restrictions on choice of cooling fluid. The second approach suits the cooling by a subcooled fluid and is used for STAR-H2 System where the CO₂ is cooled by seawater.

Brayton Cycle Optimization*

The Brayton cycle should be optimized for the cycle layout, maximum and minimum pressures and the temperatures and components designs.

* Reprinted with permission from “Cycle Analysis of Supercritical CO₂ Gas Turbine Brayton Cycle Power Conversion System for Liquid Metal-Cooled Fast Reactors”, ICONE11-36023. In: Proceedings of ICONE-11, Eleventh International Conference on Nuclear Engineering, Tokyo, Japan, April 20-23, 2003. Copyright 2003 by the Japan Society of Mechanical Engineers.

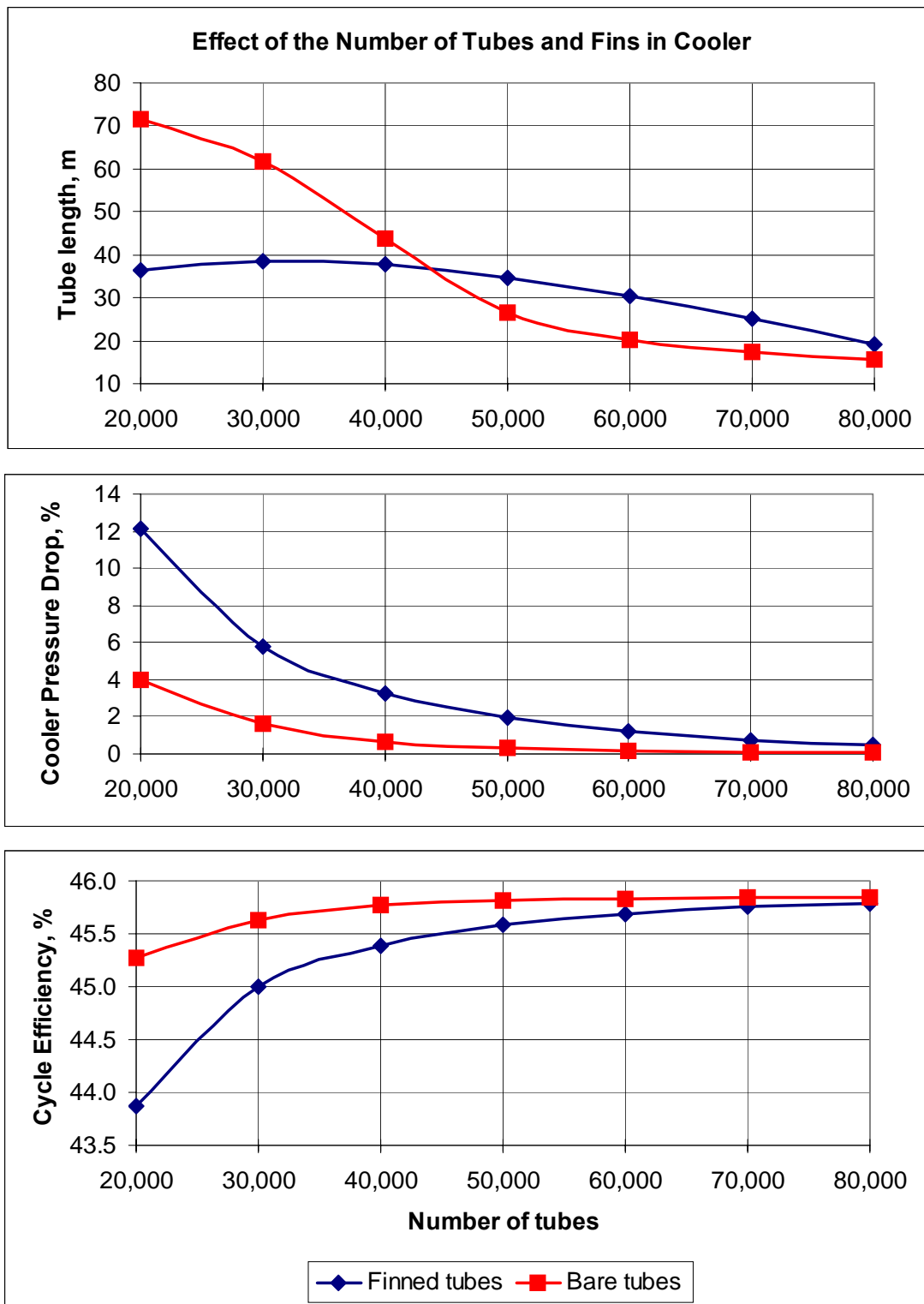


Figure 12. Results of the cooler module calculations.

The optimization criterion is a cycle thermal efficiency which is defined as the ratio of the electricity produced to the amount of heat supplied to the cycle. The estimation was made (Table 2) to show the potential benefit from cycle optimization.

Table 2. Estimation of benefit from increase in cycle efficiency by 1%

Thermal power	400	MW
Original efficiency	0.45	
Plant design power	180	MWe
Average capacity factor	0.9	
Average plant power	162	MWe
New efficiency - 1% higher	0.46	
New electrical power	165.6	MWe
Power gain	3.6	MWe
Increase (from this 1%) in electricity produced per day	86400	kW-hr
Electricity price	2.5	c/kW-hr
Net gain per day	2.16	K\$/day
Gain per year (330 days)	0.788	M\$/yr
Total gain for lifetime (40 years)	31.54	M\$

Simple Brayton Cycle

Simple Brayton cycle (Figure 13) consist of reactor heat exchanger (RHX), turbine connected to generator, recuperator, precooler, intercooler, and two compressors.

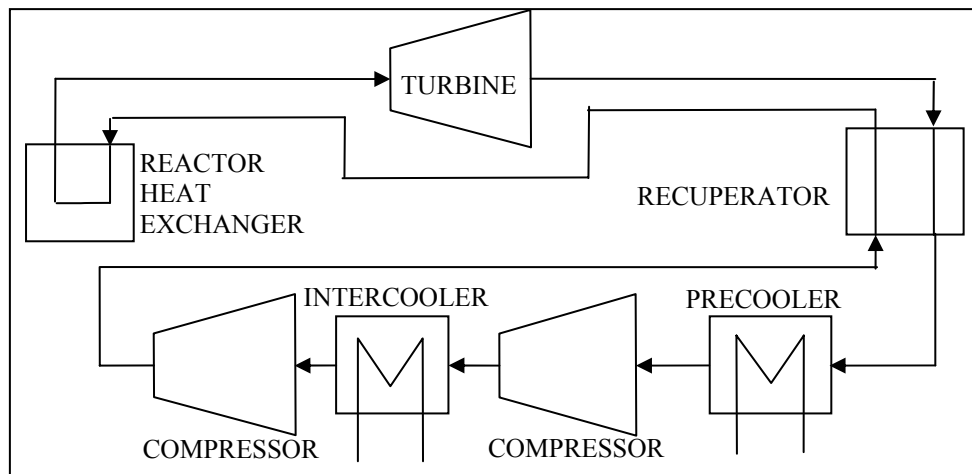


Figure 13. Simple Brayton cycle.

It is shown that the cycle efficiency increases with maximum (turbine inlet) temperature. Calculations were made for both real and ideal recuperators. Although the efficiency of the cycle with ideal recuperator was about 5 % higher than that of cycle with a real recuperator, it was still rather low ($\sim 38\%$ for $T_{max}=550\text{ }^{\circ}\text{C}$).

To determine the reason for this low efficiency, the effect of intercooling was investigated. The cycle efficiency was plotted as a function of the amount of intercooling (in $^{\circ}\text{C}$). The results (Figure 14) show that eliminating the intercooler increases efficiency. To see where this trend goes, the intercooler was replaced by interheater, i.e. CO_2 was heated between the compressors. It can be seen from Figure 14 that there is an optimum in temperature change inside the intercooler (interheater).

The reasons why the cycle efficiency increases with eliminating the intercooler can be explained using Figure 5. There is a region in the recuperator inlet (compressor outlet) temperature, where the recuperator effectiveness is minimal. Conditions further away from this region increase the recuperator effectiveness and, therefore, the cycle efficiency, overtaking the fact that heating CO_2 between the compressors decreases its density resulting in higher compression work.

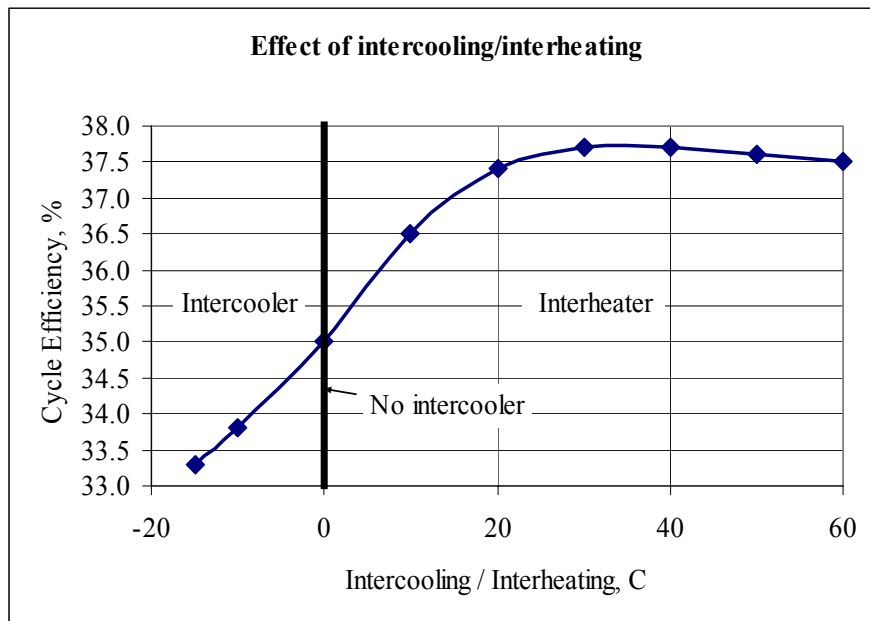


Figure 14. Effect of intercooling and interheating.

Recompression Brayton Cycle

Even the increased efficiency of a simple Brayton cycle is too low to take advantage of CO₂. To increase the cycle efficiency it was proposed (Dostal et al., 2002) to split the flow after the recuperator. A fraction of the flow goes to the cooler, compressor and recuperator. The second part of the flow is compressed by another compressor and returns to the recuperator in the middle. For convenience, the recuperator is divided into two parts, a low temperature recuperator (LTR), where only a fraction of the CO₂ flows on the cold side and a high temperature recuperator (HTR) with full mass flow rates on both sides. This cycle is called a recompression Brayton cycle and is shown in Figure 1.

The reasons why the efficiency of the recompression S-CO₂ Brayton cycle is higher than that of simple Brayton cycle can be understood from equations (2) and (3). At some ratio of mass flow rates on the hot and cold sides, the cold outlet temperature can achieve a hot inlet temperature, resulting in 100 % effectiveness. In the recompression Brayton cycle the fraction of flow which goes to LTR can be adjusted to achieve the maximum recuperator effectiveness. In the end, the benefit from the increased recuperator performance is greater than the loss from higher compression work in the second compressor (flow goes to the compressor without being cooled).

The ratio of the mass flow rates (and, therefore, fraction of the flow sent to the LTR), which gives the maximum recuperator effectiveness, depends on the difference in specific heats for two flows. This difference is defined by the difference in pressures; thus, the optimal flow split will depend on pressures in cycle.

The minimum pressure (7.4 MPa) is set to be as close as possible to critical point. The maximum pressure is an optimization parameter and it should be optimized together with the flow split. Figure 15 show the optimization process for the maximum pressure and flow split. Indeed, the optimal flow split depends on the maximum pressure. Although the cycle efficiency increases with pressure, there is small gain in the cycle efficiency for pressures above 20 MPa. Therefore, 20 MPa and 60 % flow split (fraction of flow to the LTR) are selected as optimal values.

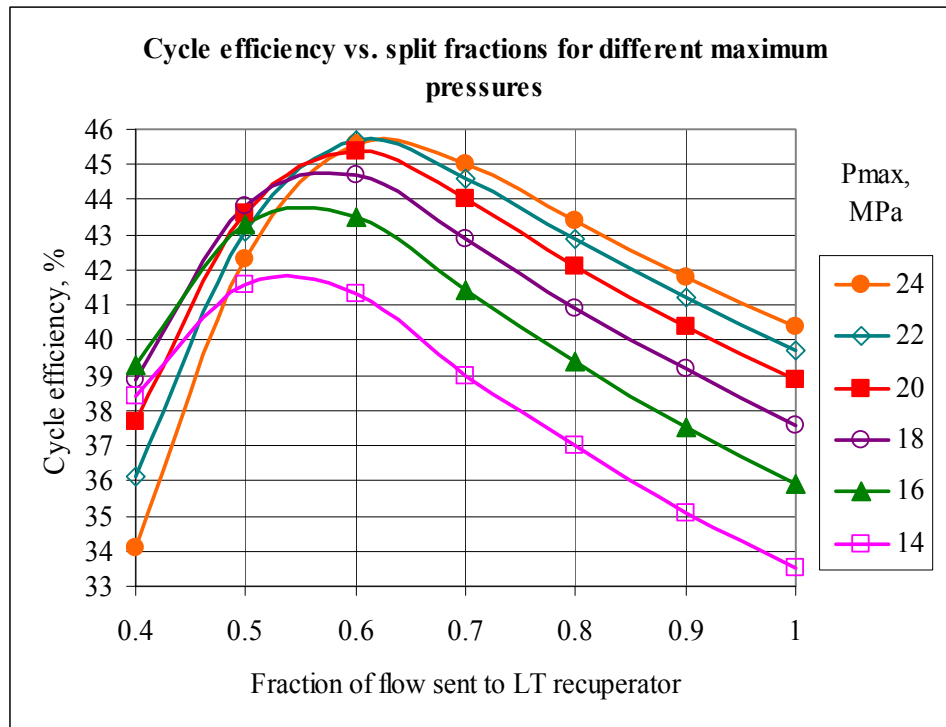


Figure 15. Maximum pressure and flow split optimization.

The cycle efficiency of about 45% can be achieved with the recompression cycle. The minimum temperature in the cycle, i.e. the temperature before the compressor #1 is to be optimized as well. It can be estimated from the behavior of CO₂ density (Figure 3) that the closer the minimum temperature to the critical temperature, the better is the cycle efficiency. Figure 16 confirms this hypothesis and shows that the minimum temperature should be held as close as possible to the critical point. An increase of 1 °C will drop the cycle efficiency by more than 3%.

Recuperators Design Optimization

It was shown previously in the simple Brayton cycle section that the difference in cycle efficiency between ideal and real recuperator can be as significant as 5%. Therefore, the recuperator design should be optimized to be as close as possible to an ideal recuperator limit.

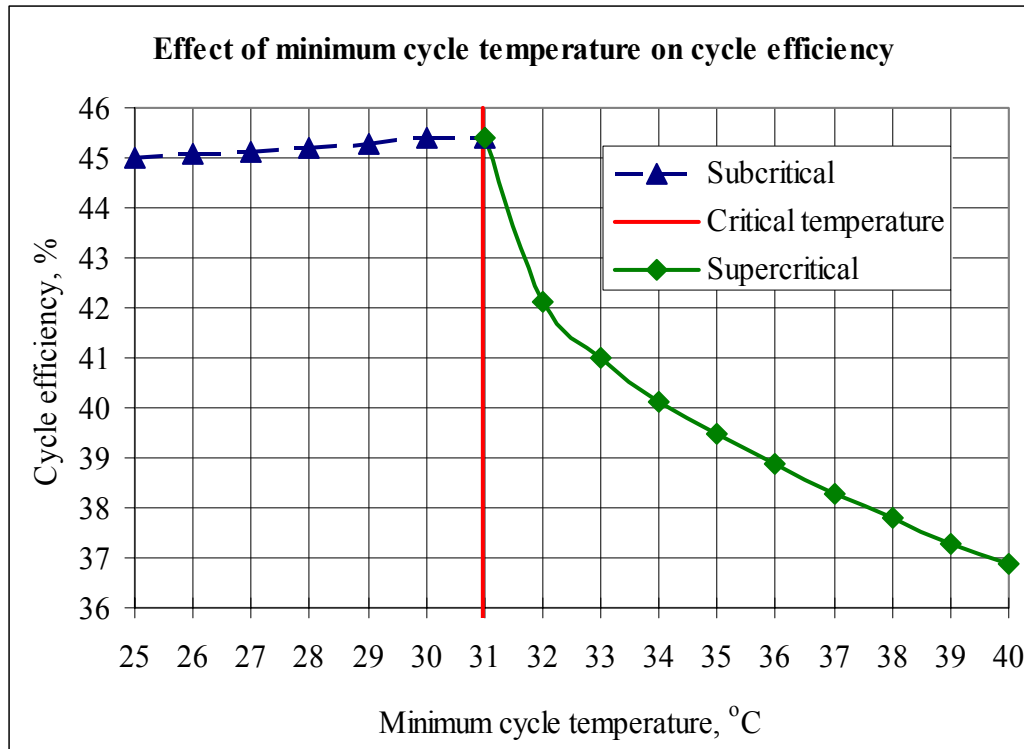


Figure 16. Minimum temperature optimization.

Each of the recuperators serves to transfer heat from one CO₂ flow (hot) to the other flow (cold). According to the cycle layout (Figure 1), the hot flow is the flow after the turbine and, therefore, at low pressure (near compressor-inlet pressure of 7.4 MPa). The cold flow is the flow after compressor and its pressure is the highest in the cycle, 20 MPa. The difference in pressures of the two flows in the recuperators is about 14.5 MPa which is too large for the plate type heat exchanger which is usually used for gases.

There are two types of heat exchangers that can withstand such pressure difference. First, the shell-and-tube type heat exchanger is used widely but it is not very effective for gasses. The second type is a printed circuit heat exchanger, produced by HEATRIC Company (HEATRIC website). This is a new concept and it has not been used a lot, however it has the potential to achieve the gas-to-gas heat exchange goals better. Both these type were modeled and optimized for the S-CO₂ Brayton cycle.

Shell-and-tube heat exchanger

The shell-and-tube heat exchanger is a tank with tubes inside it. One flow (usually one with higher pressure) goes inside the tubes; the other flow goes outside the tubes (shell side). The counter-current design where the flows go in opposite directions is used here because it has the potential to heat up the cold flow to the hot flow inlet temperature (in co-current design the cold flow could be heated only up to hot flow outlet temperature). The heat transfer area is the total surface area of the tubes. Since the heat transfer is proportional to the heat transfer area, it is desirable to have the area as large as possible. For this reason, the tube diameter was selected to be as small as practically achievable (1 cm), and the number of tubes (80,000) was selected such that the total diameter of the heat exchanger would be at fabrication limit of 6 m.

Fins on Tube Surfaces

To further increase the heat transfer area, tubes with longitudinal fins on the inside and outside surfaces were investigated. The fins increase the heat transfer area, which affect the heat transfer through an increase in wetted perimeter (Equation (4)). However, the fact that the fin temperature is slightly different from the tube temperature, the fins have an efficiency (<1), Equation (4), which was calculated using the approach described by (Özişik, 1985). Figure 17 shows the example of a fin attached to the outer surface of a tube and equation for fin efficiency calculation. Also the fact that the fins block some flow area was taken into account for accurate calculations.

Table 3 summarizes the benefits of using fins on the inner, outer, or both surfaces in the recuperator tube in comparison with a bare-tube design and an ideal recuperator. The cycle efficiency as well as both recuperators' effectiveness are shown. The cycle efficiency increases from 44.3% without fins to 46.3% if double-finned tubes are used in both recuperators, which is very close to the performance of ideal recuperators (47.3%).

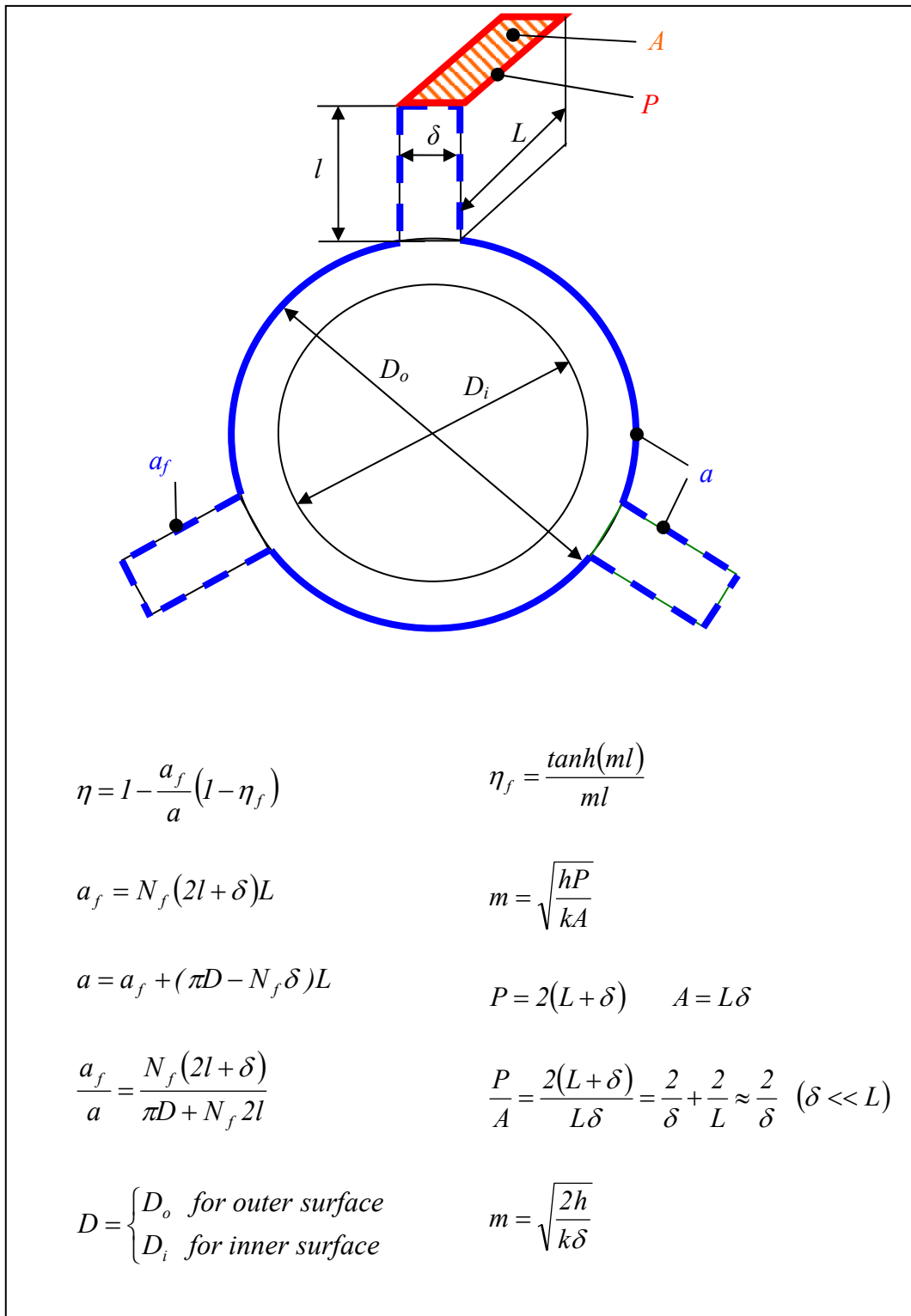










Figure 17. Fins and their efficiency.

Table 3. Effect of tube fins on recuperators' effectiveness and cycle efficiency

		LT recuperator				
						Ideal
$\eta_{\text{cycle}}, \%$						
$\varepsilon_{\text{HTR}}, \%$						
$\varepsilon_{\text{LTR}}, \%$						
HT recuperator		44.3	45.0	44.9	45.6	45.6
		83.8	84.1	84.0	84.2	84.2
		89.9	96.0	94.8	99.8	100.0
		45.0	45.6	45.5	46.3	46.8
		85.6	86.0	85.9	86.3	86.4
		85.4	91.4	89.8	96.5	100.0
		44.8	45.5	45.4	46.1	46.5
		85.2	85.5	85.4	85.7	85.8
		86.7	92.9	91.4	98.1	100.0
		45.1	45.7	45.6	46.3	47.1
		86.0	86.4	86.3	86.7	87.0
		84.1	89.6	88.1	94.2	99.8
	Ideal	45.3	45.9	45.8	46.5	47.3
		86.0	86.4	86.3	86.7	87.1
		83.9	89.4	87.9	94.0	99.5

The last recuperator parameter which should be optimized is the recuperator length. Figure 18 shows the increase in cycle efficiency through an increase in recuperator length. A 10 m double-finned tube design seems to be optimal because the increase in length beyond 10 m does not produce much benefit in the cycle efficiency.

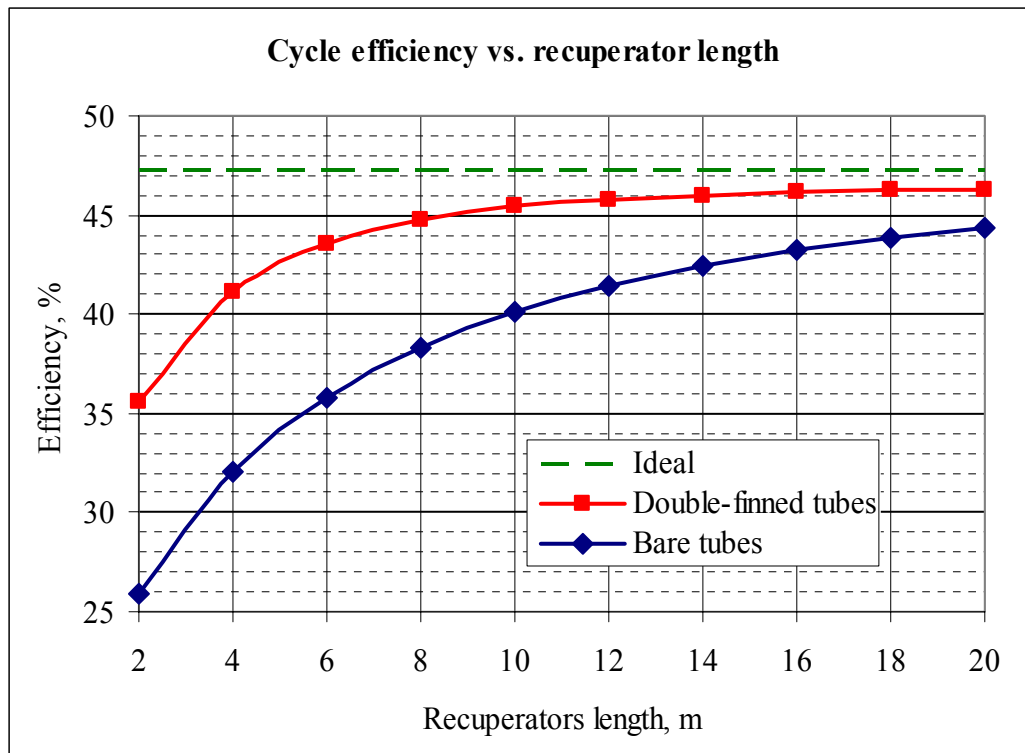


Figure 18. Recuperator length optimization.

The HEATRIC Heat Exchanger

The other possibility to increase heat transfer area is to use printed circuit heat exchangers. This heat exchanger (produced by HEATRIC Company) is made of several metallic plates. Each plate has semicircular channels chemically milled on one side. The plates are bounded together, forming a metal cube with semicircular channel inside it. The CO₂ flows inside these channels in the counter-current directions (Figure 19). This technology makes it possible to have very small channels (0.5 mm), which increases the heat transfer area significantly.

The HEATRIC heat exchanger was modeled to be used in the S-CO₂ Brayton cycle. The design was optimized for the same parameters as the shell-and-tube heat exchanger, which are channel diameter, pitch-to-diameter ratio, and length and side dimensions. Figure 20 shows the optimization process for a high temperature

recuperator. The cycle efficiency values are different from those in the previous tables and figures because the optimization was performed for the different cycle conditions. However, the optimal parameters can be found and the heat exchanger performance can be compared to that of the shell-and-tube heat exchanger under the same cycle conditions.

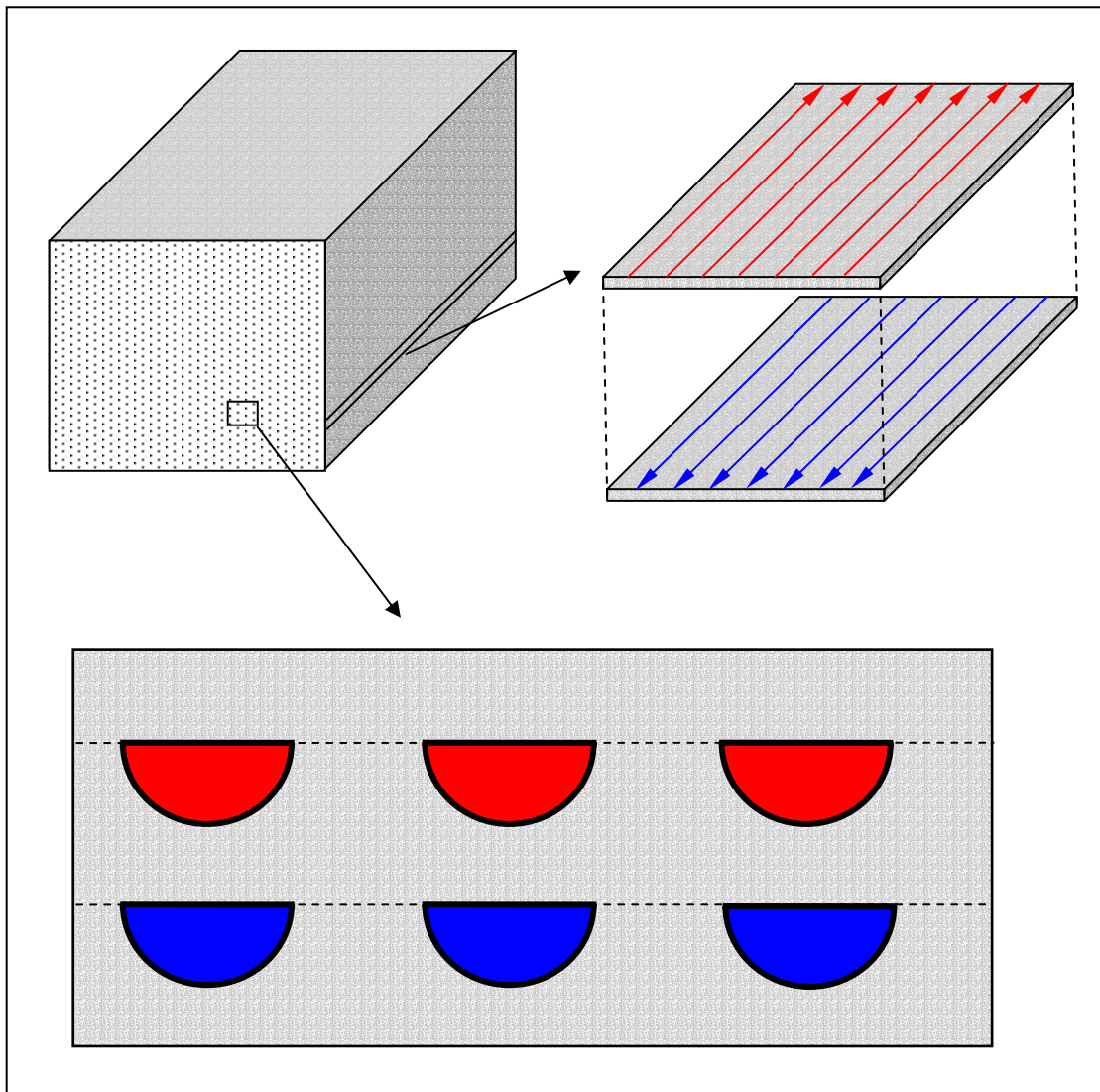


Figure 19. HEATRIC heat exchanger.

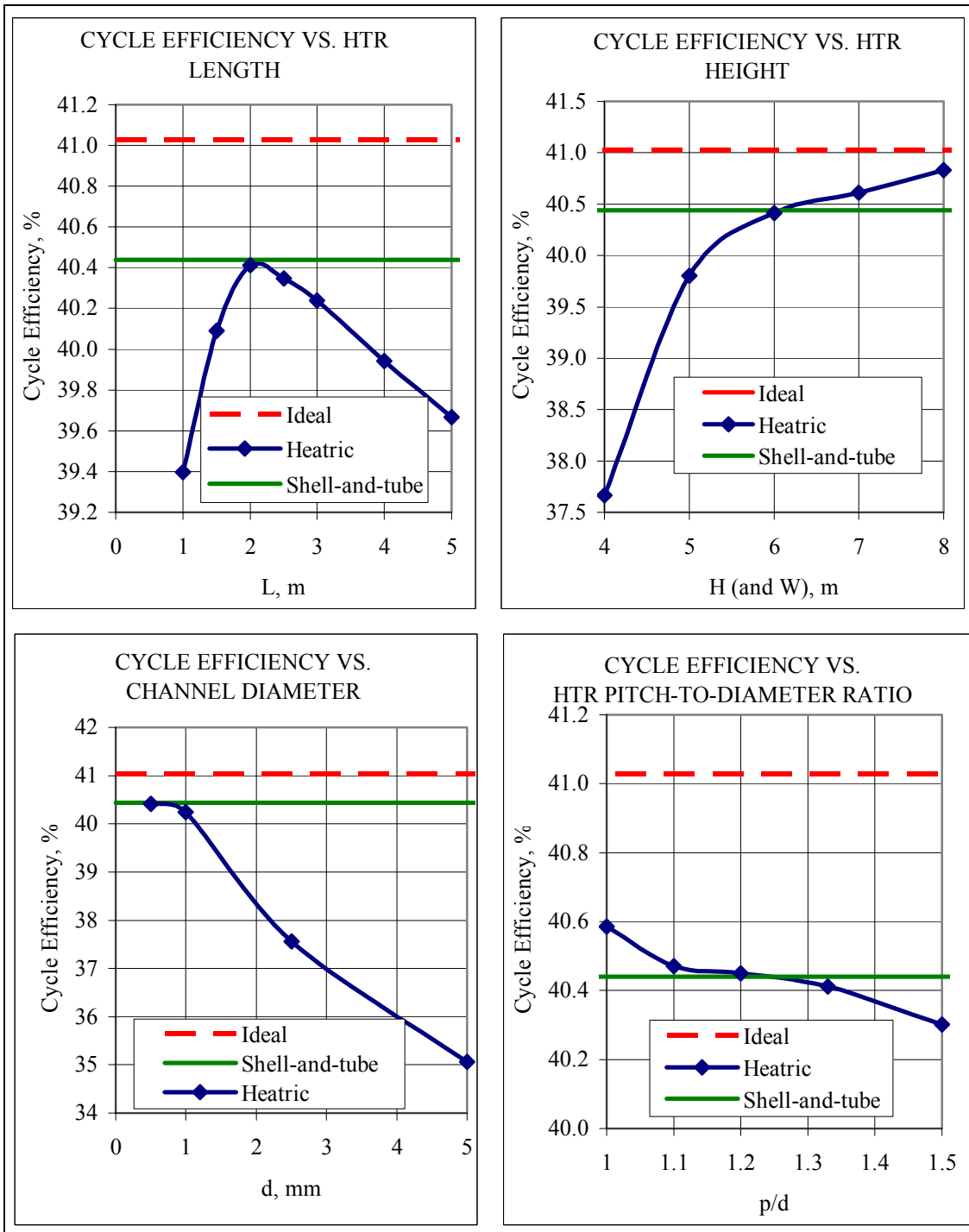


Figure 20. HEATRIC heat exchanger parameters optimization.

Figure 20 shows that the channel for the HEATRIC heat exchanger should be small (0.5 mm). This small diameter provides for a very large heat transfer area. At the same time, a small channel means large friction losses. This becomes more significant for a long heat exchanger where the loss from friction is greater than the gain from a small channel. Therefore, there is an optimal heat exchanger length (2.0 m), where the cycle efficiency is the highest.

Overall, the HEATRIC heat exchanger is more compact (2m x 6m x 6m) than the shell-and-tube heat exchanger (10 m x 6mD), but performance of these two heat exchangers is essentially equal. Besides, as it was stated before, the printed circuit heat exchanger is a new technology and it can be more expansive than the shell-and-tube design. The final judgment should be made on the basis of the cost-benefit comparison, which is beyond the scope of this work. Thus, no preferences could be made at this point; hence both concepts are included in the code, giving the user a choice.

Cooler Optimization

The number of tubes for the heat exchanger was optimized previously (Figure 12). The recuperator length is not an optimization parameter, since the length is selected in such a way that the cooler outlet temperature is equal to the given minimum temperature. However, the cooler design affects the choice of this minimum temperature.

As was shown before (Figure 16) the cooler outlet temperature should be as close to the critical temperature as possible to increase the cycle efficiency. 31.0 °C was selected originally (critical temperature is 30.98 °C). The peak in specific heat near the critical point (Figure 3) means that significant transfer of heat would be required to cool the CO₂ down to 31.0 °C. This means that the cooler should be long in this case. This was confirmed by the cooler calculations (Table 4), which determined that the required cooler length is 26.5 m. This is very long, compared to 10m of recuperator length.

At the same time, the cooler length can be significantly reduced by increasing the minimum temperature by a fraction of a degree (just enough to stay to the right of the

peak) based on the specific heat behavior (Figure 3). In this case, the amount of heat to be removed from the cycle, which is equal to the integral of specific heat, would be much lower. Table 4 shows that if 31.25 °C is selected for the minimum cycle temperature, the required cooler length drops by more than a half, down to 12 m. This is comparable to the recuperator length. The price for this reduction in tubing is decreased cycle efficiency. Since the increase in the minimum temperature would decrease the CO₂ density at the compressor inlet, the compression work will increase, resulting in the lower cycle efficiency (by about 2% compared to the 31.0 °C case).

Table 4. Minimum temperature in cycle and cooler length

T_{min}, °C	31.00	31.25
Cooler tube length, m	26.5	12.1
Compressor #1 work, MW	27.6	40.0
Cycle efficiency, %	45.8	43.8
T _{min} control mechanism	Cooling by fluid which boils at just below 31 °C	Barrier in <i>C_p</i> requires additional 14 m of cooler to cool CO ₂ down to 31.0 °C

However, there is one more consideration which affects the choice of the minimum temperature. For compressor durability reasons it is necessary to avoid two-phase flow in the compressor. Therefore, the CO₂ temperature should be maintained above the critical temperature all the time. 31.0 °C is too close to the critical point (just 0.02 °C higher) to maintain an above-critical temperature by any active control scheme. Thus, some passive control is required, for example, cooling the CO₂ by some fluid which boils at just below 31.0 °C. This will assure that the CO₂ temperature will not drop below the critical temperature. However, such a fluid, even if found, can be expensive.

At the same time, staying to the right of the specific heat peak (at 31.25 °C) would provide a passive barrier for cooling the CO₂ below the critical temperature. Indeed, it follows from Table 4 that the additional 14 m of a cooler will be required to cool the CO₂ from 31.25 to 31.0 °C. This allows for active control of the CO₂ temperature and for maintaining it above the critical point. It is estimated that the cooling flow rate should be increased by about 33% to overcome the specific heat barrier and to decrease the CO₂ temperature from 31.25 to 31.0 °C for the same cooler design.

Also, Table 4 compares the cycle efficiency while cycle conditions stay the same. However, as shown before, the optimal flow split depends on the difference in specific heats for two flows in a low temperature recuperator. Changing the CO₂ minimum temperature causes the change in the CO₂ parameters at the LTR inlet. So, the optimal flow split should be different for different minimum temperatures. It was calculated that 65% / 35% flow split is optimal for 31.25 °C (compared to 60/40 split for 31.0 °C). The cycle efficiency is about 44 % for 65/35 flow split and 31.25 °C minimum temperature. So, the loss in cycle efficiency is even lower than reported in Table 4.

Thus, 31.25 °C is selected as the minimum temperature in the Brayton cycle for further calculations.

Modification in the Brayton Cycle for the STAR-H2 System

The Brayton cycle for the STAR-H2 system differs, while not significantly, from that used in the STAR-LM system.

First, as mentioned above, the CO₂ is cooled in a cooler by seawater at 25 °C.

Second, there is an additional heat supply to the cycle from a chemical plant through the beds R4 and R5 (Figure 2). Since the detailed design of these beds is beyond the scope of this work, only the change in CO₂ temperature in these beds is calculated through the heat supplied to the cycle.

Third, the CO₂ cycle should produce steam at about 125 °C for a hydrogen production plant. So, two additional heat exchangers were added to the bottom of the cycle: a brine boiler and a steam superheater (Figure 2). In the brine boiler, the portion

of the seawater flow after the cooler is being boiled. The steam produced in the brine boiler is superheated to 125 °C in the steam superheater. To be able to produce the steam at 125 °C, the CO₂ temperature at the brine boiler and the steam superheater (after the low temperature recuperator) should be increased to about 130 °C. Also, some further adjustment to the CO₂ temperature should be made to produce as much steam as required for hydrogen production (increasing in the CO₂ temperature increases the amount of heat available above the water boiling temperature). This increase in the CO₂ temperature is achieved by adjusting the CO₂ flow split. So, in the STAR-H2 system the flow split is defined by the steam production requirements (not by the optimal cycle efficiency).

Reactor Submodel

The reactor (Figure 1) consists of a core, reactor heat exchanger (RHX), coolant, reactor vessel and Reactor Vessel Air Cooling System (RVACS).

The core consists of cylindrical fuel rods. Each fuel rod has three layers: fuel (uranium or trans-uranium nitride), bond (liquid metal, lead), and cladding (stainless steel SS-316 for the STAR-LM and silicon carbide for the STAR-H2). Each fuel rod has a fission gas plenum above the active core.

The fuel rods are cooled by the coolant (lead). Then the heat transferred from the lead into a secondary fluid in the RHX (some fraction of the flow can bypass the RHX). The RVACS removes some fraction of the reactor power and cools the coolant slightly after the RHX. Then coolant returns to the core. There are several flow distribution plates below the core. Also, there is core support plate at the bottom of the core.

The reactor operates on natural circulation, i.e. there are no primary coolant pumps in the system. To assure natural circulation, the RHX should be elevated above the core. This creates the driving force, since in the upper plenum (the region above the core) the coolant is hot and, therefore, lighter than the coolant in down comer (the region below the RHX). The difference in mass creates a pressure head which should be sufficient to overcome all resistance to the flow in the core and RHX.

The goal of the reactor submodel is to calculate coolant, cladding and fuel temperatures inside the reactor. The submodel uses natural circulation equation (Sienicki and Petkov, 2003) to calculate the speed of the coolant in the core:

$$u = \left(\frac{g \cdot \beta \cdot Q \cdot L_{diff}}{2 \cdot \bar{\rho} \cdot \bar{c}_p \cdot A_{core} \cdot K} \right)^{1/3}, \quad (57)$$

where

g – gravitation acceleration,

β – coolant thermal expansion,

Q – core thermal power,

L_{diff} – difference between thermal centers of core and RHX,

$\bar{\rho}, \bar{c}_p$ – average coolant density and specific heat In core,

A_{core} – core flow area,

K – total loss coefficient,

$$K = \left(\frac{L_{core}}{D_{h,core}} f_{core} + \frac{1}{4} \sum_i K_{i,core} \right) + \left(\frac{(1-Y)A_{core}}{A_{HX}} \right) \left(\frac{L_{HX}}{D_{h,HX}} f_{HX} + \frac{1}{4} \sum_i K_{i,HX} \right)$$

L_{core}, L_{HX} – core and RHX rod length,

$D_{h,core}, D_{h,HX}$ – core and RHX hydraulic diameters,

$K_{i,core}, K_{i,HX}$ – core and RHX pressure loss coefficients (contraction and

expansion),

f_{core}, f_{HX} – core and RHX friction factors,

Y – fraction of flow that bypass RHX,

A_{HX} – RHX flow area.

Equation (57) is modified to take into an account the fact that the fraction of core nominal power (F_{RVACS}) is removed by the RVACS, and not by the RHX. The effective difference between the core and RHX thermal centers is used instead of an actual difference:

$$L'_{diff} = L_{diff} - \frac{H_{HX}}{2} \frac{F_{RVACS} \cdot Q_{nom}}{Q} \frac{\bar{c}_p}{\bar{c}_p^{DC}} \quad (58)$$

where

H_{HX} – elevation of the bottom of the RHX above the bottom of core (downcomer length – where RVACS remove heat),

Q_{nom} – nominal core power,

\bar{c}_p^{DC} – average specific heat in the downcomer.

The coolant temperature is calculated for both average and hot channels. In an average channel the coolant temperature rise is defined by the core power and coolant speed:

$$\Delta T = \frac{Q}{\bar{\rho} \cdot u \cdot \bar{c}_p \cdot A_{core}} \quad (59)$$

Temperature rise in a hot channel is equal to the temperature rise in an average channel multiplied by a hot channel factor. Coolant temperatures are calculated at three axial locations: the bottom, middle, and top of the core. The temperature at the bottom of the core (the core-inlet temperature) is give and the same for both average and hot channels. The temperature at the top of the core (core-outlet) is equal to the inlet temperature plus ΔT . The coolant temperature at the middle of the core is an average between core-inlet and core-outlet temperatures (it is assumed that the power profile is axially symmetric in the core).

The cladding and fuel temperatures are calculated at the same axial locations for both average and hot channels. At every location, two cladding temperatures, at the outer (T_{clad}^o) and the inner (T_{clad}^i) surfaces, and two fuel temperatures, at the outer surface (T_f^o) and at the centerline (T_f^{CL}), are calculated (Figure 21):

$$\left\{ \begin{array}{l} T_{clad}^o = T_{cool} + q'' \frac{1}{h} \\ T_{clad}^i = T_{clad}^o + q'' \frac{R_{clad}^o}{k_{clad}} \ln \left(\frac{R_{clad}^o}{R_{clad}^i} \right) \\ T_f^o = T_{clad}^i + q'' \frac{R_{clad}^o}{k_{bond}} \ln \left(\frac{R_{clad}^i}{R_f^o} \right) \\ T_f^{CL} = T_f^o + q'' \frac{R_{clad}^o}{2k_f} \end{array} \right. \quad (60)$$

where

T_{cool} – coolant temperature at the location,

q'' - heat flux,

h – heat transfer coefficient,

$R_{clad}^o, R_{clad}^i, R_f^o$ - outer and inner cladding and outer fuel radii (Figure 21),

k_{clad}, k_{bond}, k_f – cladding, bond, and fuel thermal conductivity.

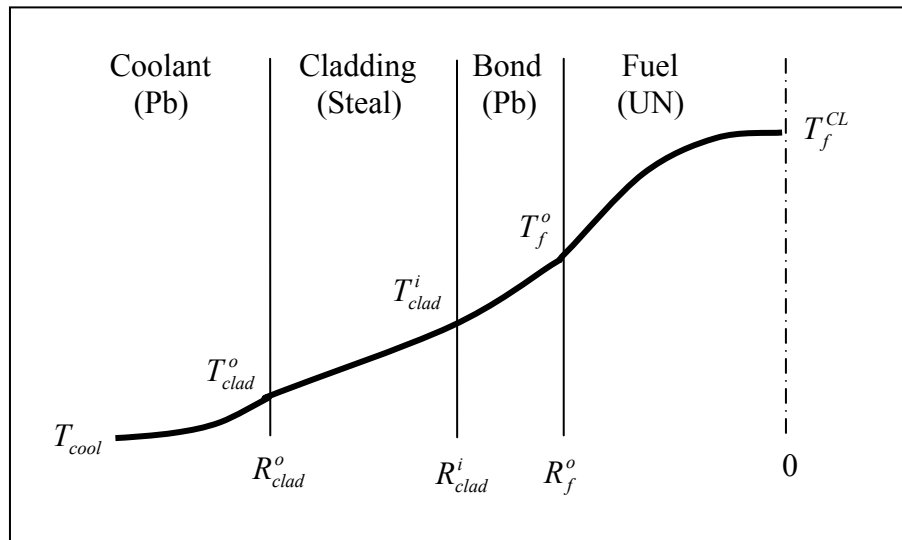


Figure 21. Coolant, cladding, and fuel temperatures.

The heat flux for an average channel is calculated as the ratio of core power to the total fuel pin surface area. Heat fluxes at the edge of the core and in a hot channel are calculated by multiplying the average-channel heat flux by the corresponding peaking factor.

The coolant heat transfer coefficient is calculated using the correlation recommended by Kirillov and Ushakov (Kirillov and Ushakov, 2001).

The temperature dependent properties of lead and the temperature dependent thermal conductivity of steel and uranium nitride (Fink, 1998; Hayes et al., 1990; Leibowitz and Blomquist, 1988; Lyon and Poppendiek, 1954; Ofte and Wittenberg, 1963; Saar and Ruppertsberg, 1987) are used in calculations.

The fuel average temperature (needed for the reactivity feedback) is an average between fuel temperatures at the outer surface and at the centerline.

It follows from Equations (57) – (60) that all temperatures, including peak cladding temperature are functions of the resistance to flow in the heat exchanger. This fact was used to select the heat exchanger height in order to get the desirable cladding temperature.

Hydrogen Production Plant and Intermediate Loop Submodel (STAR-H2)

Hydrogen Production Plant

The three-step thermochemical process is used to break water into hydrogen and oxygen:

1. $\text{CaBr}_2 + \text{H}_2\text{O} + \text{Q} \rightarrow \text{CaO} + 2\text{HBr}$
2. $2\text{HBr} + \text{plasma} + \text{E} \rightarrow \text{H}_2 + \text{Br}_2$
3. $\text{CaO} + \text{Br}_2 \rightarrow \text{CaBr}_2 + 0.5\text{O}_2 + \text{Q}$

The first reaction transforms calcium bromide into calcium oxide and hydrogen bromide. This reaction should be maintained at 700-750 °C; hence the heat should be supplied to the tanks where the reaction takes place. The steam should also be supplied at 750 °C. According to the hydrogen production plant design (Doctor and Matonis, 2003),

these reactors are called beds and have numbers R1, R2, R3, B1, B2, and B3, and they are referenced here as beds R1-B3.

The second reaction splits hydrogen bromide into hydrogen and bromine. The special equipment (plasmatron) was designed (Doctor and Matonis, 2003) to conduct the reaction.

In the third reaction (which takes place in the beds R4 and R5) the calcium bromide is reformed. The reaction occurs at 600 °C and produces heat which is supplied to the Brayton cycle.

For the purpose of this work, the hydrogen production plant was modeled as the three heat exchangers: beds R1-B3, reagent steam superheater, and beds R4-R5. The following requirements should be met:

1. The amount of heat supplied to beds R1-B3 should meet heat requirements of hydrogen production plant;
2. The heat should be supplied at temperature above 700 °C;
3. The reagent steam, as much as needed, should be supplied at 750 °C;
4. The amount of heat available from beds R4-R5 is specified;
5. The amount of electricity produced by the Brayton cycle should be enough to run the plant's pumps and plasmatron.

The electricity requirements for the plasmatron are 0.47 MWe for every 1 MWt supplied to the beds R1-B3, plus about 10% of that is required to run pumps of the hydrogen production plant.

Intermediate loop

The goal of the intermediate loop in the STAR-H2 system is to transfer heat from the reactor to the hydrogen production plant and the Brayton cycle. The original idea was to use helium as a working fluid in the intermediate loop. However, as the calculations have shown, it will take too much energy to pump helium, because of its

low density. So, helium was substituted by molten salt. Li_2BeF_4 (also known as flibe) was selected because of its high density and specific heat.

The intermediate loop (Figure 2) consists of the reactor heat exchanger (RHX), beds R1-B3 of the chemical production plant, the reagent steam superheater, the molten salt-to- CO_2 heat exchanger (MS- CO_2 HX), and a pump. Since both beds R1-B3 and the reagent steam superheater require high-temperature heat, the flibe flow is split after the RHX, one part goes to beds, and the other goes to the steam superheater.

The goal of the intermediate loop module is to calculate temperature distribution of the flibe in the loop. The flibe temperature before the RHX is given. The flibe temperature after the RHX and split fraction are selected such that the flibe temperature after the beds is above $700\text{ }^\circ\text{C}$ and the steam temperature after the steam superheater is exactly $750\text{ }^\circ\text{C}$. The flibe mass flow rate is selected to remove all required heat from the RHX. The steam superheater (and the molten salt-to- CO_2 heat exchanger) module is similar to the recuperator module. The temperature before the MS- CO_2 HX is calculated based on heat conservation for the merged flow. The CO_2 temperature after the heat exchanger is a result of the heat exchanger calculations.

The pressure drop is calculated for the RHX, the steam superheater, and the MS- CO_2 HX. The amount of energy required to pump the working fluid is (Waltar and Reynolds, 1981):

$$W_{pump} = \frac{\dot{m} \cdot \Delta p}{\rho} \quad (61)$$

where

\dot{m} - flibe mass flow rate,

Δp - total pressure drop in the loop,

ρ - flibe density.

The pressure drop itself is proportional to the mass flow rate squared over the density. Therefore, the mumping power is reciprocal to the square of fluid density. So,

the pumping power for helium ($\rho=0.03 \text{ kg/m}^3$ at 1 atm) would be several orders of magnitude higher than the pumping power required for flibe ($\rho=2000 \text{ kg/m}^3$ at 1 atm). For these reasons, the molten salt is used in the intermediate loop instead of helium.

The hydrogen production rate (and, therefore, heat requirements and reagent steam mass flow rate) was selected so that the amount of electricity produced by the Brayton cycle will be sufficient to run the plasmatron and on-site pumps.

Reactor Heat Exchanger Module

The heat exchanger inside the reactor vessel (RHX) serves to transfer the heat from the reactor core coolant to the secondary fluid. In both the STAR-LM and the STAR-H2 designs the primary coolant is lead (Pb), while the secondary fluids are different. The STAR-LM system uses supercritical carbon dioxide (S-CO₂) and the STAR-H2 design uses molten salt (flibe). Although different fluids have different properties, the physical principles are the same, so in further discussions, there will be no difference between those systems, and the secondary fluid (S-CO₂ or flibe) will be referred to as “secondary fluid” (or “S.F.” for short in the figures).

Due to the reactor vessel design, the volume available for the heat exchanger is an annulus between the core and the vessel wall (Figure 22). There are also several places (gaps) in the annulus which are not available for the heat exchanger.

The heat exchanger length is limited since the reactor vessel height is limited and a natural circulation requires specific elevation of the heat exchanger thermal center above the core thermal center.

There are several possible designs (Heat Exchanger Design Handbook, 1983) of the heat exchanger, which could fit into the geometry shown on Figure 22. These designs could be based on U-tubes, straight tubes and concentric tubes. The STAR-H2 system also allows for the plate-type HX since both lead and flibe flows are at atmospheric pressure, and hence, there is no pressure gradient in the HX. Some of the possible designs were modeled and they are described below in detail.

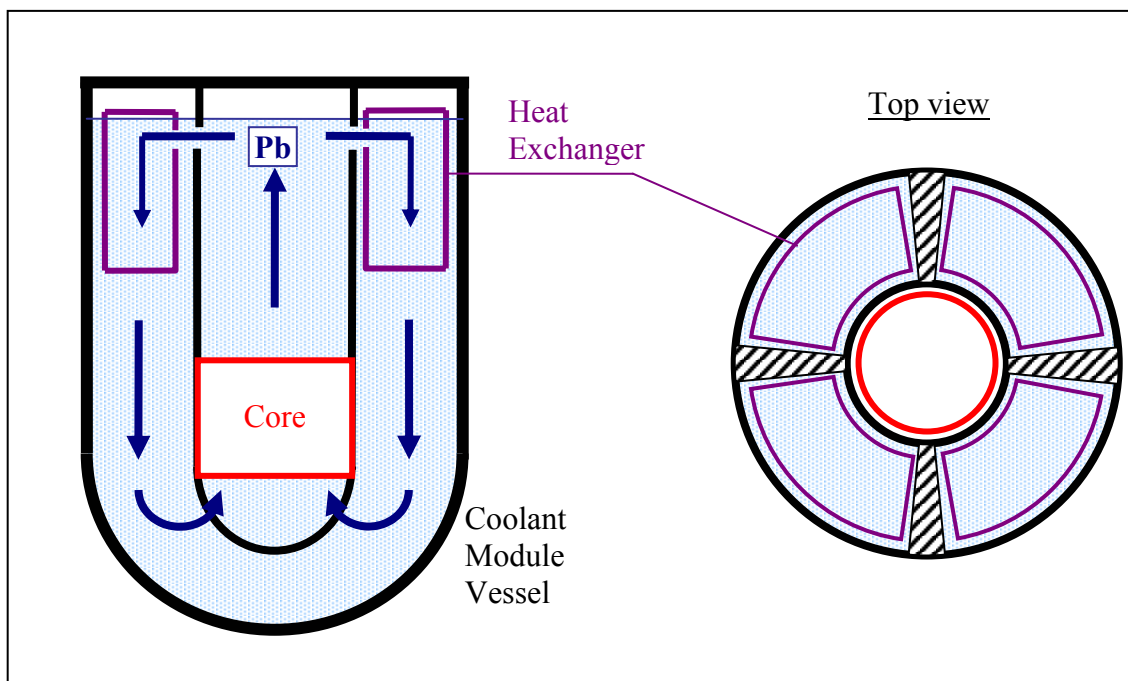


Figure 22. Reactor heat exchanger.

Independent of design, the goal of the RHX model is to calculate the outlet temperature for lead and secondary fluid, given the inlet temperatures and mass flow rates. The models are based on the average channel meaning that the temperature change calculated for one average channel and this then represents the entire heat exchanger. The fluid mass flow rate through one channel is the total flow rate through the heat exchanger divided by number of channels.

RHX Type 1: Stacked U-tubes Heat Exchanger

The first approach to the RHX design is to use U-tubes for the secondary fluid. The cold secondary fluid flow enters tubes from the top; the hot secondary fluid flow leaves tubes also at the top but at a different location. The lead flows downwards outside the tubes. U-tubes are organized into rows such as the tubes in the bottom portion are located one atop another (APPENDIX A, Figure A.1).

Number of Tubes

The number of tube rows and the number of tubes in each row depend on a choice of the HX lattice. There are two common choices: a triangular lattice and a square lattice. The equations to find the number of tubes and the number of rows, based on tube outer diameter (d), tube pitch (p), heat exchanger annulus outer and inner diameters (D_o and D_i), the number of the heat exchangers (N_{HX}), and gap thickness (gap) are presented in Table 5 for different lattice layouts.

Table 5. Number of tubes for the stacked U-tube HX

Lattice	Square	Triangular
Layout		
Equation for number of tubes in a row	$\frac{D_o - D_i}{2} = 2 \cdot N_t^{row} \cdot p$	$\frac{D_o - D_i}{2} = 2 \cdot N_t^{row} \cdot p + \frac{p}{2}$
Number of tubes in a row	$N_t^{row} = \frac{D_o - D_i}{4 \cdot p}$	$N_t^{row} = \frac{1}{2} \left(\frac{D_o - D_i}{2p} - \frac{1}{2} \right)$
Equation for number of tube rows	$\pi \frac{D_o + D_i}{2} - N_{HX} \cdot gap = N_{rows} \cdot p$	$\pi \frac{D_o + D_i}{2} - N_{HX} \cdot gap = N_{rows} p \frac{\sqrt{3}}{2}$
Number of tube rows	$N_{rows} = \frac{\pi \frac{D_o + D_i}{2} - N_{HX} \cdot gap}{p}$	$N_{rows} = \frac{\pi \frac{D_o + D_i}{2} - N_{HX} \cdot gap}{p \frac{\sqrt{3}}{2}}$
Total number of tubes	$N_{tube} = N_{rows} \cdot N_t^{row}$	

Since the number of tubes in a row is an integer, the lattice pitch should be corrected using first equations from Table 5 after the number of tubes in a row is calculated and rounded to the nearest integer.

Approach to Solve for Outlet Temperatures

A U-tube of the HX is show on the Figure 23.

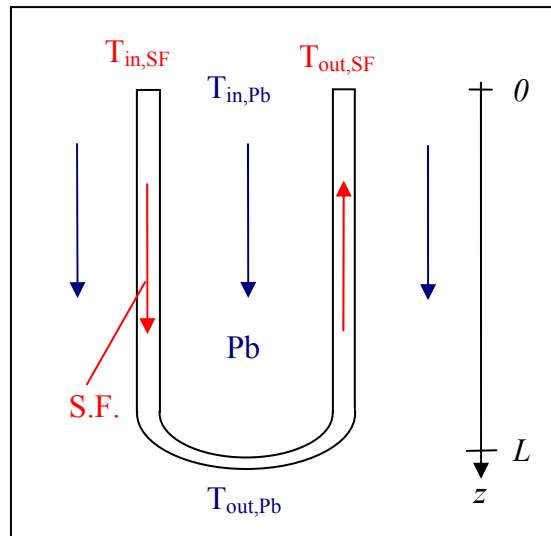


Figure 23. U-tube.

Index 1 is used for the Pb flow, index 2 for the down coming secondary fluid flow, and index 3 for the upper coming secondary fluid flow. Since heat is transferred from lead to both secondary fluid flows, there are two heat flows in this system. The first is from the lead to the down coming secondary fluid. The second heat flow is from lead to the upper coming secondary fluid. Both of these heats are defined by the temperature differences between the heat exchanging flows and the total heat transfer coefficients:

$$\begin{aligned} q_{12}(z) &= H_{12}(T_1(z) - T_2(z)) \\ q_{13}(z) &= H_{13}(T_1(z) - T_3(z)), \end{aligned} \quad (62)$$

where
$$H_{1,j} = \frac{1}{\frac{1}{2\pi \cdot R_o \cdot h_1} + \frac{\ln(R_o/R_i)}{2\pi \cdot k_w} + \frac{1}{2\pi \cdot R_i \cdot h_j}}$$

R_i, R_o – tube inner and outer radii,

h – heat transfer coefficient,

k_w – tube wall thermal conductivity.

The amount of heat transferred in tube length dz from or to the fluid defines the change in its temperature on dz . This change is negative for flows #1 and #3 since temperature decreases with z and positive for the flow #2:

$$\begin{aligned} m_1 \cdot Cp_1 \cdot dT_1 &= -(q_{12}(z) + q_{13}(z))dz \\ m_2 \cdot Cp_2 \cdot dT_2 &= q_{12}(z) \cdot dz \\ m_3 \cdot Cp_3 \cdot dT_3 &= -q_{13}(z) \cdot dz \end{aligned} \quad (63)$$

Equations (62) and (63) can be written as a system of differential equations:

$$\begin{cases} \frac{dT_1}{dz} = -\frac{1}{m_1 \cdot Cp_1} [H_{12}(T_1(z) - T_2(z)) + H_{13}(T_1(z) - T_3(z))] \\ \frac{dT_2}{dz} = \frac{1}{m_2 \cdot Cp_2} H_{12}(T_1(z) - T_2(z)) \\ \frac{dT_3}{dz} = -\frac{1}{m_3 \cdot Cp_3} H_{13}(T_1(z) - T_3(z)) \end{cases} \quad (64)$$

The boundary conditions for the system (64) are known inlet temperatures of lead and secondary fluid, $T_1(0)$ and $T_2(0)$, respectively, and the matching secondary fluid temperatures at the middle of the tube, $T_2(L)=T_3(L)$. It is assumed that the U-tube is represented by two straight tubes of length L , i.e. heat transfer in U-turn of the tube is neglected. The justification for this assumption is provided below.

Although the system (64) is a system of ordinary differential equations, the analytical solution can be complicated. Instead, it is proposed to separate the lead flow into two flows, one for each secondary fluid flow and neglect the heat exchange between those lead flows. This approach is similar to the one used in the reactor core calculations, where the core is divided into independent channels with no interchanging of a coolant and heat between channels. The difference between these two approaches is discussed at the end of this section.

Under the assumptions described above, Figure 23 is converted into Figure 24 where index 1 is used for one lead flow (around the downward secondary fluid flow), index 3 is used for the other lead flow and indexes 2 and 4 are used for the corresponding secondary fluid flows:

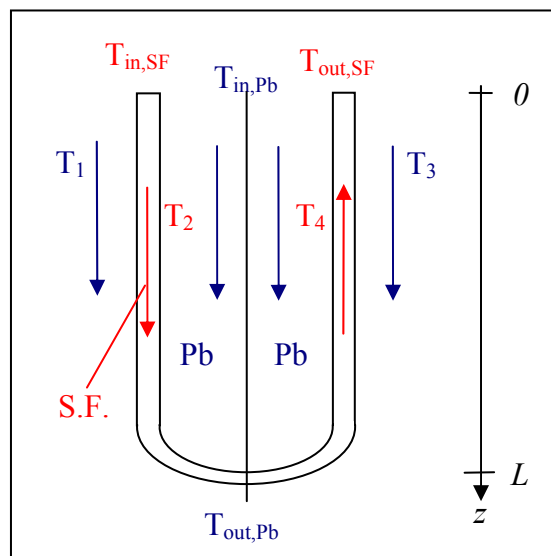


Figure 24. RHX tube with two lead flows.

Neglecting heat transfer between different lead flows allows decoupling of the system (64). This lets the system of equations to be re-written as:

$$\begin{cases} \frac{dT_1}{dz} = -\frac{1}{m_1 \cdot Cp_1} H_{12}(T_1(z) - T_2(z)) \\ \frac{dT_2}{dz} = \frac{1}{m_2 \cdot Cp_2} H_{12}(T_1(z) - T_2(z)) \end{cases} \quad (65)$$

$$\begin{cases} \frac{dT_3}{dz} = -\frac{1}{m_3 \cdot Cp_3} H_{34}(T_3(z) - T_4(z)) \\ \frac{dT_4}{dz} = \frac{1}{m_4 \cdot Cp_4} H_{34}(T_3(z) - T_4(z)) \end{cases} \quad (66)$$

The boundary conditions are similar to those for the system (64):

$$\begin{cases} T_1(0) = T_{in,Pb} \\ T_2(0) = T_{in,SF} \end{cases} \quad (67)$$

$$\begin{cases} T_3(0) = T_{in,Pb} \\ T_4(L) = T_2(L) \end{cases} \quad (68)$$

Introducing the following variables

$$k_{12} = \frac{H_{12}}{m_1 \cdot Cp_1} \quad n_{12} = \frac{m_1 \cdot Cp_1}{m_2 \cdot Cp_2} \quad (69)$$

$$k_{34} = \frac{H_{34}}{m_3 \cdot Cp_3} \quad n_{34} = \frac{m_3 \cdot Cp_3}{m_4 \cdot Cp_4} \quad (70)$$

Systems (65) and (66) can be written in the following form:

$$\begin{cases} \frac{dT_1}{dz} = -k_{12} \cdot T_1(z) + k_{12} \cdot T_2(z) \\ \frac{dT_2}{dz} = k_{12} \cdot n_{12} \cdot T_1(z) - k_{12} \cdot n_{12} \cdot T_2(z) \end{cases} \quad (71)$$

$$\begin{cases} \frac{dT_3}{dz} = -k_{34} \cdot T_3(z) + k_{34} \cdot T_4(z) \\ \frac{dT_4}{dz} = -k_{34} \cdot n_{34} \cdot T_3(z) + k_{34} \cdot n_{34} \cdot T_4(z) \end{cases} \quad (72)$$

If coefficients k and n are constant, solutions of systems (71) and (72) are very similar to the system for recuperator model, except for system (71) the minus sign will appear everywhere before n_{12} :

$$\begin{cases} T_1(z) = A_{12}(z) \cdot T_1(0) + (1 - A_{12}(z)) \cdot T_2(0) \\ T_2(z) = C_{12}(z) \cdot T_1(0) + (1 - C_{12}(z)) \cdot T_2(0) \\ T_3(z) = A_{34}(z) \cdot T_3(0) + (1 - A_{34}(z)) \cdot T_4(0) \\ T_4(z) = C_{34}(z) \cdot T_3(0) + (1 - C_{34}(z)) \cdot T_4(0) \end{cases} \quad (73)$$

where

$$\begin{aligned} A_{12}(z) &= \frac{n_{12} + e^{-k_{12} \cdot (n_{12}+1) \cdot z}}{n_{12} + 1} \\ C_{12}(z) &= \frac{n_{12} - n_{12} \cdot e^{-k_{12} \cdot (n_{12}+1) \cdot z}}{n_{12} + 1} \\ A_{34}(z) &= \frac{n_{34} - e^{k_{34} \cdot (n_{34}-1) \cdot z}}{n_{34} - 1} \\ C_{34}(z) &= \frac{n_{34} - n_{34} \cdot e^{k_{34} \cdot (n_{34}-1) \cdot z}}{n_{34} - 1} \end{aligned}$$

In the solution (73) the first two temperatures could be found immediately once coefficients k and n are known. Note that the solution assumes that these coefficients are constant along the tube. This is not actually true since these coefficients depend on the fluid properties (temperatures). Instead, the multi-region iterative approach can be used, which divides the tube length is into several regions. The coefficients k and n are calculated for each region based on the average temperatures found in previous iterations. In that case, the solution (73) is still applicable to each region except the initial conditions are temperatures at the region's boundary (not tube-inlet temperatures).

From the solution, $T_2(L)$ specify boundary condition for a second part of the U-tube, since $T_4(L)=T_2(L)$.

The approach to solve for T_3 and T_4 is more complicated since $T_4(0)$ is not given. The approach here is similar to that used in the recuperator model. The solution in each region can be written as a linear combination of the temperatures at $z=0$:

$$\begin{aligned} T_3^i &= F_i \cdot T_3(0) + (1 - F_i) \cdot T_4(0) \\ T_4^i &= L_i \cdot T_3(0) + (1 - L_i) \cdot T_4(0) \end{aligned} \quad i=1,2,\dots,N \quad (74)$$

The algorithm for finding coefficients F and L is described in the recuperator module section.

The relations (74) hold for each region including the last one:

$$\begin{aligned} T_3(L) &\equiv T_3^N = F_N \cdot T_3(0) + (1 - F_N) \cdot T_4(0) \\ T_4(L) &\equiv T_4^N = L_N \cdot T_3(0) + (1 - L_N) \cdot T_4(0) \end{aligned} \quad (75)$$

The initial condition for the solution (73) can be found:

$$T_4(0) = \frac{T_4(L) - L_N \cdot T_3(0)}{1 - L_N} \quad (76)$$

Once the initial conditions are known, T_3 and T_4 could be found using the same multi-region iterative approach as for T_1 and T_2 .

Pressure Change

Since properties of secondary fluid depend on pressure, pressure drop for each region is calculated for the secondary fluid flows on every iterative step, using properties for average pressure and temperature from previous iteration.

Outlet Temperatures

From Figure 24, the outlet temperature for the secondary fluid is just the outlet temperature of the flow #4, i.e. $T_4(0)$. Since the mass flow rates of lead are equal on both lead flows, the outlet temperature for lead is an average of the outlet temperatures of flows #1 and #3:

$$\begin{aligned} T_{out,SF} &= T_4(0) \\ T_{out,Pb} &= \frac{T_1(L) + T_3(L)}{2} \end{aligned} \quad (77)$$

Comparison of the Two Approaches

In order to compare the two approaches described above (one with one lead flow and the other with two lead flows), system (64) was solved numerically using the MathCAD software and the results were compared to the solution (73). 550 °C and 400 °C were selected as initial conditions for inlet temperatures of lead and secondary fluid (the secondary fluid is assumed to have the CO₂ properties). For comparison purposes, one region approach was used with lead and CO₂ properties calculated at average temperature, i.e. 475 °C. The results are shown in Figure 25 where the solid lines represent a numerical solution of the system (64) and the dashed lines represent the solution (73). Table 6 shows the comparison of these two methods in terms of outlet temperatures. Figure 25 and Table 6 demonstrate that the difference between these two methods is not significant, though the second method is easier and faster since it represents decoupled system. However, even in the first approach, lead flow temperatures around tubes with different secondary fluid temperature will be different, resulting in a gradient in lead temperature. Therefore, the actual lead temperature distribution will be somewhere in between the first approach, which assume complete intermixture of lead flows around different tubes, and the second approach, which assumes no lead intermixture. Thus, results of the second approach would be even closer to actual results than it appears in Table 6.

This U-tube rows RHX design has a large distance between downward and the upward sections of a section of the U-tube for an average tube. Also, the downward sections of the U-tubes are combined together, as well as the upward sections, which means that the average tube in the middle of the bundle “sees” lead around similar portions (upward or downward) of tubes. Therefore, the second approach is expected to give more accurate result for this RHX design.

The RHX design #2 (U-tubes), which is described in the next section, assumes one lead flow; and the system (64) is solved numerically for that design.

It can be seen from Figure 25 that the temperature difference between the lead and the secondary fluid flow is minimal at $z=L$, i.e. at the U-turn. It follows from Equation (62) that the heat transfer at this location is small compared to the average heat transfer in a tube. Therefore, the assumption of neglecting the heat transfer at the U-turn does not significantly affect the results.

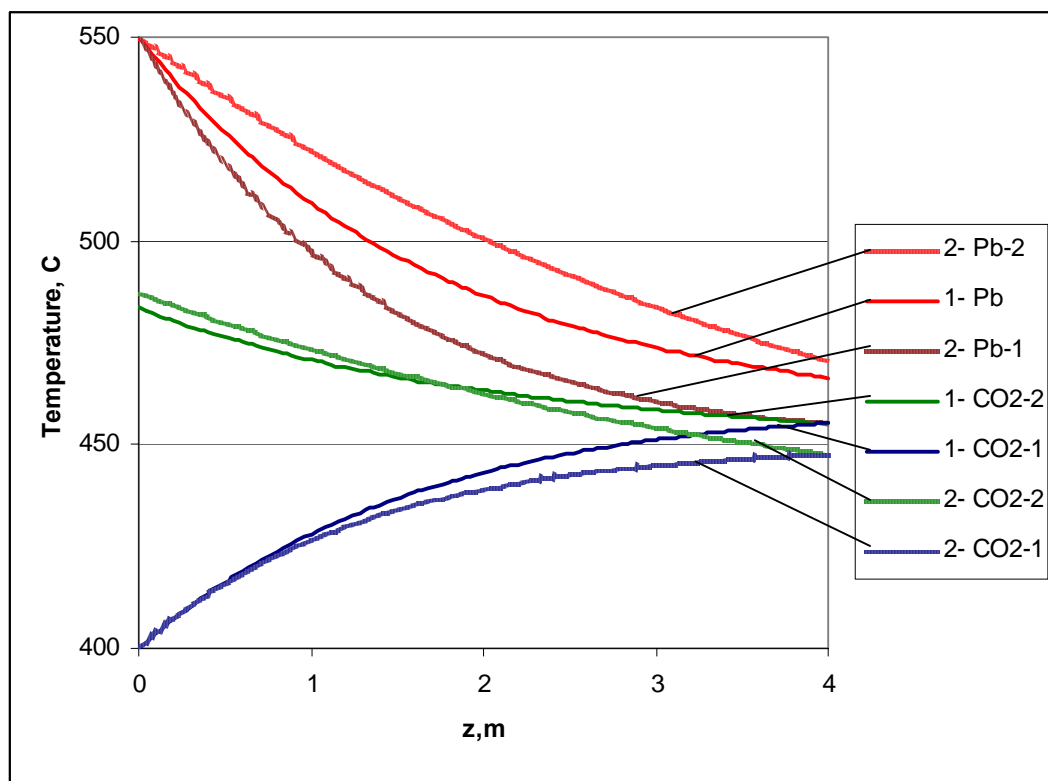


Figure 25. Comparison of two approaches.

Table 6. Results for outlet temperatures

RHX outlet temperatures, °C	First Approach System (64)	Second Approach Solution (73)
Pb	466.5	462.8
CO ₂	483.5	487.2

RHX Type 2: U-tubes Heat Exchanger

The second approach to the RHX design also utilizes U-tubes, but they are not organized into rows. In this case, the upward and downward portions of the U-tubes are mixed inside the heat exchanger (APPENDIX A, Figure A.2). Because of this, the lead flows around the upward and downward sections of the U-tube are so close to each other that the lead is expected to have the same temperature. This means that the decoupling of the system (64) (like in the previous design) should produce a larger error, and that the system should be solved without decoupling.

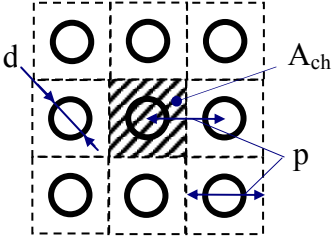
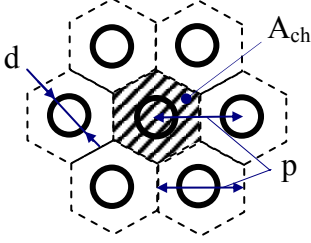
Number of Tubes

The number of tubes is found by the ratio of the total cross section area of all heat exchangers to the cross section area occupied by one tube. The total cross section area of all heat exchangers is (see Figure 22 and figures from Table 5):

$$A_{total} = \left(\pi \frac{D_o^2 - D_i^2}{4} - N_{HX} \cdot gap \right) \cdot \frac{D_o - D_i}{2} \quad (78)$$

The area occupied by one tube depends on the tube lattice, as shown in Table 7.

Table 7. RHX cross section area occupied by a tube

Lattice	Square	Triangular
Layout		
Channel Area	$A_{ch} = p^2$	$A_{ch} = \frac{\sqrt{3}}{2} p^2$
Tube area (two channels)	$A_t = 2 \cdot A_{ch} = 2 \cdot p^2$	$A_t = 2 \cdot A_{ch} = \sqrt{3} p^2$

Approach to solve for outlet temperatures

System (64) is to be solved using the trapezoidal rule approximation. First, similar to the Stacked U-tubes HX, the system can be written in the form:

$$\begin{cases} \frac{dT_1}{dz} = -(k_{12} + k_{13}) \cdot T_1(z) + k_{12} \cdot T_2(z) + k_{13} \cdot T_3(z) \\ \frac{dT_2}{dz} = k_{12} \cdot n_{12} \cdot T_1(z) - k_{12} \cdot n_{12} \cdot T_2(z) \\ \frac{dT_3}{dz} = -k_{13} \cdot n_{13} \cdot T_1(z) + k_{13} \cdot n_{13} \cdot T_3(z) \end{cases} \quad (79)$$

where

$$k_{12} = \frac{H_{12}}{m_1 \cdot Cp_1} \quad n_{12} = \frac{m_1 \cdot Cp_1}{m_2 \cdot Cp_2} \quad (80)$$

$$k_{13} = \frac{H_{13}}{m_3 \cdot Cp_3} \quad n_{13} = \frac{m_3 \cdot Cp_3}{m_1 \cdot Cp_1} \quad (81)$$

The boundary conditions are:

$$\begin{cases} T_1(0) = T_{in,Pb} \\ T_2(0) = T_{in,SF} \\ T_3(L) = T_2(L) \end{cases} \quad (82)$$

It is convenient to write down system (79) in a matrix form:

$$\frac{d}{dz} \bar{T} = D \bar{T} \quad (83)$$

where

$$\bar{T} = \begin{pmatrix} T_1 \\ T_2 \\ T_3 \end{pmatrix}$$

$$D = \begin{pmatrix} -(k_{12} + k_{13}) & k_{12} & k_{13} \\ k_{12} \cdot n_{12} & -k_{12} \cdot n_{12} & 0 \\ -k_{13} \cdot n_{13} & 0 & k_{13} \cdot n_{13} \end{pmatrix}$$

Using the trapezoidal rule for the region i , where $i=0$ and $i=N$ refer to boundaries at $z=0$ and $z=L$, correspondingly, and assuming constant properties (i.e. k 's and n 's are constant) at this region, the system (83) can be written as:

$$\bar{T}^i = \bar{T}^{i-1} + \int_{z_{i-1}}^{z_i} D_i \bar{T}(z) dz \approx \bar{T}^{i-1} + D_i \cdot \frac{\bar{T}^{i-1} + \bar{T}^i}{2} \Delta z \quad (84)$$

Collecting temperatures at the next region border on the left hand side:

$$\left(I - D_i \frac{\Delta z}{2} \right) \bar{T}^i = \left(I + D_i \frac{\Delta z}{2} \right) \bar{T}^{i-1}$$

Introducing matrices B_i and C_i :

$$B_i \bar{T}^i = C_i \bar{T}^{i-1} \quad (85)$$

where

$$\begin{aligned} B_i &= I - D_i \frac{\Delta z}{2} \\ C_i &= I + D_i \frac{\Delta z}{2} \end{aligned} \quad (86)$$

Since B_i is a 3x3 matrix with determinant close to 1 for a small region length ($\Delta z \rightarrow 0$), it can be easily inverted, and Equation (85) can be solved for the next-boundary temperatures:

$$\bar{T}^i = A_i \bar{T}^{i-1} \quad (87)$$

where $A_i = B_i^{-1} C_i$

If the properties are known at every region (say, from previous iteration) the matrices A_i can be constructed for every region. Then, the values at $z=L$ can be linked to the value at $z=0$:

$$\bar{T}(L) \equiv \bar{T}^N = A_N \bar{T}^{N-1} = \dots = A_N A_{N-1} \dots A_1 \bar{T}^0 = A \bar{T}^0 \equiv A \bar{T}(0) \quad (88)$$

Returning to the equation form:

$$\begin{cases} T_1(L) = a_{11}T_1(0) + a_{12}T_2(0) + a_{13}T_3(0) \\ T_2(L) = a_{21}T_1(0) + a_{22}T_2(0) + a_{23}T_3(0) \\ T_3(L) = a_{31}T_1(0) + a_{32}T_2(0) + a_{33}T_3(0) \end{cases} \quad (89)$$

In system (89), the coefficients a_{ij} of matrix A are known (they are calculated through the properties at the temperatures obtained in the previous iteration); $T_1(0)$ and $T_2(0)$ are given. Using the third boundary condition from (82), $T_3(0)$ can be calculated:

$$T_2(L) = T_3(L) \Rightarrow a_{21}T_1(0) + a_{22}T_2(0) + a_{23}T_3(0) = a_{31}T_1(0) + a_{32}T_2(0) + a_{33}T_3(0) \quad (90)$$

$$\Rightarrow T_3(0) = \frac{(a_{31} - a_{21}) \cdot T_1(0) + (a_{32} - a_{22}) \cdot T_2(0)}{a_{23} - a_{33}}$$

Once $T_3(0)$ is found, all three temperatures at all the region boundaries can be found using (87). Then, the average temperatures for every region are:

$$T_j^{i,av} = \frac{T_j^i + T_j^{i-1}}{2}, \quad i = 0 \dots N, \quad j = 1, 2, 3 \quad (91)$$

The properties and coefficients k 's and n 's are to be recalculated at these average temperatures and matrices B_i , B_i^{-1} , C_i , A_i , A and temperatures are recalculated, if necessary.

The outlet temperatures are:

$$T_{out,Pb} = T_1(L)$$

$$T_{out,SF} = T_3(0) \quad (92)$$

Although presented here for the trapezoidal rule, this approach can easily be adopted for any other numerical approximation. The logic remains the same, and only the coefficients of matrices B_i and C_i in Equation (86) would change.

RHX Type 3: Concentric Tubes Heat Exchanger

In this design concentric tubes for the secondary fluid are used. The secondary fluid comes down inside the inner tube, enters the outer tube at the bottom of the heat exchanger, comes up inside the outer tube and leaves the heat exchanger at the top. Lead flows around the outside tube (APPENDIX A, Figure A.3).

The number of the tubes is found similar to that in the U-tubes HX, with d meaning the outer diameter of the outer tube.

Tube Diameters

Although the diameters of the inner and outer tubes can be set directly by the user, for the purpose of this work the tube dimensions is selected such that the flow areas for both the secondary fluid flows are equal. This will provide equal speed for the flows. From Figure 26, the equal flow areas condition gives:

$$\frac{\pi \cdot d_i'^2}{4} = \frac{\pi \cdot d_i^2}{4} - \frac{\pi \cdot d_o'^2}{4} \quad (93)$$

$$d_i = \sqrt{d_i'^2 + (d_i' + 2 \cdot t_w)^2}$$

$$d_o = d_i + 2 \cdot t_w$$

where t'_w and t_w – inner and outer tube wall thicknesses, respectively.

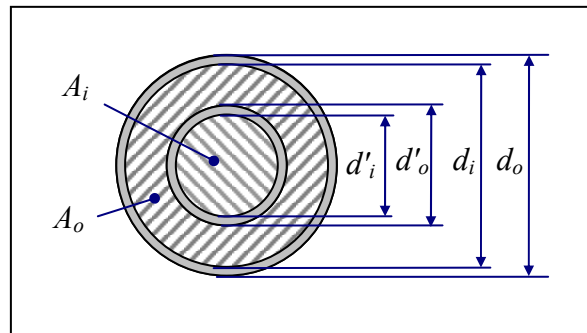


Figure 26. Flow areas in concentric tubes.

Approach to Solve for Outlet Temperatures

The approach to the solution is very similar to the previous case. If we assign index 1 to the upward secondary fluid flow, index 2 to the downward secondary fluid flow and index 3 to the lead, the equations described for the U-tubes HX remain the same with few exceptions.

The heat transfer coefficients now reflect heat transfer through the inner and outer walls of the outer tube:

$$H_{12} = \frac{1}{\frac{1}{2\pi \cdot r'_o \cdot h_1} + \frac{\ln(r'_o/r'_i)}{2\pi \cdot k_w} + \frac{1}{2\pi \cdot r'_i \cdot h_2}}$$

$$H_{13} = \frac{1}{\frac{1}{2\pi \cdot r_i \cdot h_1} + \frac{\ln(r_o/r_i)}{2\pi \cdot k_w} + \frac{1}{2\pi \cdot r_o \cdot h_3}}$$

where r'_i, r'_o – inner tube inner and outer radii,
 r_i, r_o – outer tube inner and outer radii.

The boundary conditions are:

$$\begin{cases} T_3(0) = T_{in,Pb} \\ T_2(0) = T_{in,SF} \\ T_1(L) = T_2(L) \end{cases}$$

Because of the different boundary conditions, Equation (90) is to be solved for $T_1(0)$, instead of $T_3(0)$.

The outlet temperatures are:

$$\begin{aligned} T_{out,Pb} &= T_3(L) \\ T_{out,SF} &= T_1(0) \end{aligned}$$

RHX Type 4: Straight Tubes Heat Exchanger

In this design, the secondary fluid flows through the straight tubes upward from the bottom of the heat exchanger. The secondary fluid is delivered to the bottom of the heat exchanger through the areas which are blocked for the lead flow (APPENDIX A, Figure A.4). Then the secondary fluid is distributed through the tubes and flows inside the tubes.

Number of Tubes

To find the number of the tubes, first it is necessary to determine the area required for the downward secondary fluid. The condition used here is similar to that used in the Concentric tubes HX analysis: the total flow area for the downward secondary fluid is equal to the total flow area of the upward secondary fluid. From Figure 27 these areas are:

$$A_{\downarrow} = \frac{D_o - D_i}{2} \cdot \Delta g \cdot N_{HX} \quad (94)$$

$$A_{\uparrow} = f_{SF} \cdot A_{HX}$$

where

D_o, D_i – heat exchanger annulus outer and inner diameters,

Δg – width of the area for down coming secondary fluid measured at the annulus' middle diameter,

N_{HX} – number of the heat exchangers,

f_{SF} – fraction of HX cross section area occupied by the secondary fluid (see Table 8),

A_{HX} – HX cross section area:

$$A_{HX} = \left[\pi \frac{D_o + D_i}{2} - N_{HX} (gap + \Delta g) \right] \cdot \frac{D_o - D_i}{2}$$

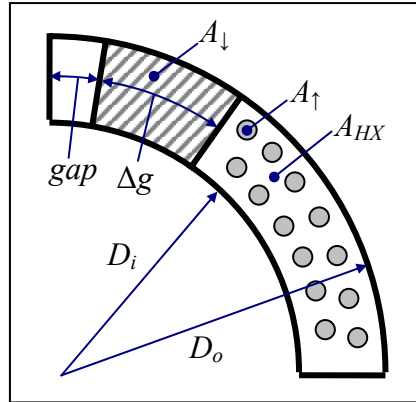


Figure 27. Straight tubes HX flow areas.

Table 8. Fraction of RHX cross section area occupied by secondary fluid

Lattice	Triangular	Square
Channel area	$A_{ch} = \frac{\sqrt{3}}{4} p^2$	$A_{ch} = p^2$
Secondary fluid area per channel	$A_{SF} = \frac{1}{2} \frac{\pi \cdot d_i^2}{4}$	$A_{SF} = \frac{\pi \cdot d_i^2}{4}$
$f_{SF} = \frac{A_{SF}}{A_{ch}}$	$f_{SF} = \frac{\pi}{2\sqrt{3}} \left(\frac{d_i}{p} \right)^2$	$f_{SF} = \frac{\pi}{4} \left(\frac{d_i}{p} \right)^2$

Setting the flow area of equation (94) equal to each other, the Δg could be found:

$$\frac{D_o - D_i}{2} \cdot \Delta g \cdot N_{HX} = f_{SF} \cdot \left[\pi \frac{D_o + D_i}{2} - N_{HX} (gap + \Delta g) \right] \cdot \frac{D_o - D_i}{2} \quad (95)$$

$$\Rightarrow \Delta g = \frac{f_{SF} \cdot \left[\pi \frac{D_o + D_i}{2} - N_{HX} \cdot gap \right]}{N_{HX} (1 + f_{SF})}$$

The number of tubes in the heat exchanger can now be found in a similar way to the U-tubes HX (Equation (78)) except that the gap should be increased by Δg and the tube area in Table 7 should be equal to the channel area since for the straight tubes one channel means one tube.

Approach to Solve for Outlet Temperatures

Since this is a simple shell-and-tube counter flow heat exchanger, the approach to solve for the outlet temperatures is exactly the same as the one used for a recuperator model.

It is assumed that there is no heat transfer to the downward secondary fluid. This is a good assumption since a channel for the downward secondary fluid is very large while the secondary fluid heat transfer coefficient is low. Under this assumption, the temperature of the secondary fluid entering tubes from the bottom is equal to the secondary fluid temperature at the heat exchanger inlet, which is given.

RHX Type 5: Straight Annuli Heat Exchanger

This concept is similar to the Straight tubes HX. The secondary fluid is delivered to the bottom of a heat exchanger, is distributed to between tubes and flows upward in the tubes. The difference of this RHX type is that it uses the concentric tubes, like in the Concentric tubes HX. However, the lead flows inside the inner tube and outside the outer tubes and the secondary fluid flows between the inner and outer tubes (APPENDIX A, Figure A.5). This approach is advantageous because it increases heat transfer surface, since there are two tube walls instead of one.

Number of tubes

The number of the tubes is calculated similar to the Straight tubes HX. The only difference is the secondary fluid flow area per channel (Table 8), which is now defined as:

$$A_{SF} = \begin{cases} \frac{1}{2}\pi(r_i^2 - r_o'^2) & \text{for triangular lattice} \\ \pi(r_i^2 - r_o'^2) & \text{for square lattice} \end{cases} \quad (96)$$

where

r_i – inner radius of outer tube,

r'_o – outer radius of inner tube.

Approach to Solve for Outlet Temperatures

If we assign indexes to the flows such as 1 will mean the lead flow outside the tubes, 2 will mean the secondary fluid flow between the tubes and 3 will be the lead flow inside the inner tube; then the heat balance equation (system (64)) for this system will look like this:

$$\begin{cases} \frac{dT_1}{dz} = -\frac{H_{12}}{m_1 \cdot Cp_1} (T_1(z) - T_2(z)) \\ \frac{dT_2}{dz} = -\frac{H_{12}}{m_2 \cdot Cp_2} (T_1(z) - T_2(z)) - \frac{H_{32}}{m_2 \cdot Cp_2} (T_3(z) - T_2(z)) \\ \frac{dT_3}{dz} = -\frac{H_{32}}{m_3 \cdot Cp_3} (T_3(z) - T_2(z)) \end{cases} \quad (97)$$

where

$$H_{12} = \frac{1}{\frac{1}{2\pi \cdot r_o \cdot h_1} + \frac{\ln(r_o/r_i)}{2\pi \cdot k_w} + \frac{1}{2\pi \cdot r_i \cdot h_2}}$$

$$H_{32} = \frac{1}{\frac{1}{2\pi \cdot r'_i \cdot h_3} + \frac{\ln(r'_o/r'_i)}{2\pi \cdot k_w} + \frac{1}{2\pi \cdot r'_o \cdot h_2}}$$

r_i, r_o – outer tube inner and outer radii,

r'_i, r'_o – inner tube inner and outer radii (see Figure 26).

The mass flow rates of lead flows are found based on a condition that the frictional pressure drop for both flows is equal. Assuming that the properties (density and friction factors) of these flows are approximately equal, the frictional pressure loss is proportional to the square of the flow speed. Therefore, the squares of the speed, or speeds, are equal to both flows. The speed is related to the mass flow rate and the flow area:

$$m = \rho \cdot u \cdot A \quad \Rightarrow \quad u = \frac{m}{\rho \cdot A} \quad (98)$$

Again, assuming equal properties, the ratio of the mass flow rate to the flow area is the same for both flows. Using a condition that the total mass flow rate per tube of lead (m_{pb}) is given, the mass flow rates for both lead flows can be found:

$$\begin{aligned} m_1 &= m_{pb} \frac{A_1}{A_1 + A_3} \\ m_3 &= m_{pb} \frac{A_3}{A_1 + A_3} \end{aligned} \quad (99)$$

where A_1 and A_3 – flow areas of the lead flows, i.e. flow area outside the tubes and inside inner tube, respectively.

The boundary conditions for the system (97) are:

$$\begin{cases} T_1(0) = T_{in,Pb} \\ T_2(L) = T_{in,SF} \\ T_3(0) = T_{in,Pb} \end{cases} \quad (100)$$

Introducing the coefficients k and n , like before, the system (97) can be rewritten as:

$$\begin{cases} \frac{dT_1}{dz} = -k_{12}(T_1(z) - T_2(z)) \\ \frac{dT_2}{dz} = -k_{12} \cdot n_{12}(T_1(z) - T_2(z)) - k_{32} \cdot n_{32}(T_3(z) - T_2(z)) \\ \frac{dT_3}{dz} = -k_{32}(T_3(z) - T_2(z)) \end{cases} \quad (101)$$

$$\text{where } k_{12} = \frac{H_{12}}{m_1 \cdot Cp_1} \quad n_{12} = \frac{m_1 \cdot Cp_1}{m_2 \cdot Cp_2}$$

$$k_{32} = \frac{H_{32}}{m_3 \cdot Cp_3} \quad n_{32} = \frac{m_3 \cdot Cp_3}{m_2 \cdot Cp_2}$$

The solution is similar to the process described for the Concentric tubes HX with the following matrix D :

$$D = \begin{pmatrix} -k_{12} & k_{12} & 0 \\ -k_{12} \cdot n_{12} & k_{12} \cdot n_{12} + k_{32} \cdot n_{32} & -k_{32} \cdot n_{32} \\ 0 & k_{32} & -k_{32} \end{pmatrix} \quad (102)$$

The initial value for the secondary fluid temperature is found from the second boundary condition (100) and solution (83):

$$T_2(0) = \frac{T_{in,SF} - (a_{21} + a_{23})T_{in,Pb}}{a_{22}} \quad (103)$$

The heat exchanger outlet temperatures for the secondary fluid flow and the lead flow are:

$$\begin{cases} T_{out,SF} = T_2(L) \\ T_{out,Pb} = \frac{m_1 T_1(L) + m_3 T_3(L)}{m_1 + m_3} \end{cases} \quad (104)$$

RHX Type 6: Helical Coil Heat Exchanger

This heat exchanger uses helical coil tubes rather than straight tubes. As in the Straight tubes HX, the secondary fluid is delivered to the bottom of the heat exchanger through the central section, which consists of the straight portions of tubes collected together. Then the tubes turn around and the fluid flows upward through helical portion of the tubes around the straight tube bundle. The tubes are collected into several groups (rings) (APPENDIX A, Figure A.6).

Number of tubes

First, it is necessary to calculate the number of the heat exchangers (tube bundles), i.e. the number of circles that can be fitted into the heat exchanger annulus. The maximum possible diameter of the heat exchanger is the annulus width. The available space for the heat exchangers is the distance between the gaps (Figure 28).

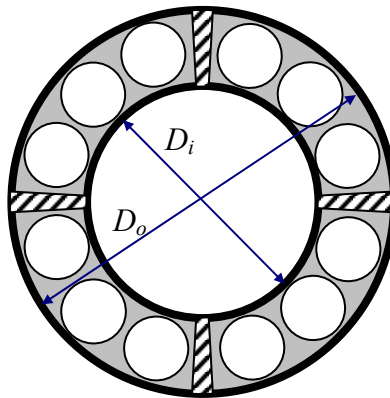


Figure 28. Number of the helical coil HXs.

The ratio of these two distances gives the number of heat exchangers that can be fitted between the two gaps; this number is multiplied by the number of gaps to get the total number of heat exchangers:

$$N_{HX} = \left[\frac{\frac{\pi \frac{D_o + D_i}{2} - gap}{N_{gap}}}{\frac{D_o - D_i}{2}} \right] N_{gap} \quad (105)$$

with square brackets meaning taking the nearest integer of the argument.

Since the number of the heat exchangers is rounded to an integer number, the outer diameter of the heat exchanger might differ from the annulus width:

$$D_{max} = \min \left\{ \frac{\pi \frac{D_o + D_i}{2} - N_{gap} \cdot gap}{N_{HX}}, \frac{D_o - D_i}{2} \right\} \quad (106)$$

The number of tubes per one ring is the ratio of a tube elevation per one twist to the tube pitch in vertical direction (Figure 29) (Smith, 1997):

$$n = \frac{H_1}{p_H} = \frac{H/k}{p/\cos(\varphi)} = \frac{H}{k \cdot p} \frac{1}{\sqrt{1 + \left(\frac{H}{k \cdot \pi \cdot D} \right)^2}} \quad (107)$$

where

H – heat exchanger height,

p – tube lattice pitch, measured in the direction perpendicular to the tube axis,

k – number of twists of one tube in the heat exchanger,

D – tube ring diameter,

p_H – pitch in vertical direction = $\frac{p}{\cos(\varphi)}$,

H_1 – elevation per one twist = $\frac{H}{k}$,

$$\varphi - \text{tube elevation angle, } \cos(\varphi) = \frac{\pi \cdot D}{\sqrt{(\pi \cdot D)^2 + (H_1)^2}} = \frac{1}{\sqrt{1 + \left(\frac{H_1}{\pi \cdot D}\right)^2}}$$

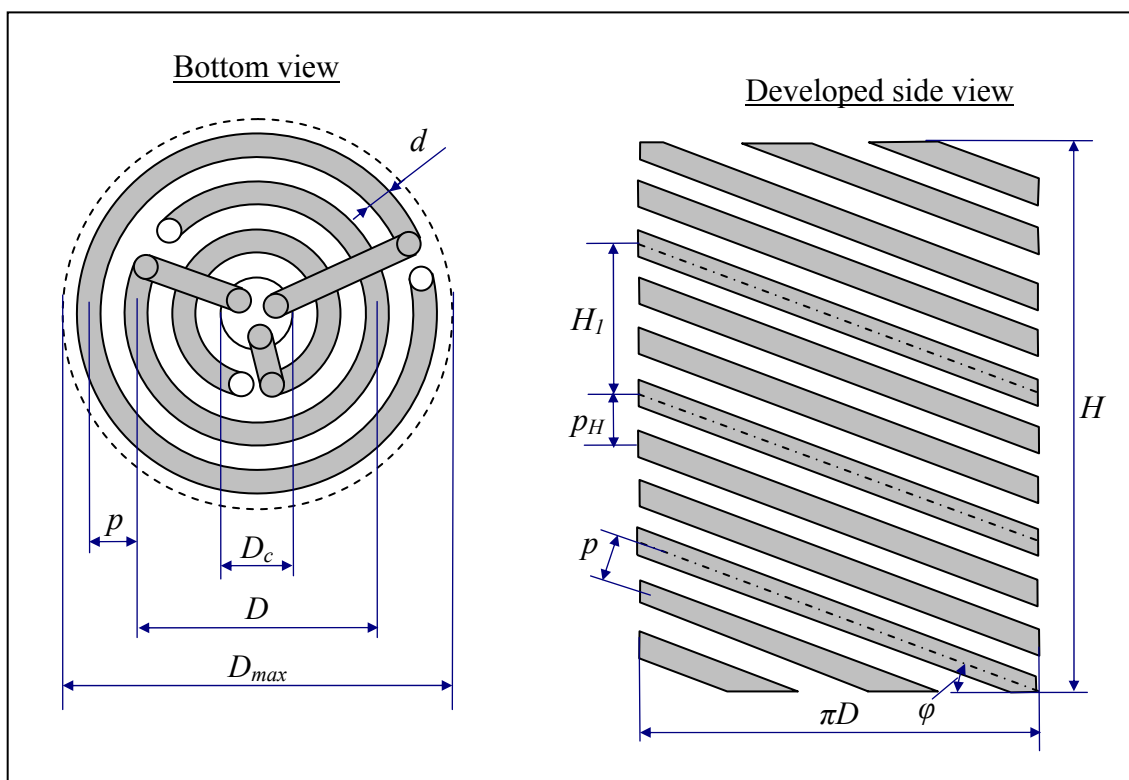


Figure 29. Dimensions of helical coil HX.

The diameter of the j^{th} ring, which defines through (107) the number of tubes in that ring, is:

$$D_j = D_c + 2 \cdot p \cdot j - 2 \cdot \frac{p}{2} = D_c + (2j - 1)p \quad (108)$$

where D_c – diameter of the central part of the HX (Figure 29).

The condition to find the number of rings (J) per one heat exchanger is that the diameter of the outer ring plus one tube pitch is not greater than the diameter of the heat exchanger:

$$D_c + 2 \cdot J \cdot p \leq D_{\max} \quad (109)$$

Since the central part of the heat exchanger is the bundle of all tubes, its cross sectional area is equal to the cross sectional area of the bundle of the tubes packed with triangular pitch equal to the tube diameter:

$$\frac{\pi \cdot D_c^2}{4} = \sum_{j=1}^J n_j \cdot \frac{\sqrt{3}}{2} d^2 \quad (110)$$

As it follows from Equation (107), the number of the tubes in each ring depends on the ring's diameter, which is the function of D_c (Equation (108)). Moreover, the total number of rings also depends on the D_c (equation (109)). Therefore, the diameter of the central part cannot be found directly. Instead, it is assumed that the total number of tubes in all rings is approximately equal to the number of tubes in an “average” ring, times the number of rings:

$$\sum_{j=1}^J n_j \approx \bar{n} \cdot J \quad (111)$$

where the number of the tubes in average ring is calculated by (107) for the average ring

$$\text{diameter } D = \frac{D_{\max} + D_c}{2}.$$

And the diameter of the central part is a function of the number of rings becomes:

$$D_c(J) = \sqrt{\frac{2\sqrt{3}}{\pi} \bar{n} J d} \quad (112)$$

Still, the average ring diameter is the function of D_c , so iterations on the diameter of the central section are required. Inside each iteration, the number of rings is increased (1,2,3,...) to find the maximum value at which the condition (109) holds.

When the number of rings, the diameter of the central part and the average ring diameter are found, the number of the tubes per heat exchanger can now be defined by (111) and the total number of tubes is:

$$N_t = N_{HX} \cdot \bar{n} \cdot J \quad (113)$$

where \bar{n} is calculated by (107) at average ring diameter D .

Approach to Solve for Outlet Temperatures

The approach to solve for temperatures at the RHX outlet is similar to that used for the Straight tube HX. The differences are the number of tubes (defined by (113)), the tube length and the heat transfer and friction factor correlations.

The tube length could be found from Figure 29:

$$L = k \cdot L_1 = k \cdot \sqrt{(\pi \cdot D)^2 + (H_1)^2} = k \cdot \pi \cdot D \cdot \sqrt{1 + \left(\frac{H}{k \cdot \pi \cdot D}\right)^2} \quad (114)$$

The heat transfer and friction factor correlations used here for the secondary fluid inside the tubes are those recommended by Mori and Nakayama (Smith, 1997) for helical coil heat tubes.

RHX Type 7: Plate Type Heat Exchanger with U-Turn

In the STAR-H2 system both the primary lead loop and the secondary molten salt loop operate at atmospheric pressure. No pressure difference between the two flows in the RHX makes it possible to use a plate type heat exchanger. Since the secondary fluid enters and leaves the heat exchanger at the top, the secondary fluid flow should turn around at the bottom (APPENDIX A, Figure A.7).

Number of Channels

One channel is considered to be the secondary fluid layer and the lead layer (Figure 30). The secondary fluid flow is either upward or downward direction, so there are two channels per one secondary fluid-lead layer. The number of the channels is two times the number of layers which can fit into the annulus region:

$$N_{ch} = 2 \cdot N_l = 2 \cdot \frac{\frac{D_o - D_i}{2}}{p} = \frac{D_o - D_i}{p} \quad (115)$$

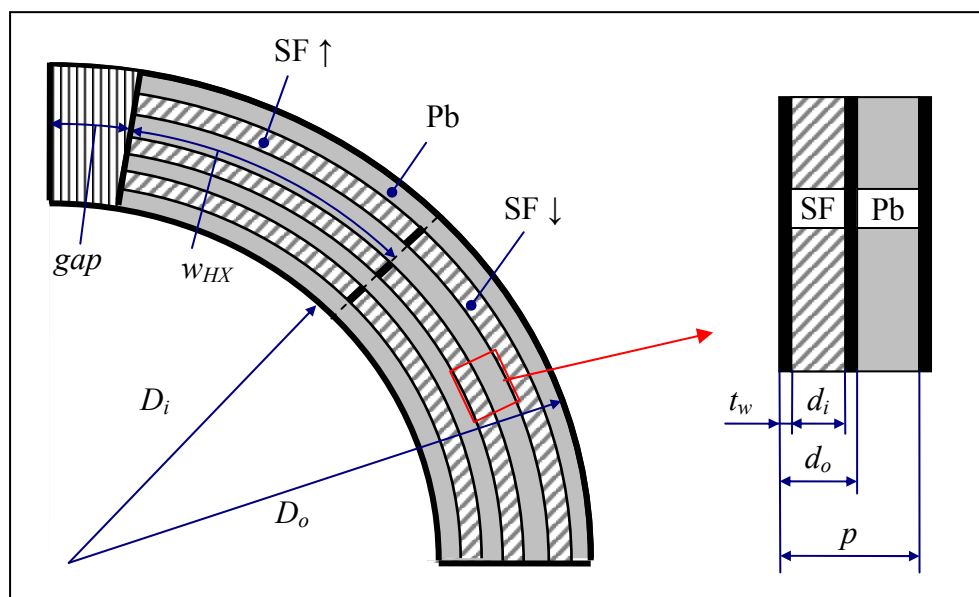


Figure 30. Plate type RHX.

The channel width, w , is defined as (Figure 30):

$$w = N_{HX} \cdot w_{HX} = \frac{\pi \frac{D_o + D_i}{2} - N_{HX} \cdot gap}{2} \quad (116)$$

The approach used to solve for the outlet temperatures is identical to that used for the Stacked U-tubes HX. The difference will occur in the heat transfer coefficient, which in the case of plate geometry is:

$$H_{1j} = \frac{w}{\frac{1}{h_1} + \frac{t_w}{k_w} + \frac{1}{h_j}}, \quad j = 2,3 \quad (117)$$

RHX Type 8: Counter Flow Plate Type Heat Exchanger.

This design for the heat exchanger is something between the Straight tubes and the Plate type with U-turn designs. It uses plate geometry, like Plate type with U-turn HX, but instead of the U-turn, the secondary fluid is delivered to the bottom of the heat exchanger through a separated area, like in the Straight tubes HX (Appendix I, Figure I.8).

Number of Channels

As in the Straight tube HX, it is first necessary to find the width of the area needed for the downward secondary fluid. The approach is the same, i.e. the cross section area for the upward and downward secondary fluid flows is the same. The flow area for the downward secondary fluid is exactly as it is defined in equation (94); the flow area for the upward secondary fluid flow is (Figure 30):

$$A_{\uparrow} = N_{ch} \cdot w \cdot d_i \quad (118)$$

where

$$w = N_{HX} \cdot w_{HX} = \pi \frac{D_o + D_i}{2} - N_{HX} \cdot (gap + \Delta g) \quad \text{- channel width,}$$

$$N_{ch} = N_l = \frac{\frac{D_o - D_i}{2}}{p} = \frac{D_o - D_i}{2p} \quad \text{- number of channels.}$$

Note that in this case the number of channels is equal to the number of layers since there is only one secondary fluid flow in the heat exchanging area.

From equations (94) and (118), the width of the down coming secondary fluid area is:

$$\Delta g \cdot \frac{D_o - D_i}{2} \cdot N_{HX} = N_{ch} \cdot d_i \cdot \left[\pi \frac{D_o + D_i}{2} - N_{HX} \cdot (gap + \Delta g) \right] \quad (119)$$

$$\Rightarrow \Delta g = \frac{N_{ch} \cdot d_i \cdot \left[\pi \frac{D_o + D_i}{2} - N_{HX} \cdot gap \right]}{N_{HX} \left[\frac{D_o - D_i}{2} + N_{ch} \cdot d_i \right]}$$

The approach to solve for the outlet temperatures is the same is that used for the Straight tube HX with the exception of heat transfer coefficient, which is to be calculated for this case using Equation (117).

RHX Type 9: HEATRIC Heat Exchanger

HEATRIC heat exchanger is a printed circuit heat exchanger where both fluids flow through semi-circular channels. These channels are chemically milled inside the metal plates (Figure 31). This technology can produce very small channels, as low as 0.5mm in diameter. Since HEARTIC is a counter-flow heat exchanger, the secondary

fluid is delivered to the bottom of the heat exchanger through the special channel, similar to the straight tube design. (APPENDIX A, Figure A.9)

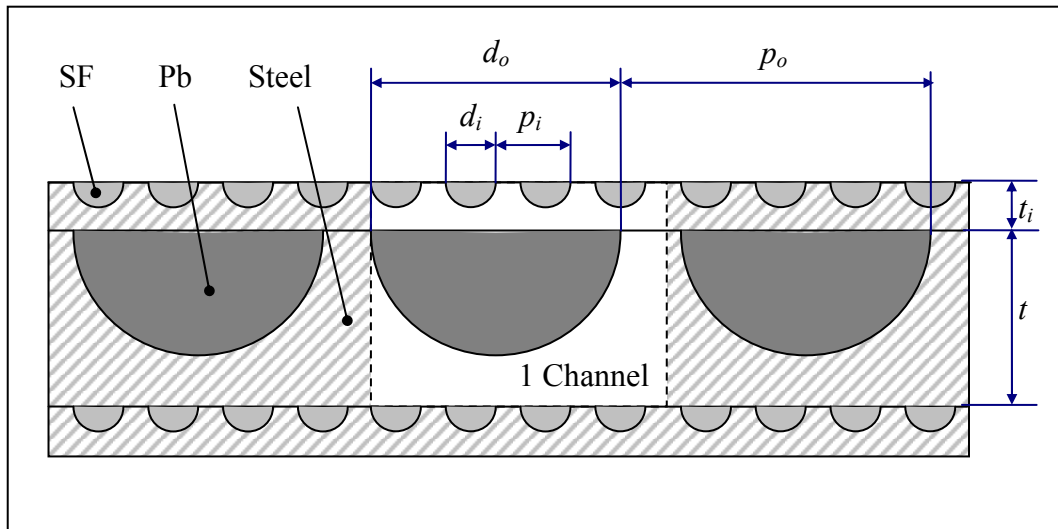


Figure 31. HEATRIC HX channel.

To simplify the calculations, several assumptions were made:

- p/d on the lead side is equal to the p/d on the secondary fluid side, $p_i/d_i = p_o/d_o$
- Lead channel diameter is a multiple of the secondary fluid channel diameter, $d_o = kd_i$
- Heat transfer occurs from a lead channel to the secondary fluid channels which are close to the lead channels (upper secondary fluid layer on the Figure 31).
- Secondary fluid channel layer thickness is equal to the channel diameter, $t_i = d_i$
- Lead channel layer thickness is the channel radius plus 2 mm, $t = d_o/2 + 2 \text{ mm}$

First two assumptions provide the integer number of the secondary fluid channels per one lead channel. The last two assumptions reduce the number of parameters for the HX performance optimization.

Number of Channels

The number of rows (lead and secondary fluid layers) can be calculated through the heat exchanger annulus and the row thickness:

$$n_{rows} = \frac{\frac{D_o - D_i}{2}}{t + t_i} = \frac{\frac{D_o - D_i}{2}}{t + \frac{d_o}{k}} \quad (120)$$

To calculate the number of channels per one layer, the place occupied by the downward secondary fluid should be calculated first. The algorithm to find the width of this area, Δg , is similar to that described for the Straight tube HX (Equations (94) – (95)) with fraction of cross section area occupied by the secondary fluid defined from Figure 31:

$$f_{SF} = \frac{\frac{1}{2} \frac{\pi \cdot d_i^2}{4} k}{(t + t_i) \cdot p_o} = \frac{\pi \left(\frac{d_o}{k}\right)^2 k}{8 \left(t + \frac{d_o}{k}\right) \cdot (p/d) \cdot d_o} = \frac{\pi}{8} \frac{1}{\left(k \frac{t}{d_o} + 1\right) \cdot (p/d)} \quad (121)$$

Then, the number of the channels per one row is:

$$N_{ch}^{row} = \frac{\pi \frac{D_o + D_i}{2} - N_{HX}(gap + \Delta g)}{p_o} = \frac{\pi \frac{D_o + D_i}{2} - N_{HX}(gap + \Delta g)}{(p/d)d_o} \quad (122)$$

And the total number of channels is:

$$N_{ch} = N_{ch}^{row} n_{rows} \quad (123)$$

The number of lead channels is equal to the N_{ch} , while the number of the secondary fluid channels is k times bigger.

Approach to Solve for Outlet Temperatures

The approach to solve for the outlet temperature is similar to the Straight tube HX with a total heat transfer coefficient calculated under assumption of heat transfer from the wall to the row of tubes. This assumption is good since the lead channel is much larger than the secondary fluid channel (k is large) and the lead channel could be approximated as a wall for a secondary fluid channel. The total heat transfer coefficient for one secondary fluid channel is (VanSant, 1983):

$$HP_1 = \frac{1}{\frac{1}{2\pi \cdot r_i \cdot h_2} + \frac{1}{2\pi \cdot k_w} \ln \left\{ \frac{t_i}{\pi \cdot (d_i/p_i) \cdot r_i} \sinh \left[2\pi \cdot (d_i/p_i) \cdot \left(1 + \frac{k_w}{t_i h_2} \right) \right] \right\}} \quad (124)$$

where

h_1, h_2 – heat transfer coefficients on lead and secondary fluid sides, respectively,

k_w – wall thermal conductivity.

Since the amount of heat transferred per one lead channel is equal to the sum of heats transferred for all secondary fluid channels, the total heat transfer coefficient for one lead channel is (using assumptions described above):

$$HP = k \cdot HP_1 = \frac{k}{\frac{1}{\pi \cdot d_i \cdot h_2} + \frac{1}{2\pi \cdot k_w} \ln \left\{ \frac{2p/d}{\pi_i} \sinh \left[\frac{2\pi}{p/d} \left(1 + \frac{k_w}{d_i h_2} \right) \right] \right\}} \quad (125)$$

Heat Transfer and Friction Factor Correlations

The following heat transfer correlations were used in the model:

- Secondary fluid flow inside the straight or U-tubes:

$$Nu = 0.023 \cdot Re^{0.8} \cdot Pr^{0.3} \text{ - Dittus-Boelter (Todreas and Kazimi, 1990).}$$

- Lead flow outside the tube bundle:

$$Nu = 7.55 \cdot (p/d) - 14/(p/d)^5 + 0.007 \cdot (Re \cdot Pr)^{0.64+0.246 \cdot p/d} \text{ (Zhukov et al., 2002).}$$

- Secondary fluid flow inside helical coiled tubes:

$$Nu = \frac{Pr \cdot Re^{0.8} \cdot (d/D)^{0.1} \left[1 + \frac{0.098}{Re \cdot (d/D)^2} \right]}{26.2 \cdot Pr^{0.666} - 0.074} \text{ - Mori and Nakayama (Smith, 1997).}$$

For the friction factor the following correlations were used:

- Secondary fluid flows inside straight tubes and lead flow:

$$\frac{1}{\sqrt{f}} = 1.74 - 2 \log \left(\frac{2k}{d} + \frac{18.7}{Re \sqrt{f}} \right) \text{ - Colebrook and White (Kestin, 1960).}$$

- Secondary fluid flow inside helically coiled tubes:

$$f = \frac{0.305 \left[1 + \frac{0.112}{Re \cdot (d/D)^2} \right] \sqrt{(d/D)}}{4 \left[Re \cdot (d/D)^2 \right]^{0.2}} \text{ - Mori and Nakayama (Smith, 1997).}$$

Heat Transfer Enhancement

The results of the reactor heat exchanger module calculations, which will be discussed in more details below, showed that the heat exchanger performance is far from its theoretical limits. In particular, the secondary fluid outlet temperature is below the lead inlet temperature. To improve the RHX performance, the effect of the tube projections on the heat transfer was investigated.

The projections (Figure 32) rough the tube surface and, therefore, increase heat transfer and friction losses. The projections are characterized by the projection height (e), pitch (t), and angle (α). Usually, the projection height and pitch are measured relative to the tube diameter, e/d and t/d respectively, and the angle is measured relative to 90 degrees, $\alpha/90$.

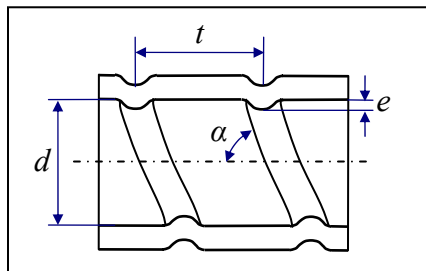


Figure 32. Tube projections.

The range of possible projections parameters is:

$$e/d: 0.01 \text{ to } 0.1$$

$$t/d: 0.25 \text{ to } 10.0$$

$$\alpha/90: 0.2 \text{ to } 1.0.$$

The two sets of correlations proposed by Bergles (Bergles, 1988; Ravigururajan and Bergles, 1985) and Zukauskas (Zukauskas and Kalinin, 1988) were analyzed for the Straight tube heat exchanger (Figure 33). Although the results are similar, the Zukaskas correlations do not include the projection angle dependence. Hence, the Bergels

correlations for heat transfer and friction enhancement compared to those of the straight tube were used in the further analysis:

$$\frac{Nu}{Nu_s} = \left\{ 1 + \left[2.64 \text{Re}^{0.036} \text{Pr}^{-0.024} (e/d)^{0.212} (p/d)^{-0.21} (\alpha/90)^{0.29} \right]^7 \right\}^{1/7}$$

$$\frac{f}{f_s} = \left\{ 1 + \left[29.1 \text{Re}^{(0.67-0.06 p/d-0.49 \alpha/90)} (e/d)^{(1.37-0.157 p/d)} \right. \right. \\ \left. \left. \times (p/d)^{(-1.66 \times 10^{-6} \text{Re}-0.33 \alpha/90)} (\alpha/90)^{(4.59+4.11 \times 10^{-6} \text{Re}-0.15 p/d)} \right]^{5/16} \right\}^{16/15}$$

RHX Parameters Optimization

The goal of this study is to find the optimum heat exchanger parameters that yield the maximum performance of the heat exchanger. The following parameters could vary:

- Tube diameters, inner and outer tube where applicable, (tube-based designs)
- Tube pitch-to-diameter ratio (tube-based designs)
- Tube lattice, triangular or square, (tube-based designs)
- Secondary fluid and lead channels width (plate type designs)
- Heat exchanger height
- Tube projections parameters

The optimization parameters were the Brayton cycle efficiency for the STAR-LM system and the peak cladding temperature for the STAR-H2 system. The restricting parameters are peak cladding temperature and RHX pressure drop for the STAR-LM and the STRA-H2 systems, respectively.

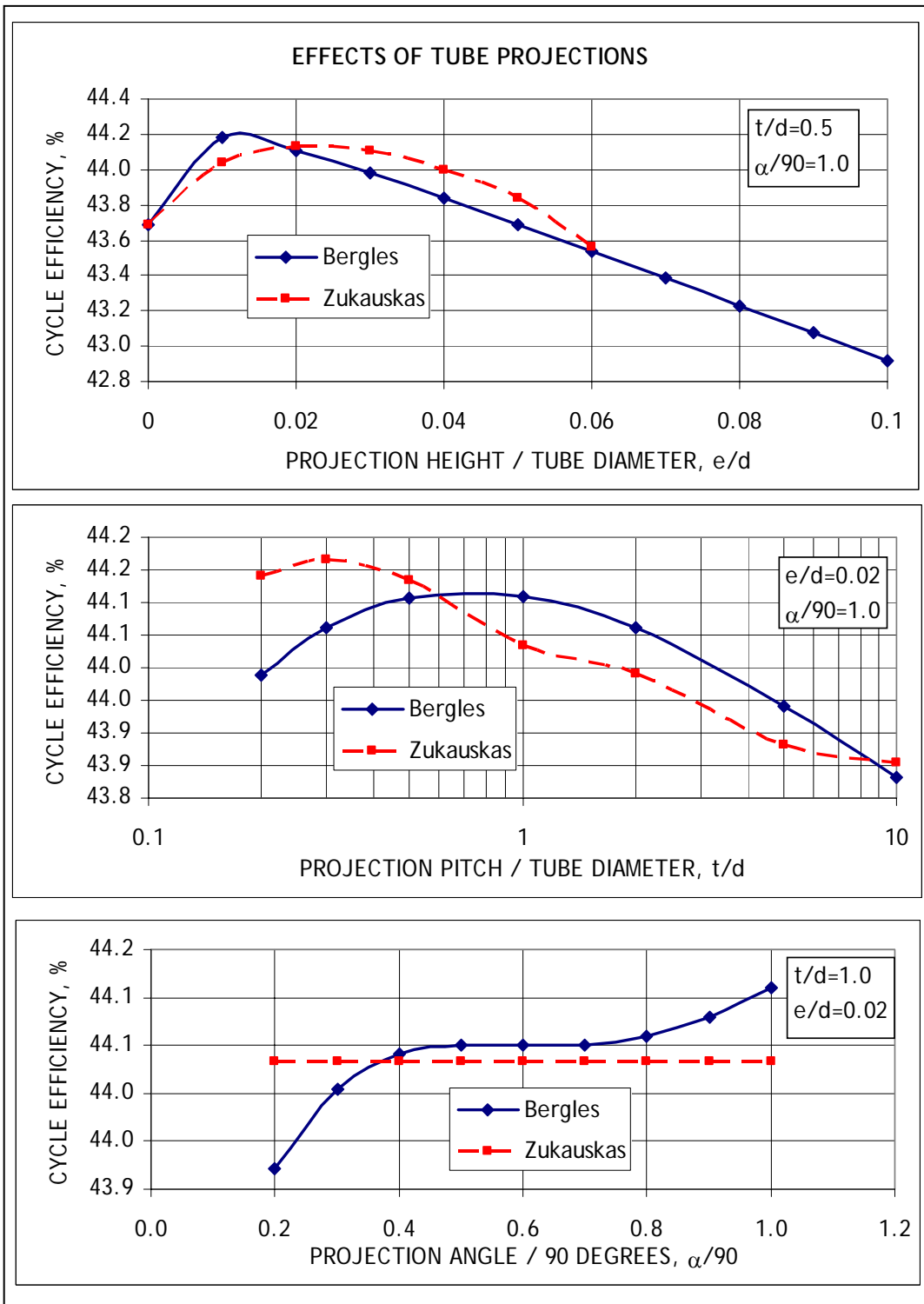


Figure 33. Comparison of the tube projections correlations.

For every type (unless stated otherwise) of heat exchanger the optimization includes the following steps:

- For fixed heat exchanger height, the tube diameter and tube pitch-to-diameter ratio was changed to find the optimal combination for triangular and square lattices.
- (Straight annuli heat exchanger only). Based on the results from the previous step, the best diameter of inner tube was selected and annulus width was optimized simultaneously with tube pitch-to-diameter ratio.
- (Helical coil heat exchanger only). The number of tube twists was optimized based on the tube diameter selection from the previous step.
- Based on the results from the previous steps, the best tube diameters (and number of twists) were selected; and tube pitch-to-diameter ratio and the heat exchanger height were changed to find the optimum performance.
- (STAR-LM only). For the designs that gave the best results (straight tubes and straight annuli), the projection height, pitch and angle were optimized.
- (STAR-LM only). With the optimal projections, and heat exchanger height selected such that the peak cladding temperature was at its limit, the optimal pitch-to-diameter ratio and optimal annulus width (for straight annuli heat exchanger) were recalculated.

The optimization process is presented in the APPENDIX B for the Straight annuli heat exchanger for the STAR-LM system.

Results and Design Comparison

The results are presented in Table 9 and Figure 34 for the STAR-LM and in Table 10 and Figure 35 for the STAR-H2 systems. The designs are compared for the CO₂ outlet temperature (and cycle efficiency) (the higher is better) for the STAR-LM system and peak cladding temperature (the lower is better) for the STAR-H2 system. Both of these parameters reflect the efficiency of the RHX. The performance is calculated at optimal heat exchanger parameters, which are also shown in the tables.

Table 9. Results of RHX optimization (STAR-LM)

No.	Type	Optimized Cycle Eff, %	Lattice	p/d	d' _i , cm	d _i ,cm	Height, m	T _{CO2} (max), °C
1	STACKED U-TUBES	41.5	Square	1.3	-	1.0	5.625	490.2
2	U-TUBES	40.0	Triangular	1.33	-	1.5	5.729	461.6
3	CONCENTRIC TUBES	39.3	Triangular	1.25	1.5	2.4	5.311	461.5
4	STRAIGHT TUBES	43.7	Triangular	1.6	-	1.0	7.076	531.5
5	STRAIGHT ANNULI	44.2	Triangular	1.2	2.0	3.0	6.147	543.0
6	HELICAL COIL	43.5	k=3.0	1.4	-	1.0	6.719	533.3
7	HEATRIC	44.1	-	1.2	0.05	1.15	2.759	546.9

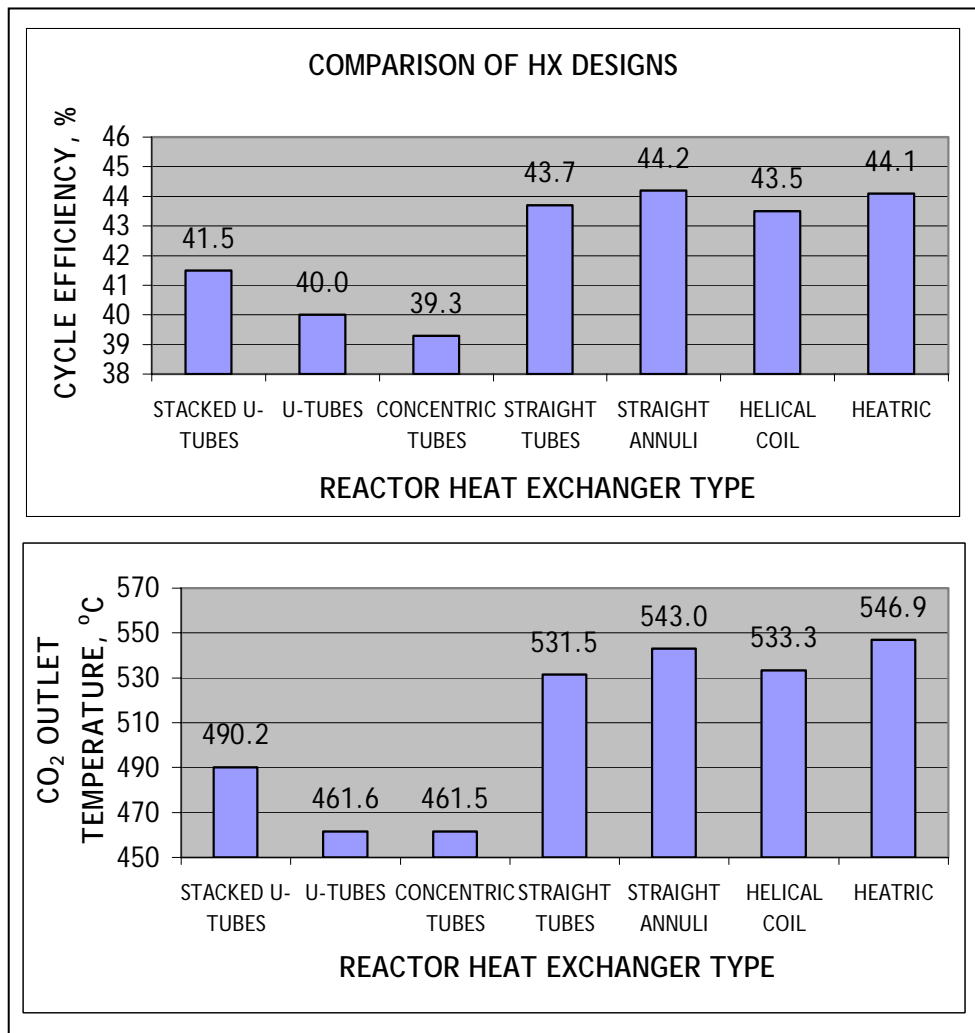
**Figure 34. Comparison of RHX designs (STAR-LM).**

Table 10. Results of RHX optimization (STAR-H2)

Type	Description	Peak Tel, °C	Lattice	p/d	d _i , cm	d _i ,cm	H,m	ΔP, atm	Core Tout, °C
1	Stacked U-Tubes	927.9	Square	1.65	-	1.0	5.0	0.18	842.9
2	U-Tube	940.0	Triangular	1.75	-	1.0	4.0	0.14	856.0
3	Concentric Tubes	929.7	Square	1.4	1.0	1.56	4.5	0.27	844.6
4	Straight Tube	903.4	Triangular	2.0	-	1.0	8.0	0.17	814.8
5	Straight Annuli	876.1	Triangular	1	2.5	2.9	3.0	2.23	787.3
6	Helical Coil	889.8	k=7.0	1.65	-	1.0	4.5	1.81	802.5
7	Plate U-Turn	922.5	Plate	5.0	-	0.25	4.0	0.65	838.6
8	Plate Type	895.4	Plate	6.0	-	0.25	7.5	0.63	807.3

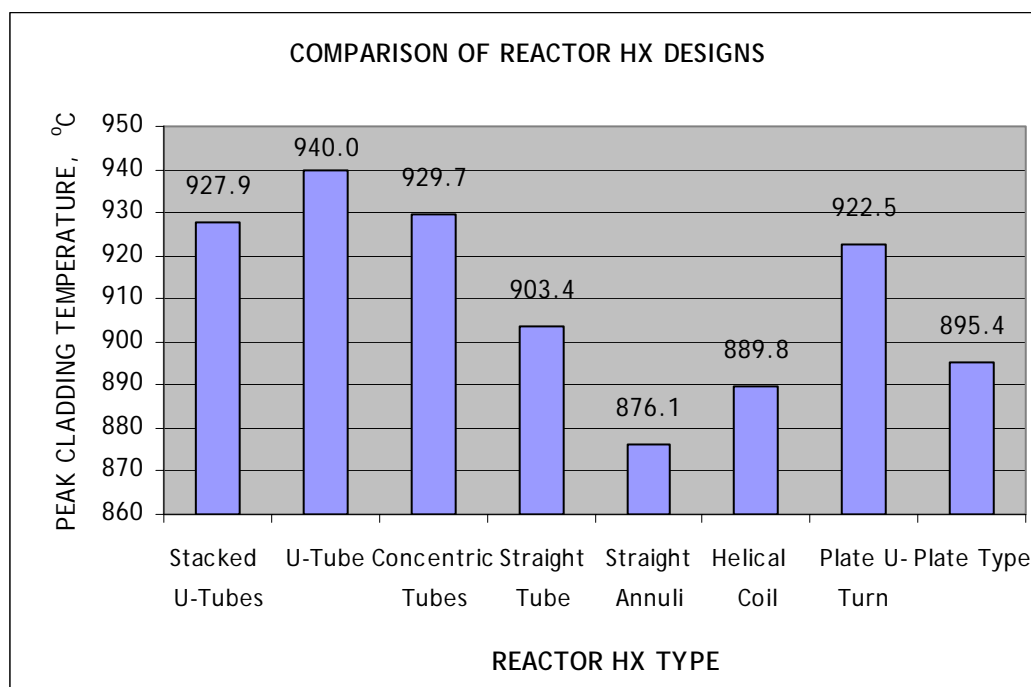
**Figure 35. Comparison of RHX designs (STAR-H2).**

Figure 36 shows (for STAR-LM) the increase in heat exchanger performance due to tube projections for the two most promising designs: the Straight tubes and the Straight Annuli heat exchangers compared to the HEATRIC design performance.

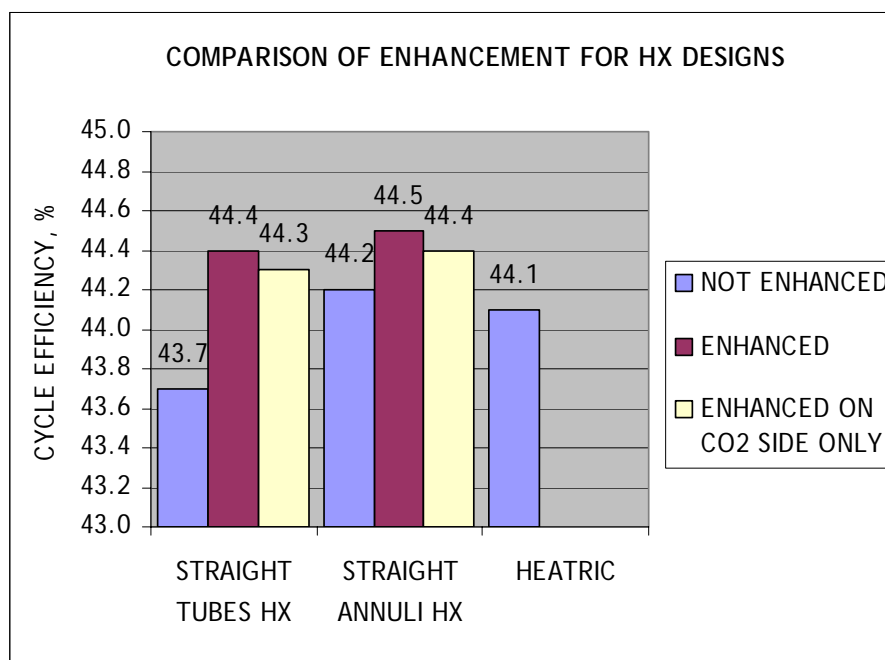


Figure 36. Effect of the tube projections.

Based on the obtained results the following observations can be made.

Straight tube designs (types 4 and 5) perform better than U-tubes and helical coil designs. The reason why the straight tubes perform better than the U-tubes can be explained using Figure 37, showing the results for the RHX types 1 (Stacked U-tubes) and 4 (Straight tubes). In the case of the U-tubes, there is a region in the bottom of the heat exchanger (large z) where the secondary fluid and the lead temperature are almost equal. Thus, based on Equation (62) the heat flow in this region is very small, meaning that there is a portion of the tube that does not work. This is not the case for the Straight tube heat exchanger, where there is the temperature difference everywhere along the tube.

The Straight Annuli design gives the best results. The reason for such performance is that this design has increased heat transfer area compared to the other designs. The secondary fluid flow area can also be selected as small as needed, which is very important for the STAR system, where the secondary fluid flow rate is approximately an order of magnitude less than the lead mass flow rate.

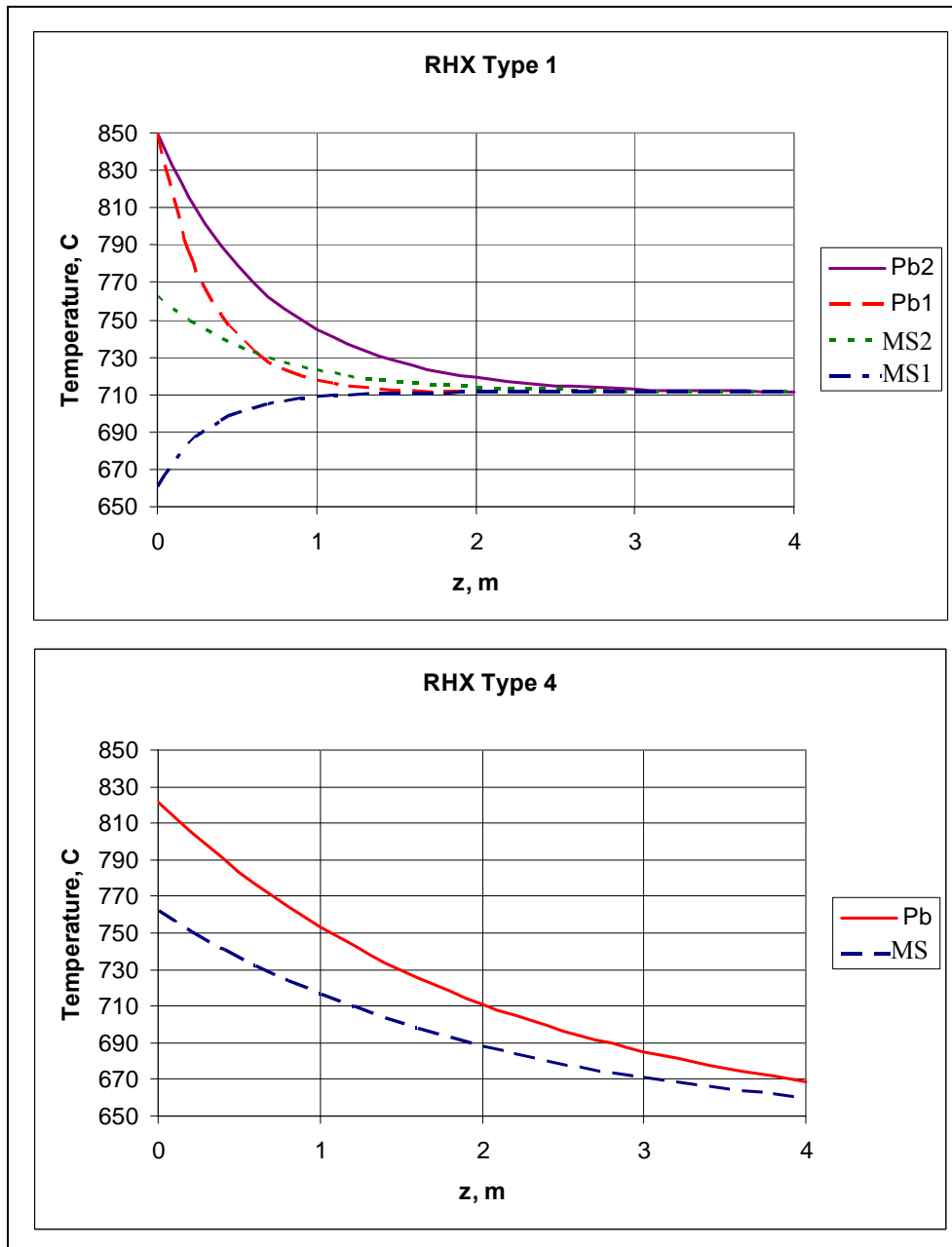


Figure 37. Temperature distribution inside U-tube (#1) and straight tube (#4).

The HETRIC heat exchanger although more compact does not perform better than the Straight annuli HX. The reason for that are narrow secondary fluid channels which increase the pressure drop in the RHX.

The triangular lattice gives better results, although the difference from a square lattice is minimal. Hence, any lattice could be selected, depending on which one is better for technological reasons. For example, for the Stacked U-tubes heat exchanger the square lattice was selected because it gives simplified upper plenum design.

The Helical coil design does not perform better than the similar straight tube design. This behavior is explained by the fact that although the tube length increases, the number of tube decreases proportionally so that the total tube length stays the same. Moreover, the cylindrical geometry of this heat exchanger leads to the loss of some space inside the annulus (Figure 28), which further decreases number of tubes in the heat exchanger, compared to the straight tube design, where the entire annulus area is available for tubes.

The Concentric tube heat exchanger with two secondary fluid flows (type 3) performs the worst. The reason for that is that heat transfer from secondary fluid to secondary fluid is worse than from lead. Therefore the downward secondary fluid is not heated as much, while taking space in the heat exchanger.

The Plate type designs do not perform much better than the tube-based designs. The possible reason can be and increase in resistance for the lead flow in a narrow channel. Increase in the channel size reduces heat transfer.

In summary, the nine different designs for reactor heat exchanger were modeled and compared. The optimal design was selected. For the two best designs, the effect of the tube projection was investigated. The total effect of this optimization and design comparison is the increase in the Brayton cycle efficiency from 40% to 44.5% for the STAR-LM system and the reduction of the peak cladding temperature in the core from 940 °C to 876 °C for the STAR-H2 system.

Results of the Steady-State Model

The input files for the steady-state model are presented in APPENDIX C. The results of calculations are shown on Figure 38 and Figure 39 for the STAR-LM and the STAR-H2 systems, respectively.

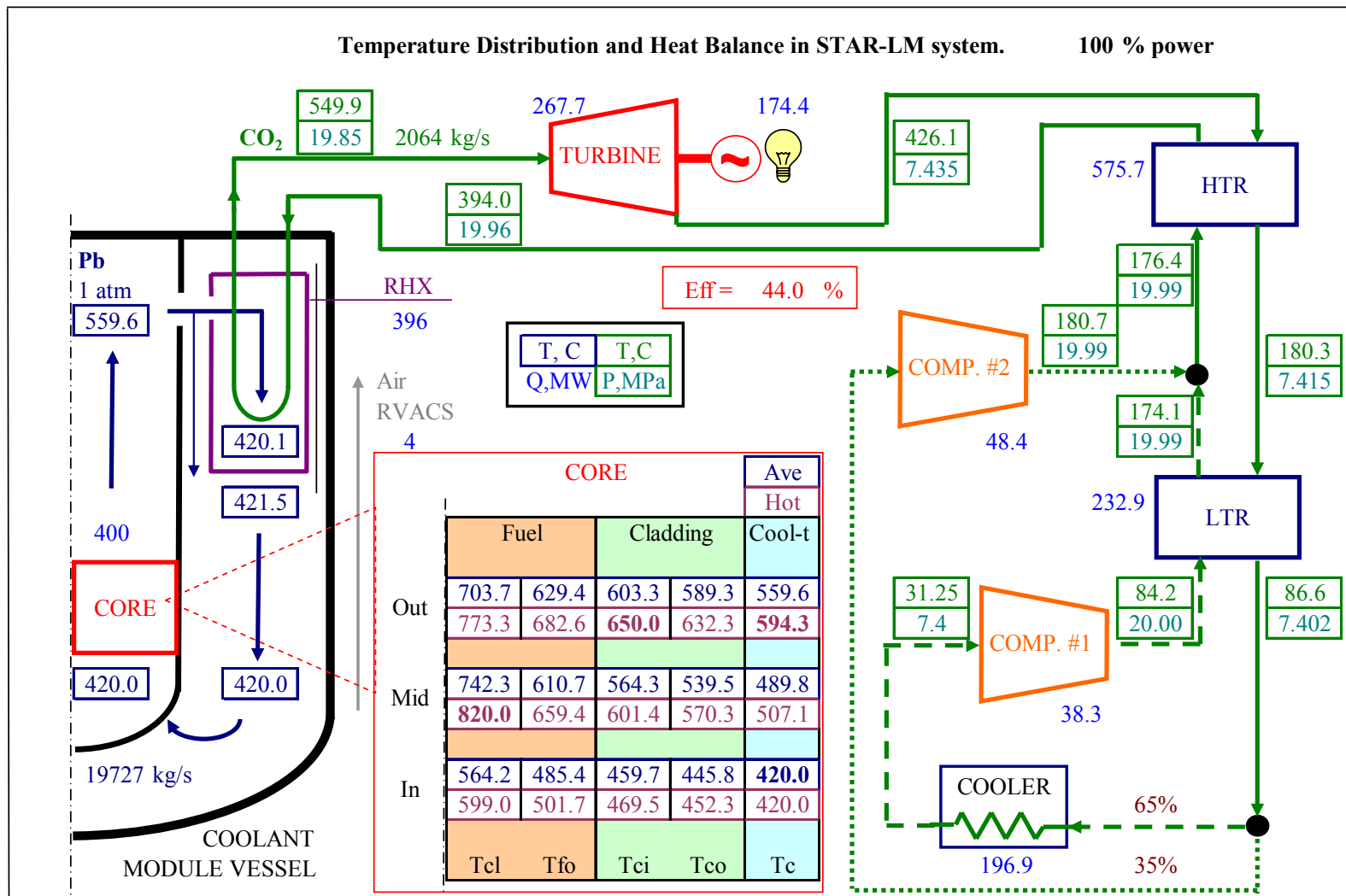


Figure 38. Result of the steady-state model (STAR-LM).

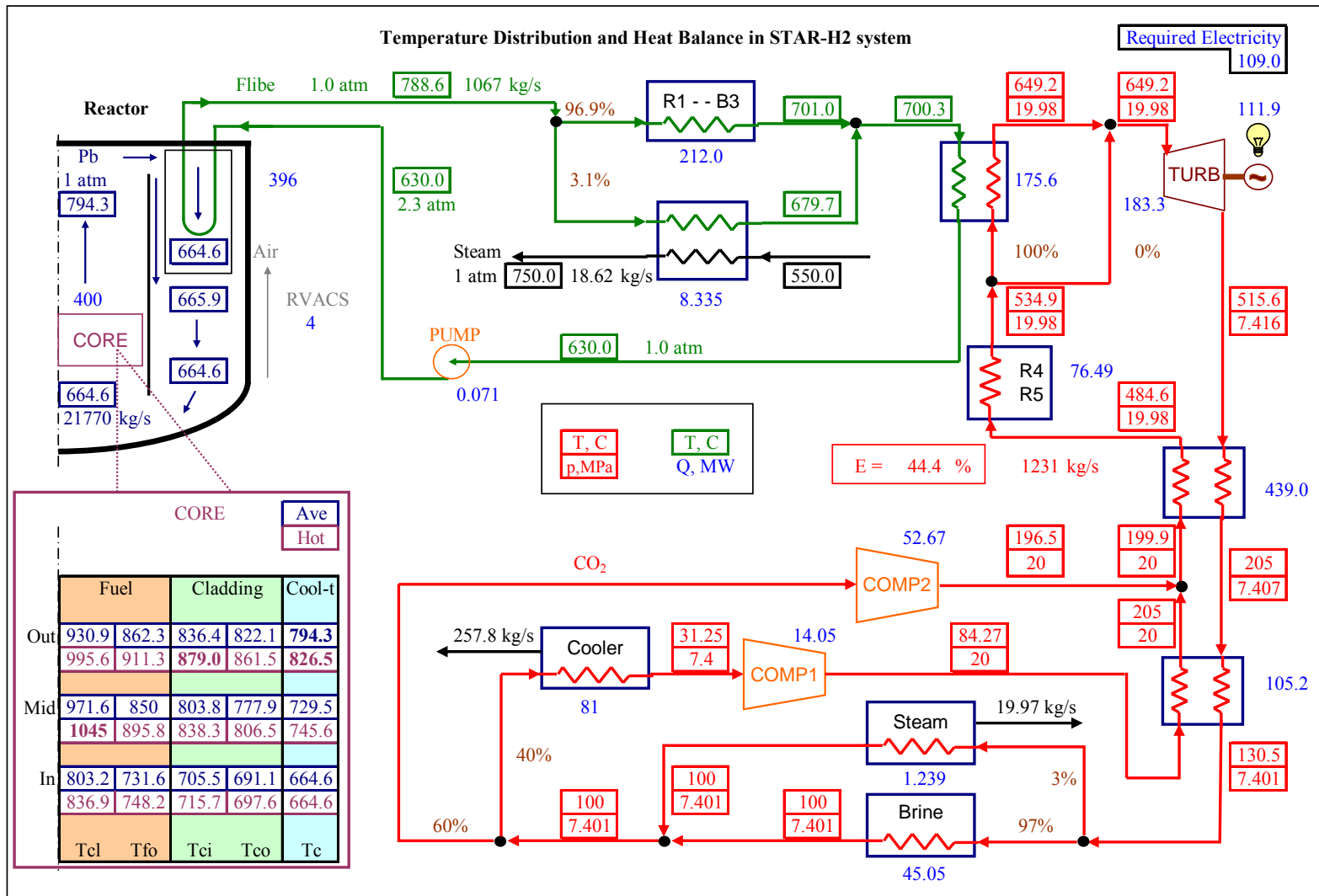


Figure 39. Results of the steady-state model (STAR-H2).

In the STAR-LM, the main safety criteria, which is peak cladding temperature (<650 °C), is satisfied. The achieved cycle efficiency is 44%.

For the STAR-H2 system, the peak cladding temperature is 879 °C, which is also below safety limit of 900 °C (Zinkle and Ghoniem, 2000). The Brayton cycle efficiency is also 44%. This was achieved, despite the fact that the CO₂ flow split is not optimal for the cycle efficiency, by increasing the CO₂ temperature at turbine inlet up to about 650°C. The hydrogen production rate (reagent steam flow rate) was selected such that the electricity produced by the Brayton cycle (111.9 MWe) is sufficient for the hydrogen production plant (109 MWe).

PASSIVE LOAD FOLLOW ANALYSIS

In the previous section the steady-state parameters for the full power systems were calculated. However, during the plant operation it is sometimes required to adjust the amount of product (either electricity or hydrogen) produced by the plant. The adjustments to the system parameters that are necessary to operate at different power levels are called load follow. These adjustments are discussed in this section.

As it will be shown below, the plant control for load follow can be performed without any control action on the reactor. The reactor power will adjust automatically to any energy demand from the balance-of-plant by passive means. The load follow strategy which does not require control action on the reactor is called passive load follow. The passive load follow eliminates any operator action on the reactor thus eliminating the operator error accidents, hence improving the overall plant safety.

The quasi-static passive load follow analysis was done for the STAR-LM and the STAR-H2 systems. Under the quasi-static approach the initial (full power) and final (reduce load) states are calculated using the steady-state model. The development of a dynamic model for the entire system transient can be very complicated and it is beyond the scope of this work. At the same time, the quasi-static approach is much simpler (it uses steady-state model rather than the complicated dynamic model) and it addresses most of the safety issues (like peak cladding temperature) for the load follow process.

The load follow analyses are different for the STAR-LM and the STAR-H2 systems, since the product (load) is deferent; the STAR-LM provides electricity, while the STAR-H2 produces hydrogen. However, the reactor response is the same because both systems use the same reactor.

Reactor Reactivity Feedbacks and Passive Load Follow

The STAR reactor was designed to adjust its power to the energy demand from the balance-of-plant. This is done by selecting design features to produce the reactivity coefficients which allow for passive load follow.

The passive load follow works on the following principals. Initially, at the steady-state operation at full power the heat produced by the reactor and heat transferred to the balance-of-plant are in balance and total net reactivity in the reactor is zero. If some control action is taken on balance-of-plant, this changes parameters (temperature and mass flow rate) of the secondary fluid at reactor heat exchanger inlet. This change causes the change of a coolant temperature (and, therefore, other temperatures) in the core. Through the reactivity feedbacks these temperature changes add or remove reactivity causing the reactor power to increase or decrease. These adjustments will continue until the heat balance in the RHX is achieved. This will be a new steady state, with zero net reactivity at a new power level.

Therefore, the equation which characterizes the changes in the reactor during the transient from one steady state to another is based on the fact that both states have zero total reactivity and, therefore, reactivity change is also zero. The reactivity of the reactor is affected by the coolant temperature, reactor power (through fuel temperature), and change in core geometry (due to core material thermal expansion). Since no control rods are used for the power control, there is no external reactivity source in the reactor. So, there are four reactivity effects which should be taken into account when calculating the change in reactivity:

1. Coolant density feedback (defined by change coolant temperature and its thermal expansion),
2. Doppler feedback (due to change in fuel temperature, which, in turn, defined by change in coolant density and power level),
3. Core radial expansion feedback (radial expansion of coolant), and
4. Core radial expansion feedback (axial expansion of fuel).

Each reactivity feedback is characterized by the reactivity coefficient. The change in total reactivity is:

$$\Delta\rho = (\alpha_D + \alpha_A)\delta T_f + (\alpha_C + \alpha_R)\delta T_c \quad (126)$$

where $\alpha_D, \alpha_A, \alpha_C, \alpha_R$ = Doppler, core axial expansion, coolant, and core radial expansion reactivity coefficients, respectively, cents/ $^{\circ}\text{C}$,

$\delta T_f = T_f - T_{f,0}$ = Change in the average fuel temperature, $^{\circ}\text{C}$,

$\delta T_c = T_c - T_{c,0}$ = Change in the average coolant temperature, $^{\circ}\text{C}$.

Average coolant and fuel temperatures are the functions of the coolant core-inlet temperature and the reactor power:

$$T_c = \frac{T_{in} + T_{out}}{2} = T_{in} + \frac{\Delta T}{2} = T_{in} + \frac{1}{2} \frac{Q}{\dot{m} \cdot c_p} = T_{in} + \frac{1}{2} \frac{Q}{\rho \cdot u \cdot A \cdot c_p} \quad (127)$$

$$T_f = T_c + \frac{Q}{S} B = T_{in} + \frac{1}{2} \frac{Q}{\rho \cdot u \cdot A \cdot c_p} + \frac{B}{S} Q \quad (128)$$

where T_{in}, T_{out} = coolant temperature at core inlet and outlet, respectively, $^{\circ}\text{C}$,

Q = reactor thermal power, W,

\dot{m} = coolant mass flow rate, kg/s,

c_p = average coolant specific heat, J/kg- $^{\circ}\text{C}$,

ρ = average coolant density, kg/m 3 ,

A = core flow area, m 2 ,

S = total fuel rod surface area, m 2 ,

B = total thermal resistance between coolant and fuel middle point (defined in System (60)), W/m 2 - $^{\circ}\text{C}$.

If the total reactivity coefficient from coolant and fuel temperature rise is negative, the increase in reactor power will add negative reactivity through temperature rise. This means that there will be a new steady-state condition with zero total reactivity.

$$\begin{aligned} 0 = \Delta\rho = & (\alpha_D + \alpha_A)\delta T_f + (\alpha_C + \alpha_R)\delta T_c = (\alpha_D + \alpha_A + \alpha_C + \alpha_R)T_{in} \\ & + \left[(\alpha_D + \alpha_A + \alpha_C + \alpha_R) \frac{1}{2 \cdot \rho \cdot u \cdot A \cdot c_p} + (\alpha_D + \alpha_A) \frac{B}{S} \right] Q \\ & - (\alpha_D + \alpha_A)T_{f,0} - (\alpha_C + \alpha_R)T_{c,0} \end{aligned} \quad (129)$$

Equation (129) relates the new power level to the new core inlet temperature. For the purposes of the load follow analysis, Equation (129) is solved for the core inlet temperature as a function of the core thermal power.

$$T_{in} = \frac{1}{(\alpha_D + \alpha_A + \alpha_C + \alpha_R)} \left\{ (\alpha_D + \alpha_A)T_{f,0} + (\alpha_C + \alpha_R)T_{c,0} + \left[-(\alpha_D + \alpha_A + \alpha_C + \alpha_R) \frac{1}{2 \cdot \rho \cdot u \cdot A \cdot c_p} - (\alpha_D + \alpha_A) \frac{B}{S} \right] Q \right\} \quad (130)$$

Equation (130) is used to calculate new core-inlet temperature for every new power level, or to calculate new reactor power, if the core-inlet temperature is known.

Load Follow for the STAR-LM System

Load Definition

The STAR-LM system is designed to produce electrical power. The steady-state calculations gave a temperature distribution inside the system at nominal power (Figure 38). However, during the plant operation there is a need to adjust electricity production according to the grid demand. This grid demand for electricity is called load for the STAR-LM system and is usually measured in percents of full power. The range of the load variation is set to be 10% to 100% of full power.

The STAR-LM system is designed such that the power reduction does not require any operator action on the reactor; the reactor power will be adjusted by the passive means to match the conditions of the Brayton cycle.

Therefore, the goal of the passive load follow analysis is to find a control scheme, as simple as possible, for the Brayton cycle which will adjust the electricity production to the required demand with no operator action on the reactor.

Instead of calculating the new system state for every load, the reverse approach is used, under which the system parameters, including the electricity output, are calculated

for a new reactor power. Then, for every desired load level, the reactor power can be found and control actions should be taken to achieve necessary power level.

Therefore, the calculations start with the reactor. The core inlet temperature is calculated (Equation (130)) for every new power level. The new reactor power and coolant temperature at core inlet specify the coolant temperature everywhere inside the reactor vessel, including the RHX inlet/outlet and the coolant mass flow rate. Then, the CO₂ conditions on the secondary side of the reactor heat exchanger are selected to match coolant temperature at the RHX outlet. Two control schemes to get such conditions on CO₂ side are proposed: the CO₂ mass flow variation and the flow split variation. They are discussed in more details below.

Mass Flow Rate Variation

In this control scheme, the CO₂ mass flow rate through the reactor heat exchanger can vary. The mass flow rate could be adjusted by supplying more or less power to the compressors:

$$W_{comp} = \dot{m} \cdot \Delta h_{comp} \quad (131)$$

where

W_{comp} = compressor work, W,

Δh_{comp} = enthalpy change in compressor, J/kg.

The change in the enthalpy is specified by the pressure ratio and the compressor shaft revolution speed. If the pressures and the shaft speed kept the same¹, then the supplying more power to the compressor will result in the increased mass flow rate.

The iterative scheme to find the conditions on the CO₂ side is following. For a given CO₂ temperature at the RHX inlet, the CO₂ mass flow rate is selected such that the lead temperature at the RHX outlet, obtained from the RHX module calculations, will

¹ For more on the pressure control see the CO₂ inventory control section

match the value from the reactor module calculations with a new power level and a new core-inlet temperature. The RHX module also gives the CO₂ temperature at the RHX outlet, which is the same as the turbine inlet.

Then, the CO₂ Brayton cycle calculations are performed for a current CO₂ mass flow rate and the turbine inlet temperature. The turbine and compressors efficiencies are calculated by the Turbine/Compressor module. This module uses the same equations as the design module does, but the blade dimensions and inlet parameters are given, while outlet parameters and efficiency are calculated. Then the outlet pressure is restored (since it is controlled), and the outlet temperature is calculated based on the inlet parameters, the outlet pressure, and new turbine or compressor efficiency.

As a result of cycle calculations, the new value for the CO₂ temperature at the RHX inlet is obtained. The new value of the CO₂ mass flow rate is calculated, as described above, and the process is repeated until they converge.

The results are produced as a set of graphs of various parameters as a function of the reactor power (APPENDIX D, Figure D.1). Among this parameters are the percentage of electricity produced by a generator (Figure D.1c), power requirements for compressors (Figure D.1h), and the heat rejection in the cooler (Figure D.1g). From the operator point of view, for every generator load needed, the reactor power is selected using Figure D.1c Then the amount of power, specified by Figure D.1h, should be supplied to the compressor and the cooling fluid mass flow rate should be adjusted to remove the required amount of heat from the cooler. These actions will specify required conditions on the CO₂ side. The reactor power will adjust automatically to the required level. It can be seen from the Figure D.1a that peak cladding is below safety limits of 650 °C for all reduced power levels. However, increase in power level will exceed this limit, so the system could not be operated above 100% power.

Figure 40 shows the example of the system state at reduced power (50% reactor power).

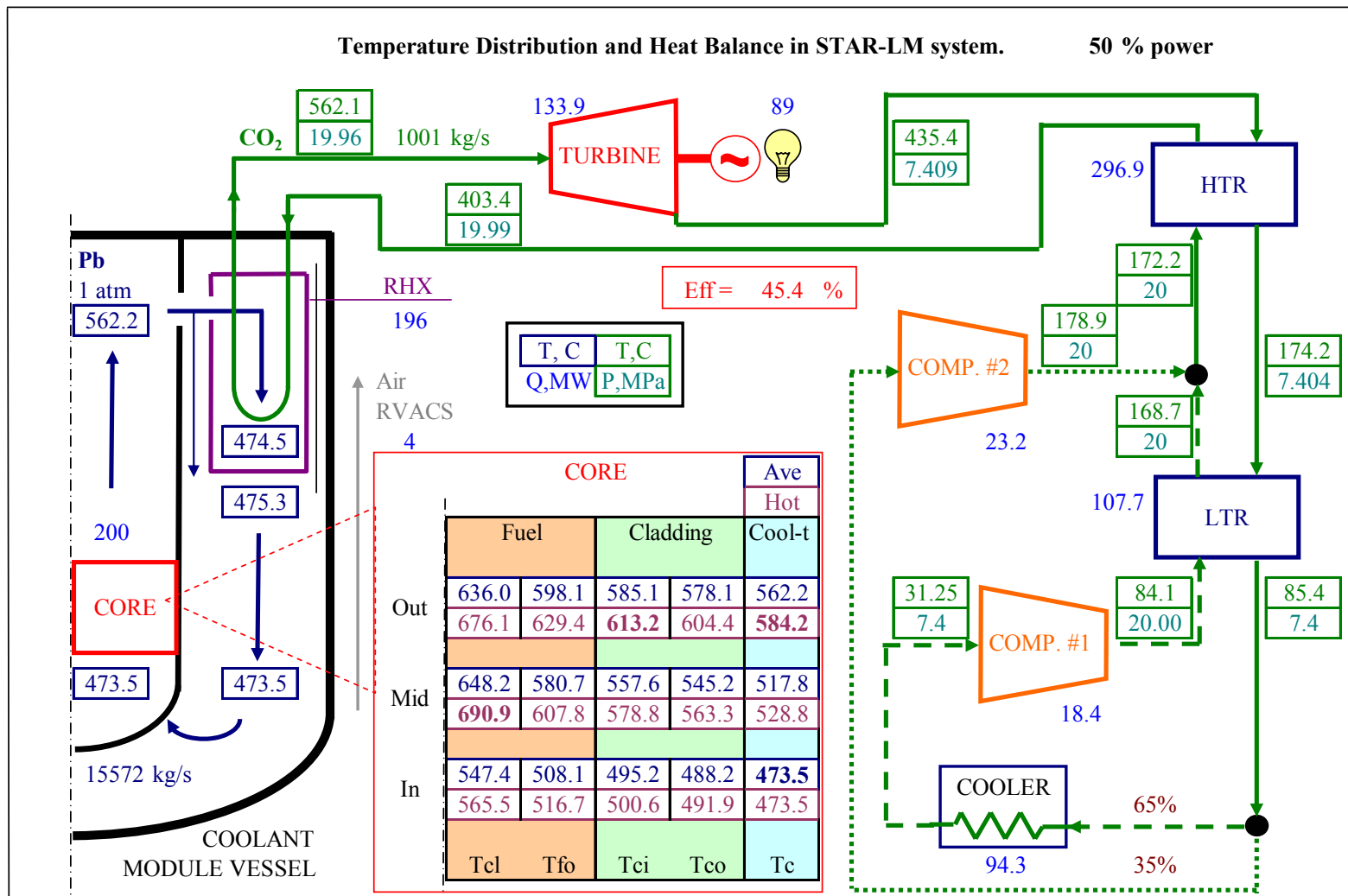


Figure 40. STAR-LM at 50 % load (mass flow rate controlled).

Flow Split Variation

In this scheme, the CO₂ mass flow rate stays the same, but the flow split between the compressors vary. This control mechanism seems to be simpler than the mass flow rate variation.

The control idea is based on the fact that at nominal power the plant operates at a nominal¹ flow split, therefore the deviation from this nominal value will result in a decrease of the cycle efficiency. The decrease in the cycle efficiency leads to less electricity production, if the reactor power stays the same. However, the reactor power changes because the change in the flow split results in the change of conditions on the CO₂ side and, hence, the lead temperatures. According to Equations (126), the change in the lead temperatures add or remove reactivity and the reactor power should adjust itself (Equation (130)) to a new steady state in order to compensate for the reactivity addition. This means that in some cases although the cycle efficiency decreases, the electricity production may increase, if the reactor power increases.

The highest value of the flow split is 1 (100 %) which means that all flow goes to the compressor #1. The lower boundary is defined by the condition when the Brayton cycle does not produce electricity (cycle efficiency approaches zero), the cooler has to reject all heat produced by the reactor. This means that there is a minimum flow rate through the cooler and, hence, through the compressor #1. It turned out that this minimal value for the flow split is about 30%.

As in the previous scheme, the pressures should be kept the same and minimum temperature should be controlled, requiring the adjustment of cooling fluid mass flow rate. The reactor power is adjusted by passive means.

The results of load follow by the flow split variation are shown in APPENDIX E (Figure E.1). All parameters are shown as a function of the flow split, which is a percent of a flow that goes through the compressor #1. It follows from Figure E.1c that the load can be followed from almost 0% up to about 120% using this scheme.

¹ Giving maximum cycle efficiency

The drawbacks of this strategy are that the reactor power is not adjusted proportionally to the load, meaning that the heat from the reactor is not used optimally at off-nominal loads. Also, since the CO₂ mass flow rate (through turbine) stays the same, the mass flow rates through each compressor changes with a fraction of flow which goes through the compressor. This means that the flow rate through each compressor should be adjusted as well. Therefore, this scheme is not simpler than the mass flow rate variation.

Figure 41 shows the example of the system state at the reduced load (60 %). The 60% load is achieved at the flow split of 40%, according to Figure E.1c.

CO₂ Inventory and Pressure Control

It is proposed to control pressures in the Brayton cycle by adding or removing the CO₂ to or from the system. To calculate the amount of the CO₂ which should be added (or removed) to the system, the CO₂ inventory is calculated at a nominal power and at every load, while the pressures in the systems remain the same. The difference between the CO₂ inventory at some power level and that at the nominal power level determines how much of the CO₂ should be added to the system to maintain required pressures.

The CO₂ inventory is calculated as the CO₂ mass inside pipes plus a sum of CO₂ masses inside every component. The CO₂ mass inside pipes is calculated as:

$$M_i^{pipe} = \rho_i \cdot L_i^{pipe} \cdot \frac{\pi (d_i^{pipe})^2}{4} \quad (132)$$

where

ρ_i = density of the CO₂ inside the pipe (assumed constant), kg/m³,

L_i^{pipe} , d_i^{pipe} = pipe length and diameter, respectively, m.

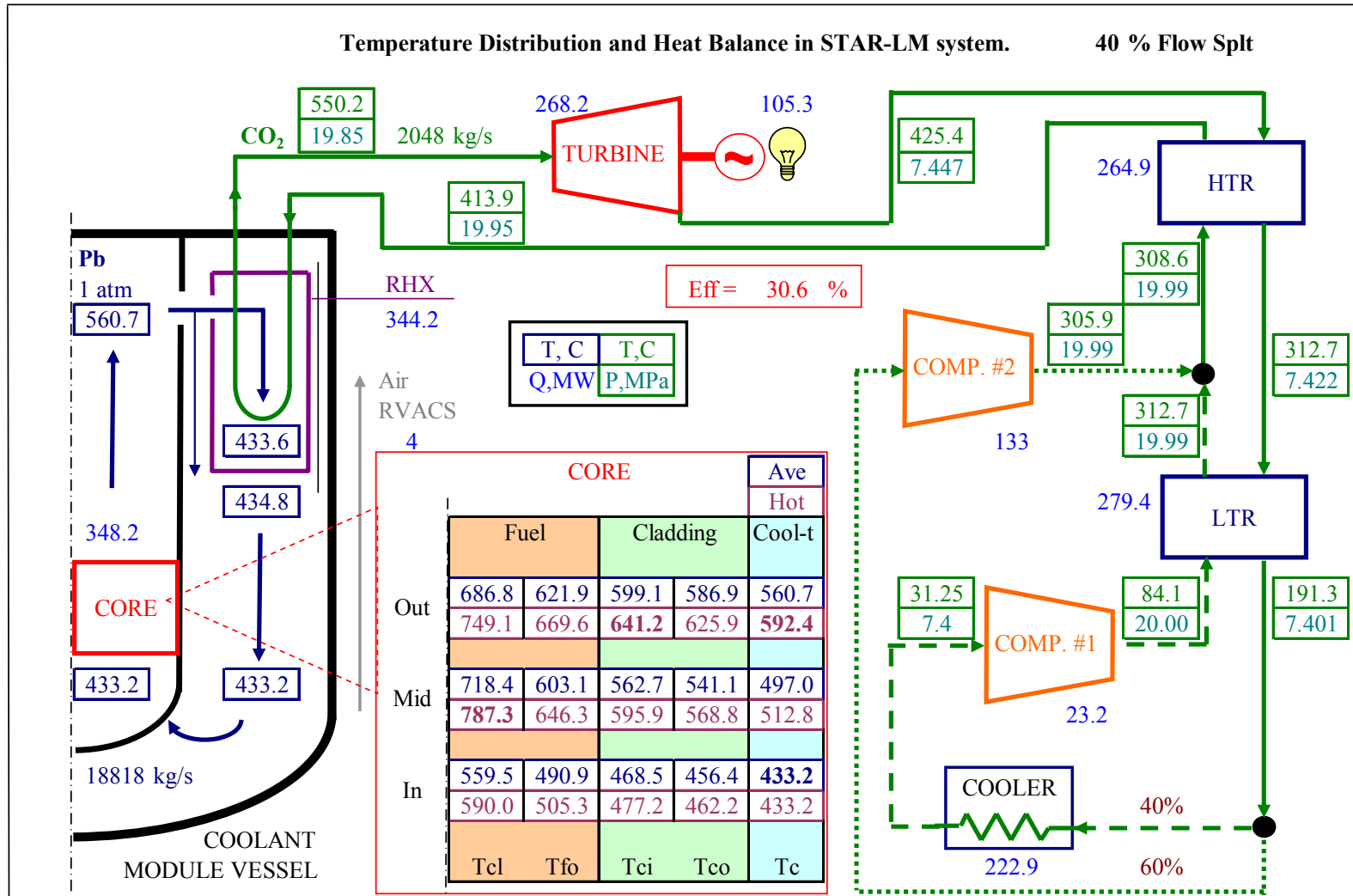


Figure 41. STAR-LM at 60 % load (flow split controlled).

The pipe lengths between every two components are estimated based on the preliminary layout of the plant components. The pipe diameter is assumed to be 0.5 m. The calculations showed that the mass inside the pipes is small compared to the mass inside the components, so the possible error in pipe length and diameter is not very important for the CO₂ inventory.

The CO₂ mass inside each component is calculated similarly. However, the CO₂ density is changing inside a component, so the average density is calculated for every region, which is used for the temperature calculations; and it is multiplied by the region's volume:

$$M_k = \sum_{j=1}^{N(k)} \rho_j \cdot dL_j \cdot A_j \quad (133)$$

where $N(k)$ = number of the regions used for component k ,

ρ_j = average density of the CO₂ for region j , kg/m³,

dL_j, A_j = region length and flow area, m and m², respectively.

For a heat exchanger, the region length is calculated as the heat exchanger length divided by the number of regions; the flow area is equal to the flow area per channel times the number of channels. For a compressor or turbine, one region means one stage, and the region length is a stage length; the flow area is an average flow area for the stage. The CO₂ mass inside the recuperators includes the mass of both flows.

Table 11 shows the CO₂ inventory distribution between each component and piping for the nominal power case.

The change in CO₂ inventory for the load follow controlled by the mass flow rate is shown in Figure 42. To compensate this change in the inventory, it is proposed to use a CO₂ tank, which is connected through the valves to the pipes with high and low CO₂ pressures. The greater the pressure difference between the pipes the faster this mechanism responds. The maximum pressure change in the cycle occurs around the compressor #1 (Figure 38).

Table 11. CO₂ inventory at nominal power

	Location	L, m	M _{CO₂} , kg
Components	RHX	5.52	2,961.2
	Turbine	0.45	10.5
	HTR	10.0	18,305.9
	LTR	10.0	31,276.6
	Cooler	9.04	9,832.9
	Compressor #1	0.80	33.4
	Compressor #2	0.80	12.6
Piping	RHX outlet - Turbine inlet	20	484.9
	Turbine outlet - HT Recuperator inlet	5	55.3
	HT Recuperator outlet - LT Recuperator inlet	2	36.9
	LT Recuperator outlet - Cooler inlet	7	190.3
	Cooler outlet - Compressor1 inlet	2	144.8
	Compressor1 outlet - LT Recuperator inlet	2	223.2
	LT Recuperator outlet - Flow merge inlet	1	56.6
	Compressor2 outlet - Flow merge inlet	2	110
	Flow merge outlet - HT Recuperator inlet	1	56
	HT Recuperator outlet - RHX inlet	20	620.3
	TOTAL		64,411.3

However, connecting this tank to the pipes immediately before and after the compressor will have two disadvantages. First, due to the temperature change inside the compressor, the tank should be maintained at some average temperature to avoid thermal stresses. Second, it would complicate the control of the CO₂ temperature at the compressor inlet. To avoid such problems, the control tank is connected on the low pressure side to the pipe before the cooler (Figure 43).

The size of a tank is defined by the condition that the pressure inside the tank should always be between 7.4 and 20 MPa. It follows from Figure 42 that the maximum change in the CO₂ mass in the tank is about 5,000 kg.

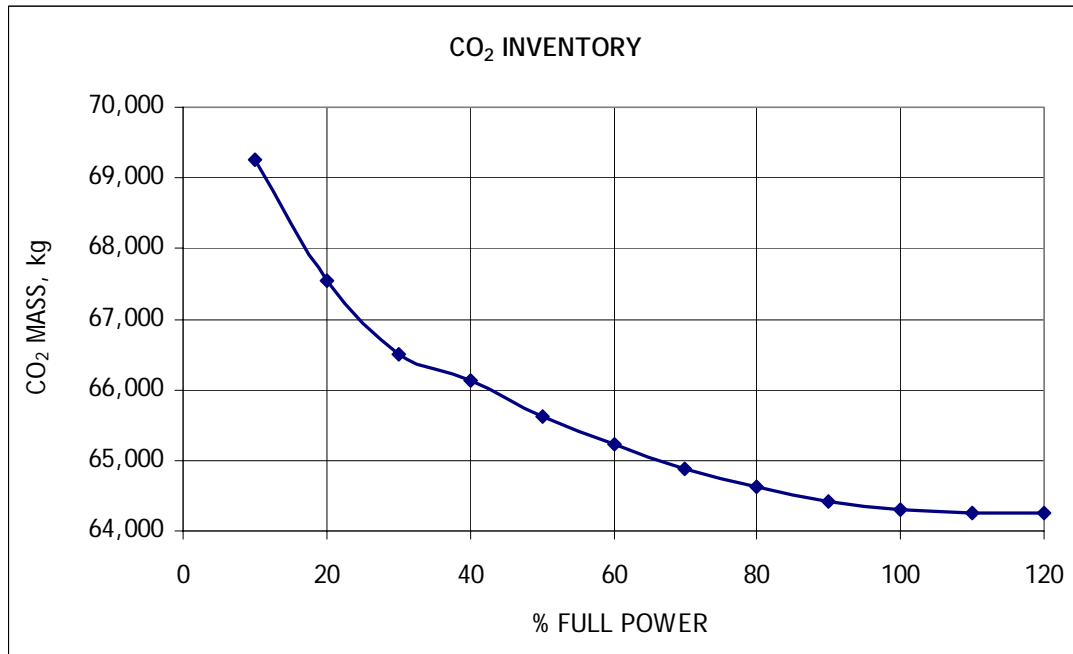


Figure 42. CO₂ inventory change.

For the tank to fulfill its functions even at 10% power (where it contains less CO₂) and to have some margin, it is proposed to use the condition that the pressure in tank is exactly 7.4 MPa after taking twice as much gas out of the tank as is required for load follow function. On the other end, adding the same 5,000 kg to the tank would not cause the pressure to go beyond 20 MPa. It is also assumed that the gas in the tank is at some average temperature, which is set to be 85 °C, according to Figure 43.

Let's assume that the tank volume is V (m³) and it contains m_0 (kg) of the CO₂ at a pressure p_0 (MPa) at nominal power; and use symbol Δm for the required mass change (5,000 kg).

Then, the assumptions described above lead to two equations for the tank's volume and mass of gas in it:

$$m_{\min} = m_0 - 2\Delta m \quad p_{\min} = 7.4 \text{ MPa} \quad T_{\min} = T = 85 \text{ }^\circ\text{C} \quad (134)$$

$$m_{\max} = m_0 + \Delta m \quad p_{\max} = 20.0 \text{ MPa} \quad T_{\max} = T = 85 \text{ }^\circ\text{C} \quad (135)$$

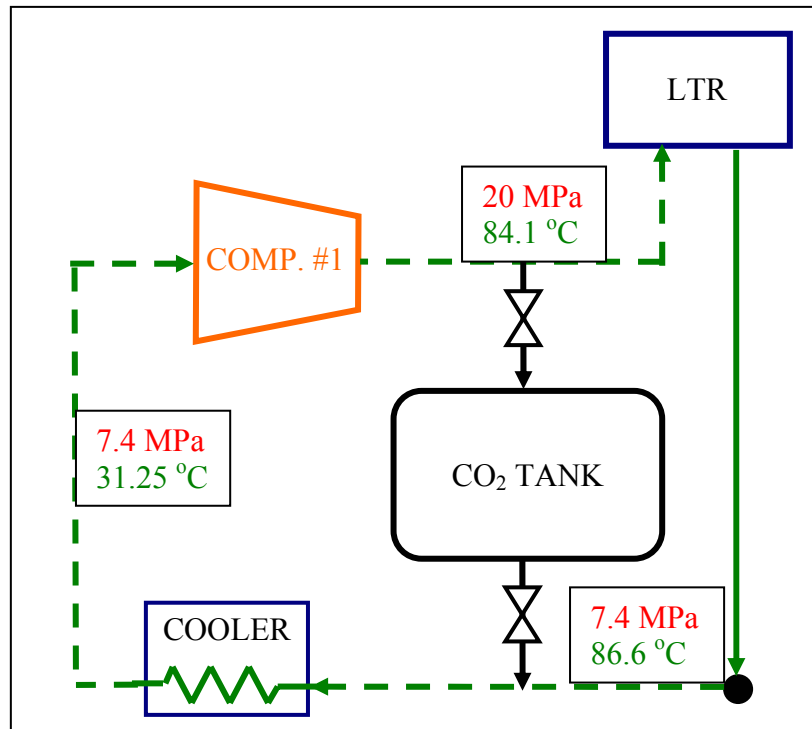


Figure 43. Inventory control system.

Since the volume stays the same, the change in mass means change in density:

$$\rho_0 = \frac{m_0}{V},$$

$$\rho_{\min} = \frac{m_{\min}}{V}, \quad (136)$$

$$\rho_{\max} = \frac{m_{\max}}{V}.$$

The densities at a minimum and maximum mass are known, since the pressure and temperature are known:

$$\rho_{\min} = \rho(7.4 \text{ MPa}, 85 \text{ }^\circ\text{C}) = 139.68 \text{ kg/m}^3,$$

$$\rho_{\max} = \rho(20 \text{ MPa}, 85 \text{ }^\circ\text{C}) = 562.68 \text{ kg/m}^3. \quad (137)$$

Equations (134), (135) and (136) give the system to find m_0 and V :

$$\begin{cases} \rho_{\min} = \frac{m_0 - 2\Delta m}{V} \\ \rho_{\max} = \frac{m_0 + \Delta m}{V} \end{cases} \quad (138)$$

The solution of System (138) is:

$$\begin{cases} V = \frac{3\Delta m}{\rho_{\max} - \rho_{\min}} = \frac{3 \cdot 5,000 \text{ kg}}{(562.68 - 139.68) \text{ kg/m}^3} = 35.5 \text{ m}^3 \\ m_0 = \rho_{\max} \cdot V - \Delta m = 562.68 \text{ kg/m}^3 \cdot 35.5 \text{ m}^3 - 5,000 \text{ kg} = 14,975 \text{ kg} \end{cases} \quad (139)$$

Assuming that the tank is a cylinder with diameter equal to the height, the tank diameter is about 3.6 m.

The initial pressure can be found as a pressure at the initial temperature and the initial density, which is equal to m_0/V :

$$\rho_0 = \frac{m_0}{V} = \frac{14,975 \text{ kg}}{35.5 \text{ m}^3} = 421.8 \text{ kg/m}^3, \quad (140)$$

$$p_0 = p(\rho_0, T) \approx 15.6 \text{ MPa}.$$

Conclusion

Two control schemes for STAR-LM were investigated to follow the load on generator from 10% to, at least, 120% without any action on the reactor, which adjusts its power by means of the reactivity feedback. It is shown that the increase in the electricity production results in an increase of the peak cladding temperature beyond the safety limit. It should be noticed here that the limit on the cladding temperature is

specified by the corrosion rate, which is proportional to the cladding temperature. While 650 °C is considered to be safe for long-term operation, small increase in the peak cladding temperature can be allowed during short-term transients. Therefore, the plant should not be permitted to operate at an increased power (above 100%) for a long time. For the partial load, all temperatures stay within the limits.

The mass flow rate variation seems to be preferable because it makes it possible to follow the load at almost constant cycle efficiency. The flow split variation, although it appears to be easier, requires changing the flow rate through each compressor as well.

It is demonstrated that the flow rate variation requires utilization of the CO₂ inventory control system. The calculations showed that the change in the CO₂ inventory in the cycle is about 5,000 kg for the power reduction from 100% down to 10%. It is estimated that this change in inventory can be compensated by using a 35.5 m³ tank with the CO₂, which is about 1/8 of a recuperator's volume.

Load Follow for the STAR-H2 System

Load Definition

The STAR-H2 system is designed for hydrogen production. So, the product is hydrogen and the load is the amount of hydrogen produced per unit of time. The hydrogen production rate is defined by the reagent steam flow rate and the amount of heat supplied to the beds of the hydrogen production plant. Therefore, the goal of the load follow analysis is to find a control strategy to adjust the plant for different levels of hydrogen production (reagent steam mass flow rate).

There is a specific feature of the hydrogen production plant which influences the load follow analysis. The input flow for the third reaction (beds R4 and R5) is bromine, which is stored in a tank and is supplied to the beds as needed. So, the bromine flow can vary independently of the reagent steam flow. Therefore, there are two independent types of load in the STAR-H2 system: reagent steam flow variation and bromine flow variation.

The goal of the plant control is to ensure that the plant can operate and produce hydrogen at partial loads. This means that several criteria must be met at these loads. First, the amount of heat, electricity, and steam supplied to the hydrogen production plant should be sufficient for the specified hydrogen production level. It follows that the reactor power level should be adjusted for the partial loads. As in case of the STAR-LM this adjustment has to be done by passive means without any control action on the reactor (passive load follow). Second, the operation at reduced loads has to be safe, i.e. temperatures and pressures should be maintained within safety limits. The most important safety parameters are cladding and coolant temperatures inside the reactor.

The control mechanism available for the STAR-H2 system are flow rates of the working fluids (flibe, CO₂, and cooling fluid), adjustment to the flow split (flibe and CO₂ loops), and pressure control. The pressures in the system are controlled by the same approach as used for the STAR-LM, i.e. by using the inventory control system. So, the pressures stay the same during load follow.

The quasi-static passive load follow analysis was done for the STAR-H2 for various loads meaning that the system parameters are calculated at an initial state (100% power) and at a final state (reduced load) using the steady-state model. The power adjustment on the reactor is done by passive means using reactivity feedbacks.

Two load schemes were investigated: the reagent steam flow variation and the bromine flow variation. In each scheme the heat duties required for the hydrogen production plant, amount of heat available from the plant and electricity requirements at reduced flow rates were considered as an input data (Doctor and Matonis, 2003). The data were provided for 25%, 50%, and 75% of full power flow rates (either bromine or steam). Also, the case of zero bromine flow rate was investigated. For every scheme the reference state (100% flow) is the system state at full power (steady-state model).

In addition, main accident scenarios (like loss of heat sink) were investigated for the STAR-H2 system.

Reagent Steam Variation

In this case, the reagent steam flow rate is reduced (25%, 50%, and 75%) while the bromine flow rate stays the same. The reduced steam flow rate means that the reactions of the hydrogen production plant slow down and as a result produce less hydrogen. At the same time, the heat duties and electricity requirements of the hydrogen production plant are reduced, requiring the adjustment of the reactor power level.

Under passive load follow the reactor power level is adjusted by varying the secondary fluid (flibe) flow rate and temperature at the RHX inlet. The flibe temperature, in turn, is controlled by the amount of heat taken from the flibe in the MS-CO₂ heat exchanger (CO₂ mass flow rate).

The steady-state model was modified to find a new steady-state with required reactor power level, amount of electricity needed from the Brayton cycle and other parameters to match different loads (reagent steam flow rates). The results are shown in APPENDIX F (Figure F.1). Figure F.1a summarizes the plant control to load follow. It shows how flow rates and energy input to compressors should be adjusted for every level of reagent steam flow rate. These control actions result in required reactor power level (Figure F.1c). Again, this power level is achieved through temperature reactivity feedbacks by changing the flibe flow rate and its temperature in reactor heat exchanger (Figures F.1e and F.1f). The other parameters of importance are also shown on Figure F.1 for every reagent steam flow rate.

It follows from Figure F.1g and F.1h that hydrogen is still being produced at a reduced rate because there is enough electricity for the hydrogen production plant and there is enough steam produced in Brayton cycle. Also, heat requirements for the hydrogen production plant are met since it is an input for the load follow calculations.

Figure F.1b shows that load follow is safe since the limiting temperatures, peak cladding temperature and maximum coolant temperature, are within their safety limits (900 °C and 800 °C, respectively) for every load.

Figure 44 shows the example of the system state at reduced load (50 %).

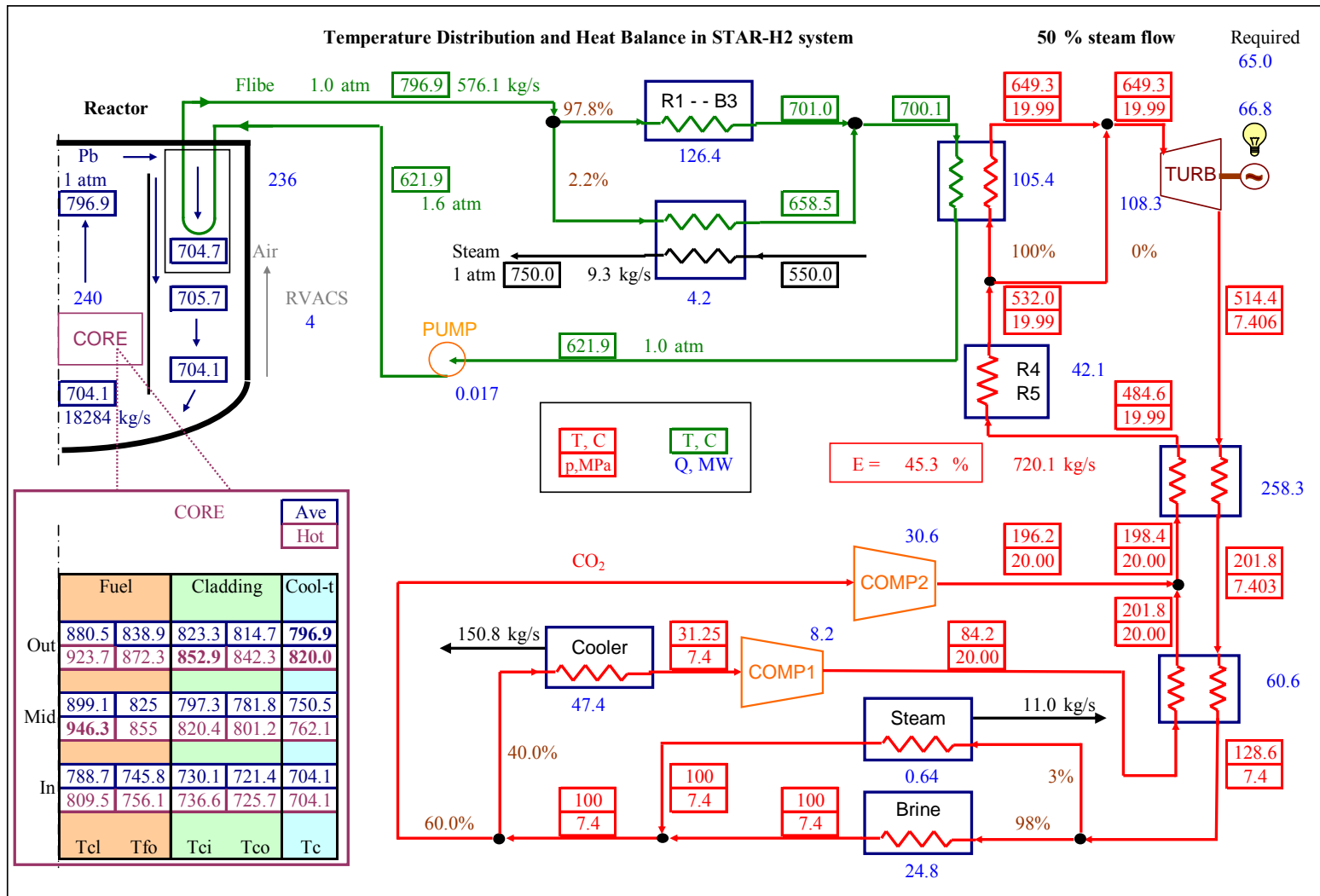


Figure 44. STAR-H2 at 50% load (reagent steam flow rate).

Bromine Flow Variation

The bromine flow rate influences the reactions in beds R4 and R5 (Figure 2). Therefore, the amount of heat available for the Brayton cycle is reduced for the reduced bromine flow. At the same time, the reagent steam flow rate remains at 100%, so the hydrogen production rate stay at 100% requiring the same amount of electricity to be supplied to the hydrogen production plant. Thus, the reduction in heat supply from beds R4 and R5 should be compensated by other means. The only way to increase the heat supply to the Brayton cycle (without taking some heat from the hydrogen production plant) is to increase the reactor power level. Again, this increase in the reactor power should be done by adjusting the condition of the secondary fluid.

The steady-state model was modified to find the required reactor power level and control parameters to achieve this power level for every bromine flow rate (25%, 50%, and 75%). Also the case with no bromine flow, assuming no heat from beds R4 and R5, was investigated. The results are shown in APPENDIX G.

Figure G.1c shows the required reactor power level for every bromine flow rate. This power level is achieved by adjusting conditions of flibe in the reactor heat exchanger (Figures G.1e and G.1f). Other plant control adjustments are also shown on Figure G.1, including the CO₂ mass flow rate (Figure G.1h), the energy input for compressors (Figure G.1i), and the amount of heat removed in the cooler (cooling fluid flow rate) (Figure G.1k). Figures G.1g and G.1l show that there are enough resources (electricity and steam) for hydrogen production at every load. Also, like in the previous scheme, heat duties for the hydrogen production plant are met since they are an input data for calculations.

Figure G.1b shows that safety requirements are met. The peak cladding temperature, although increases, is still under 900 °C; maximum coolant temperature is kept below 800 °C.

Figure 45 shows the example of the STAR-H2 system state at a reduced bromine flow (50 %).

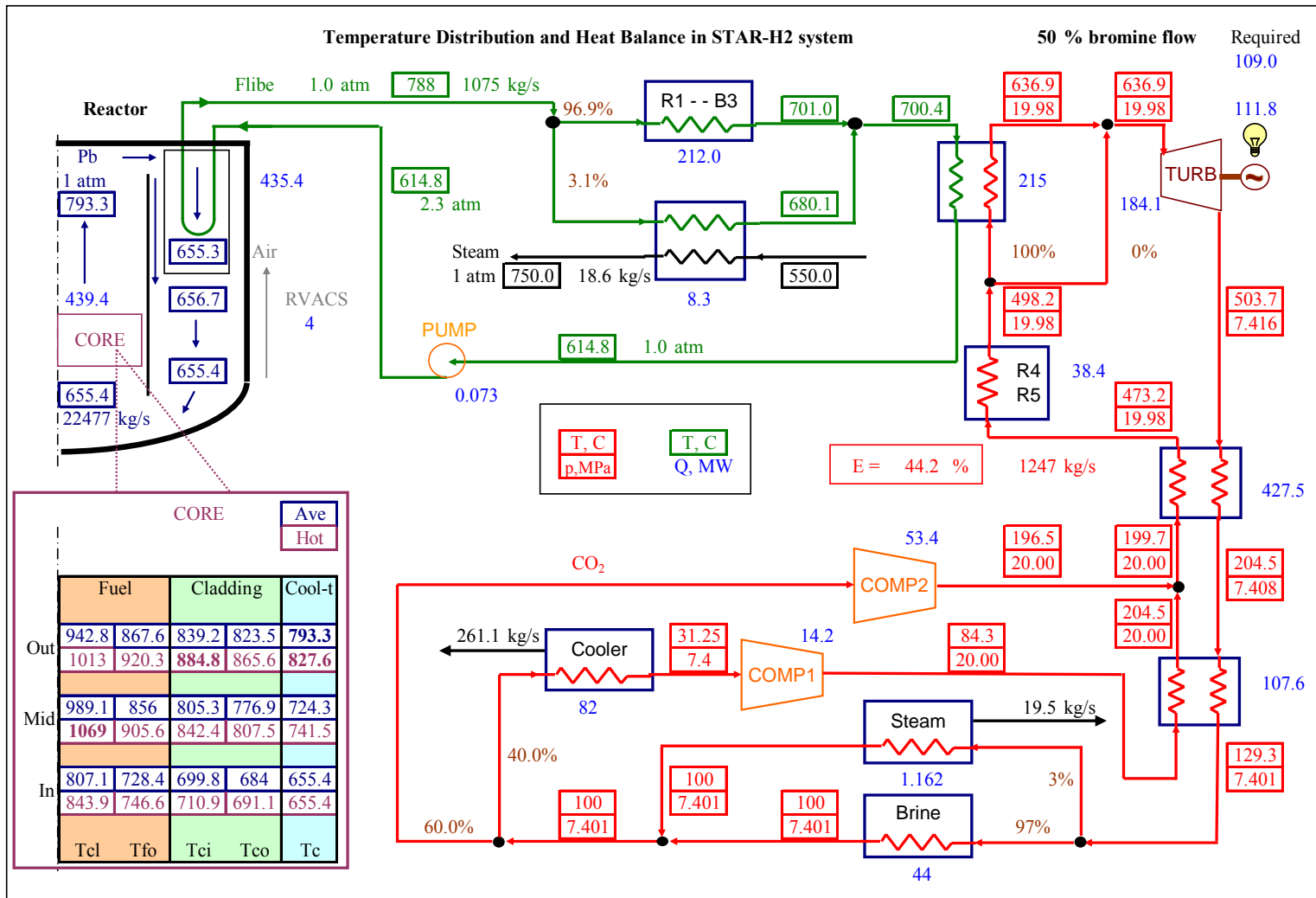


Figure 45. STAR-H2 at 50% load (bromine flow rate).

Accident Scenarios

The behavior of the STAR-H2 system under main accident conditions was investigated. Since there are no control rods in the reactor, the whole class of reactor-driven accidents is eliminated. Also, use of natural circulation eliminates primary coolant pumps, so the coolant flow is provided all times. Therefore, the only balance-of-plant-driven accidents are considered for the STAR systems.

Among the possible accident scenarios, only limiting cases were considered. A limiting scenario occurs when either flow of any working fluid stops (either due to pipe rupture or pump failure) or flow rate increases (due to pipe rupture or operator error). It is assumed that flow rate can increase, in the second case, by 115%. After that pump or compressor will trip and flow will stop, so the scenario is converted to the first type of accident. Also, the case when the hydrogen production plant quits working was considered as an accident scenario.

The accident scenarios with their descriptions are presented in Table 12.

Table 12. Accident scenarios for STAR-H2

Short name	Full Name	Description (Differences from the full power case)
100% POWER	Full Power	None
COS	(CO ₂) Compressor Over Speed	CO ₂ mass flow rate is 115% of normal.
LOBC	Loss of the Brayton Cycle	CO ₂ mass flow rate is 0. No heat sink to the Brayton cycle.
LOCP	Loss of the Chemical Plant	Chemical Plant takes and produces no heat. Reagent steam mass flow rate is 0.
LOHS	Loss of Heat Sink	Flibe mass flow rate is 0. No heat sink to the Intermediate loop.
POS	(Flibe) Pump Over Speed	Flibe mass flow rate is 115% of normal.
SBD	(Reagent) Steam Blow Down	Reagent steam mass flow rate is 300% of normal.

The response to each accident was investigated. It was assumed that there is no control action on the plant, including the reactor (ATWS class accidents). The quasi-static approach was used. The results are shown in APPENDIX H.

Figure H.1 gives the definitions of the accident scenarios in terms of working fluid mass flow rate. Figure H.2 gives the new steady-state reactor power level which is achieved through flibe temperatures. Figure H.3 shows the coolant flow rate and temperatures inside the reactor. Figure H.4 shows the heat transfer in major heat exchangers.

It follows from the Figure H.3 that the highest peak cladding temperature occurs during a compressor over speed accident. In this case, the increased heat consumption by the Brayton cycle leads to the overcooling of the flibe and reactor coolant resulting in a power increase due to negative reactivity feedbacks. Even in this case, the peak cladding temperature does not increase much over the value for normal operation and stays below the safety limit (900 °C). In all other accidents the peak cladding temperature either stays about the same as for normal operation or decreases. The coolant temperature is below 800 °C for all accidents.

Therefore, none of the major accidents leads to structural damage inside the reactor even without any control action from an operator. These results provide evidence that the STAR-H2 system is passively safe.

Figure 46 shows the system state after the worst accident condition, compressor over speed accident.

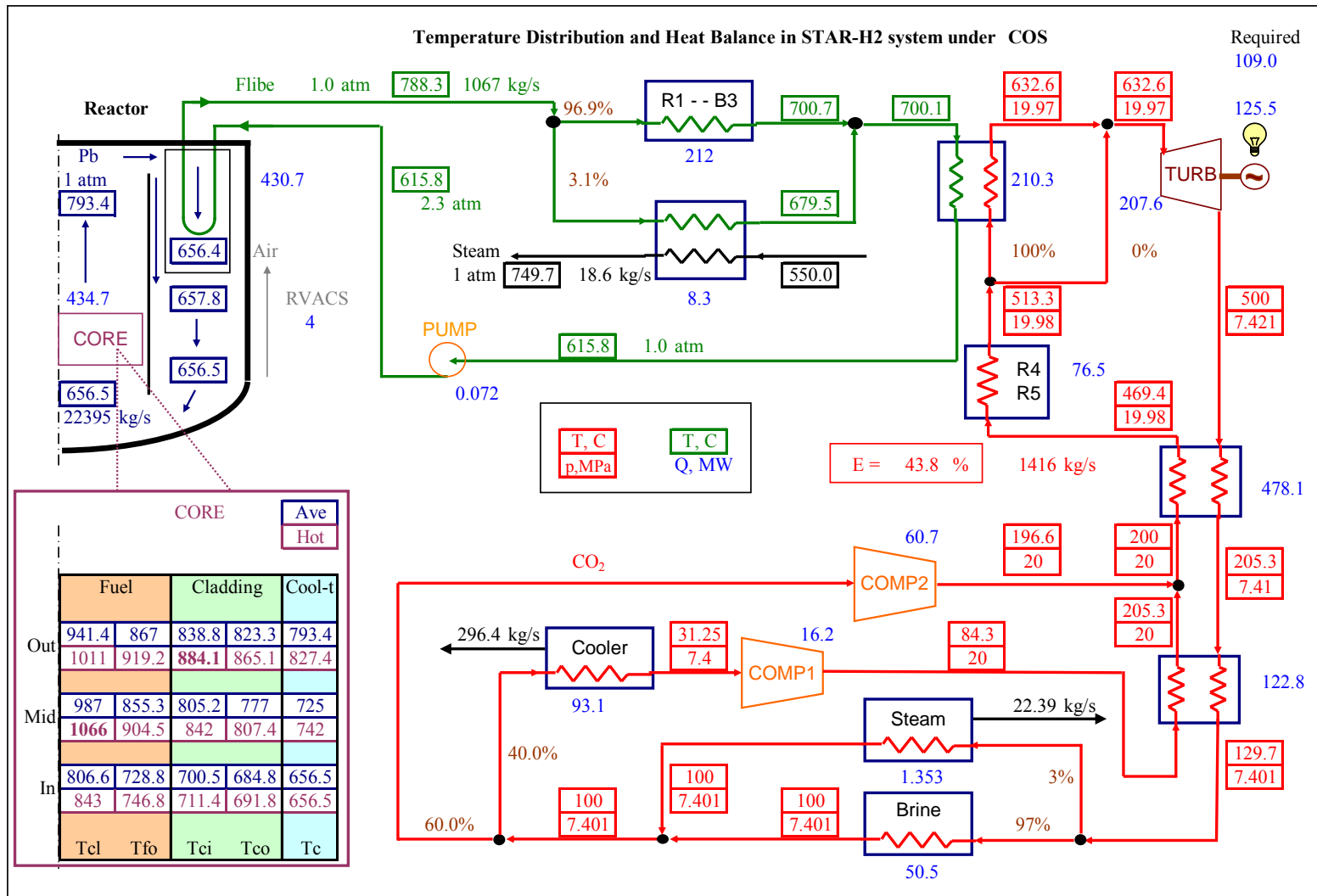


Figure 46. STAR-H2 under compressor over speed accident.

CONCLUSION

A steady-state model for the STAR-LM and the STAR-H2 systems was developed. The STAR-LM system is designed for electricity production and consists of the lead cooled reactor on natural circulation and the supercritical carbon dioxide Brayton cycle. The STAR-H2 system uses the same reactor which is coupled to the hydrogen production plant, the Brayton cycle, and the water desalination plant. The Brayton cycle produces electricity for on-site needs.

The model calculates the temperature and pressure distribution in the systems, and the heat and work balance. The model also performs design calculations for the turbine and compressors for the CO₂ Brayton cycle.

The model was used to optimize the performance of the entire system as well as every system component. The size of each component was calculated.

The efficiency of about 44 % was achieved for the Brayton cycle in both systems. For the 400 MWt reactor power, the STAR-LM produces 174.4 MWe; the STAR-H2 system produces 7450 kg H₂/hr (which correspond to the steam flow rate of 18.62 kg/s).

It was shown that the safety criteria are met. The peak cladding temperature is below 650 °C for the STAR-LM system and below 900 °C for the STAR-H2 system. The lead temperature is below 800 °C for the STAR-H2 system (for the STAR-LM system it is even lower and it is above lead melting point).

Quasi-static passive load follow model was developed for the STAR-LM and the STAR-H2 systems. It was demonstrated that the systems can follow the load from almost zero to full power. No control action on the reactor side is required for the load follow. The control strategies for balance-of-plant are developed for both systems. The safety criteria are met under load follow conditions as well for both systems.

Accident scenarios were investigated for the STAR-H2 system using quasi-static approach. It was shown that the system can passively accommodate any major accident initiating event without any control action from an operator.

REFERENCES

- Bergles, A.E., 1988. Some perspectives on enhanced heat transfer – second-generation heat transfer technology. In: Transactions of the ASME, 110, November, 1082-1096.
- Boyce, M.P., 2002. Gas turbine engineering handbook. Butterworth-Heinemann, Gulf Professional Publishing, Houston, Texas.
- Doctor, R.D., Matonis, D.T., 2003. Hydrogen generation using a calcium-bromine thermochemical water-splitting cycle. Argonne National Laboratory Intra-office memo. Argonne, Illinois, June 13.
- Dostal, V., Driscoll, M. J., Hejzlar, P., Todreas, N.E., 2002. A supercritical CO₂ gas turbine power cycle for next-generation nuclear reactors, ICONE10-22192. In: Proceedings of ICONE-10, Arlington, Virginia, April 14-18.
- Dostal, V., Hejzlar, P., Driscoll, M. J., Todreas, N.E., 2001. A supercritical CO₂ Brayton cycle for advanced reactor applications. Trans. Am. Nucl. Soc., 85, 110-111.
- Fink, J.K., 1998. Enthalpy and heat capacity of solid and liquid lead. Argonne National Laboratory Intra-office memo, June 15.
- Hayes, S.L., Thomas, J.K., Peddicord, K.L., 1990. Material properties correlations for uranium mononitride. Journal of Nuclear Materials, 171, 262-318
- Heat exchanger design handbook, 1983. Hemisphere Publishing Corporation, New York.
- HEATRIC web site, www.heatric.com. Access on October 7, 2003.
- Horlock, J.H., 1966. Axial flow turbines. Fluid mechanics and thermodynamics. Butterworth & Co. (Publishers) Ltd., London, England.
- Kestin, J., 1960. Boundary Layer Theory. McGraw-Hill Book Company, New York.
- Kirilov, P.L., Ushakov, P.A., 2001. Liquid metal heat transfer on rod bundles. Thermal Engineering (English translation of Teploenergetika), 48 (2), 127-133.
- Kulak, R.F., Therios, I.U., 2003. Turbine blade stress calculations (Draft). Argonne National Laboratory Intra-office memo, July 24.

- Leibowitz, L., Blomquist, R.A., 1988. Thermal conductivity and thermal expansion of stainless steels D9 and HT9. *International Journal of Thermophysics*, 9 (5), 873-883.
- Lyon, R.N., Poppendiek, H.F., 1954. Liquid-metal heat transfer. In: *Liquid metals handbook*, Atomic Energy Commission, Department of the Navy, Washington, D.C., 184-212.
- Mertyurek, U., 2002. NUEN 618 notes. Texas A&M University, College Station, Texas.
- Ofte, D., Wittenberg, L.J., 1963. Viscosity of bismuth, lead, and zinc to 1000°C. In: *Trans. Metallurgical Society of AIME*, 227, June, 706-711.
- Özişik, M.N., 1985. *Heat transfer. A basic approach*. McGraw-Hill Book Company, New York.
- Ravigururajan, T.S., Bergles, A.E., 1985. General correlations for pressure drop and heat transfer for single-phase turbulent flow in internally ribbed tubes. In: *Proceedings of the Winter Annual Meeting of the American Society of Mechanical Engineers*, Miami Beach, Florida, November 17-22.
- Saar, J., Ruppertsberg, H., 1987. Calculation of $C_p(T)$ for liquid Li/Pb alloys from experimental $\rho(T)$ and $(\partial P/\partial P)_s$ data. *Journal of Physics F: Metal Physics*, 17, 305.
- Sienicki, J.J., Petkov, P.V., 2003. Assessment of reactivity coefficient uncertainty effects upon STAR-LM autonomous operation and passive safety, ICONE11-36025. In: *Proceedings of ICONE-11*, Tokyo, Japan, April 20-23.
- Sienicki, J.J., Spencer, B.W., 2002. Power optimization in the STAR-LM modular natural convection reactor system, ICONE10-22294. In: *Proceedings of ICONE-10*, Arlington, Virginia, April 14-18.
- Sienicki, J.J., Spencer, B.W., Farmer, M.T., 1999. Fundamental demonstration of natural-circulation feasibility for an HLHC reactor. *Trans. Am. Nucl. Soc.*, 81, 358-364.
- Smith, E.M., 1997. *Thermal design of heat exchangers: a numerical approach – direct sizing and stepwise rating*. John Wiley & Sons Ltd., Chichester, England.

- Span, R., Wagner, W., 1996. A new equation of state for carbon dioxide covering the fluid region from the triple-point temperature to 1100K at pressures up to 800 MPa. *J. Phys. Chem. Ref. Data*, 25 (6), 1509-1596.
- Spencer, B.W., 2000. The rush to heavy liquid metal reactor coolants – gimmick or reasoned, ICONE-8428. In: *Proceedings of ICONE-8*, Baltimore, Maryland, April 2-6.
- Spencer, B.W., Hill, R.N., Wade, D.C., Hill, D.J., Sienicki, J.J., Khalil, H.S., Cahalan, J.E., Farmer, M.T., Maroni, V.A., Leibowitz, L., 2000. An advanced modular HLMC reactor concept featuring economy, safety, and proliferation resistance, ICONE-8145. In: *Proceedings of ICONE-8*, Baltimore, Maryland, April 2-6.
- Spencer, B.W., Wade, D.C., Hill, D.J., Sienicki, J.J., Farmer, M.T., 1999, Thermal-hydraulic development of a small, simplified, proliferation-resistant reactor. In: *10th Annual Engineering and Science Conference, "From the World's First NPP to the XXI Century Power,"* Obninsk, Russia, June 28-July 2.
- Todreas, N.E., Kazimi, M.S., 1990. *Nuclear Systems II*. Hemisphere Publishing Corporation, New York.
- VanSant, J.H., 1983. *Conduction heat transfer solutions*. UCRL-52863 Rev. 1, Lawrence Livermore National Laboratory, August 1983.
- Vesovic, V., Wakeham, W.A., Olchowky, G.A., Sengers, J.V., Watson, J.T.R., Millat, J., 1990. The transport properties of carbon dioxide. *J. Phys. Chem. Ref. Data*, 19 (3), 763-808.
- Waltar, A.E., Reynolds, A.B., 1981. *Fast breeder reactors*. Pergamon Press, New York.
- Zinkle, S.J., Ghoniem, N.M., 2000. Operating temperatures windows for fusion reactor structural materials. *Fusion Engineering and Design*, 51-52, 55-71.
- Zhukov, A.V., Kuzina, Yu.A., Sorokin, A.P., Leonov, V.N., Smirnov, V.P., Sila-Novitskii, A.G., 2002. An experimental study of heat transfer in the core of a BREST-OD-300 reactor with lead cooling on models. *Thermal Engineering*, 49 (3), 175-184.

Zukauskas, A.A., Kalinin, E.K., 1988. Heat transfer: soviet reviews. Volume 2: Enhancement of heat transfer. Hemisphere Publishing Corporation, New York.

APPENDIX A
REACTOR HEAT EXCHANGER DESIGNS

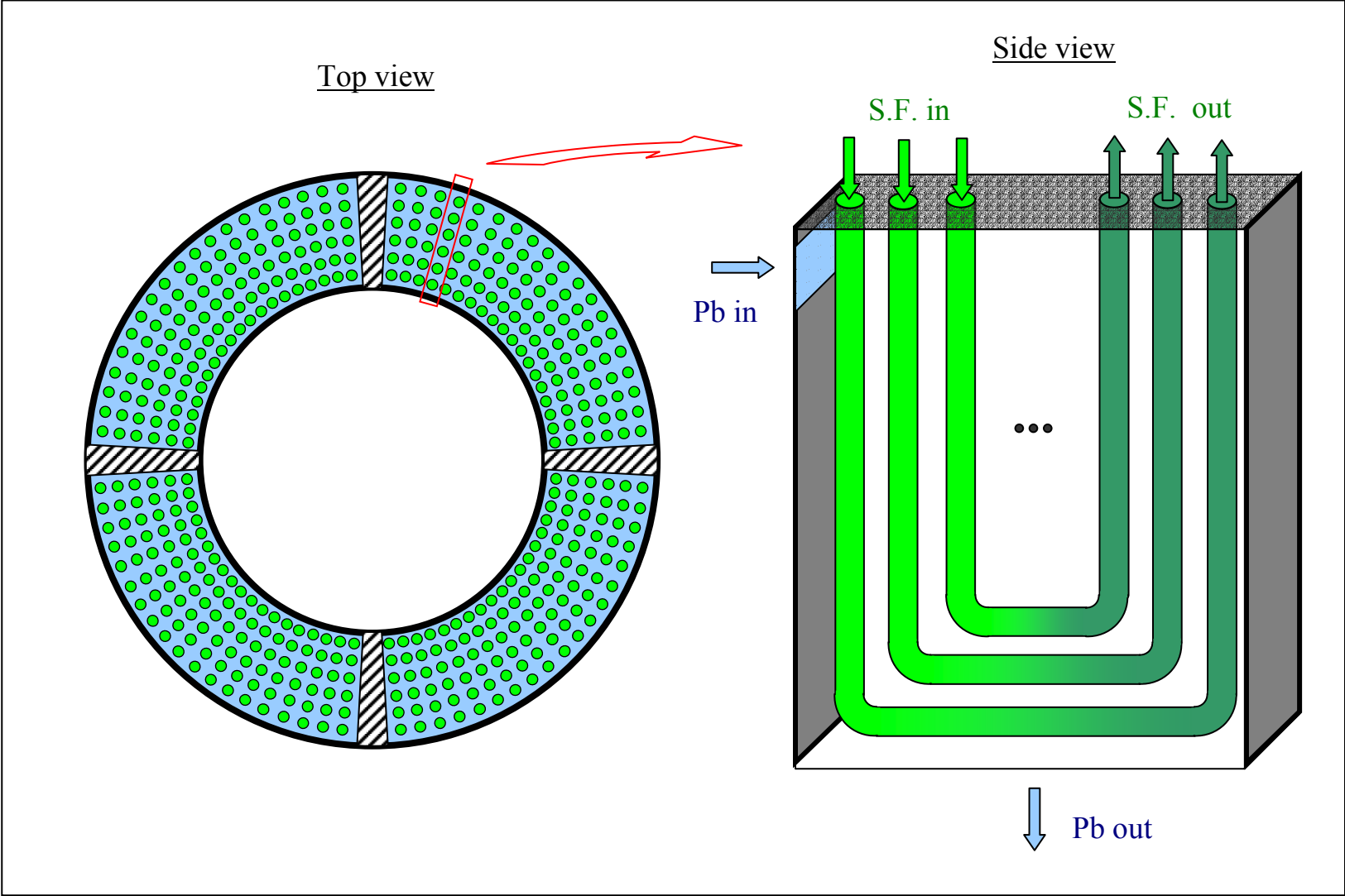


Figure A.1. Stacked U-Tubes HX.

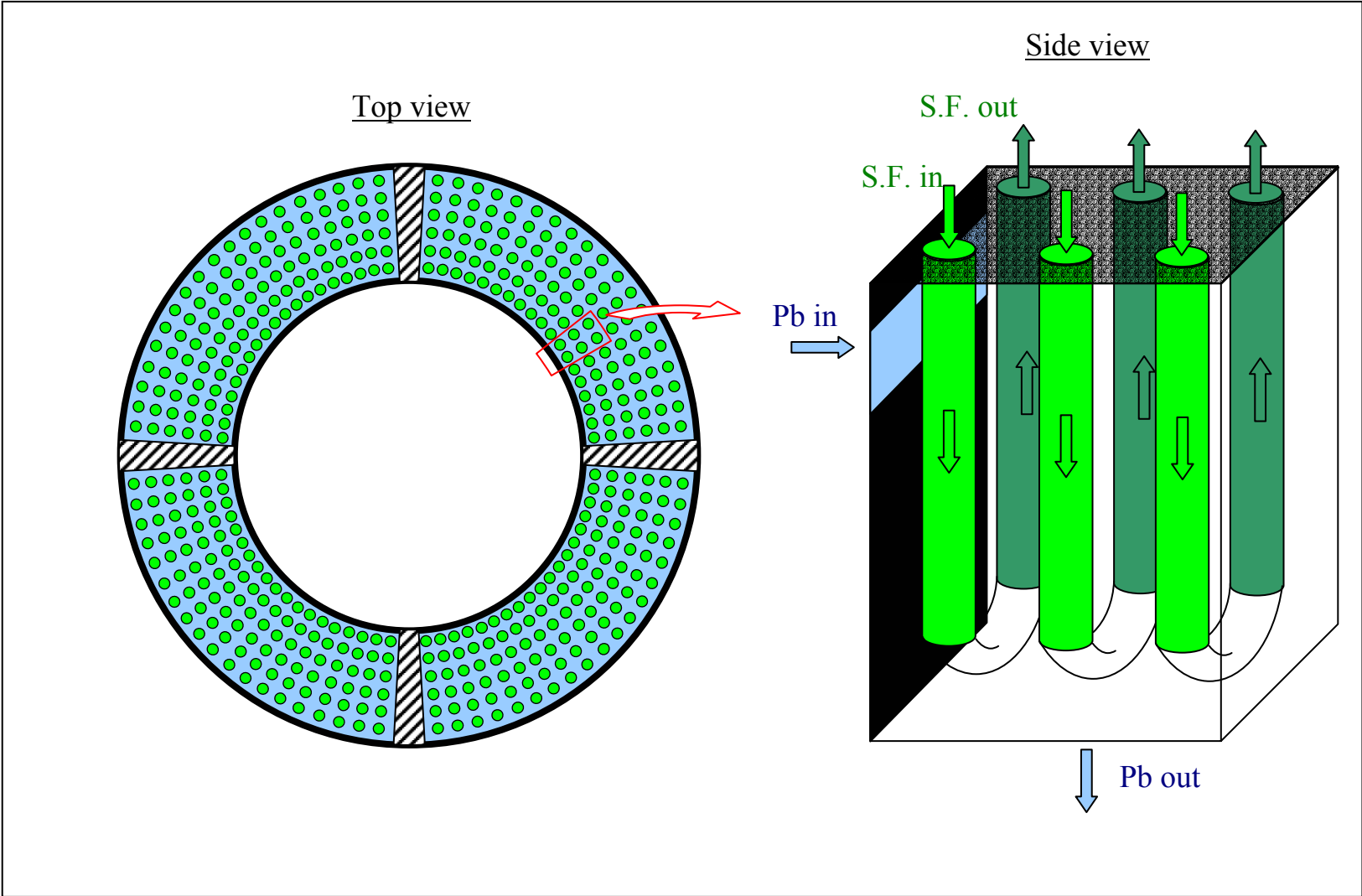


Figure A.2. U-Tube HX.

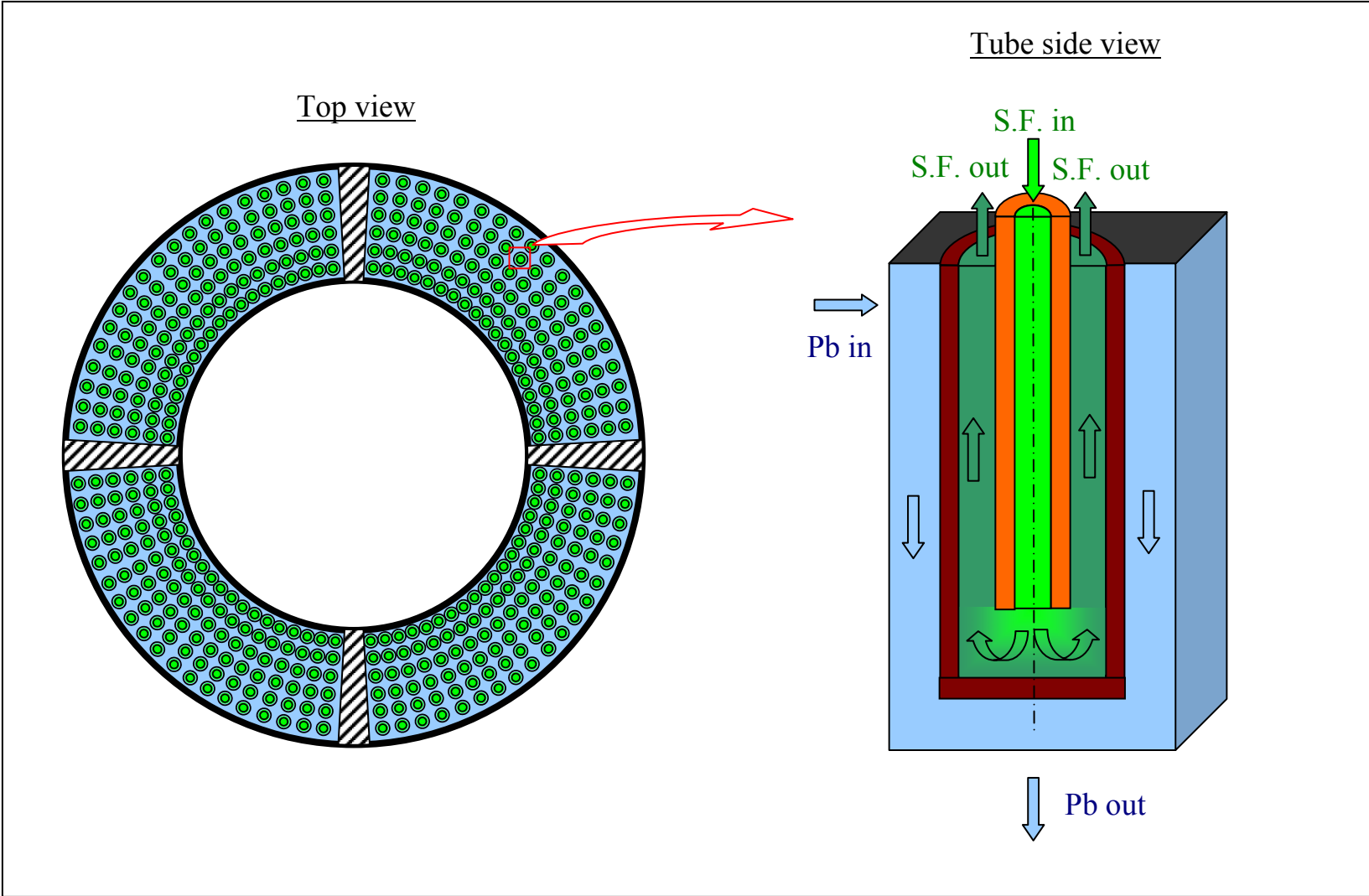


Figure A.3. Concentric Tube HX.

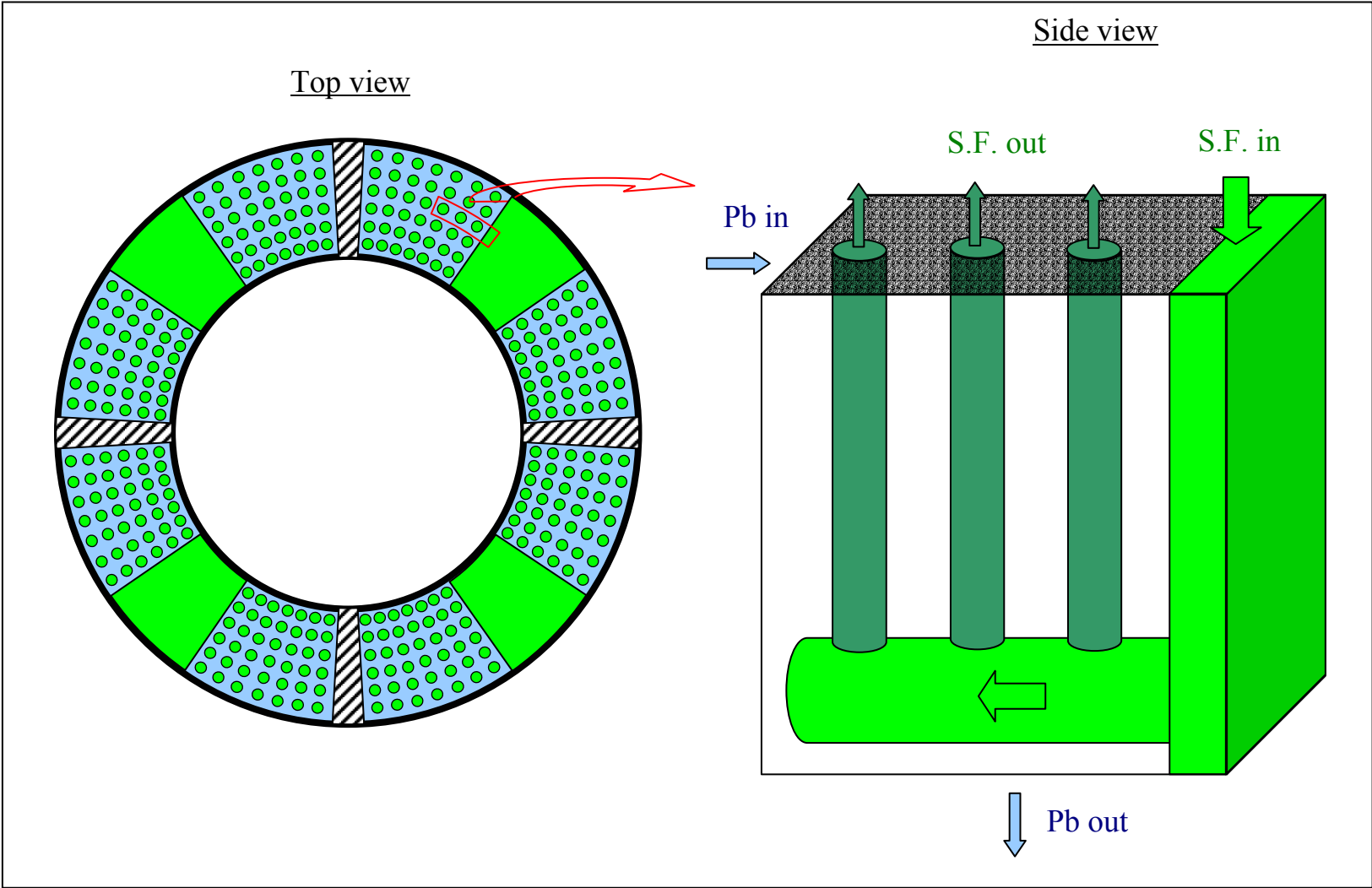


Figure A.4. Straight Tube HX.

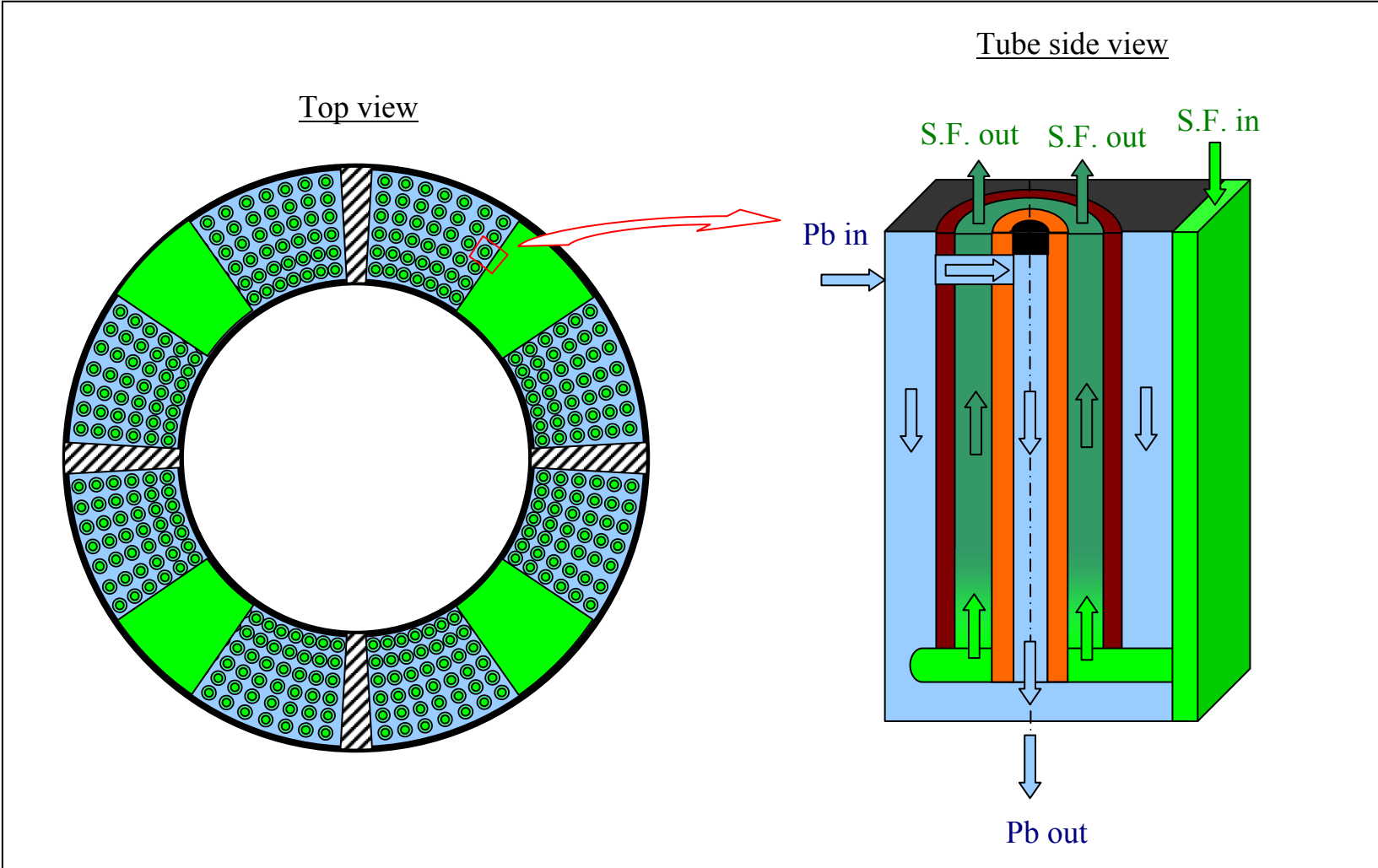


Figure A.5. Straight Annuli HX.

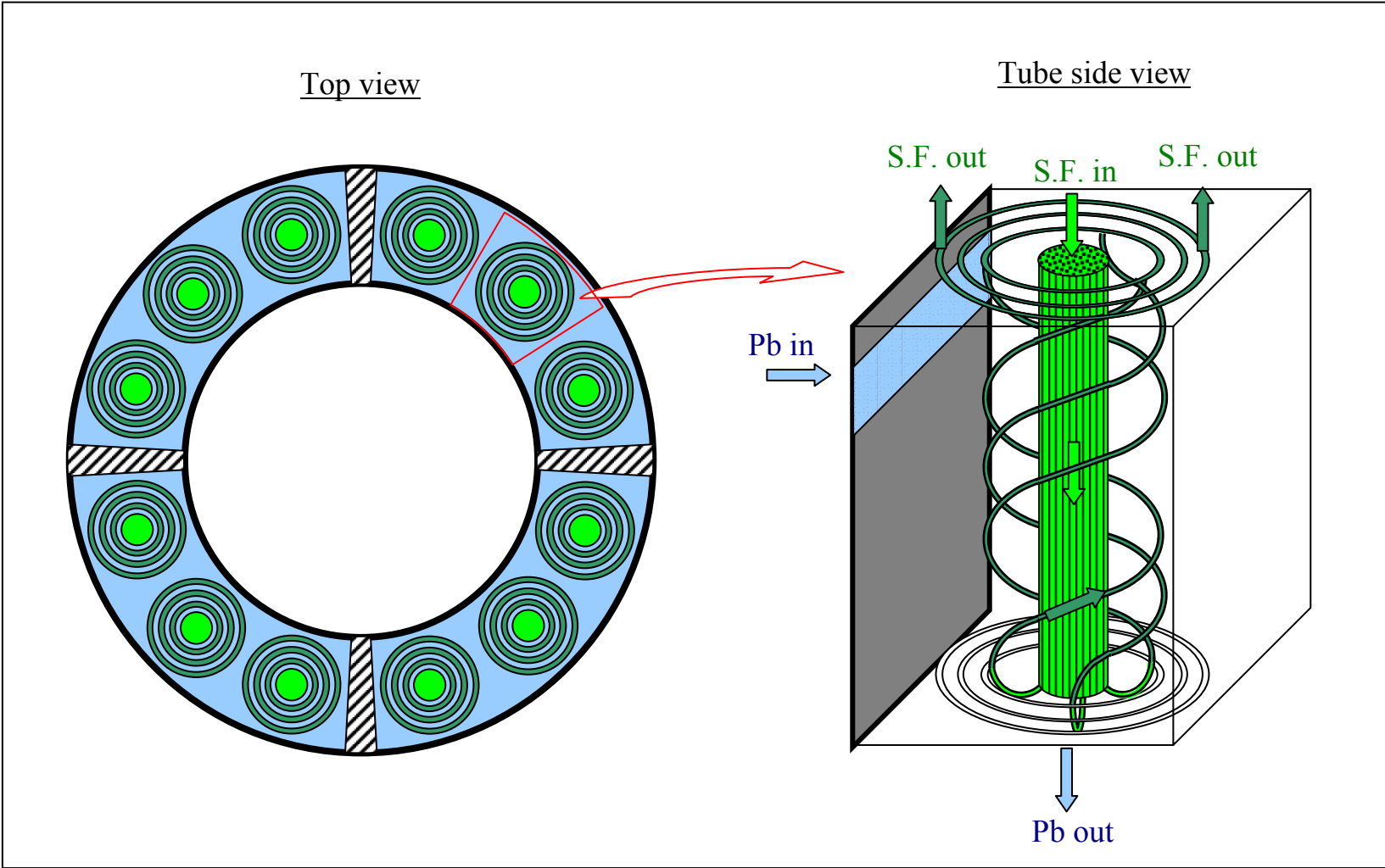


Figure A.6. Helical Coil HX.

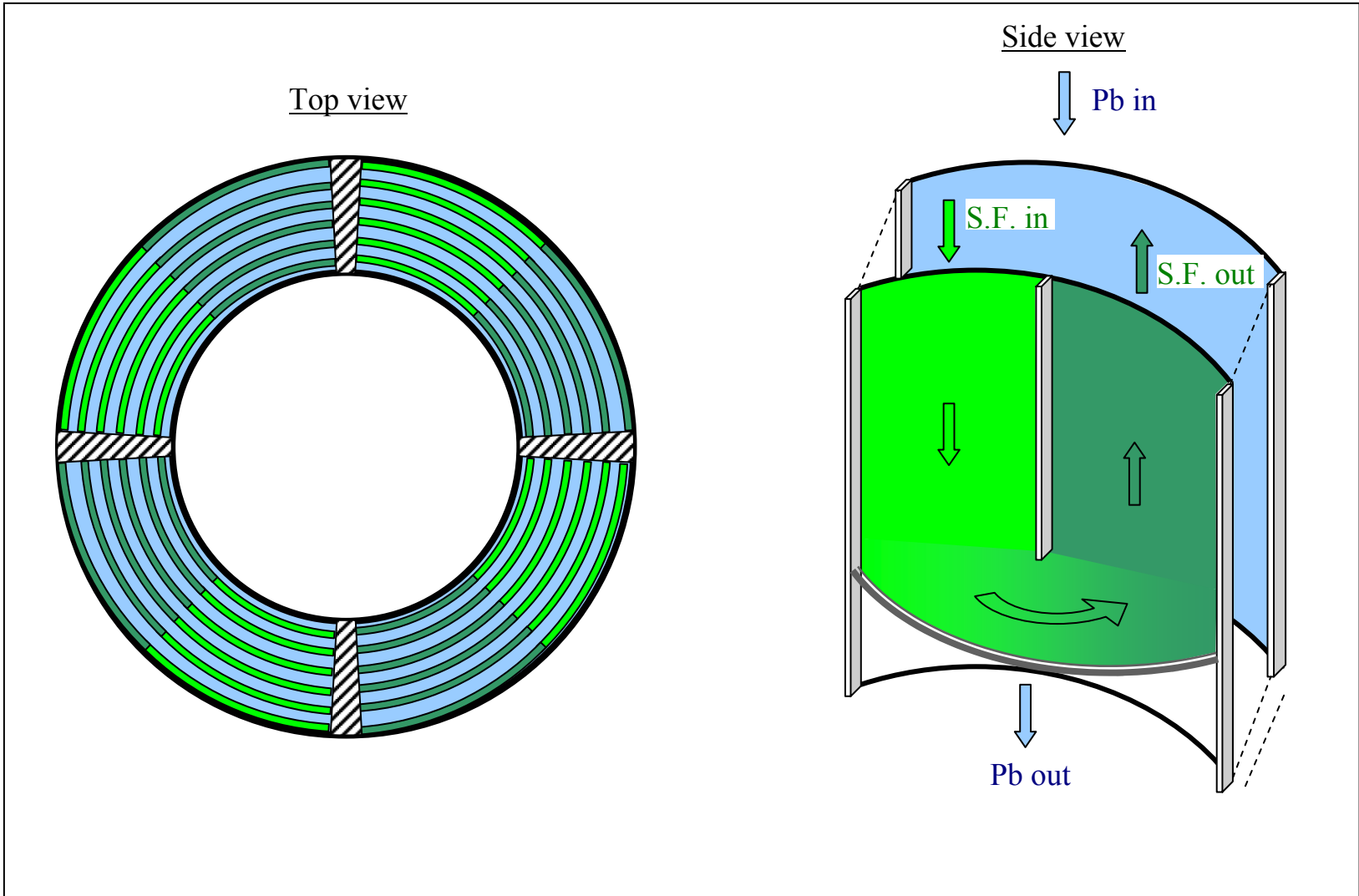


Figure A.7. Plate Type HX with U-Turn.

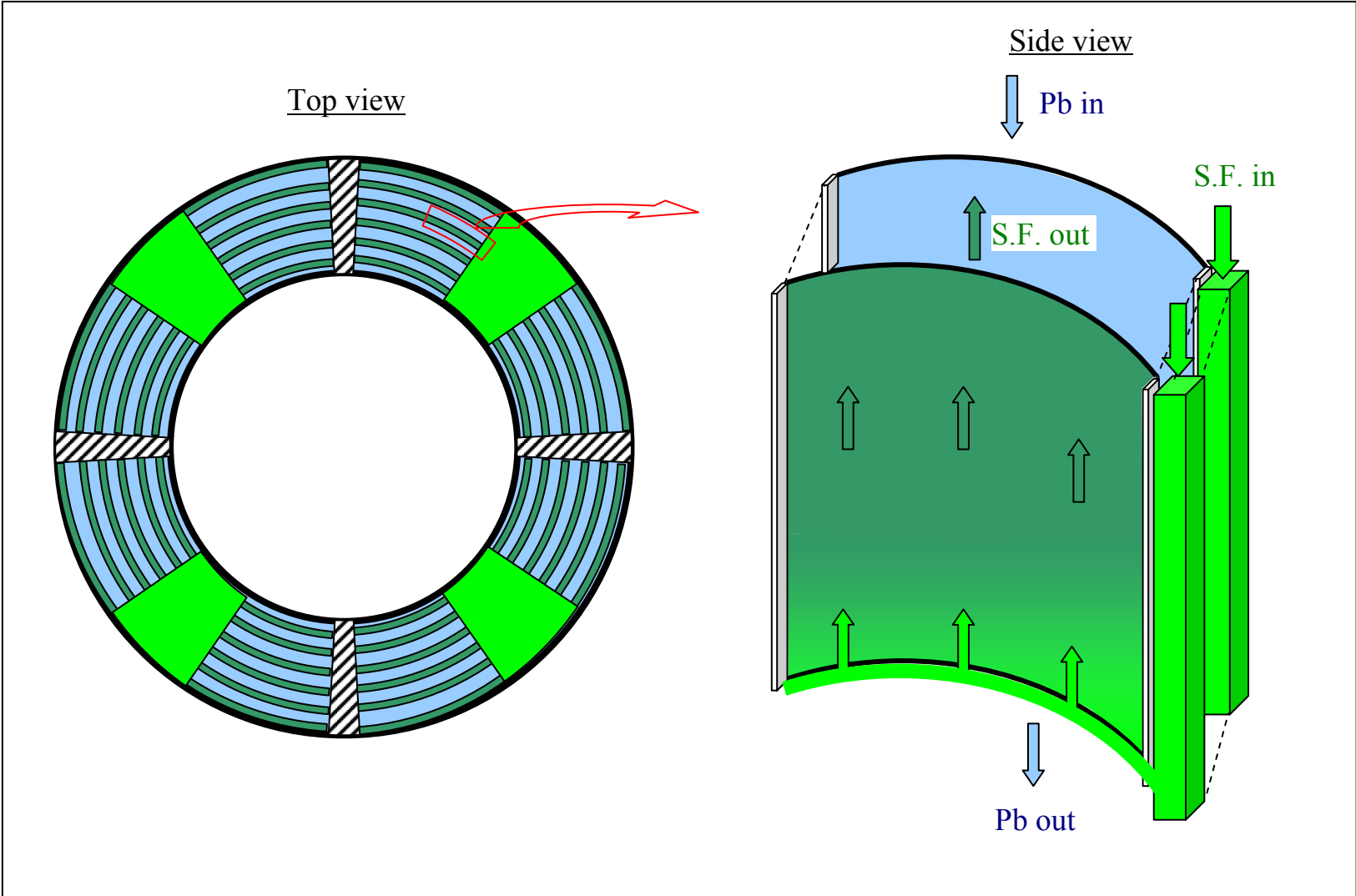


Figure A.8. Plate Type HX.

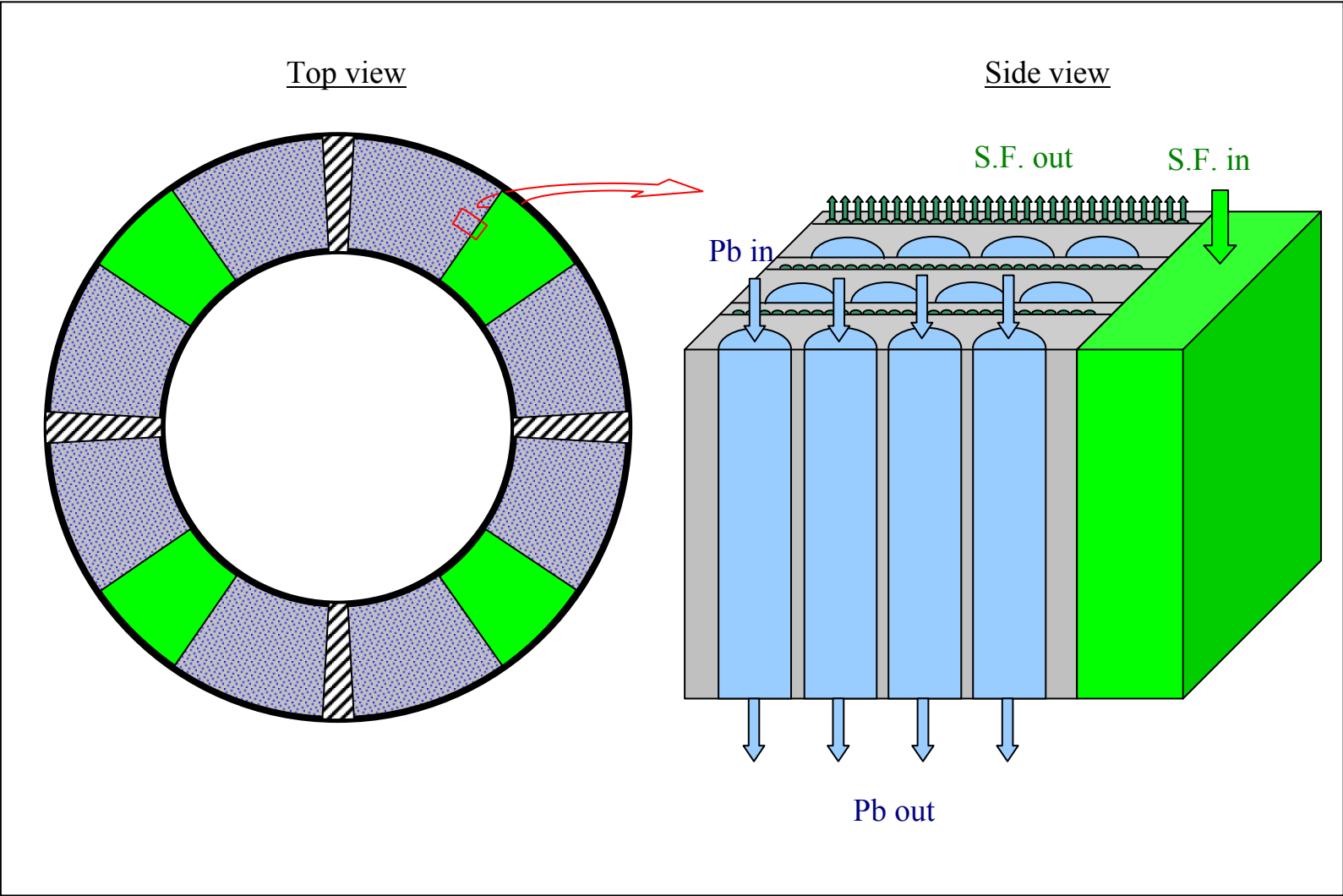


Figure A.9. HEATRIC HX.

APPENDIX B

REACTOR HEAT EXCHANGER PARAMETERS OPTIMIZATION

Straight Annuli HX, Triangular Lattice, H=6.0 m, $r_i-r'_o=2.0$ mm

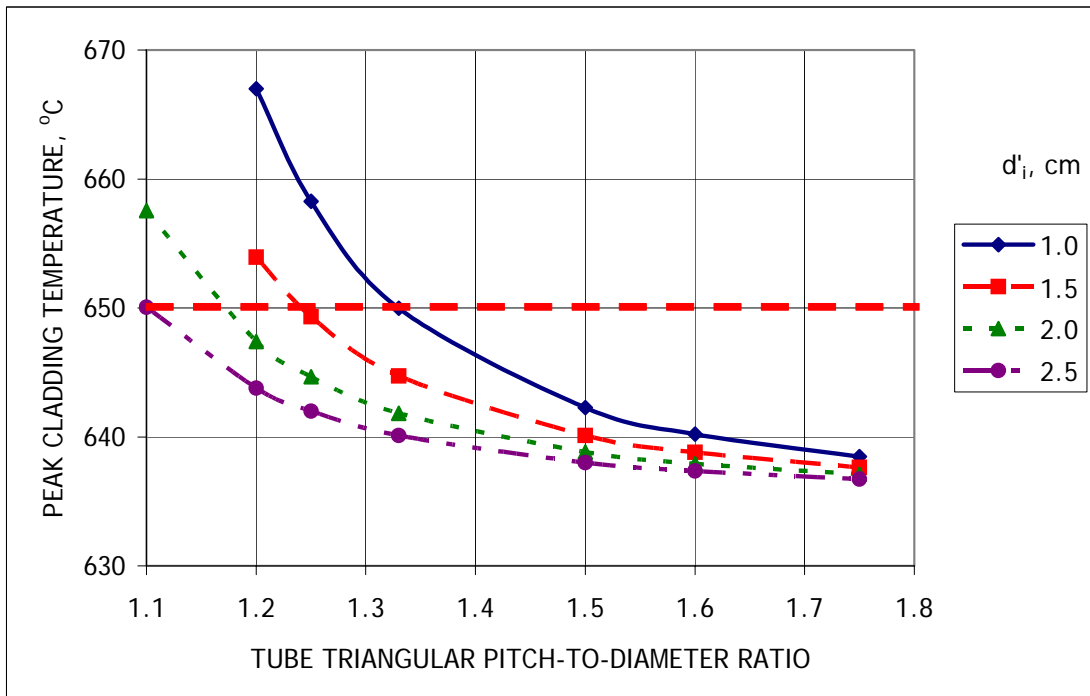
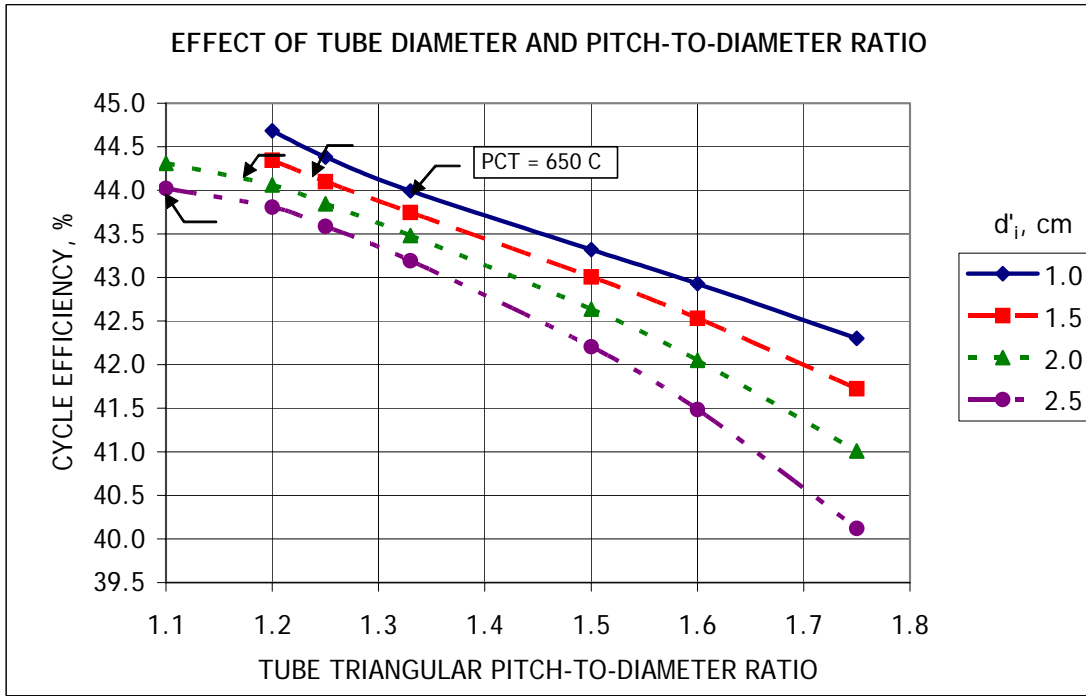


Figure B.1. Tube diameters and pitch-to-diameter ratio optimization (triangular lattice).

Straight Annuli HX, Square Lattice, $H=6.0$ m, $r_i-r'_o=2.0$ mm

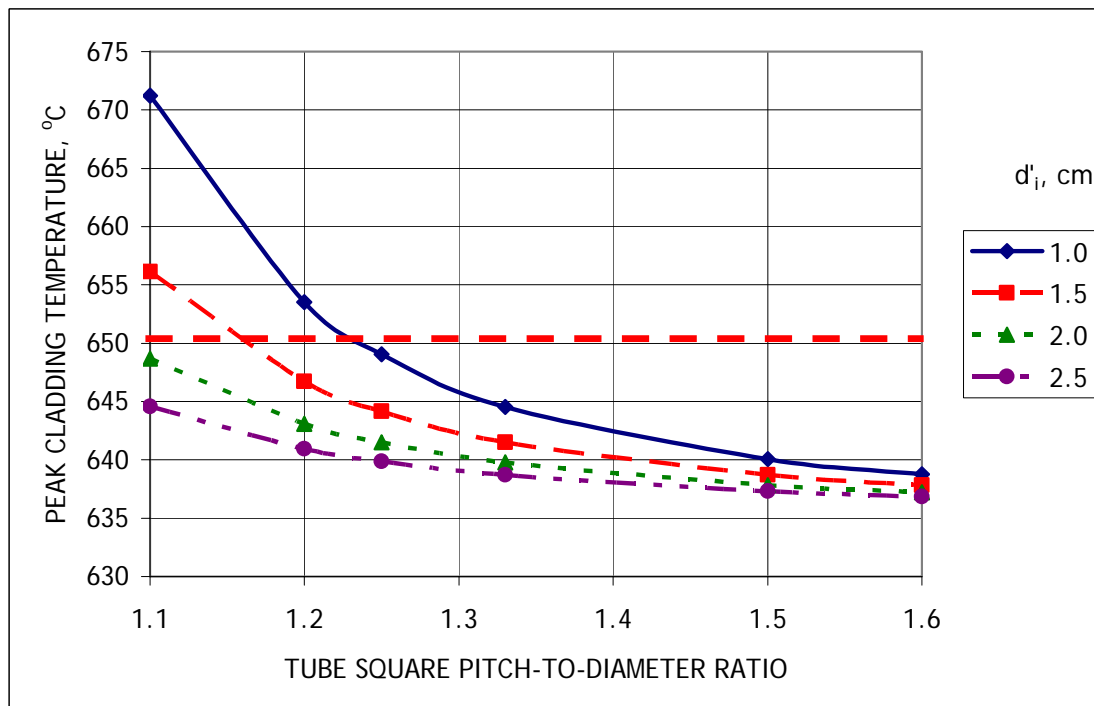
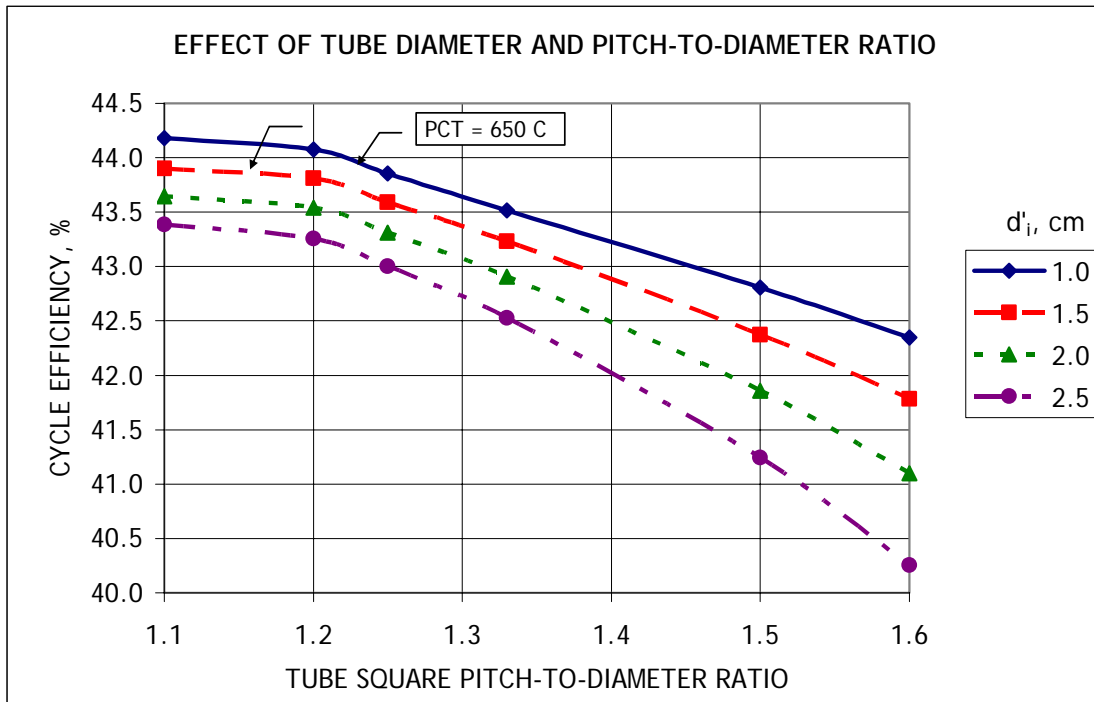


Figure B.2. Tube diameters and pitch-to-diameter ratio optimization (square lattice).

Straight Annuli HX, Triangular Lattice, $H=6.0$ m, $d'_i=2.0$ cm

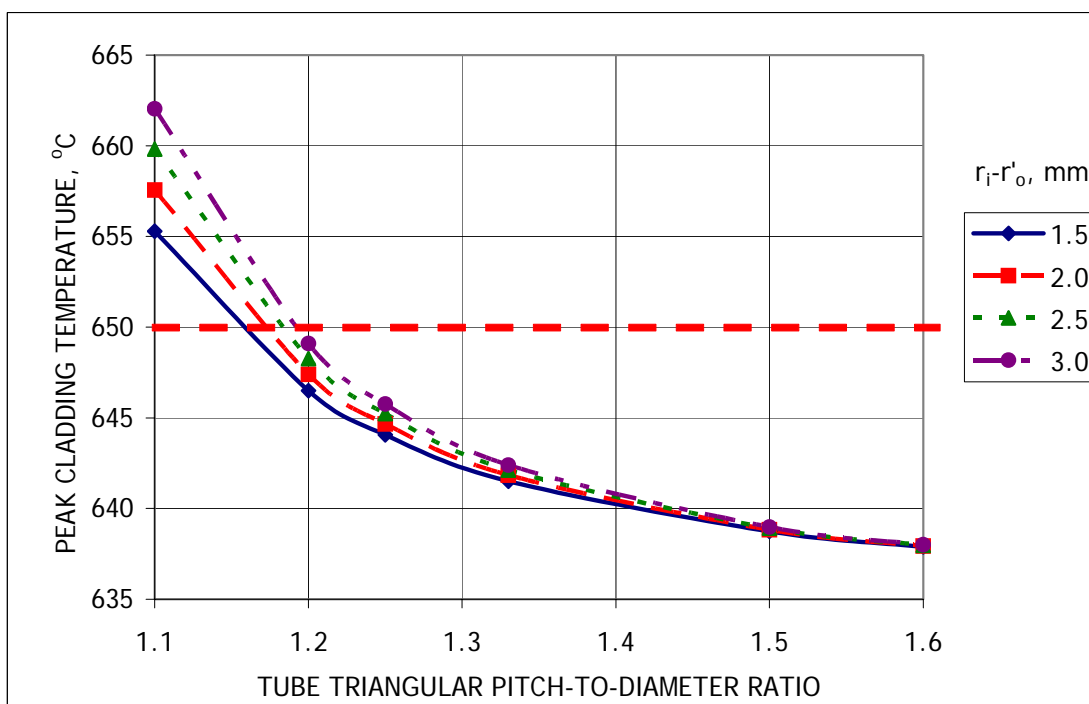
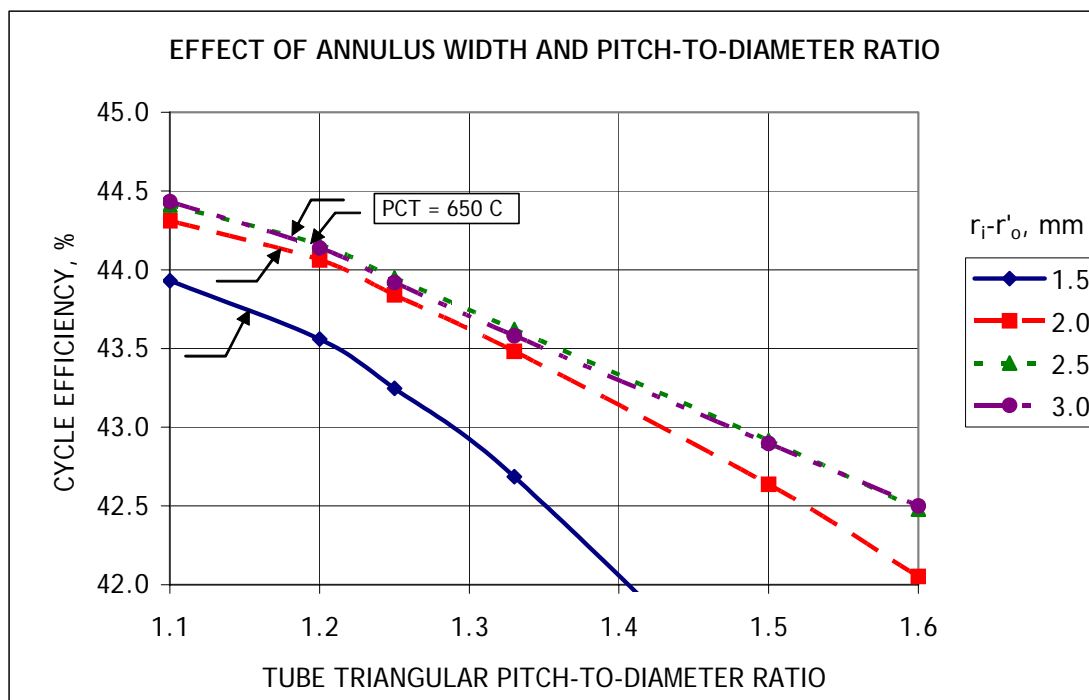


Figure B.3. Annulus width optimization.

Straight Annuli HX, Triangular Lattice, $d'_i=2.0$ cm, $d_i=3.0$ cm

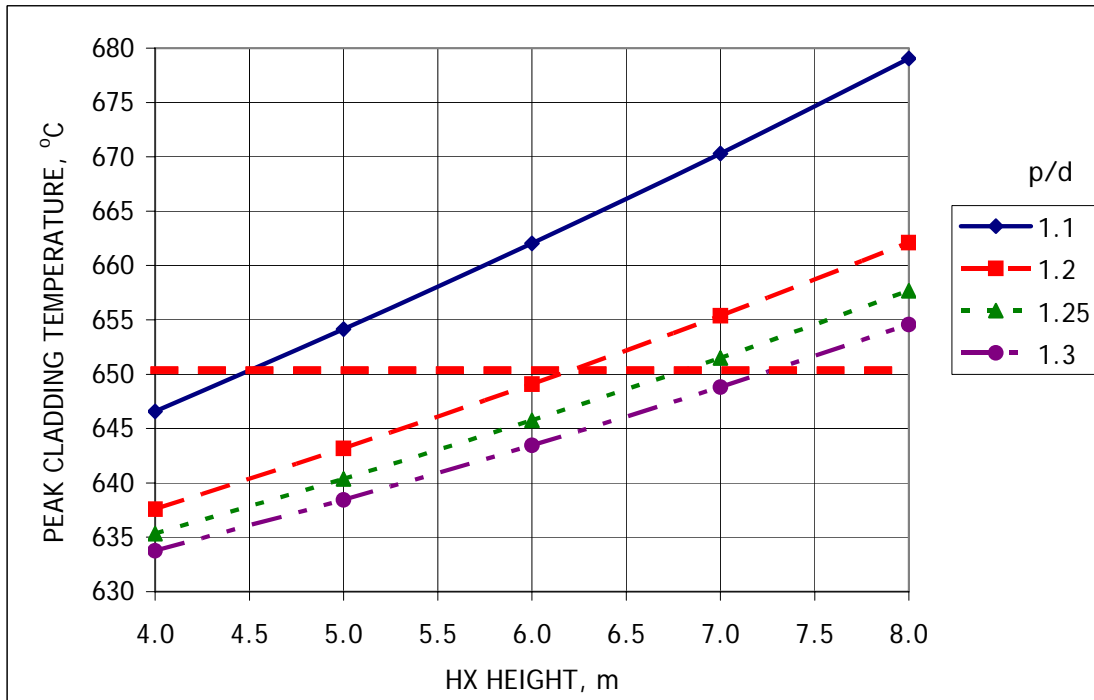
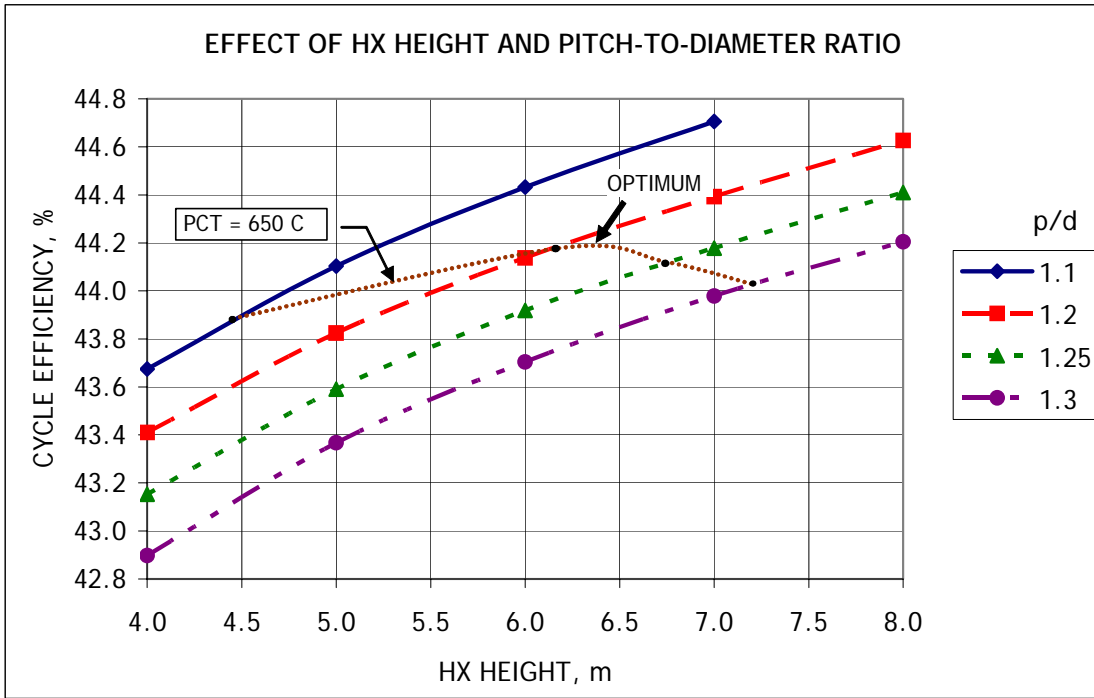


Figure B.4. RHX height optimization.

Straight Annuli HX, Triangular Lattice, $d'_i=2.0$ cm, $d_i=3.0$ cm, $p/d=1.2$

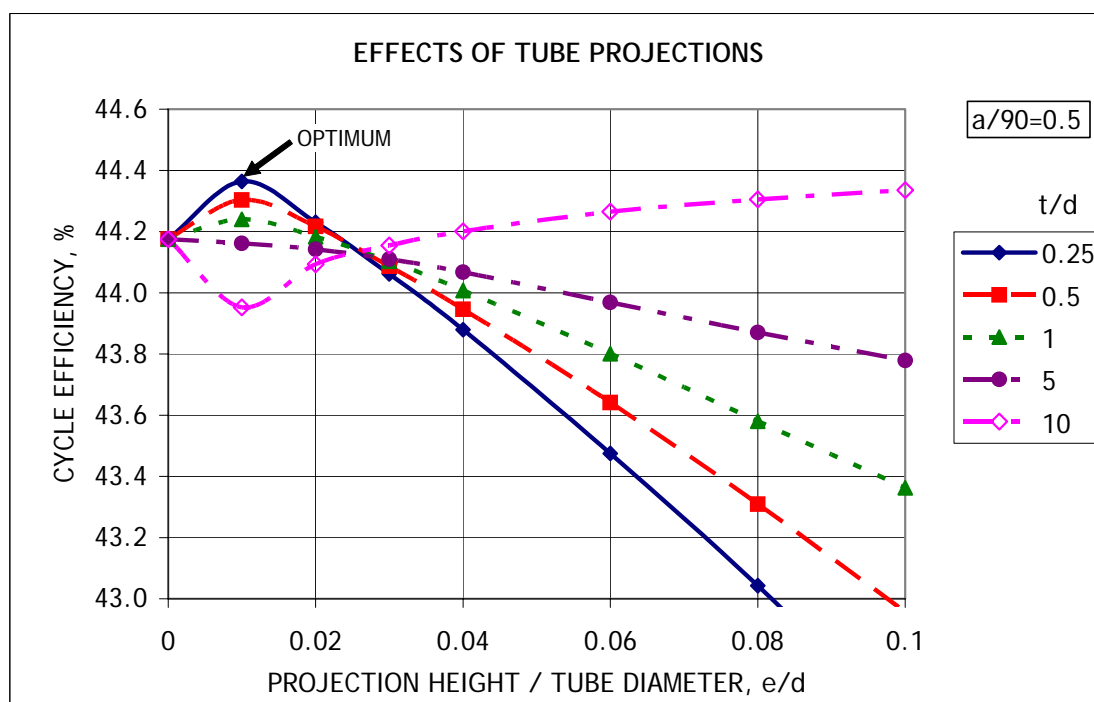
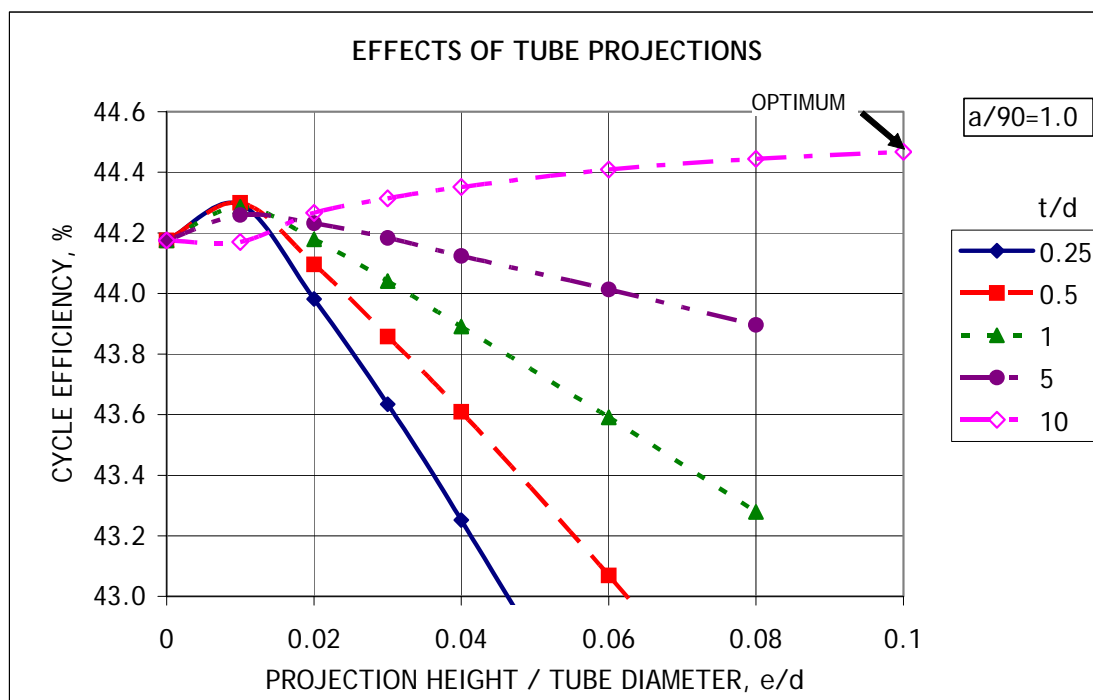


Figure B.5. Tube projections parameters optimization.

Straight Annuli HX, Triangular Lattice, $d'_i=2.0$ cm, $d_i=3.0$ cm, $p/d=1.2$

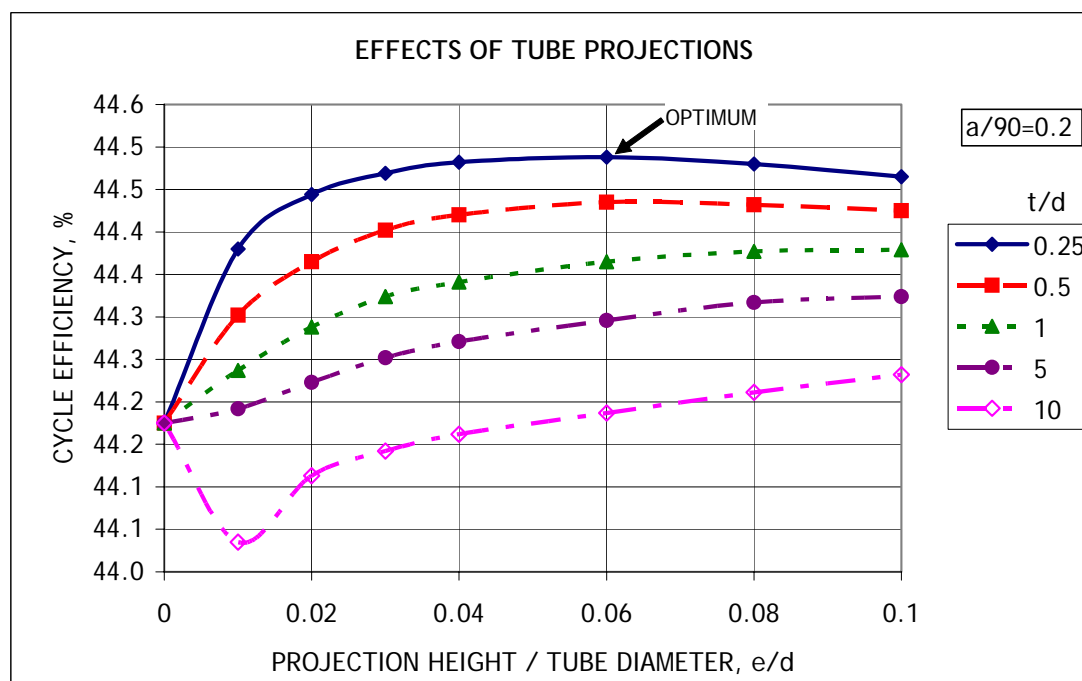
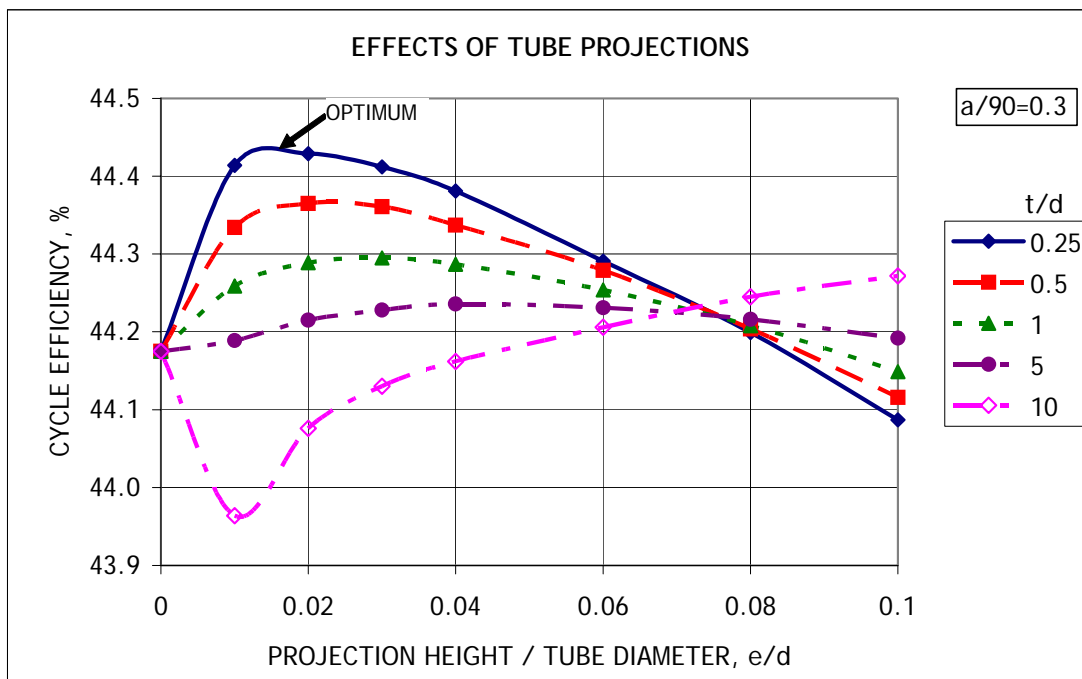


Figure B.5. (Continued) Tube projections parameters optimization.

Straight Annuli HX, Triangular Lattice, $e/d=0.06$, $t/d=0.25$, $a/90=0.2$

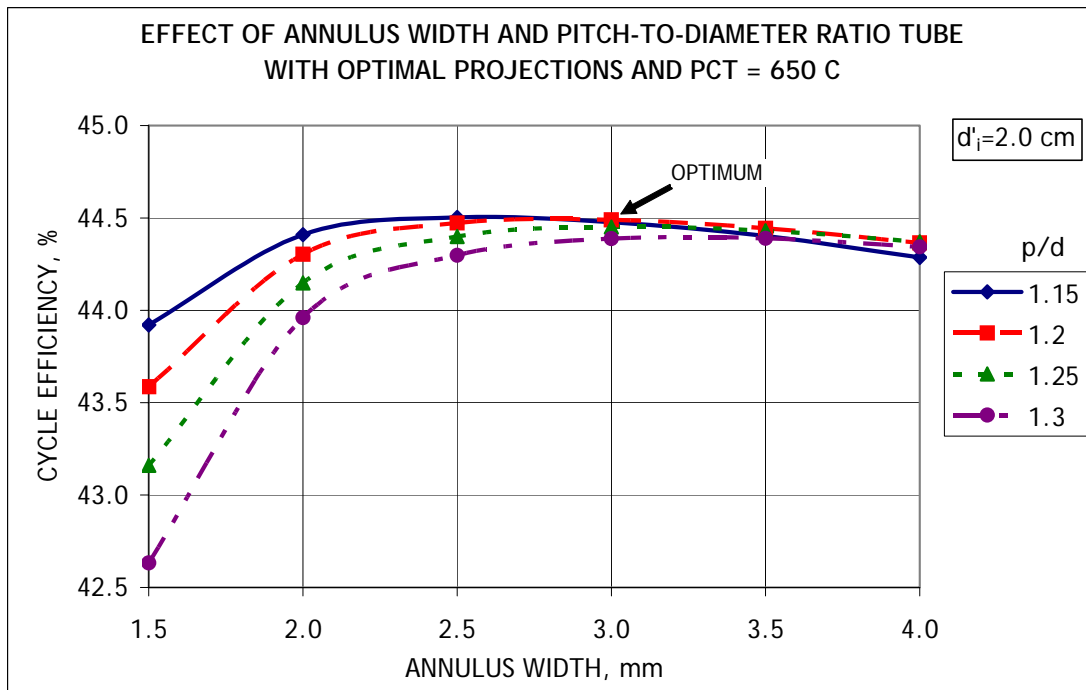
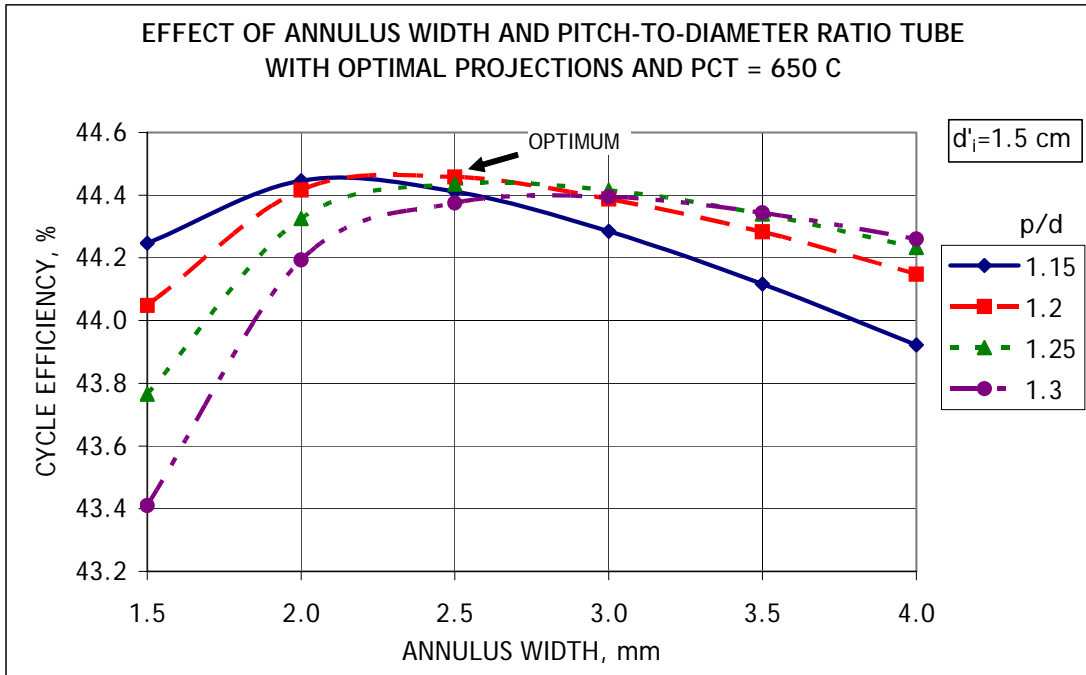


Figure B.6. Annulus width optimization for tubes with projections.

APPENDIX C

INPUT FILES FOR STEADY-STATE MODEL

***** Input data file for CO2 cycle efficiency calculations *****

Maximum pressure in cycle(MPa)
 20.0D0
 Minimum pressure in cycle (MPa)
 7.4D0
 Minimum temperature in cycle (C)
 31.25
 Turbine blade efficiency, %
 97.0
 Turbine leakage and other losses, %
 5.0
 Compressor 1 blade efficiency, %
 96.6
 Compressor 1 leakage and other losses, %
 5.0
 Compressor 2 blade efficiency, %
 94.4
 Compressor 2 leakage and other losses, %
 5.0
 Generator efficiency,%
 98.5
 Mechanical losses,%
 1.
 Fraction of flow sent to LT recuperator
 0.65
 Maximum number of iterations
 40
 Array of pipe lengths, m (10 points)
 20.0 5.0 2.0 7.0 2.0 2.0 1.0 2.0 1.0 20.0
 Array of pipe diameters, m (10 points)
 0.5 0.5 0.5 0.5 0.5 0.5 0.5 0.5 0.5 0.5
 ***** High Temperature Recuperator parameters *****
 Recuperator type (0 - Ideal, 1 - Shell-and-tube, 2 - Heatric)
 1
 ----- Shell-and-tube HX data -----
 Number of tubes in recuperator
 80000
 Recuperator length, m
 10.
 Inner and outer tube diameters, m
 0.01 0.014
 Recuperator pitch-to-diameter ratio
 1.33
 Tube material (5 characters)
 SS316
 Number of points for temperature calculations
 21
 Required accuracy (in secondary outlet temperature), C
 0.001
 Tube side (1 - Primary, 2 - Secondary)
 2
 Heat transfer correlation (DB - Dittus-Boetler, PG - Petukhov-
 Gnielinski)
 DB

```

Number of fins on inner surface per tube
12
Width of fins on inner surface ,m
0.001
Length of fins on inner surface , m
0.0015
Number of fins on outer surface per tube
12
Width of fins on outer surface ,m
0.001
Length of fins on outer surface , m
0.0025
----- Heatric HX data -----
Recuperator length, m
2.0
Recuperator width, m
6.0
Recuperator height, m
6.0
Semi-spherical channel diameter, mm
0.5
Pitch-to-diameter ratio
1.2
Layer thickness, mm
0.5
Material
SS316
Number of points for temperature calculations
11
Required accuracy (in secondary outlet temperature), C
0.01
Heat transfer correlation (DB - Dittus-Boetler, PG - Petukhov-
Gnielinski)
DB
***** Low Temperature Recuperator parameters *****
Recuperator type (0 - Ideal, 1 - Shell-and-tube, 2 - Heatric)
1
----- Shell-and-tube HX data -----
Number of tubes in recuperator (Put 0 for ideal recuperator)
80000
Recuperator length, m
10.
Inner and outer tube diameters, m
0.01 0.014
Recuperator pitch-to-diameter ratio
1.33
Tube material (5 characters)
SS316
Number of points for temperature calculations
21
Required accuracy (in secondary outlet/inlet temperature), C
0.001
Tube side (1 - Primary, 2 - Secondary)
2

```

```

Heat transfer correlation (DB - Dittus-Boetler, PG - Petukhov-Gnielinsi
DB
Number of fins on inner surface per tube
12
Width of fins on inner surface ,m
0.001
Length of fins on inner surface , m
0.0015
Number of fins on outer surface per tube
12
Width of fins on outer surface ,m
0.001
Length of fins on outer surface , m
0.0025
----- Heatric HX data -----
Recuperator length, m
1.5
Recuperator width, m
6.0
Recuperator hight, m
6.0
Semi-spherical channel diameter, mm
0.5
Pitch-to-diameter ratio
1.2
Layer thickness, mm
0.5
Material
SS316
Number of points for temperature calculations
11
Required accuracy (in secondary outlet temperature), C
0.01
Heat transfer correlation (DB - Dittus-Boetler, PG - Petukhov-
Gnielinsi)
DB
***** Cooler parameters *****
Number of tubes in cooler
50000
Inner and outer tube diameters, m
0.01 0.014
Tube material (5 characters)
SS316
Step in cooler tube length, m
0.01
Heat transfer correlation (DB - Dittus-Boetler, PG - Petukhov-Gnielinsi
DB
Number of fins on inner surface per tube
0
Width of fins on inner surface, m
0.001
Length of fins on inner surface, m
0.0015
Temperature of cooling fluid, C

```

```

30
***** Turbine *****
Shaft revolution speed (rev/s)
60
Minimum hub radius (cm)
20
Blade material density (kg/m3)
8300
Blade maximum total stress (MPa)
300
Vibrational stress factor
0.75
Maximum number of stages
6
Accuracy on exit pressure
1.D-6
----- Blade profile coefficients -----
Coefficient for Ixx
1.165D-3
Coefficient for Iyy
1.0381D-2
Coefficient for x coordinate of center of gravity
7.434D-2
Coefficient for y coordinate of center of gravity
2.738D-2
Coefficient for x coordinate of trailing edge
4.372D-1
Coefficient for y coordinate of trailing edge
-4.656D-1
Principal axes angle, degrees
60.33
Average blade angle, degrees
60
***** Compressor #1 *****
Shaft revolution speed (rev/s)
60
Minimum hub radius (cm)
10
Blade material density (kg/m3)
8300
Blade maximum total stress (MPa)
300
Vibrational stress factor
0.75
Maximum number of stages
6
Accuracy on exit pressure
1.D-6
----- Blade profile coefficients -----
Coefficient for Ixx
1.165D-3
Coefficient for Iyy
1.0381D-2
Coefficient for x coordinate of center of gravity

```

```

7.434D-2
Coefficient for y coordinate of center of gravity
2.738D-2
Coefficient for x coordinate of trailing edge
4.372D-1
Coefficient for y coordinate of trailing edge
-4.656D-1
Principal axes angle, degrees
60.33
Average blade angle, degrees
60
***** Compressor #2 *****
Shaft revolution speed (rev/s)
60
Minimum hub radius (cm)
10
Blade material density (kg/m3)
8300
Blade maximum total stress (MPa)
300
Vibrational stress factor
0.75
Maximum number of stages
6
Accuracy on exit pressure
1.D-6
----- Blade profile coefficients -----
Coefficient for Ixx
1.165D-3
Coefficient for Iyy
1.0381D-2
Coefficient for x coordinate of center of gravity
7.434D-2
Coefficient for y coordinate of center of gravity
2.738D-2
Coefficient for x coordinate of trailing edge
4.372D-1
Coefficient for y coordinate of trailing edge
-4.656D-1
Principal axes angle, degrees
60.33
Average blade angle, degrees
60

```

***** Input data for Reactor calculations *****

Reactor power, MWt
400.0
Core inlet coolant temperature, C
420.0
Maximum cladding temperature, C
650.0
Difference in elevation between top of HX and bottom of the core, m
12.0
Fraction of core power removed by RVACS
0.01
Accuracy on dT in core
1.D-6
----- Core -----
Hot channel outlet power factor
0.8263153287D00
Hot channel factor
1.248557619D00
Power peaking factor
1.47021468D0
Assembly hex size, cm
16.2379
Number of assemblies
199
Active core height, m
2.0
Fission gas plenum height, m
0.5
Fuel rod (cladding) outer diameter, cm
1.905
Cladding thickness, cm
0.1
Cladding material
HT9
Pitch-to-diameter ratio
1.5
Fuel smear density
0.78
Number of flow distributors below the core
2
Array of fractions of open flow areas in distributors
0.6 0.6
Number of spacer grids
3
Fraction of flow area blocked by the grid
0.441
----- HX -----
Number of heat exchangers
4
HX hieght, m (0 - adjust height for max cladding temperature)
0.0
HX outer diameter, m
5.13715
Ratio of HX inner diameter to core diameter


```

1.24
Gap between HX, cm
15.24
Accuracy of CO2 outlet temperature
1E-6
Fraction of flow that bypass HX
0.01
HX type:
  (   1 - Staked U-Tubes           )
  (   2 - U-tubes                   )
  (   3 - Concentric Tubes          )
  (   4 - Straight Tubes            )
  (   5 - Straight Annuli           )
  (   6 - Helical Coil              )
  (   7 - HEATRIC                   )
5
HX lattice layout (3 - triangular, 4 - square)
3
HX tube outer diameter, cm (outer tube for HX types 3&5)
3.4
HX tube inner diameter, cm (outer tube for HX types 3&5)
3.0
Pitch-to-diameter ratio
1.2
Tube material
SS316
Grooves height, relative to diameter, (e/d). 0 means no grooves.
[0<=e/d<=0.1]
0.06
Grooves pitch, relative to diameter, (t/d). [0.25<=p/d<=10.0]
0.25
Grooves angle to the tube axis, (a/90). [0.2<=a/90<=1.0]
0.2
Enhancement correlation (Z - Zukauskas, B - Bergles)
B
Heat transfer correlation on CO2 side
DB
Number of regions for temperature calculations
50
HX inner tube outer diameter, cm (for HX types 3&5 only)
2.4
HX inner tube inner diameter, cm (for HX types 3&5 only)
2.0
Number of turns per tube (Type 6 only)
3.0
----- Load Follow data -----
Number of states to calculate
0
Min and max fraction of full power (separated by space)
1.0 1.0
Fuel Doppler reactivity coefficient, cents/C
-0.153
Fuel Axial Expansion reactivity coefficient, cents/C
-0.0525

```

Core Radial Expansion reactivity coefficient, cents/C
-0.528
Coolant Density reactivity coefficient, cents/C
0.156
Maximum number of iterations
40

***** Input data for Intermediate loop calculations *****

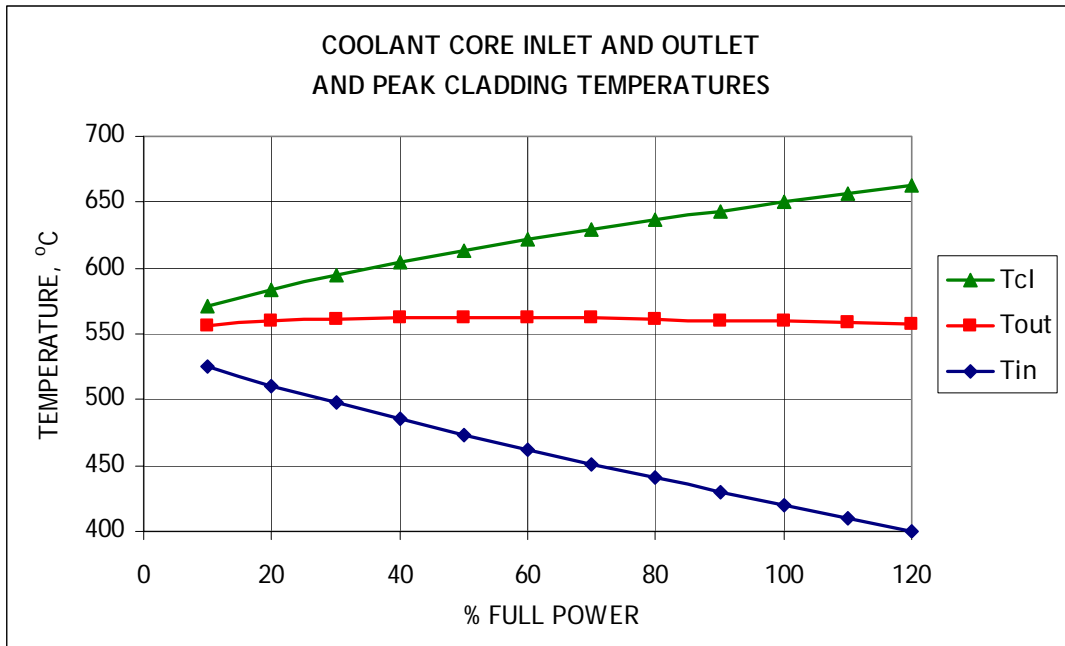
Temperature before RHX, C
 630
 CaBr2 heat duty, W
 212015145.33
 Minimum temperature at R1--B3, C
 701
 Steam mass flow rate, kmol/hr
 3721
 Steam inlet temperature, C
 550
 Steam outlet temperature, C
 750
 Steam pressure, MPa
 0.101325
 Heat available from beds R4 and R5, W
 76488670.00
 Temperature of R4 and R5 beds, C
 600
 He pressure, MPa
 0.101325
 ----- Steam superheater data (plate type HX) -----
 HX length, m
 5.0
 HX width, m
 2.0
 HX height, m
 2.0
 Wall thickness, mm
 0.5
 Space between walls, mm
 4.5
 Wall material
 SS316
 Number of regions for temperature calculations
 20
 Accuracy on steam outlet temperature
 1.D-6
 ----- MS-CO2 HX data (shell-and-tube HX) -----
 HX length, m
 5.4
 Number of tubes
 50000
 Tube outer diameter, mm
 14.0
 Tube inner diameter, mm
 10.0
 Pitch-to-diameter ratio
 1.5
 Tube wall material
 SS316
 Number of regions for temperature calculations
 100
 Accuracy on He outlet temperature

```
1.D-6
----- Load Follow data -----
Number of states to calculate
3
Array of the steam flow rates, kmol/hr
2790.75
1860
930.25
Array of the CaBr2 heat duties, W
168761338.90
126365431.70
69408052.00
Array of the heats available from beds R4 and R5, W
59467502.00
42098193.60
24748981.20
Maximum number of iterations
20
```

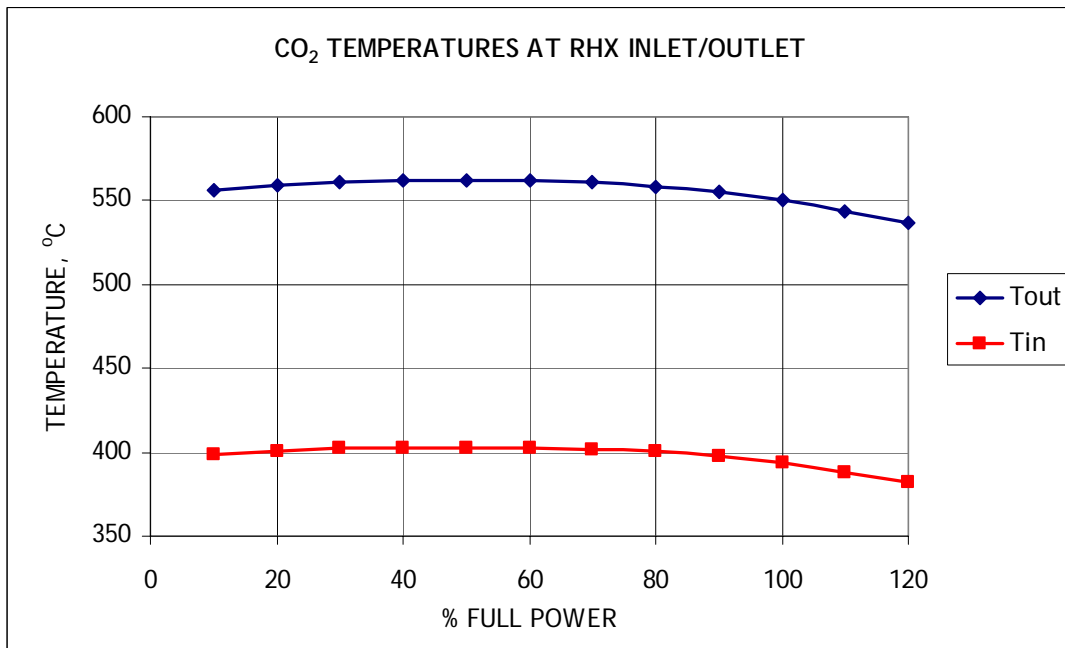
APPENDIX D

RESULTS OF LOAD FOLLOW ANALYSIS FOR STAR-LM

(MASS FLOW RATE CONTROLLED)

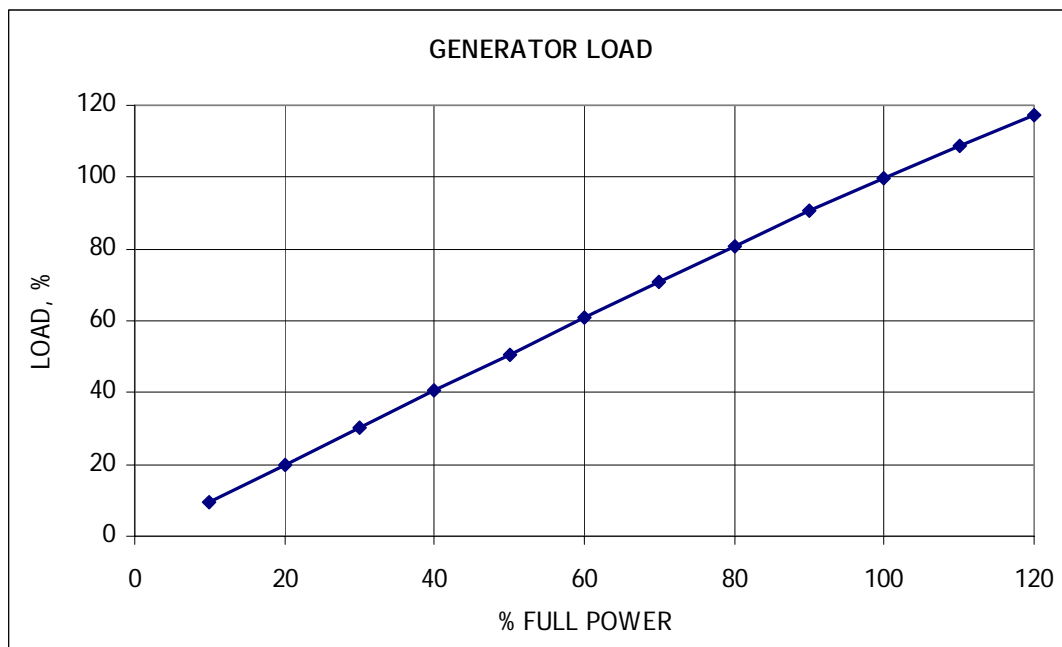


a) Temperature inside the reactor.

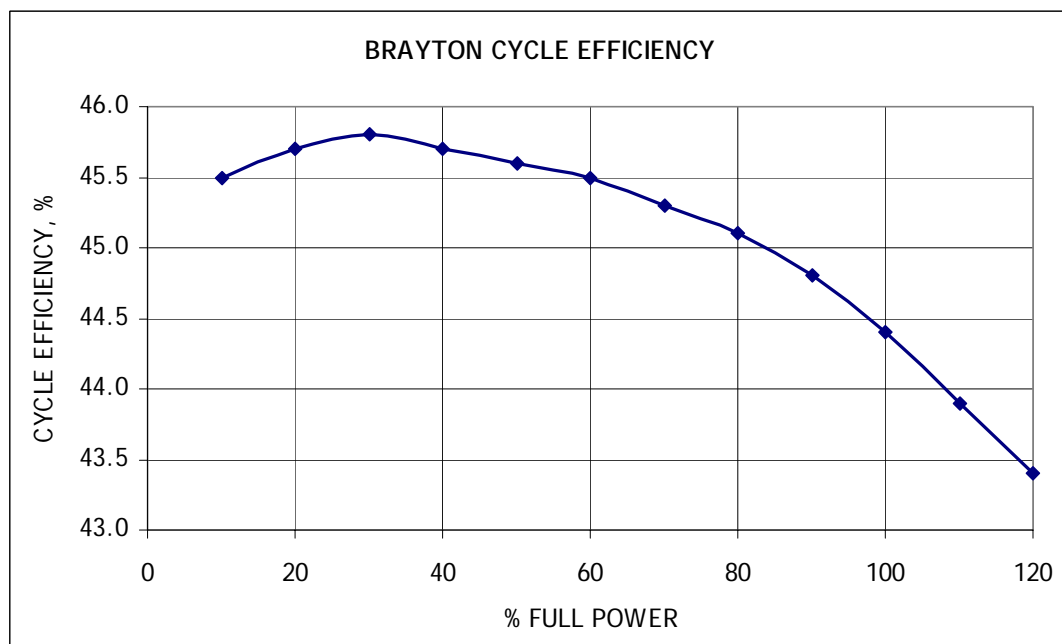


b) CO₂ temperature.

Figure D.1. Load follow by CO₂ mass flow rate control.

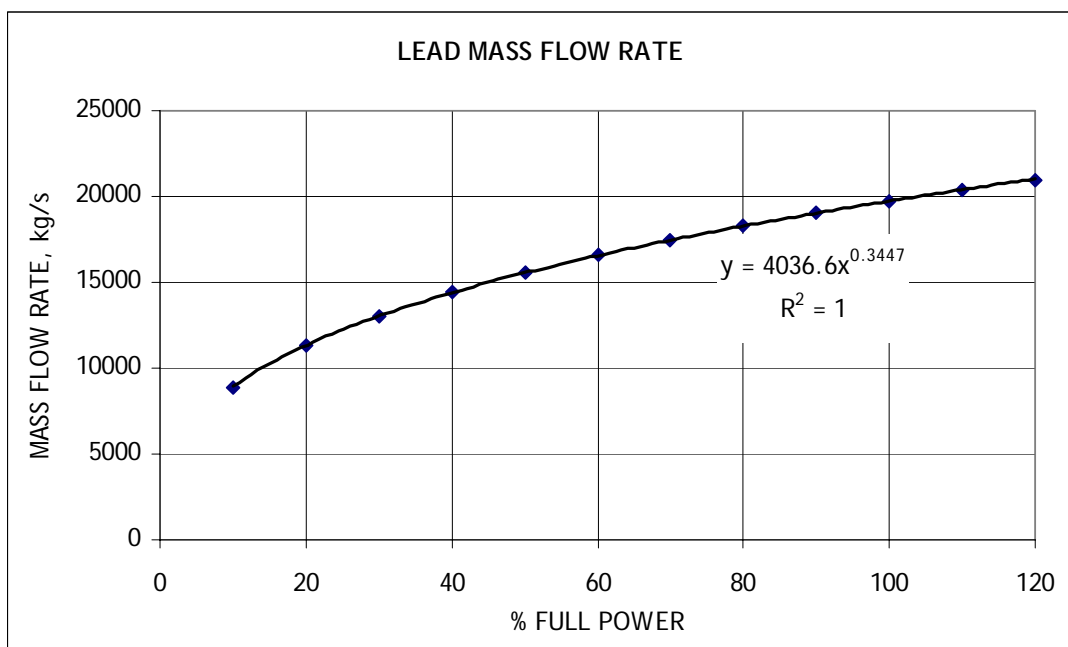


c) Generator load.

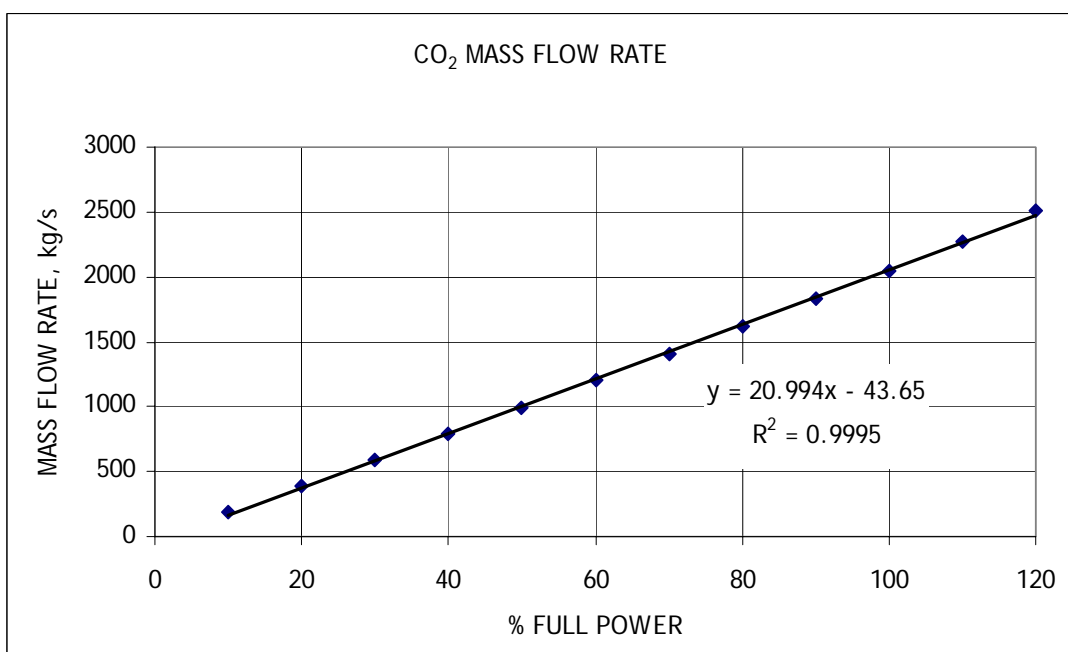


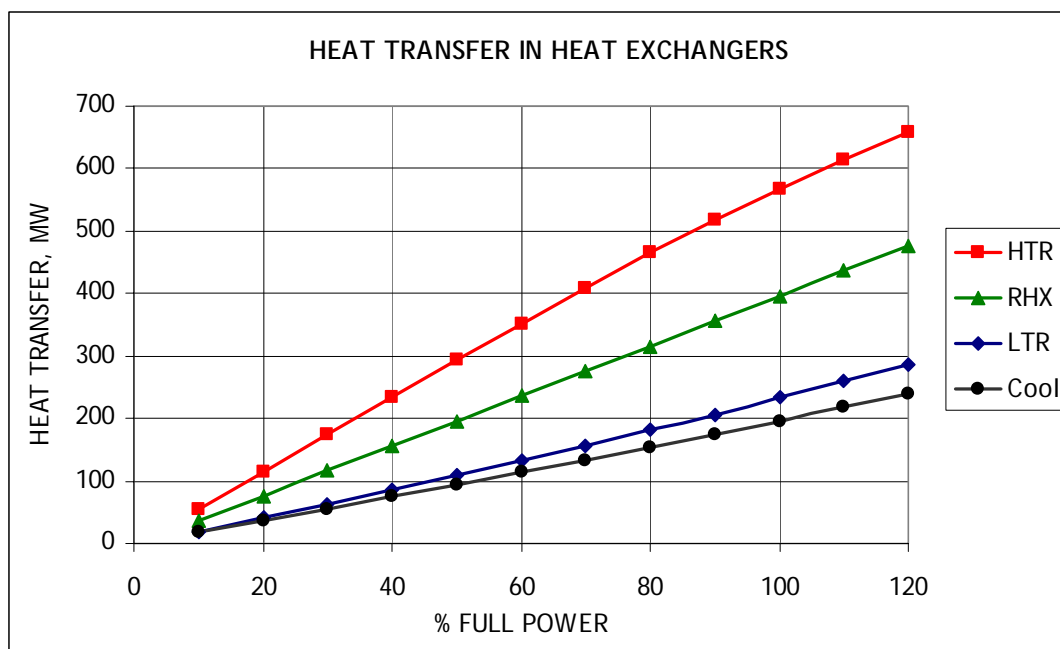
c) Brayton cycle efficiency.

Figure D.1 (Continued). Load follow by CO₂ mass flow rate control.

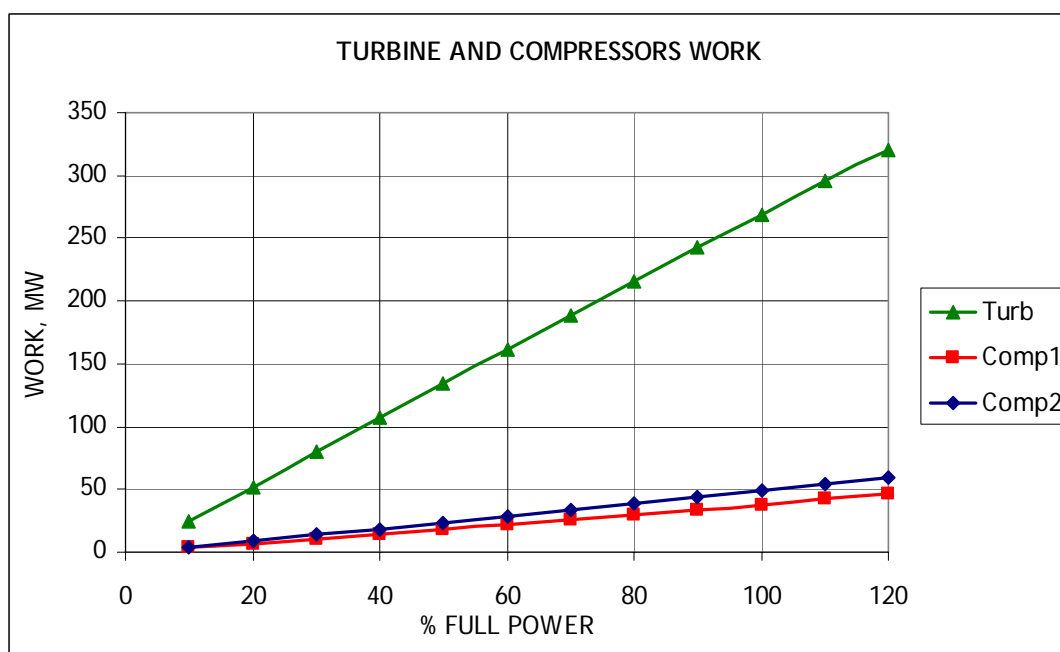


e) Reactor coolant mass flow rate.

f) CO₂ mass flow rate.**Figure D.1 (Continued). Load follow by CO₂ mass flow rate control.**



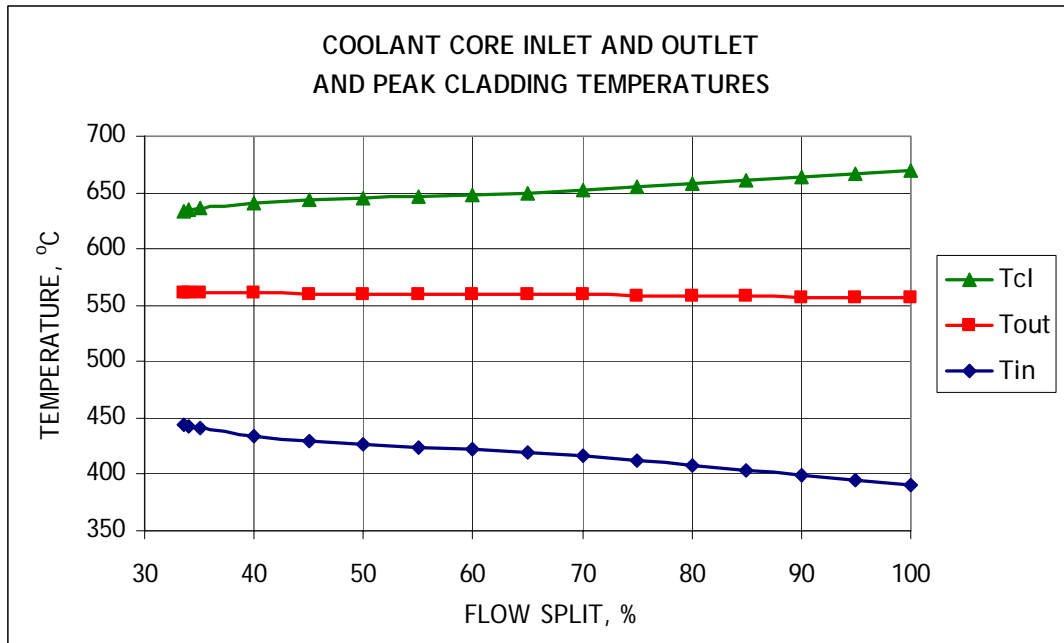
g) Heat transfer in heat exchangers.



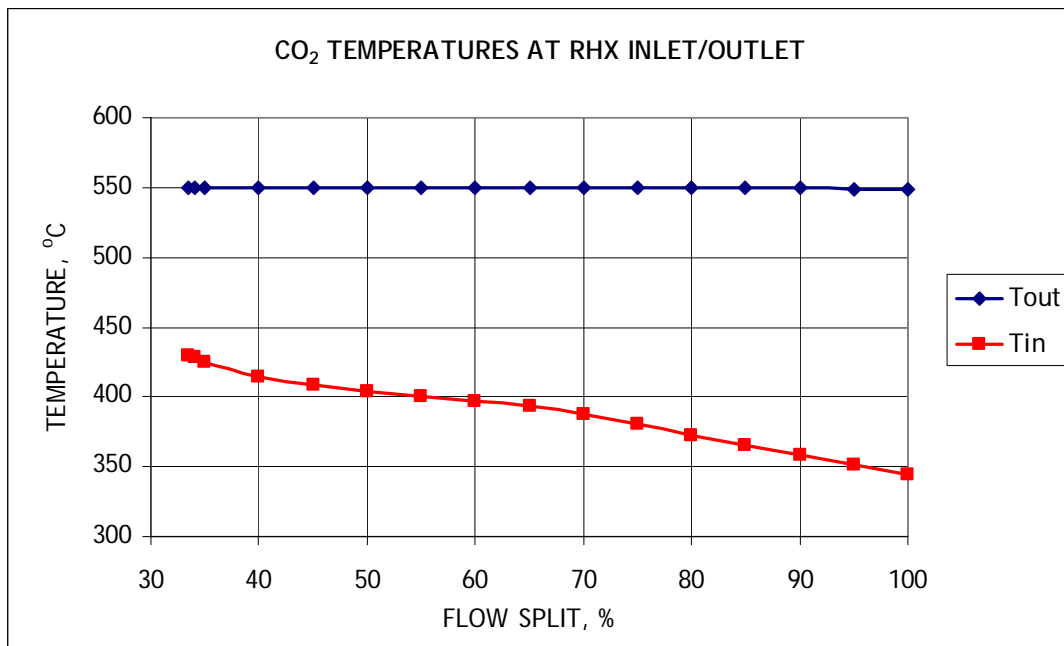
h) Turbine and Compressors Work.

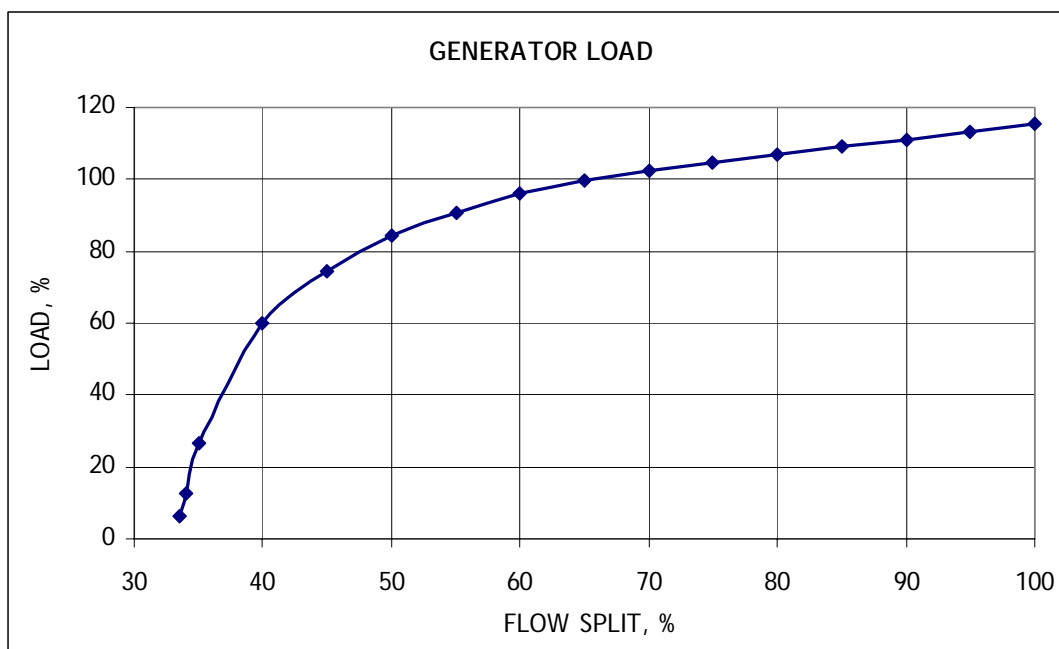
Figure D.1 (Continued). Load follow by CO₂ mass flow rate control.

APPENDIX E
RESULTS OF LOAD FOLLOW ANALYSIS FOR STAR-LM
(FLOW SPLIT CONTROLLED)

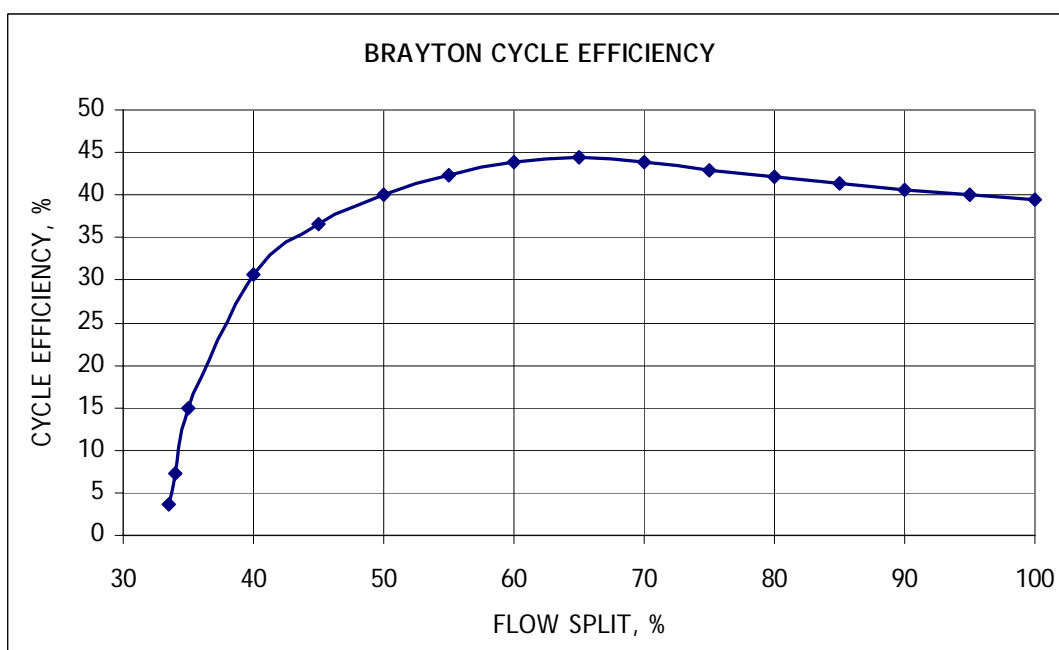


a) Temperatures inside the reactor.

b) CO₂ temperatures.**Figure E.1. Load follow by CO₂ flow split control.**

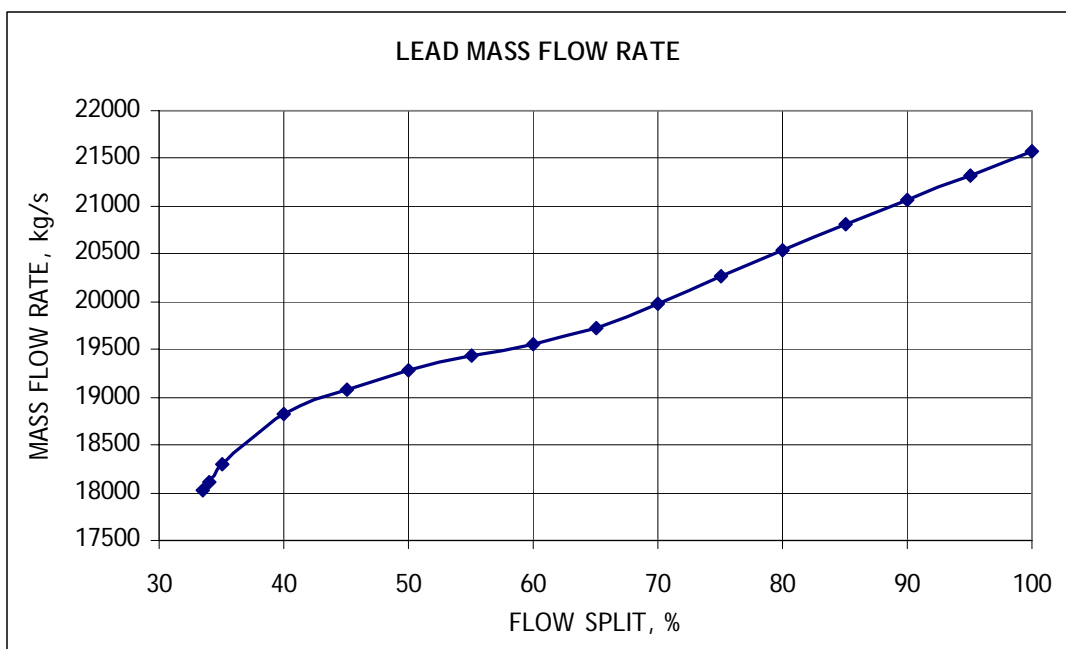


c) Generator load.

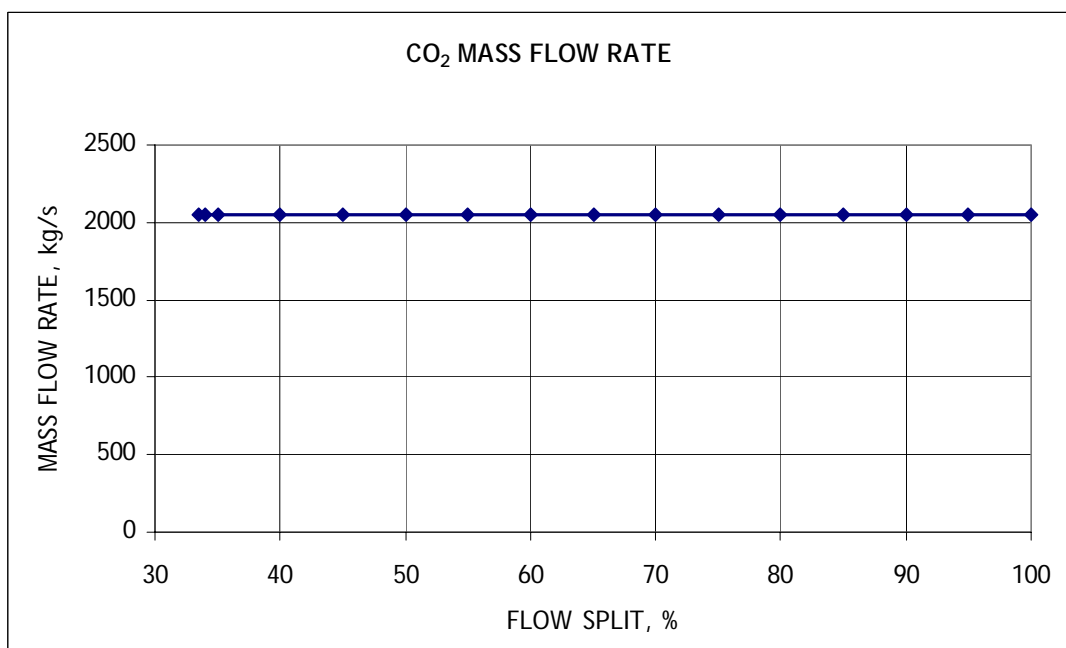


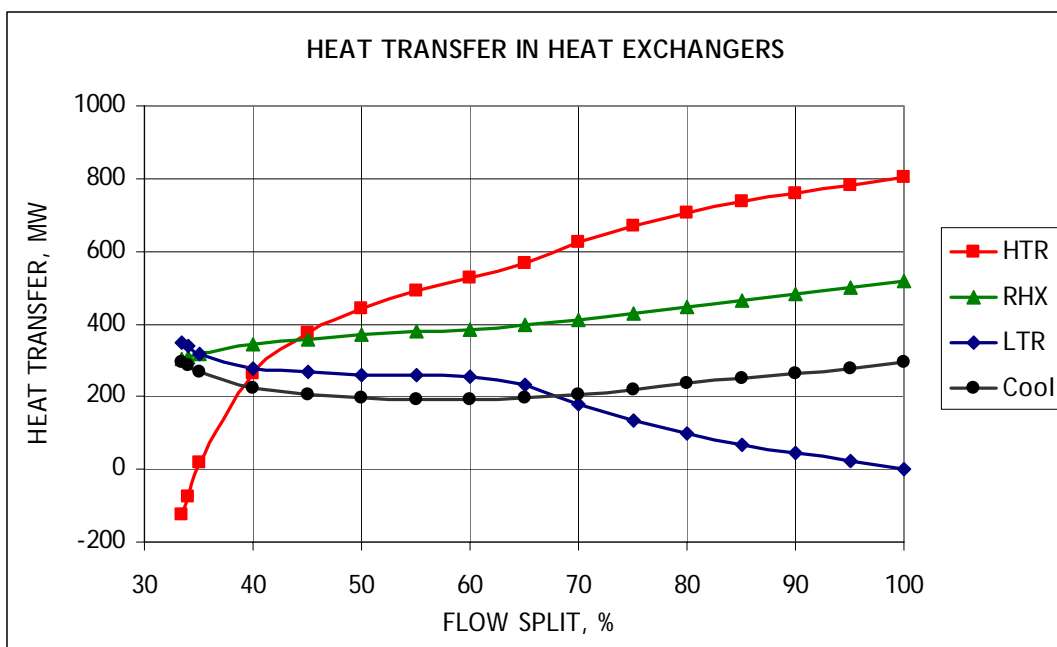
d) Brayton cycle efficiency.

Figure E.1 (Continued). Load follow by CO₂ flow split control.

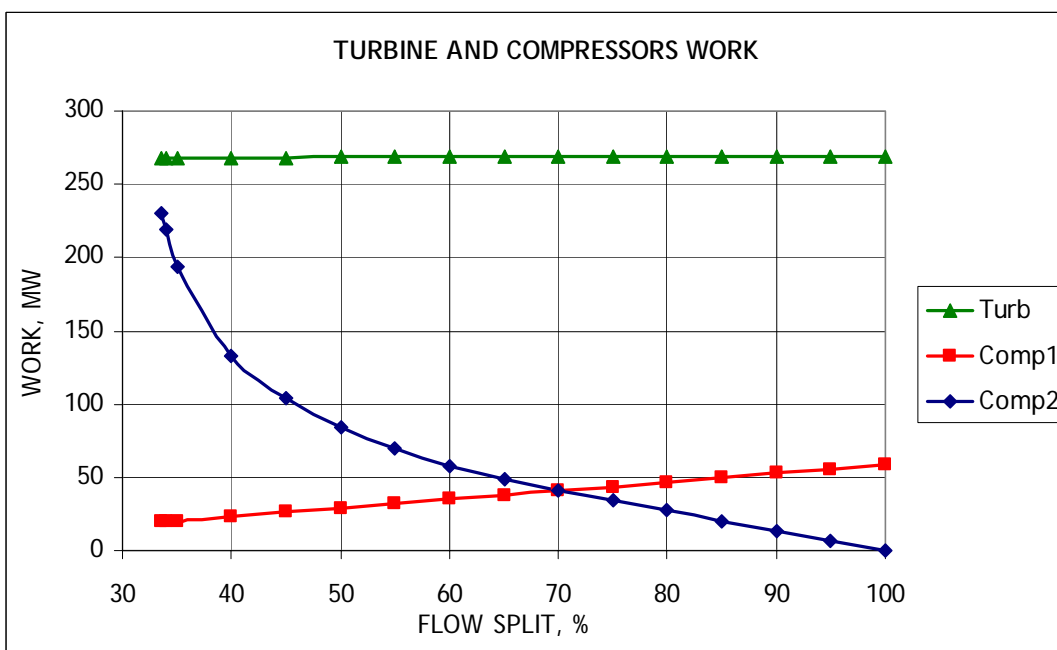


e) Reactor coolant mass flow rate.

f) CO₂ mass flow rate.**Figure E.1 (Continued). Load follow by CO₂ flow split control.**



g) Heat transfer in heat exchangers.



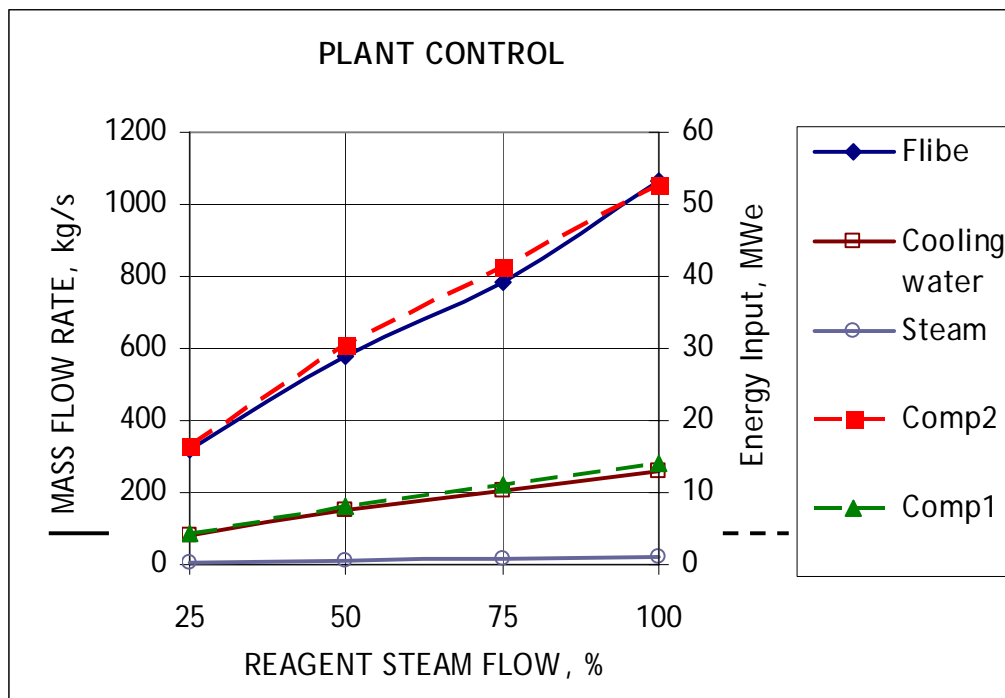
h) Turbine and compressors works.

Figure E.1 (Continued). Load follow by CO₂ flow split control.

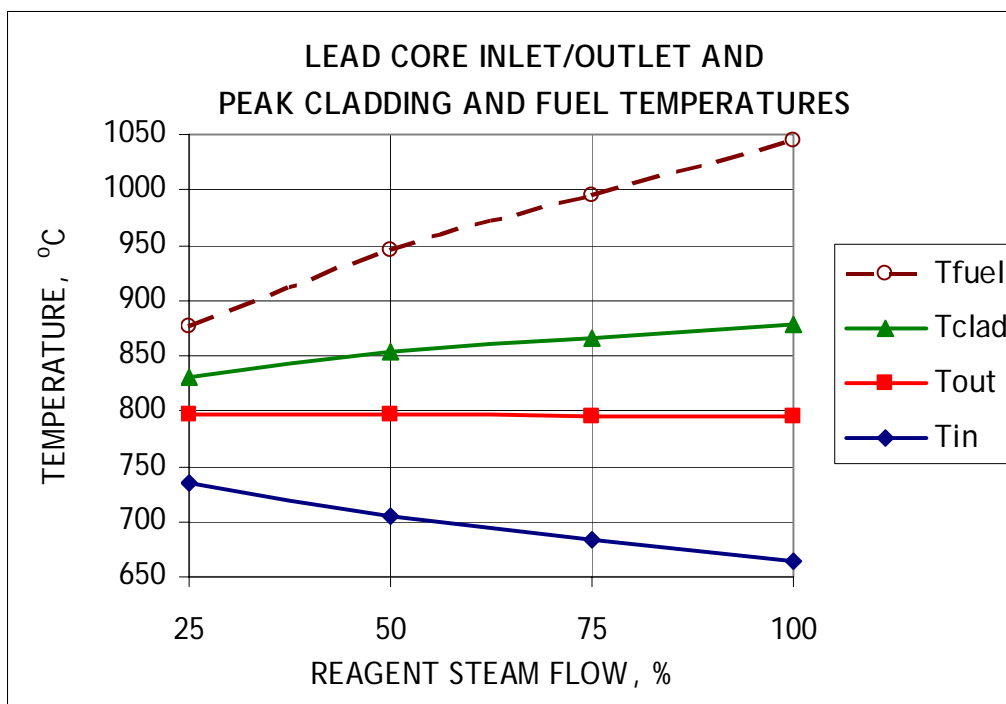
APPENDIX F

RESULTS OF LOAD FOLLOW ANALYSIS FOR STAR-H2

(REAGENT STEAM FLOW RATE VARIATION)

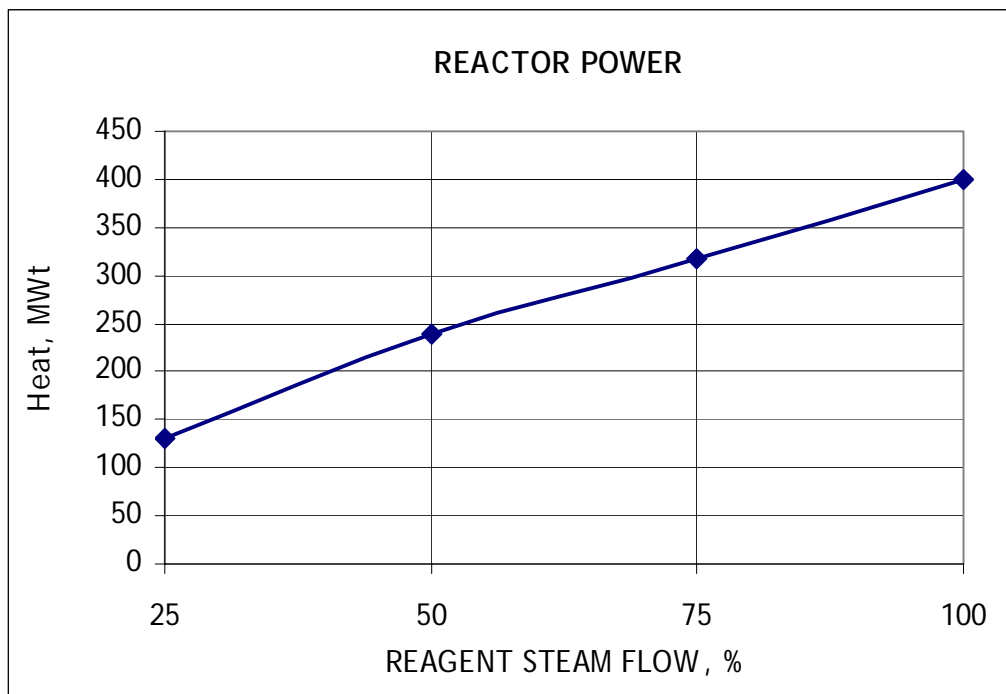


a) Plant control.

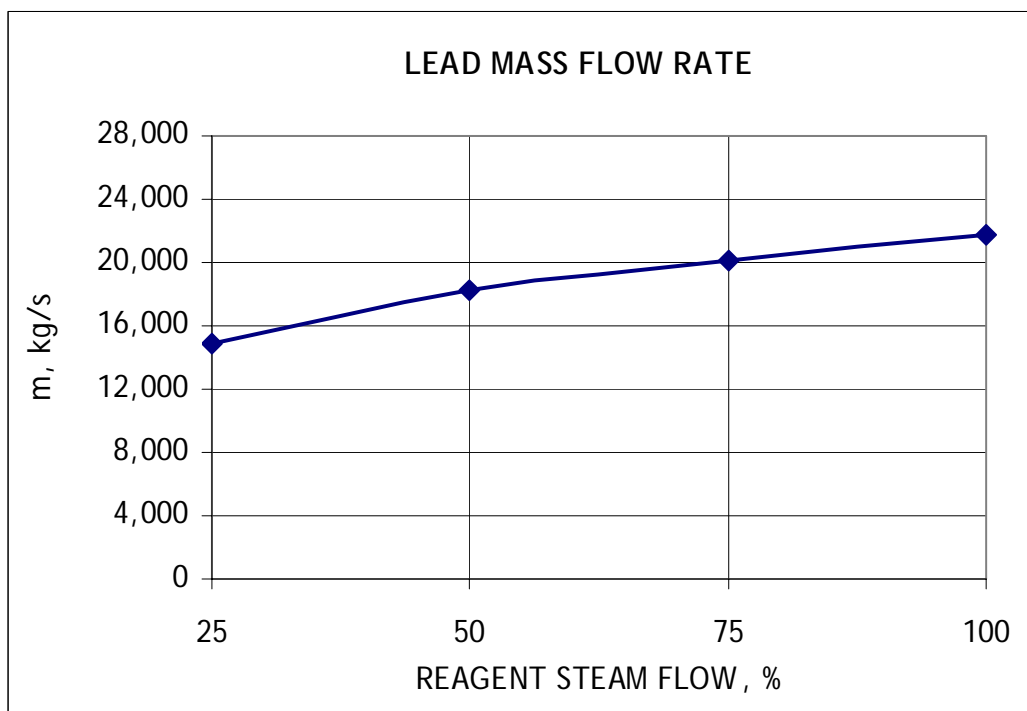


b) Temperatures inside reactor.

Figure F.1. Load follow for reagent steam flow rate variation.

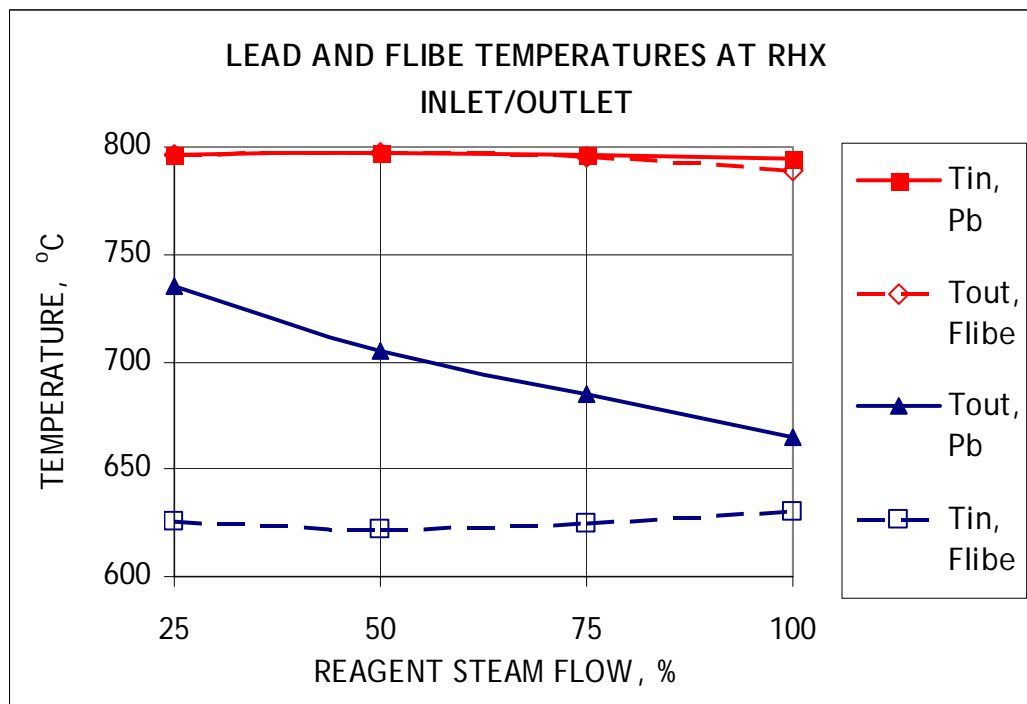


c) Reactor power.

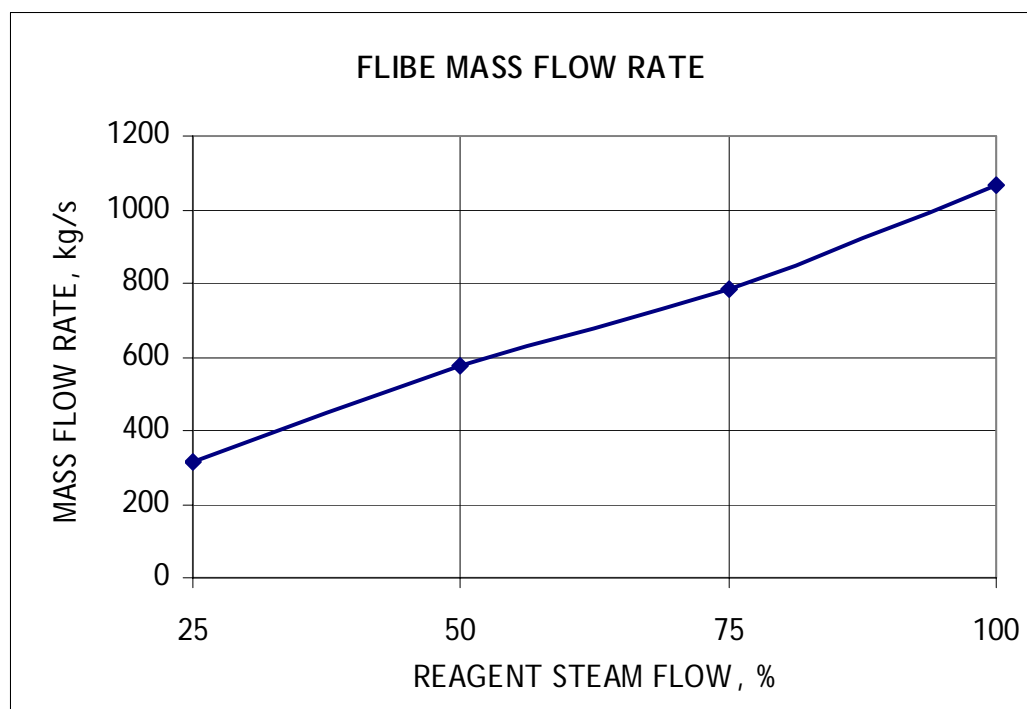


d) Reactor coolant mass flow rate.

Figure F.1 (Continued). Load follow for reagent steam flow rate variation.

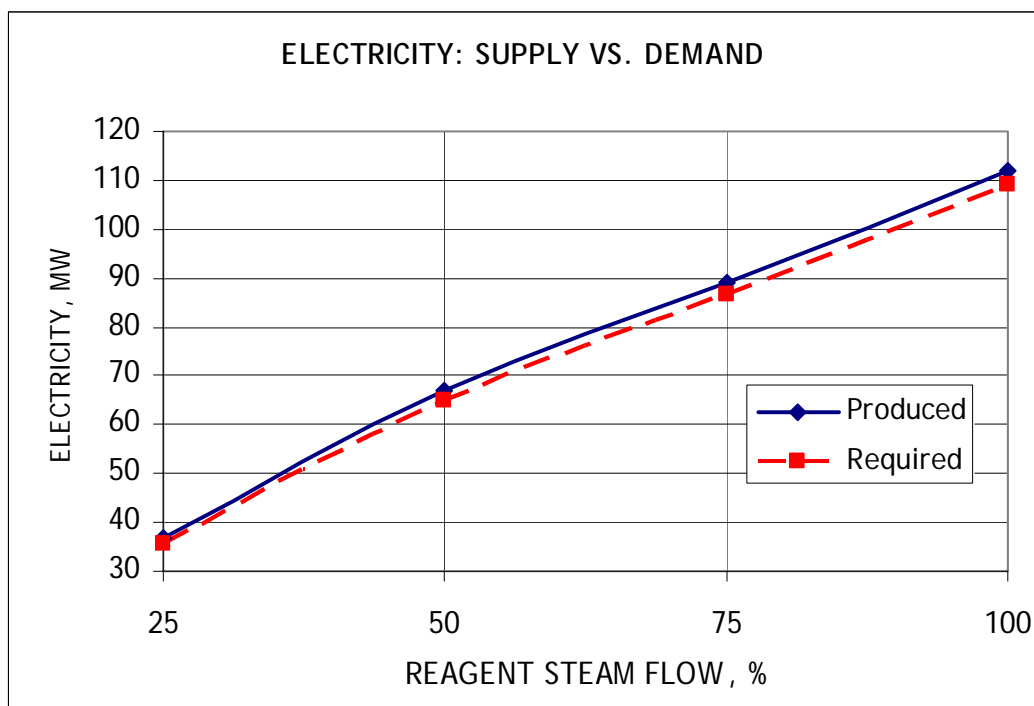


e) RHX temperatures.

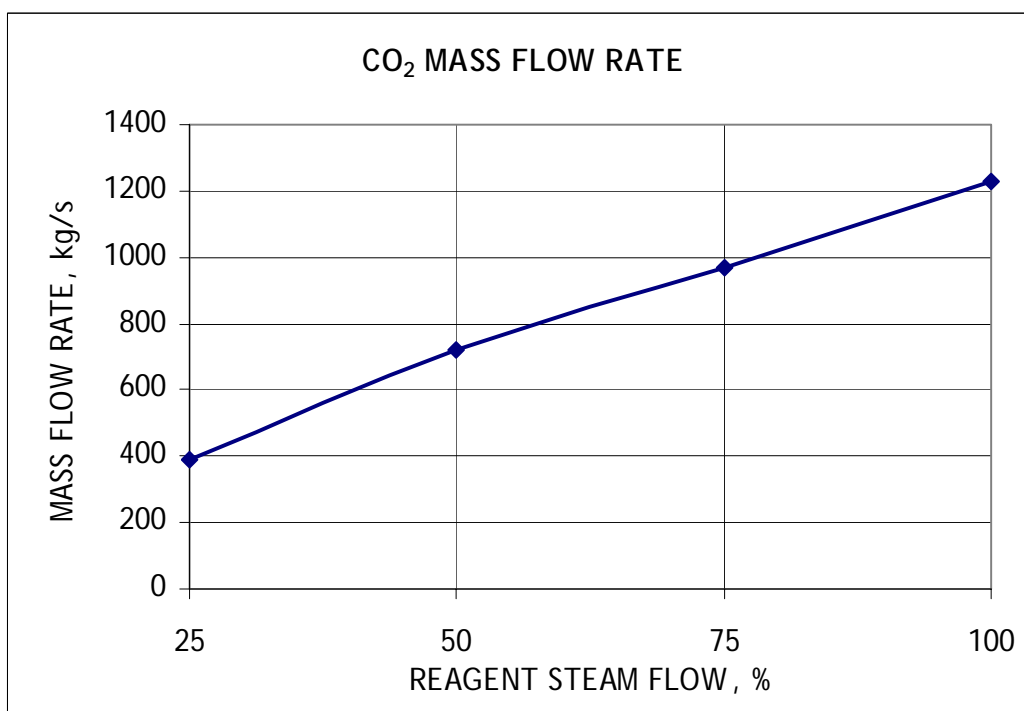


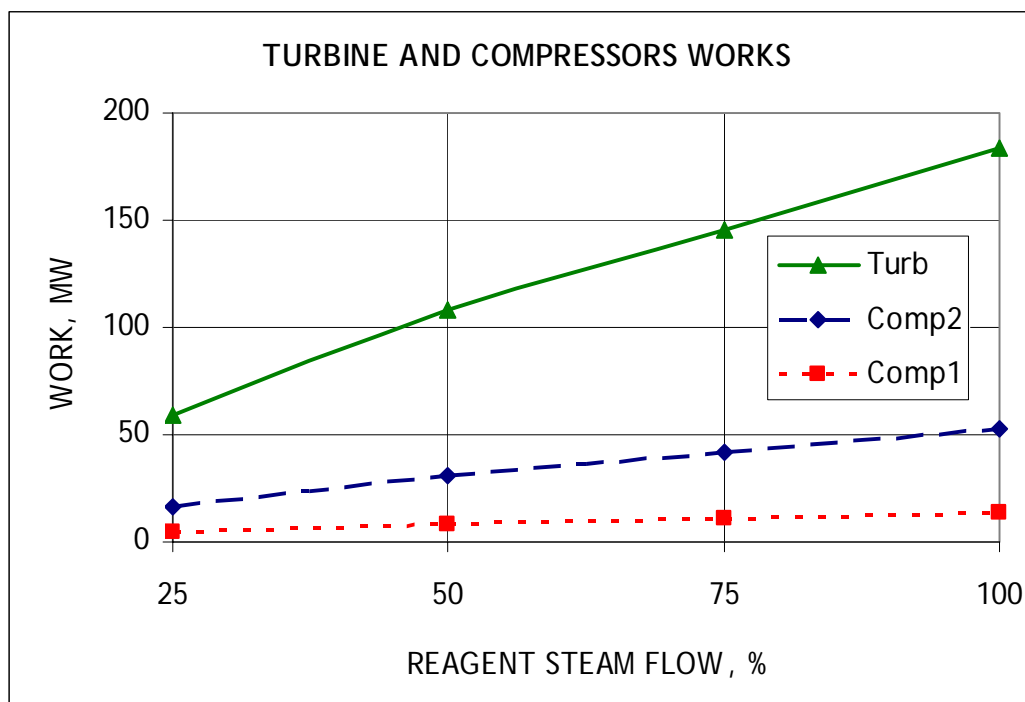
f) Flibe mass flow rate.

Figure F.1 (Continued). Load follow for reagent steam flow rate variation.

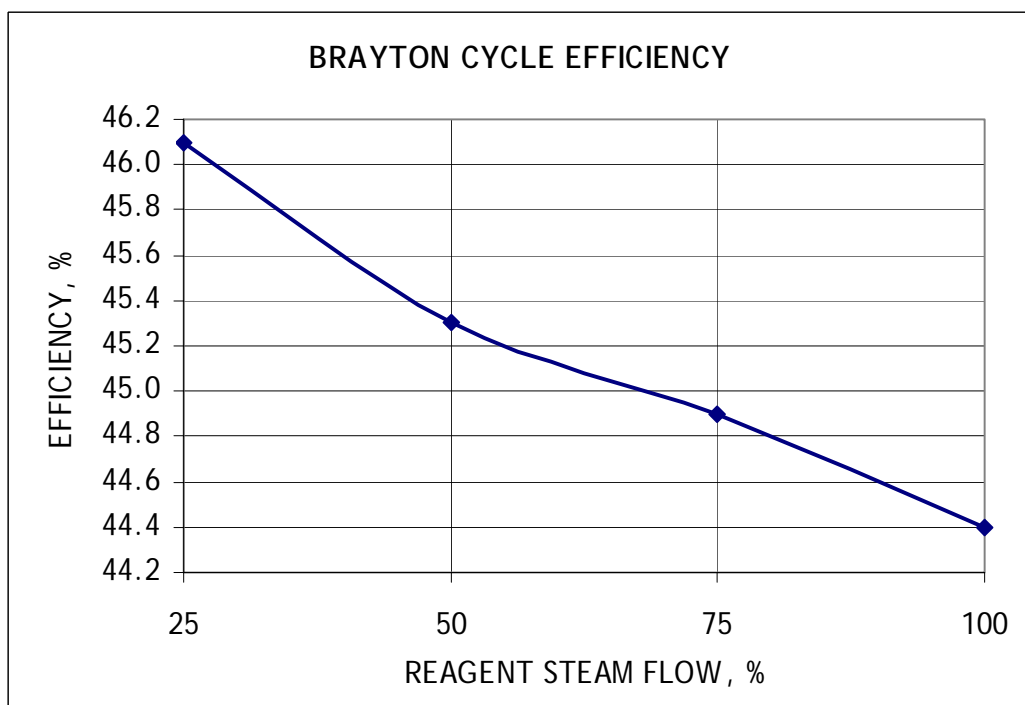


g) Electricity production.

h) CO₂ mass flow rate.**Figure F.1 (Continued). Load follow for reagent steam flow rate variation.**

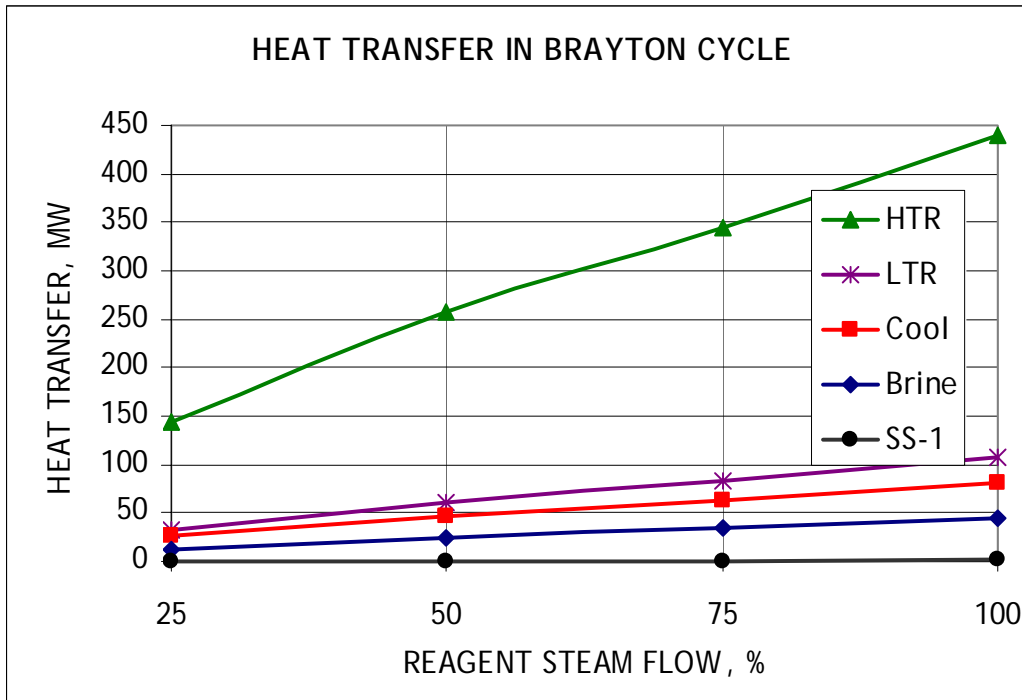


i) Turbine and compressors works.

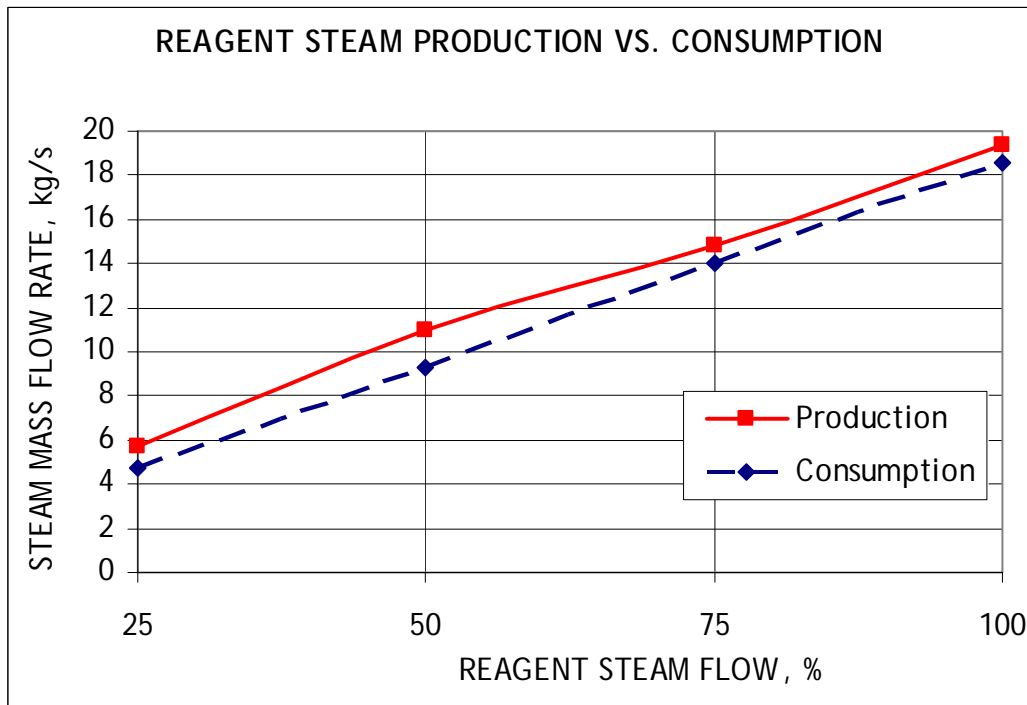


j) Brayton cycle efficiency.

Figure F.1 (Continued). Load follow for reagent steam flow rate variation.



k) Heat transfer in Brayton cycle.



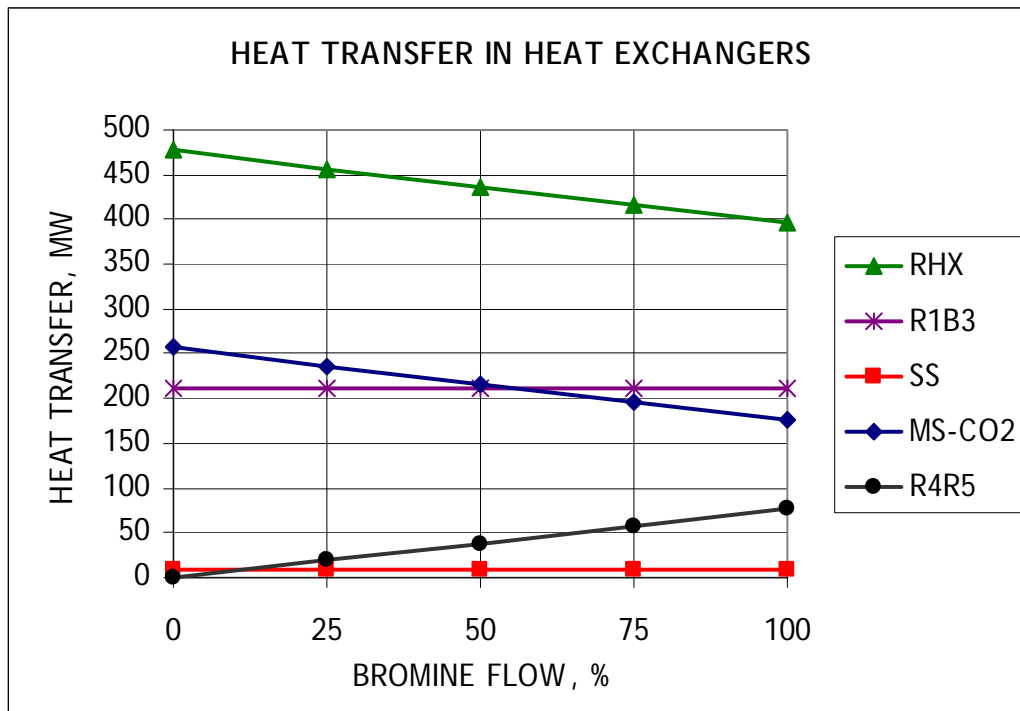
l) Reagent steam production and consumption.

Figure F.1 (Continued). Load follow for reagent steam flow rate variation.

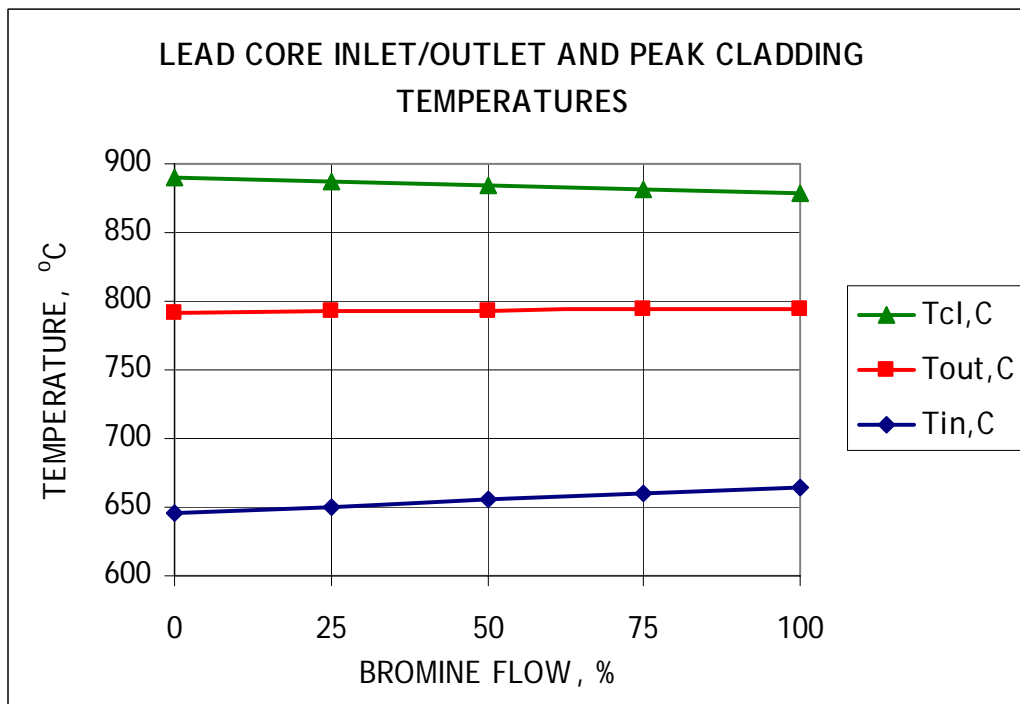
APPENDIX G

RESULTS OF LOAD FOLLOW ANALYSIS FOR STAR-H2

(BROMINE FLOW RATE VARIATION)

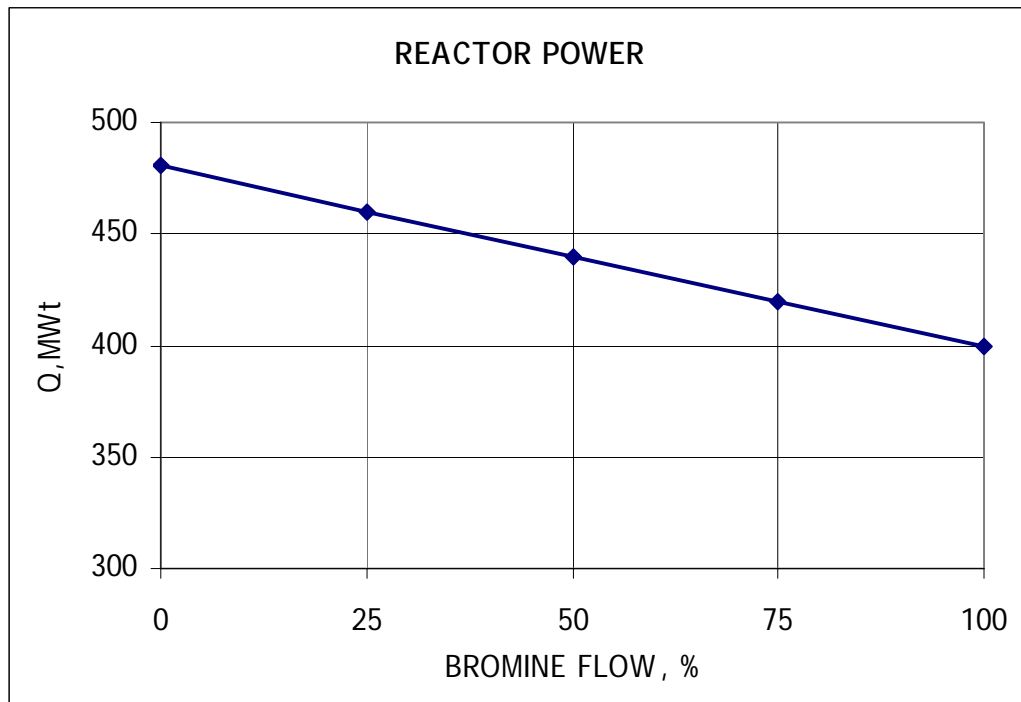


a) Heat transfer.

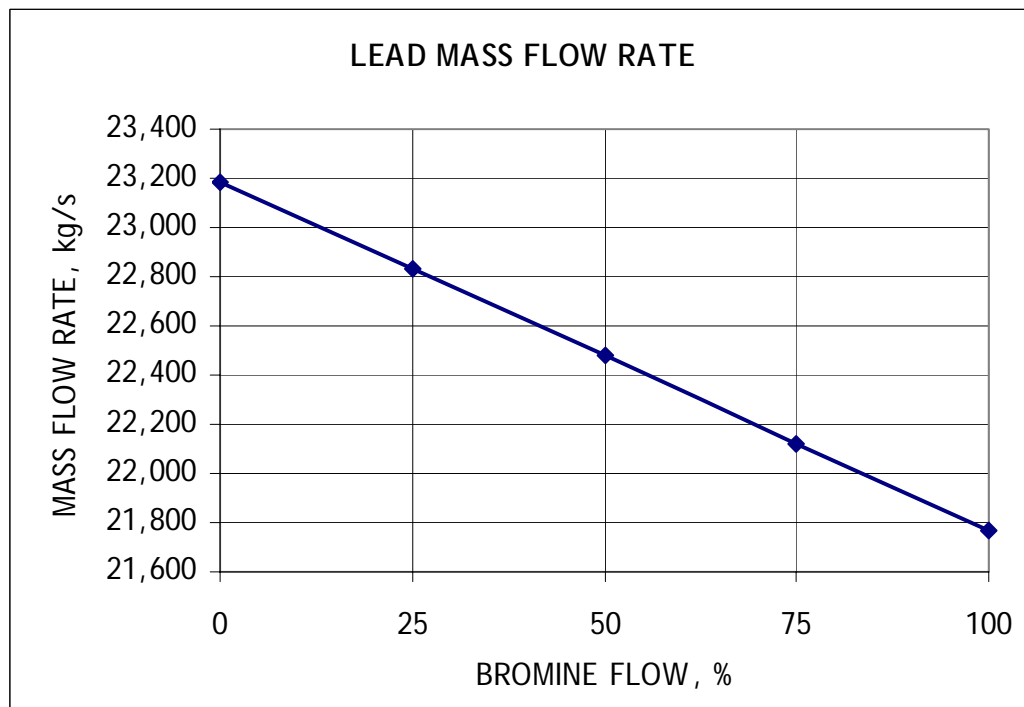


b) Temperatures inside reactor.

Figure G.1. Load follow for reagent steam flow rate variation.

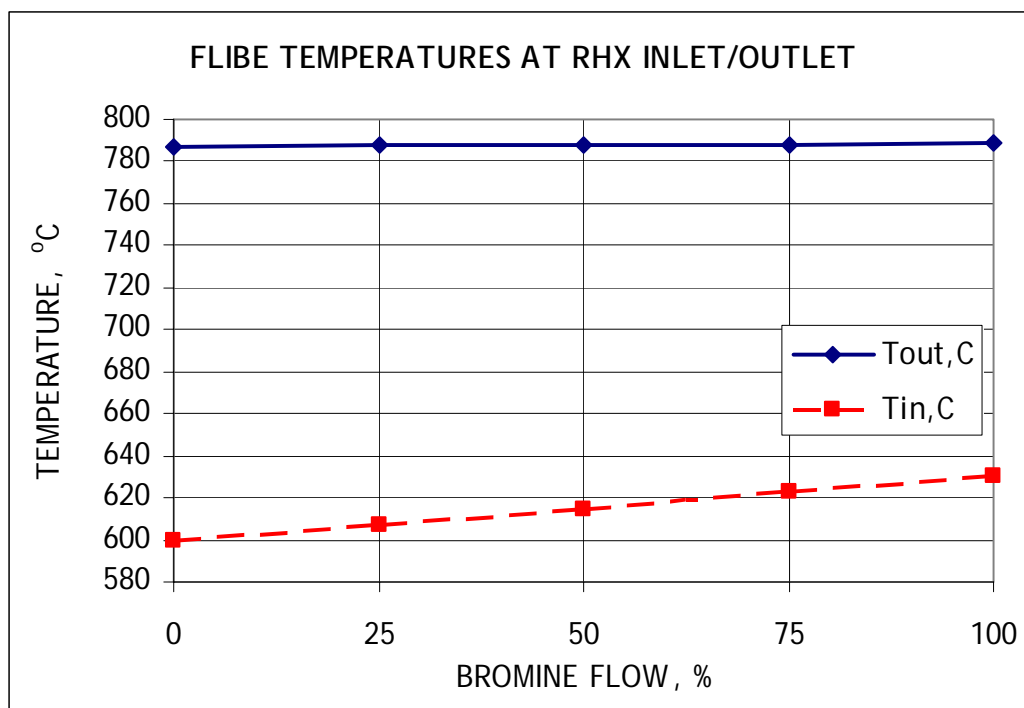


c) Reactor power.

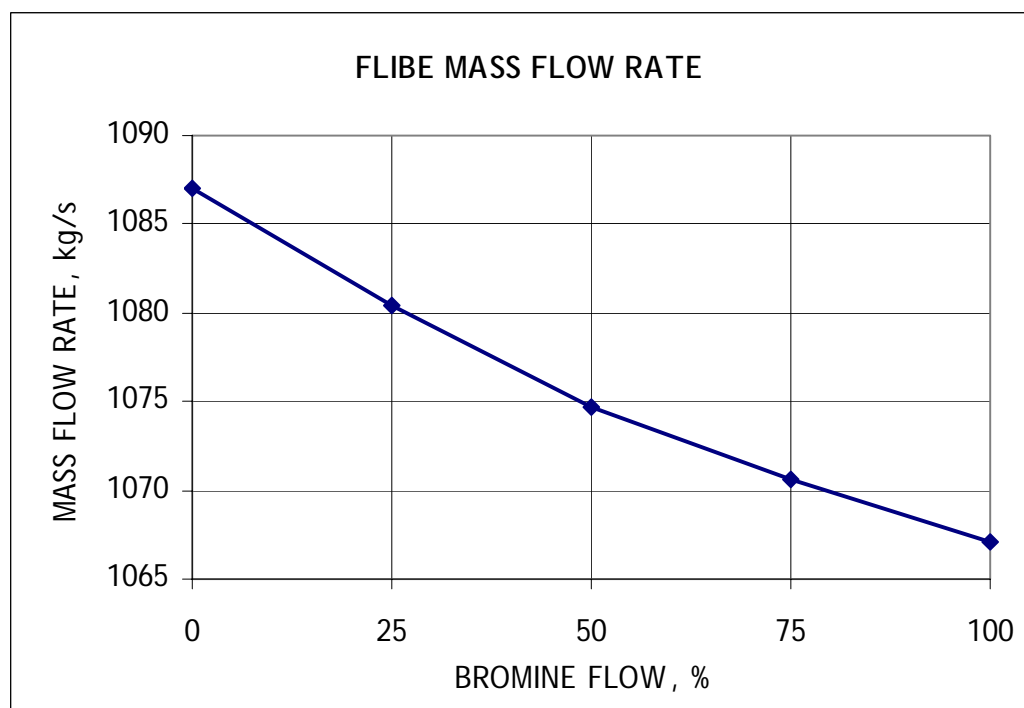


d) Reactor coolant mass flow rate.

Figure G.1 (Continued). Load follow for bromine flow rate variation.

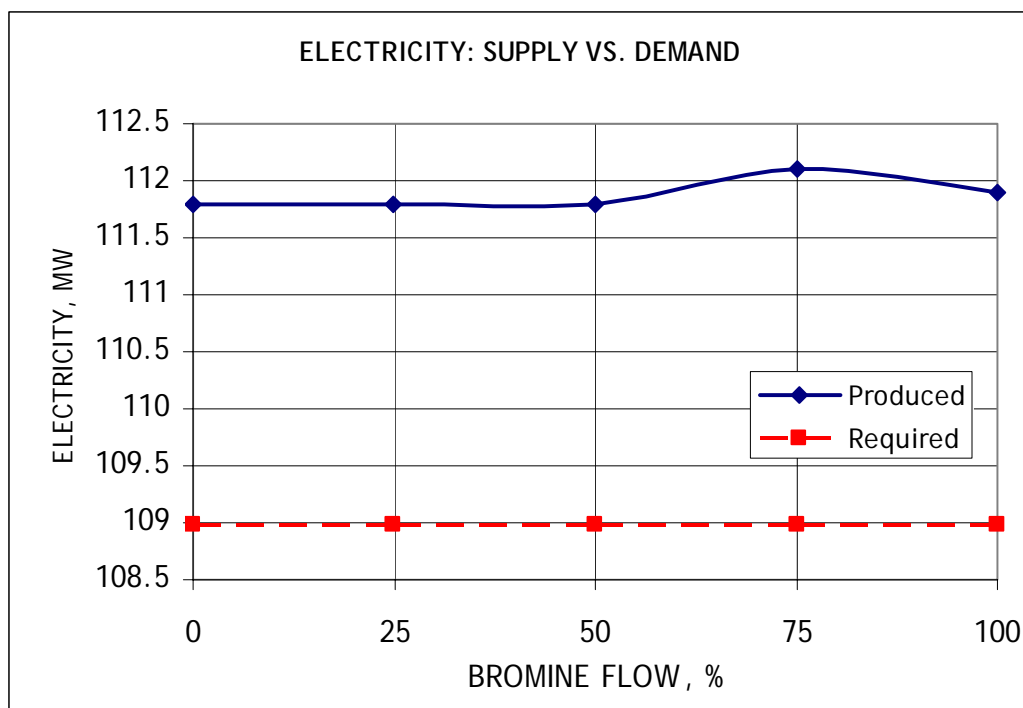


e) RHX temperatures.

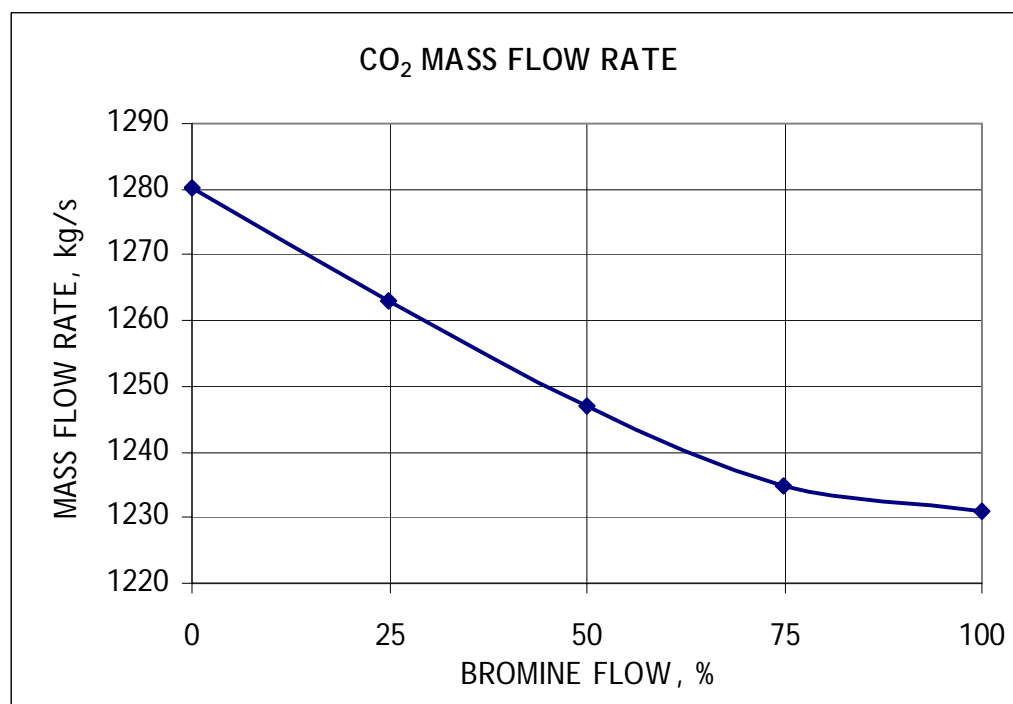


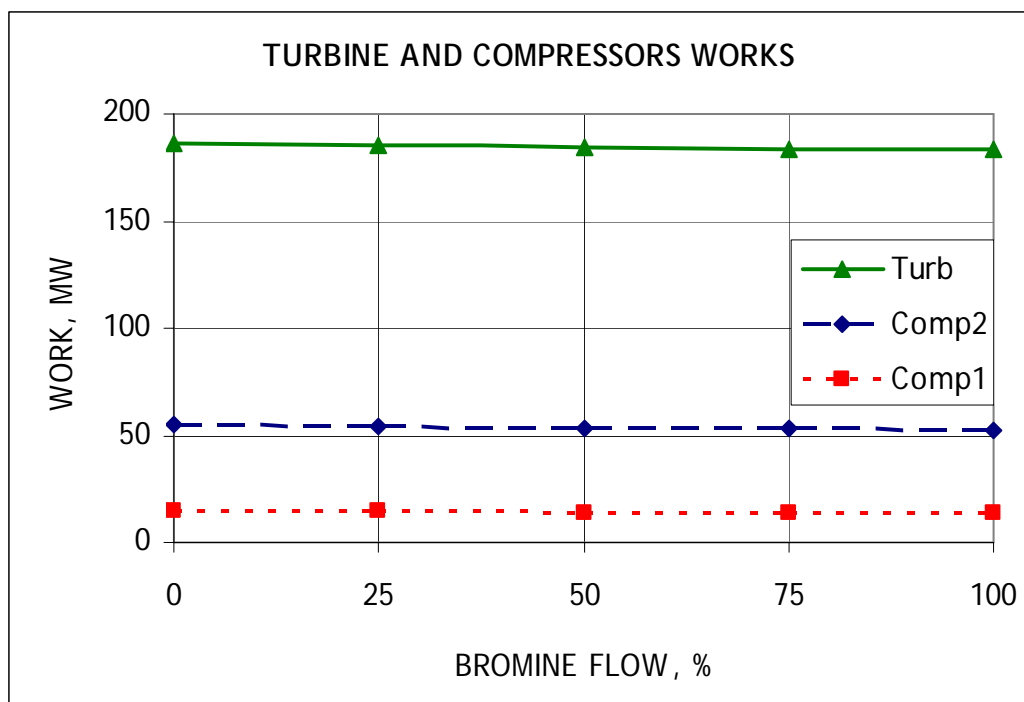
f) Flibe mass flow rate.

Figure G.1 (Continued). Load follow for bromine flow rate variation.

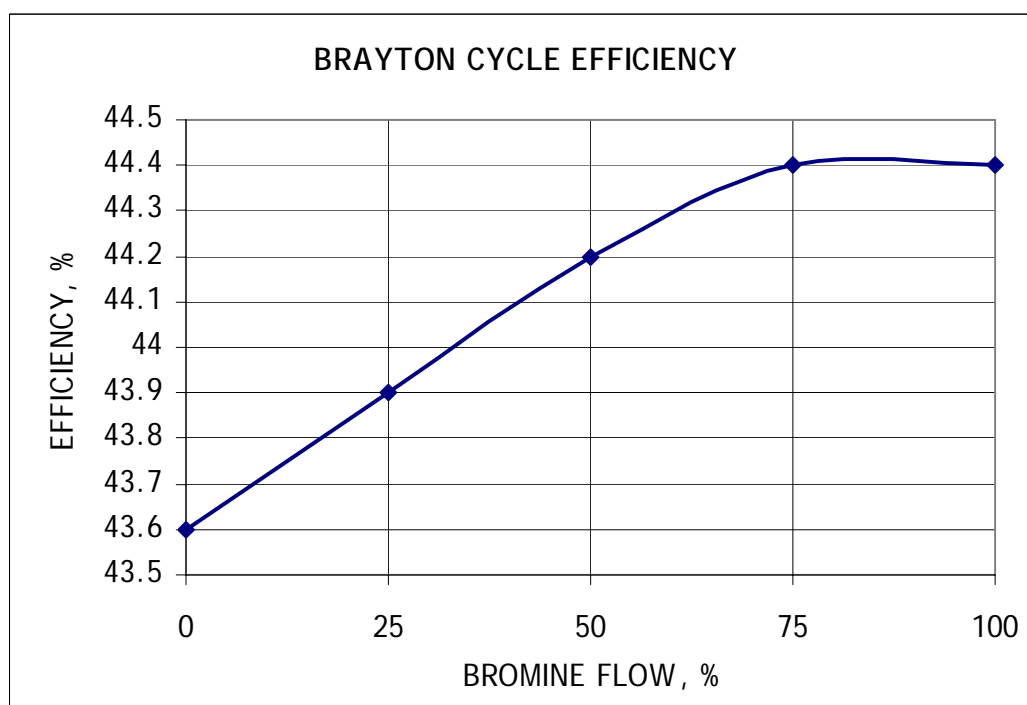


g) Electricity production.

h) CO₂ mass flow rate.**Figure G.1 (Continued). Load follow for bromine flow rate variation.**

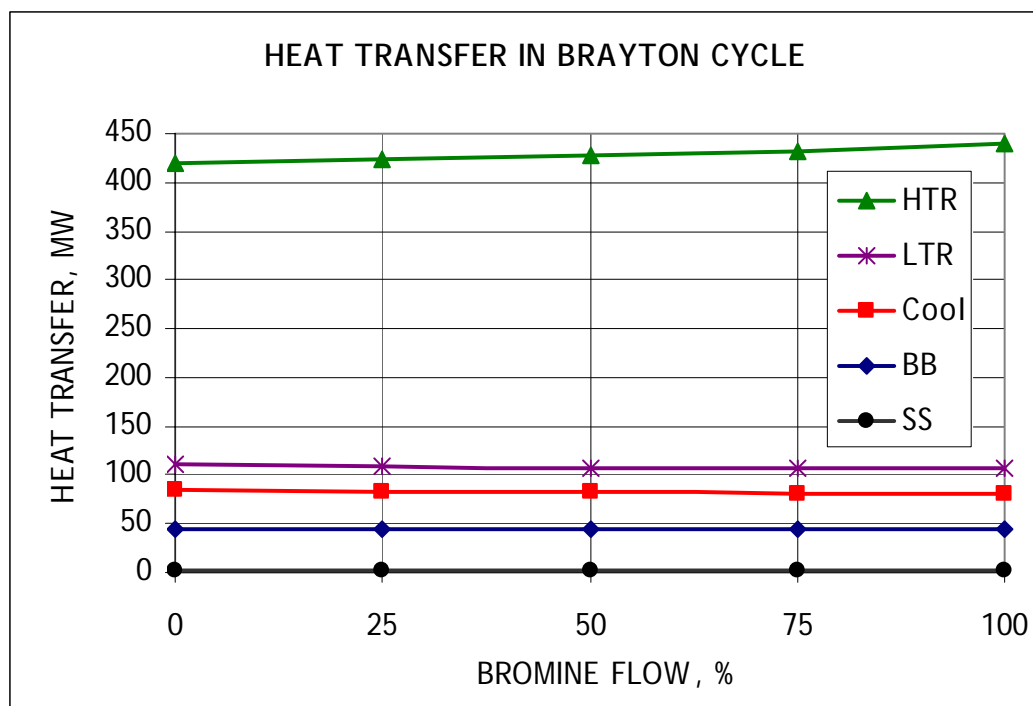


i) Turbine and compressors works.

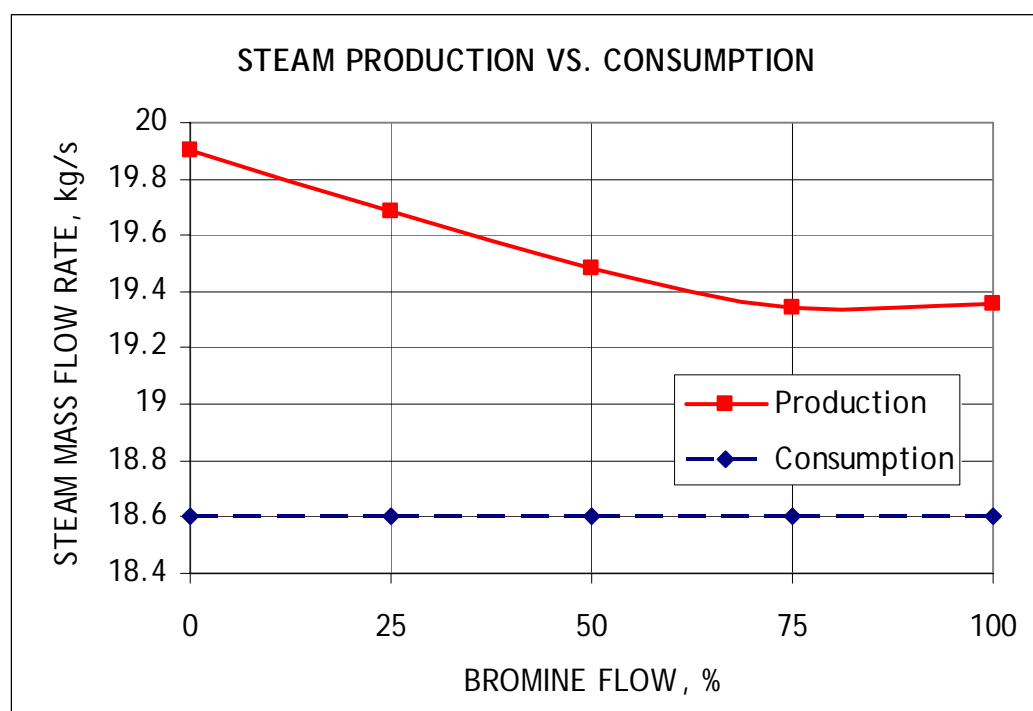


j) Brayton cycle efficiency.

Figure G.1 (Continued). Load follow for bromine flow rate variation.



k) Heat transfer in Brayton cycle.



l) Reagent steam production and consumption.

Figure G.1 (Continued). Load follow for bromine flow rate variation.

APPENDIX H
ACCIDENT SCENARIOS FOR STAR-H2

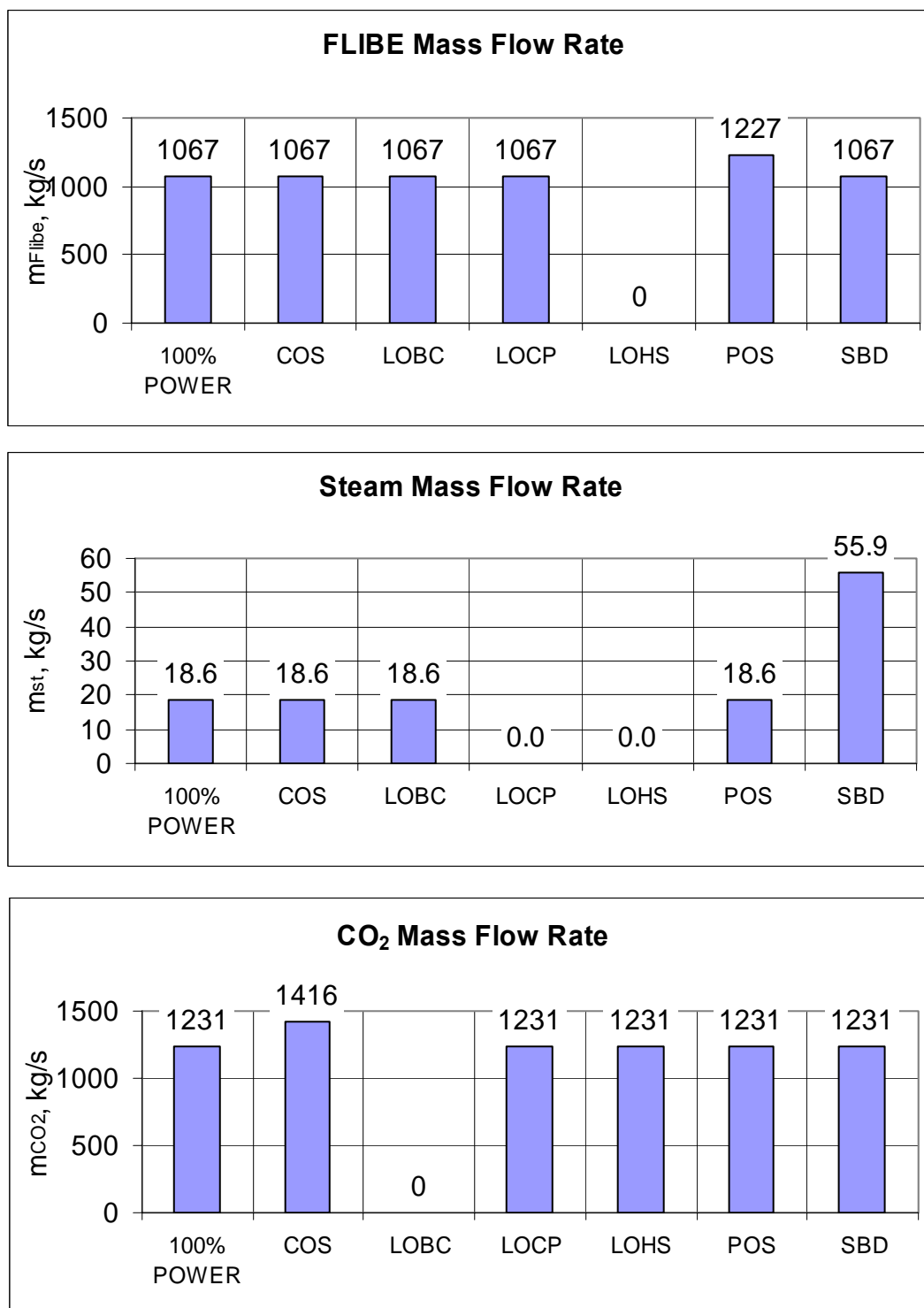


Figure H.1. Working fluid mass flow rates.

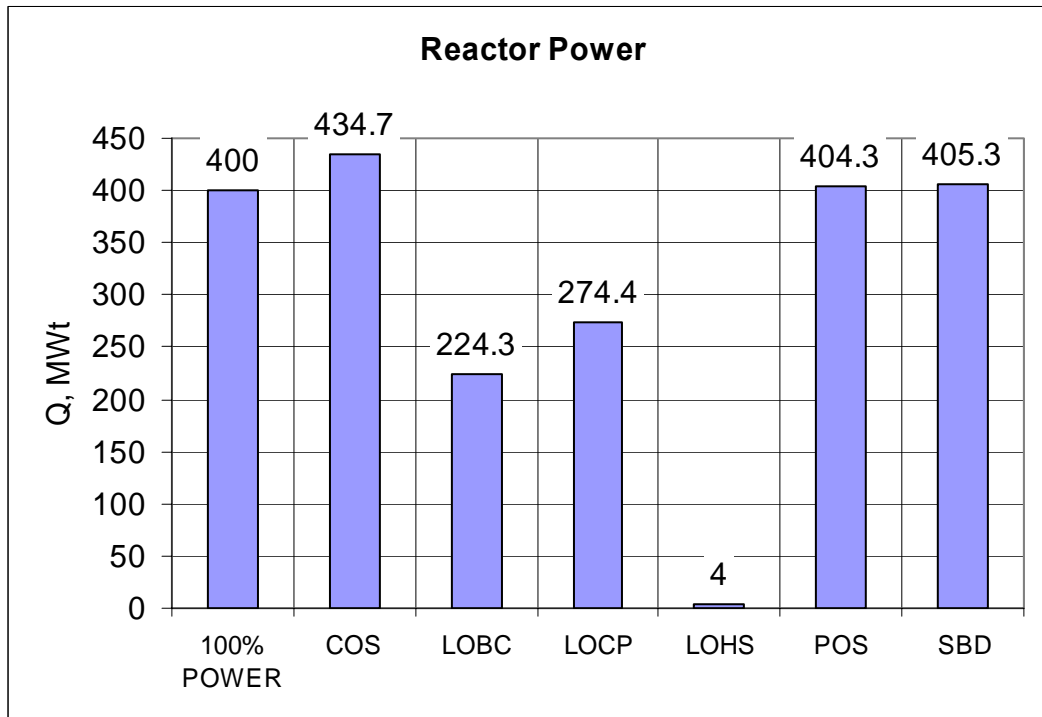
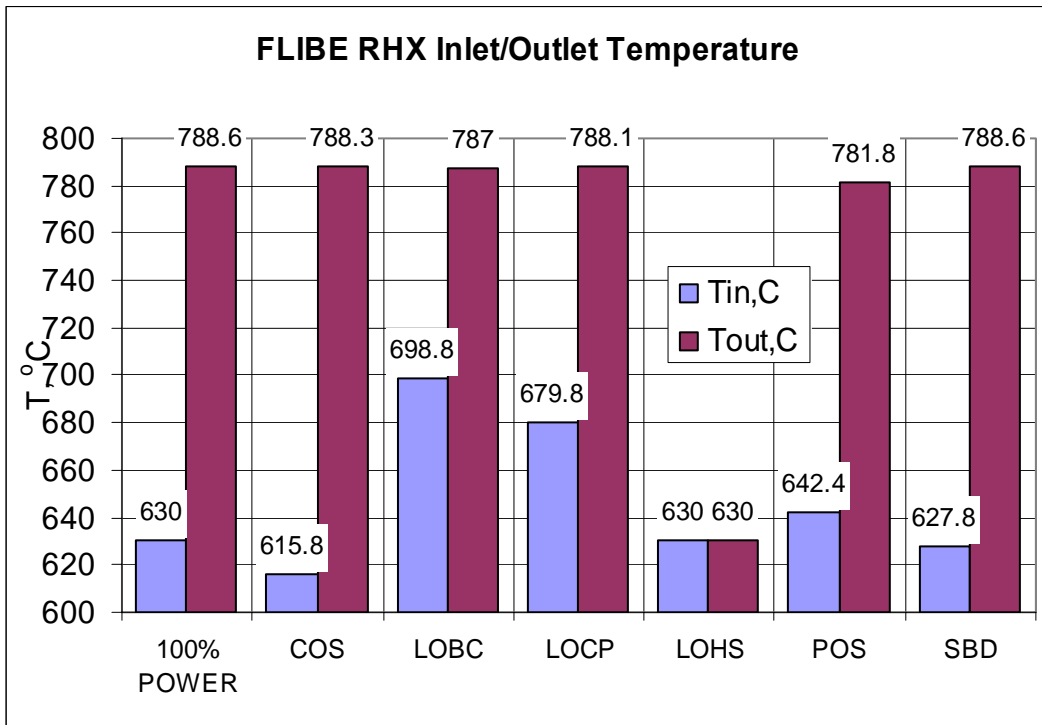


Figure H.2. Flibe temperatures and reactor power.

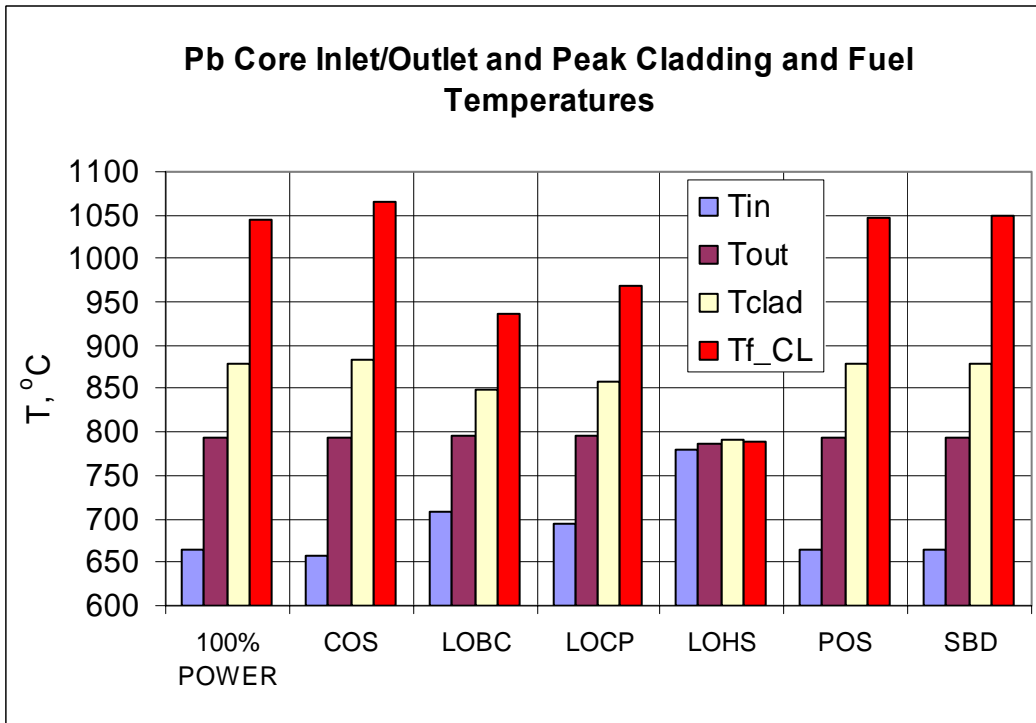
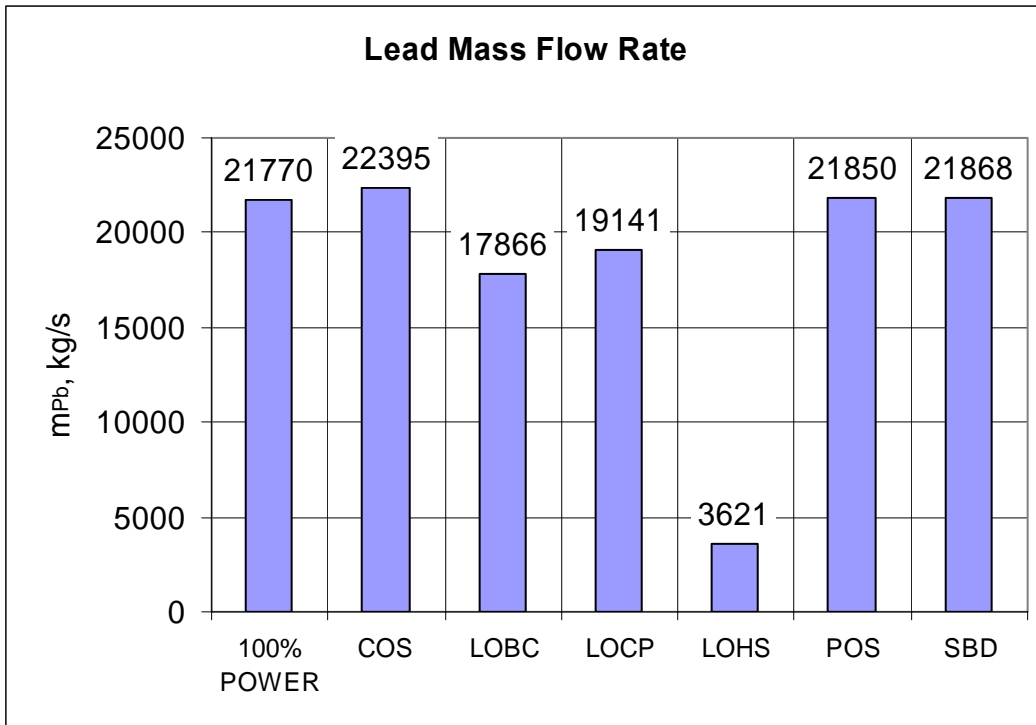


Figure H.3. Coolant mass flow rate and temperatures inside reactor.

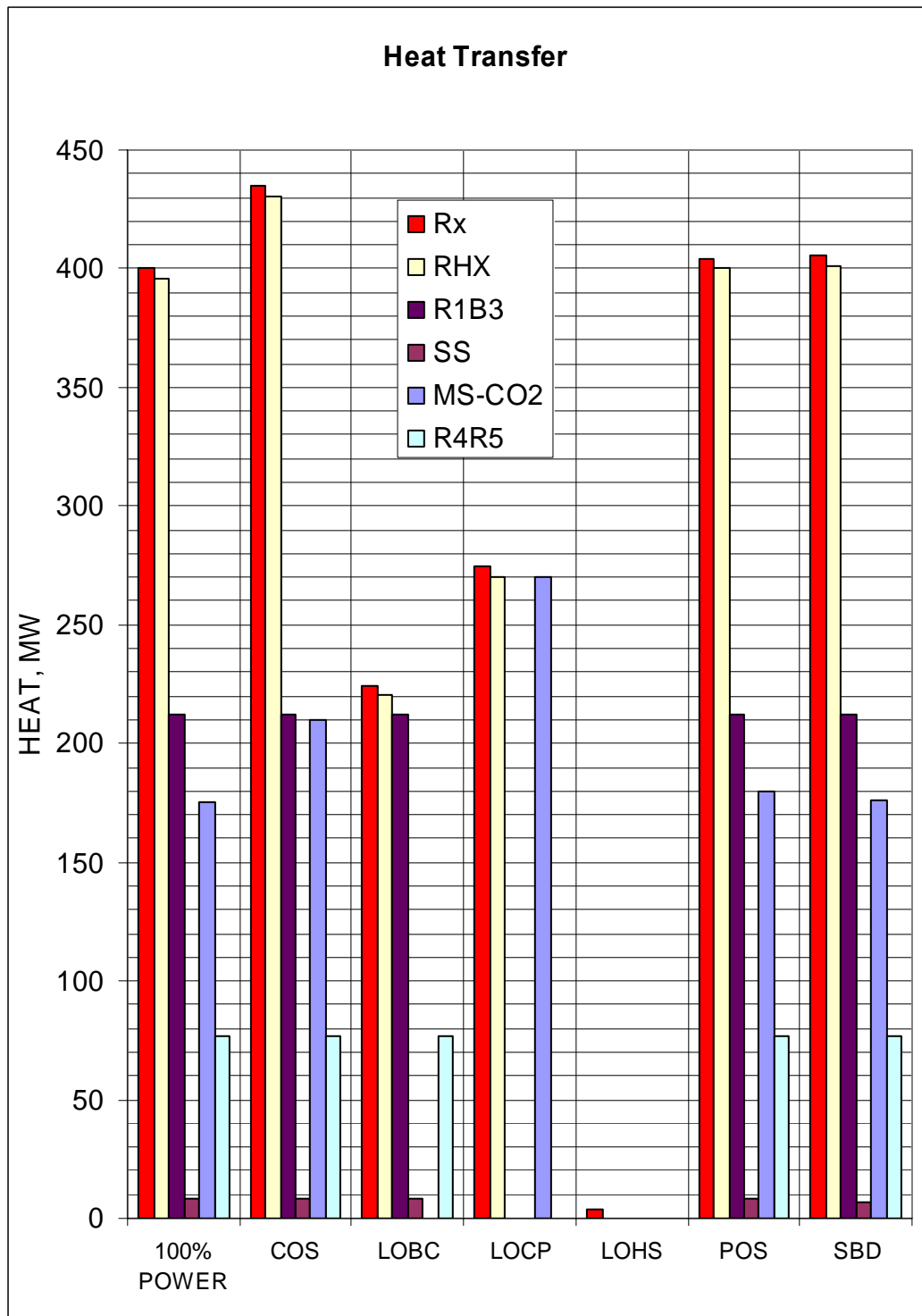


Figure H.4. Heat transfer in heat exchangers.

VITA

Anton Moisseytsev was born in Moscow, Russia in 1976. He received his B.S. degree in physics from Moscow State Engineering and Physics Institute in 1997 from the Department of Theoretical and Experimental Physics of Nuclear Reactors. He received his M.S. degree in 1999 from the same department. His thesis was in the field of Nuclear Material Safe Management.

He started his Ph.D. program in Texas A&M University at the Department of Nuclear Engineering in 2000 under the direction of Dr. Kenneth L. Peddicord. He graduated with the Ph.D. degree in December 2003.

During his Ph.D. program at Texas A&M, he worked for three summer internships at Argonne National Laboratory in Argonne, IL.

His permanent address in Russia is: Pyr'eva 14-31, Moscow, Russia, 119285.